DRY ROCK AVALANCHE PROPAGATION: UNCONSTRAINED FLOW EXPERIMENTS WITH GRANULAR MATERIALS AND BLOCKS AT SMALL SCALE

PAR

Irene MANZELLA

Laurea in ingegneria per l'ambiente e il territorio, Politecnico di Milano, Italie
et de nationalité italienne

EPFL

ÉCOLE POLYTECHNIQUE
FÉDÉRALE DE LAUSANNE

Suisse
2008

A Maya e Noemi

Nothing in life is to be feared. It is only to be understood.

Marie Curie

ACKNOWLEDGEMENTS

ABSTRACT

Rock avalanches are catastrophic phenomena which are not yet exhaustively understood. They consist of rock mass movements of more than one million cubic metres, involving a great amount of energy and travelling farther than expected with a normal sliding friction law. The present study has as main purpose to investigate the propagation mechanisms involved in rock avalanche processes and to identify parameters influencing velocity and deposit characteristics by means of laboratory experiments, i.e. dry unconstrained flows of granular materials and blocks at small scale (bricks) down an inclined board which ends with a horizontal accumulation zone.

Two main experimental campaigns have been carried out. The first represents a preliminary study which has been useful to test the experimental set-up, to improve the measuring devices and to assess significant factors governing propagation of granular avalanches. Fall height, volume, materials used (sand or gravel), releasing geometry and the number of consecutive releases have been varied and their influence on front mass velocity and on deposit characteristics has been studied.

In the second experimental campaign the varied parameters are fall height, volume, material (aquarium gravel and small bricks), slope inclination, base friction coefficient and the regularity of the pathway (sharp or curved discontinuity at the toe). Bricks are randomly poured into the releasing container before failure (loose mass) or piled orderly (structured mass). Furthermore, it has been possible to compute the morphology of the final deposit and the position of its centre of mass thanks to a new optical technique, the fringe projection method, recently developed and adapted to the laboratory conditions.

The analyses of this extensive set of parameters put in evidence the importance of the nature of the released material, the structure of the mass before failure and the topography, i.e. the slope and the regularity of the pathway. Factors causing longer runouts are: larger volume, greater fall height, lower coefficient of friction, higher slope angle, the use of bricks ordered in piles and a smoother discontinuity at the toe of the slope. Morphology is dependent on the type of material used: sand or gravel; gravel deposit seems closer to real cases. There is also a considerable difference in deposit morphology when the event is the consequence of one large volume released at once or of a progressive failure. In the latter case final deposit characteristics depend on the individual smaller volumes. By analysing the velocity of the mass front as it enters the accumulation zone, it is possible to see that a transfer of momentum occurs between the rear approaching part and the front one slowing down ahead, inducing an excessive travel distance. In the case of piled bricks the regime is mainly frictional (energy dissipated essentially by friction at the base) on the inclined panel, where the mass remains relatively structured, and then frictional-collisional (energy dissipated also by friction and collisions within the mass) in the accumulation zone. The abrupt change of flow direction seems to be the cause of the shattering of the mass activating this passage to a different regime. On the other hand, both regimes can be found from the beginning of the slope in the case of loose materials, i.e. gravel and random bricks. The length is independent from the fall height. A marked difference is detected for tests with a curved connection at the toe which show high nondimensional values of the length and of the runout against the cubic root of the volume, closer to the ones of real cases. Statistical analyses confirm the considerations made.

Keywords: Rockslides, Rock avalanches, Physical modelling, Dry granular flow, Runout, Fahrböschung, Unconstrained flow, Fringe projection method.

RÉSUMÉ

Les avalanches rocheuses sont des phénomènes catastrophiques qui ne sont pas encore totalement compris. Celles-ci consistent en des mouvements de masses rocheuses de plus d'un million de mètres cubes, impliquant des grandes quantités d'énergie et des déplacements plus importants que ceux prédits par un modèle de frottement simple. Cette recherche a pour principal objectif d'examiner les mécanismes de propagation de tels processus, et d'identifier les paramètres influençant la vitesse et les caractéristiques du dépôt. Des expériences en laboratoire permettent cette identification au moyen d'écoulements non contraints de matériaux granulaires secs ou de blocs à petite échelle (briquettes) sur un plan incliné qui se termine par une zone d'accumulation horizontale.

Deux campagnes expérimentales principales ont été menées. Dans un premier temps, une étude préliminaire a permis de tester les installations expérimentales, afin d'améliorer les instruments de mesure et d'évaluer les facteurs significatifs influençant la propagation d'avalanches granulaires. Les paramètres contrôlés sont: hauteur de lâcher, volume, matériaux utilisés, géométrie de départ de la masse et séquence de lâcher. Leur influence sur la vitesse du front de la masse et sur les caractéristiques du dépôt a été étudiée.

Dans la seconde campagne ont été contrôlés: hauteur de lâcher, volume, matériaux utilisés, inclinaison de la pente, coefficient de frottement à la base, régularité du chemin parcouru par la masse (pied discontinu ou incurvé). Les briquettes sont soit déversées de manière aléatoire dans le réservoir avant le lâcher (masse en vrac), soit empilées de façon ordonnée (masse structurée). La morphologie du dépôt final et la position de son centre de gravité ont pu être déterminées grâce à la technique de projection des franges, récemment développée.

Les analyses, qui portent sur ce large éventail de paramètres, ont mis en évidence l'importance de la nature du matériau lâché, de la structure de la masse avant la rupture et de la topographie, à savoir la pente et la régularité du chemin parcouru. Les facteurs qui induisent des distances de parcours plus grandes sont: volume plus grand, plus grande hauteur de chute, coefficient de frottement plus faible, inclinaison de la pente plus grande, empilement de briques de manière ordonnée et discontinuité plus douce au pied de la pente. La morphologie dépend du type de matériau utilisé: sable ou gravier; les dépôts de gravier semblent plus proches de cas réels. La morphologie du dépôt diffère lorsque l'événement résulte d'un seul lâcher de grand volume ou d'une rupture progressive. Dans le dernier cas, les caractéristiques du dépôt final dépendent des petits volumes individuels. En analysant la vitesse du front de masse entrant dans la zone d'accumulation, on observe un transfert de moment entre la partie arrière de la masse et la partie frontale dont la vitesse décroit, ce qui induit une distance de parcours plus grande. Dans le cas de briquettes empilées, le régime de frottement prédomine (l'énergie est dissipée principalement par le frottement à la base) sur le plan incliné, là où la masse reste relativement structurée. Puis, le régime de collision – frottement (énergie dissipée aussi par frottement et par des chocs à l'intérieur de la masse) devient prépondérant dans la zone d'accumulation. Le brusque changement dans la direction de l'écoulement semble être la cause de la perte de structure de la masse, ce qui engendre ce changement de régime. Au contraire, les deux régimes sont présents dès le début de la chute dans le cas des matériaux, graviers ou briques, en vrac. La longueur est indépendante de la hauteur de chute. Les tests effectués sur le plan incurvé au pied de la pente donnent de grandes valeurs adimensionnelles de la longueur et de la distance de parcours, ce qui est plus proche des cas réels. Les résultats obtenus sont confirmés par des analyses statistiques.

Mots clés: Eboulis, Avalanches rocheuses, Modélisation physique, Ecoulement granulaire sec, Distance de parcours, Fahrböschung, Ecoulement non contraint, Méthode de projection de franges.

TABLE OF CONTENTS

LIST OF SYMBOLS

H   Total fall height (pp. 11, 12, 23, 24, 25,)

h_v Height of the centre of mass before failure (pp. 11, 36, 37, 115, 127, 128, 129, 130, 131, 134, 135, 136, 137, 165)

L   Travel distance or runout (pp. 11, 12, 23, 24, 25, 57)

L_{CM} Distance travelled by the centre of mass (pp. 11, 28, 29)

L*   Length of the deposit (pp. 11, 24, 36, 37, 56, 95, 127, 128, 129, 130, 131, 135, 136, 137, 165, 166)

ϕ Basal coefficient of friction (pp. 11, 26, 27, 28, 29, 54, 123, 134, 135, 136, 137, 138, 153, 156)

α or ϕ_{ap} Fahrböschung or apparent coefficient of friction (pp. 11, 23, 95, 96, 99, 104, 108, 135, 136, 137, 138)

ϕ_{CM} Travel angle of the centre of mass (pp. 12, 95, 96, 102, 103, 104, 107, 113, 119, 135, 136, 137)

L_e Excessive travel distance (Hsü, 1975) $L_e = L - \dfrac{H}{\tan 32°}$ (pp. 12, 24, 117)

H_a Hazard (pp. 15, 16)

R_t Total risk (pp. 15, 16)

V_u Vulnerability (pp. 15, 16)

E_r Elements at risks (p. 16)

f Equal to H/L (p. 23, 25)

V Volume (pp. 23, 24, 25, 51, 60, 92, 93)

Lr   Index of the degree of mobility of large landslides (Corominas, 1996)

                     $L_r = \dfrac{L_e}{H / \tan(\phi)}$ (pp. 24, 117, 118, 165)

S   Area covered by the deposit (p. 24)

M   Mass (pp. 26, 27, 28, 123)

β Slope angle (pp. 26, 27, 28, 29, 49, 123)

v Velocity (pp. 26, 28, 123)

F $F = \dfrac{z_{max}}{\Delta\varphi_{max}}$ (p. 87)

$\Delta\varphi$ $\Delta\varphi = \left(\varphi_{obj} - \varphi_{ref}\right)$ (pp. 86, 87)

X_{CM} Distance travelled by the centre of mass on the horizontal panel (pp. 95, 96, 106, 107, 108, 127, 135, 136, 137)

Z_{CM} Final deposit height of the centre of mass (p. 96)

E_{lt} Total loss of energy (p. 120, 121)

E_{lf} Loss of energy by friction at the base (pp. 120, 121)

h_{CM} Difference in height of the centre of mass before and after failure (p. 120)

h_f Height representing the energy loss of the mass by basal friction (p. 120)

$\Delta E/E_{lt}$ Relative energy loss $\dfrac{\Delta E}{E_{lt}} = \dfrac{E_{lt} - E_{lf}}{E_{lt}} = \dfrac{Mg\Delta h}{Mgh_{CM}} = \dfrac{\left(h_{CM} - h_f\right)}{h_{CM}}$ (pp. 120, 121, 139)

a Acceleration of the centre of mass (p. 123)

r   Radius of curvature (pp. 123, 124, 127)

$\phi_{C\,0}$ Dynamic friction angle at the base back-analysed from the tests with a lumped mass model which account the centripetal acceleration (pp. 124, 125, 126)

$\phi_{C=0}$ Travel angle computed with the lumped mass model without accounting the centripetal acceleration (pp. 124, 125, 126)

Δh_{CM} Difference between the height of centre of mass of the idealised lumped mass model and the real one measured in laboratory (p. 125)

R/h*   Normalized runout (pp. 127, 129, 130, 131)

$E(\vec{c})$ Estimated value of the coefficients of the model (p. 133)

$E(\vec{e})$ Estimated values of the error (p. 133)

SS   Total sum of squares (p. 133)

K Degree of structure (pp. 134, 135, 136, 137)

S Degree of smoothness of the connection at the toe (pp. 134, 135, 136, 137)

$\dfrac{W}{h^*}$ Normalized width (pp. 135, 136, 137)

$\dfrac{X_{CM}}{h^*}$ Normalized X_{CM} (pp. 135, 136, 137)

δ Deflection angle (p. 144)

α_d Deflection plane true dip angle (p. 144)

1.   Introduction

Long runout rock avalanches, or Sturzstroms as called by Heim (1932), are defined as an extremely rapid, massive, flow-like motion of fragmented rock derived from a bed-rock failure and which exhibits much greater mobility than could be predicted using frictional models (Hungr et al, 2001). They are rare but catastrophic events, the most dangerous and lethal of all landslides phenomena. In particular developing countries are affected by the larger number of fatalities; here the sometimes uncontrolled increase of population density in mountainous regions puts a great number of people in danger. Therefore it becomes of the greatest importance to develop tools which could improve the prevention of this risk and give a better standard of living to all human beings.

The volume of the mass in question is more than one million cubic metres and energy involved could reach 10^{14} Joule. The most effective way to prevent rock avalanches from causing victims and damages would be to be able to forecast their runout and consequently to define areas that could be affected by their occurrence. Mechanisms involved in these phenomena are still for most part unknown; several theories have been put forward to explain their extended travel distance but at the present time no general agreement has been achieved and there are still many questions to be answered (Hungr, 1990 and Legros, 2002).

Since the number of well documented real cases is limited, due to the rareness of these catastrophic phenomena, several authors have resorted to laboratory tests. Experiments usually reproduce idealized conditions and results are used not only in numerical models

validation but also to better understand the propagation mechanisms and to identify parameters influencing velocity and deposit characteristics. Despite the difficulty in matching the scaling laws, the use of a physical model enables studying the influence of each parameter of interest, by controlling and changing one at a time, with known and consistent experimental conditions. In addition several dimensional studies have arrived to the conclusion that with the exception of some particular phenomena, granular avalanches at small scale should realistically reproduce major features of large-scale rock avalanches.

In this framework it is possible to affirm that the present research aims to study main mechanisms involved in granular avalanches laboratory tests in order to improve the understanding of phenomena engaged in real events and consequently the causes of the excessive mobility of rock avalanches. This goal is also pursued by means of comparison with existing theories and data coming from real cases and finally by formulation and validation of empirical models. As a complementary part of the research, tests have been also used to compare and validate numerical codes. Therefore a multi-tool approach is used: intuitive, empirical and statistical methods are applied to analyse the experimental results.

An extensive experimental study has been carried out for this purpose at the rock mechanics laboratory of the EPFL (Ecole Polytechnique Fédérale de Lausanne). The basic phenomenon under investigation is the propagation in an ambient gaseous medium at atmospheric pressure, of a mass triggered from rest that flows on a solid slope under gravity. At the toe of the slope follows a horizontal plane where the mass spreads and translates coming to rest when the momentum acquired from the fall is totally dissipated by collisions between the grains, intergranular and basal friction (Davies and McSaveney, 1999). The development of an innovative optical method based on fringes projection has made it possible in this study to systematically locate the centre of mass of the final deposit and consequently to analyse its governing parameters. The present study concerns mainly phenomena related to unobstructed free-spreading dry rock avalanches. Analysis of the relationships between parameters describing both the instable mass (e.g. volume, material characteristics) and the path (e.g. local morphology, slope) and deposit characteristics will allow a better understanding of the phenomena and improvements to the state of the art in assessing rock avalanche propagation.

1.1.   Synopsis of the chapters

After having defined the rock avalanche phenomenon with the support of some case histories and the definition of commonly used terms, Chapter 2 gives an overview of the main hypotheses concerning Sturzstroms excessive mobility and of the empirical, analytical and experimental models developed in the past. In particular laboratory experiments carried out in this field will passed in review and analysed in details and starting from these works the main purpose of the present research will be defined.

In Chapter 3 the experimental set-up is defined in details; in particular the front velocity measurement device is explained. Factors and characteristics studied within the preliminary experimental campaign will be listed and described. Results of this first testing campaign are then presented. The first part of the present experimental study has consisted of about a hundred and fifty tests. Fall height, volume, number of releases, geometry before failure and materials used for testing have been varied and their influence on deposit characteristics (such as length, width, height, runout and morphology) and on the front mass velocity has been studied. The approach for this campaign has been mainly intuitive and qualitative; analyses are based on observations and comparison with known real events. Despite the intuitive approach the results have been really useful for phenomenological studies and assessment of relevant physical parameters influencing rock avalanches propagation. In addition they represent the contribution of the EPFL rock mechanics laboratory to the INTERREG IIIA "Rockslidetec" project between Italian, French and Swiss partners.

In Chapter 4 results obtained with the first campaign are extended with tests performed with an improved experimental set-up and measuring devices; this will allow confirming and quantifying previous findings and studying additional factors and characteristics. This second part of the present experimental study has consisted of about two hundreds tests. The basic phenomenon studied is the same as the one of the preliminary campaign: unconstrained flow of a mass of granular material down an inclined plane. In this case the mass can consist of dry rigid non-cohesive grains or little bricks, randomly poured into the reservoir before failure or piled orderly. The choice of the latter arrangement was motivated to model an idealised rock mass affected by discontinuity sets at the start. Additional factors considered are the slope of the tilting panel, the roughness of the basal surface, and the effects of a progressive discontinuity at the toe of the slope. The fringe projection method,

an optical technique, allows retrieving the profilometry of the final deposit and then to compute the position of its centre of mass. Therefore additional characteristics have been as well evaluated, i.e. the apparent coefficient of friction, the distance travelled by the centre of mass on the horizontal panel and the angle to the horizontal of the straight line connecting the centre of mass at the start and after deposition. Therefore the approach for this campaign has been more quantitative and it has been possible to formulate empirical models describing the relationship of the factors varied against the different responses considered. These formulations are as well compared to existing models and data coming from real cases.

Complementary experiments and a benchmark exercise are described in Chapter 5. Changes in the experimental set-up have been made to carry out a particular test which has made the object of an international benchmark exercise for "the 2007 International Forum on Landslide Disaster Management, Hong Kong - Landslide Runout Analysis Benchmarking Exercise". The particularity of these tests is that a deflection is placed as an obstacle in the flow direction. The experimental set-up has been consequently modified and the fringe projection method has been adapted to measure the thickness of the flow during motion. Results of this exercise are not yet available but a small experimental campaign has been carried out with these test conditions. Considerations are drawn and interesting developments of research in this field are suggested. In the last part of this chapter, the results of a benchmark exercise made in the framework of the INTERREG "Rockslidetec" project are shown. One of the experiments made with the standard geometry of the set-up, has been simulated with the codes developed by the partners.

Chapter 6 finally summarises the whole work and draws the main conclusions.

# 2.	Rock avalanches and granular flows

Studying the Elm and Goldau events in Switzerland, Heim (1932) noticed that they have certain peculiarities: they both involve a volume of millions of cubic metres engaging a great amount of energy and their travel distance is longer than expected considering a normal sliding friction law. Since that moment, all rockslides corresponding to these characteristics were identified as different phenomena and classified as large rockslides, rock avalanches or "sturzstorms".

Even if these kinds of phenomena are relatively rare, the enormous volumes involved make them really dangerous and destructive. Therefore, since the stabilization of millions of cubic metres of rock mass would be extremely difficult and expensive, if not totally unfeasible, the best way to prevent damages and fatalities is to be able to define areas that could be affected by their occurrence. For this reason in the last fifty years, many studies have been carried out to better understand rock avalanches and to predict their propagation. Different models have been conceived to describe and predict their behaviour, but at the present state of the art in this field, there are still a large number of unknown factors as well as various and contradictory hypotheses about the cause of their abnormal runout.

Since the number of well documented real cases is limited, due to the rareness of these catastrophic phenomena, several authors have resorted to laboratory tests. Experiments usually reproduce idealized conditions and in most cases they consist in triggering a granular flow on a simple geometry. Results can constitute a significant sample to fill up partly the limited amount of reliable data used for numerical model validation. Moreover, they also contribute in better understanding the propagation mechanisms and in identifying parameters which influence velocity and deposit characteristics of rock avalanches, giving a

significant help to verify or invalidate the various hypotheses about the cause of their high-mobility. These contributions constitute the principal aim of the work carried out at the EPFL.

In this chapter, after a detailed definition of the terms related to this phenomenon, an overall review is made of the principal theories, approaches and models, used to explain, describe and simulate the rock avalanche propagation and mechanisms.

2.1.   Landslide classification

A landslide is a general term defining a gravity-driven geological movement of a mass of rock and/or earth down a slope (Cambridge dictionary). This is a large sense definition that needs a deeper distinction depending on characteristics such as materials involved, mechanisms and velocity. Among the classification made in the past, the ones of Varnes (1978) and Cruden and Varnes (1996), Hungr et al (2001) and Hungr and Evans (2004) are among the most complete and used. In 2005 Hungr et al have summarized and homogenized them in a table, which is reported in Table 2-1with some additions and adaptations.

According to Cruden and Varnes (1996) the different kinematics listed in Table 2-1 are described as follow:

- Slide: "downslope movement of a soil or rock mass occurring dominantly on surfaces of rupture or on relatively thin zones of intense shear strain".

- Fall: "detachment of soil or rock from a steep slope along a surface on which little or no shear displacement takes place". The rock blocks mainly fall, bounce or roll on the slope.

- Topple: "the forward rotation out of the slope of a mass of soil or rock about a point or axis below the centre of gravity of the displaced mass".

- Flow: "spatially continuous movement in which surfaces of shear are short-lived, closely spaced, and usually not preserved. The distribution of velocities in the displacing mass resembles that in a viscous liquid".

Table 2-1 Classification of landslide types
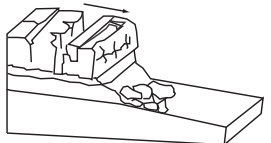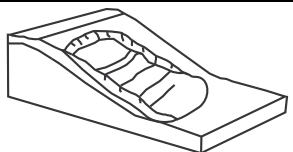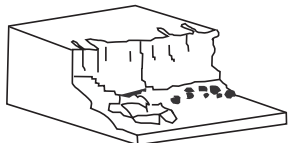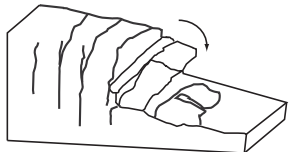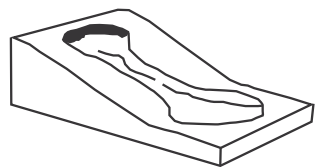
TYPE	VELOCITY CLASS*							COMMENT
	ES	VS	S	M	R	VR	ER	
SLIDES IN ROCK								
Translational (or Wedge) Rock Slide							■	
Rotational Rock Slide (Slump)	■	■	■	■	■			Very weak rock mass
Compound Rock Slide	■	■	■	■	■	■		Various types of mechanisms
Rock Collapse								Strong rock, joints, rock bridges
SLIDES IN SOIL								
Clay Slump (Rotational)	■	■	■	■				
Clay Slide (Compound)	■	■	■	■				
Sand (Gravel, Talus, Debris) Slide								Usually shallow
FALLS								
Rock (Debris) Fall							■	Fragmental fall, small volume
TOPPLES								
Rock Block Topple							■	Single or multiple blocks
Rock Flexural Topple	■	■	■	■	■			Very weak rock mass
FLOW-LIKE LANDSLIDES								
Dry Sand (Silt, Gravel, Talus Debris) Flow	■	■	■	■				No cohesion
Sand (Silt, Debris, Peat) Flow Slide						■	■	Liquefaction involved
Clay Flow Slide						■	■	Quick clay
Debris Avalanche						■	■	Non-channelized
Debris (Mud) Flow					■	■	■	Channelized
Debris Flood					■	■	■	High water content
Earth Flow	■	■	■	■				Plastic clay
Rock Avalanche							■	Begins in bedrock
Rock Slide- Debris Avalanche							■	Entrains debris

* ES: extremely slow; VS: very slow; S: slow; M: moderate; R: rapid; VR: very rapid; ER: extremely rapid

Table 2-1 Classification of landslide types (adapted from Hungr et al, 2005; sketches inspired from www.geonet.org.nz)

2.1.1. Definition and classification of rock avalanches

Among the landslide types described in Table 2-1, the one which interests the present study is rock avalanches. An avalanche has been described in general terms by Pudasaini and Hutter (2007) as a transient, three-dimensional gravity driven free surface motion of a mass system made up of an assemblage of granular fragments, initiated by instability of a granular layer and flowing down to the run-out zone on an arbitrarily topography. A rock avalanche can be consequently defined as an avalanche originated from the instability of a rock mass, in contrast with debris avalanche which is originated in unconsolidated material or snow avalanche deriving from the instability of snow layers.

A rock avalanche is considered as belonging to the flow-type landslides, which means that it can be seen as moving essentially like a liquid over a rigid bed. Its speed usually exceeds 100 km/hr, its travel distance can be of several kilometres and its volume is greater than 10^6 m^3 (Hsü, 1975). The large quantity of mass in movement can develop a considerable energy, greater than the one developed by an earthquake of magnitude 6 (~$3*10^{13}$J), e.g. in the case of Val Pola (Italy) $40*10^6$ m^3 of material developed an energy of the order of $8*10^{14}$ J (Bouzid, 1999). To have a better visualization, Erissmann (1979) affirmed that the energy developed by the prehistoric Flims landslide ($9000*10^6$ m^3) would be enough to cover the total world's energy consumption during ten hours at that time and to accelerate the Cheops pyramid into a satellite orbit. This enormous energy developed in a short time has tremendous power of destruction, that can cause irreparable damages, changes in the landscape and sadly a large number of fatalities, as in the case in 1949 of the Khait rock avalanche (Tajikistan), which destroyed the entire town of Khait with the loss of 12000 persons (Leoniv, 1960).

The term rock avalanche, now largely accepted and used to describe these catastrophic, gravity driven events, has evolved in literature passing from "rock slide-debris avalanche" as defined by Varnes (1978) to the simpler term "rock avalanche". Hungr et al (2001) describe a rock avalanche or sturzstrom as an extremely rapid, massive, flow-like motion of fragmented rock derived from a bed-rock failure which exhibits much greater mobility than could be predicted using normal sliding frictional laws.

It is important to distinguish different types of rock avalanches according to the topography of the slope and of the propagation zone. They can be classified mainly as: *unconstrained* or

unobstructed landslides (Figure 2-1a) when there are no obstacles or confinements in the downslope movement and *confined* (Figure 2-1b) in the opposite case. More in details it is possible to distinguish different characteristics of the path (Corominas, 1996) such as: *deflections* (Figure 2-1d), when the presence of topographic obstacles forces a change in the direction of propagation of more than 60°, and *bends* (Figure 2-1e) when it is less than 60°; it is called *free-spreading* when the mass of debris is free to expand laterally and downwards. Other attributes of the path could be channeling, *opposite wall* obstruction (Figure 2-1c), simple runup, thickening on a fan, confining, etc. Unconfined rock avalanches, with free-spreading in the downhill zone, are the phenomena which are of major interest for the present research. The presence of deflections along the path is also considered in a complementary part of the present study.

An additional interesting distinction concerning morphology and energy dissipation has been made by Nicoletti and Sorriso-Valvo (1991), inspired from the one made by Abele (1974). They distinguish rock avalanches in three categories:

-   High-mobility rock avalanche, determined by low energy dissipation and which shows elongated hour glass shape (Figure 2-1b). In this case the mass is usually channelized down a narrow valley and spreads out in a more open area at the toe. An example of this kind of rock avalanche is the Pandemonium creek one (see Figure 2-2a) which took place in 1959 in the southern Coast Mountains of British Columbia; approximately $5 \times 10^6 \, \text{m}^3$ of debris travelled 9.0 km along a highly irregular path, descending a vertical distance of 2 km along a low-angle stream valley (6–9 degrees) into a lake. Debris may have reached velocities of up to 100 metres per second (Evans et al, 1989).

-   Intermediate mobility rock avalanche, determined by moderate energy dissipation and which shows a nearly oval, lengthened trapezium or tongue shape (Figure 2-1a). This kind of landslide usually spreads onto a broad valley or plain. It consequently belongs to the unconstrained rock avalanche type mentioned before and which constitutes the main object of the present study. The Frank slide in the southern Rocky Mountains of Canada is an example of this kind of rock avalanche (see Figure 2-2b). In 1903, $36.5 \times 10^6 \, \text{m}^3$ of limestone crashed from the summit of Turtle Mountain and covered approximately three square kilometres of the valley, killing more than 70 people.

- Low mobility rock avalanche, determined by high energy dissipation and which shows deformed T-shape (Figure 2-1c). This shape derives mainly from the perpendicular impact of the mass against the opposite slope. The impact leads often to runup, partition of the debris and fall-back ridges which indicate forced stopping and important energy dissipation. A typical example of this kind is the Valpola rock avalanche in 1987 in Italy (see Figure 2-2c). It took place after a period of heavy rainfall and involved 34 millions cubic meters of fractured rock. It fell approximately 800 m, impacting on the opposite side, devastating the bottom of the valley over a distance of 4 km and killing 27 people (Azzoni et al, 1992)
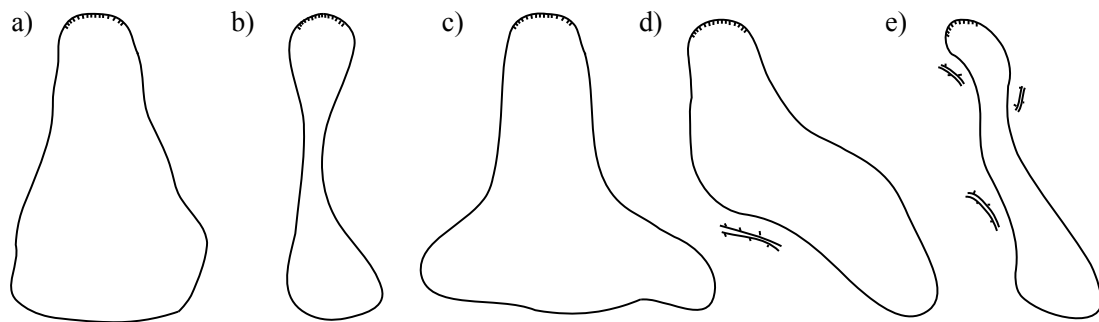
Figure 2-1 Landslides classification according to morphology of the path inspired from Nicoletti and Sorriso-Valvo (1991) and Corominas (1996)
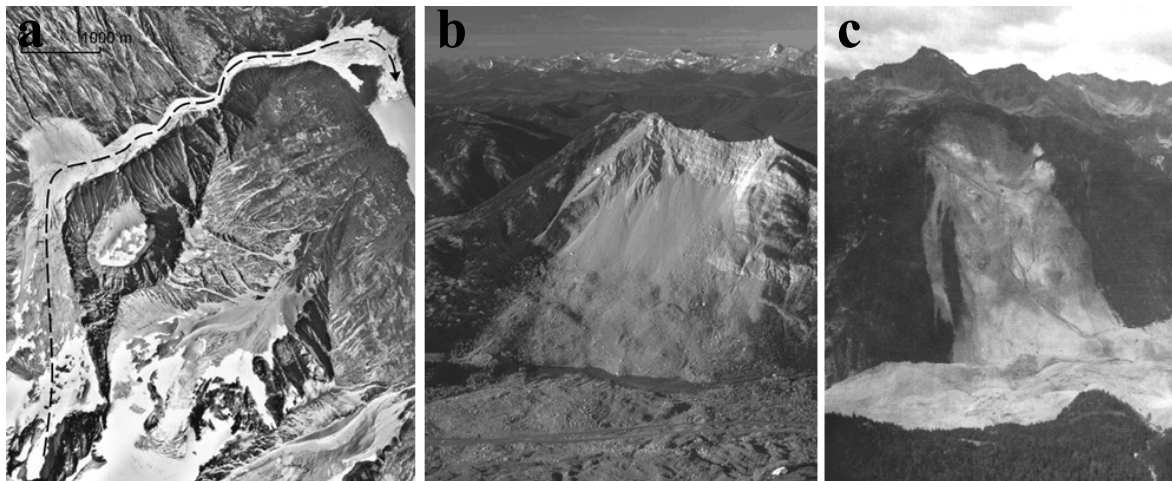
Figure 2-2 Three examples of rock avalanche: a) Pandemonium creek (source: Province of British Columbia), b) Frank slide (source: Alberta Community Development) and c) Valpola (source: Azzoni et al, 1992)

In the field of rock avalanche studies there are several recurrent terms that it is necessary to recall here. As in literature it is possible to find different definitions of the same word, here

are considered the ones which seem the most universally accepted; some additional definitions are also reported which will be useful for the following sections.

- Total fall height, H (see Figure 2-3): the elevation difference between the crown of the head scarp and the toe of the deposit.

- Height of the centre of mass before failure, h_v (see Figure 2-3) defined by Davies and McSaveney (1999) as the "vertical distance of the original centre of mass above the runout plane".

- Travel distance or runout, L (see Figure 2-3): the horizontal projection of the line connecting the crown of the head scarp with the most distal end at the toe of the deposit along the midstream path of the mass.

- Distance travelled by the centre of mass L_{CM} (see Figure 2-3): the horizontal projection of the line connecting the centre of mass before failure and after deposition along the midstream path of the mass.

- Length of the deposit, L* (see Figure 2-3): longitudinal spreading of the mass, the horizontal projection of the line connecting the rear and the front of the final deposit along the midstream path of the mass.

- Basal coefficient of friction, ϕ: the coefficient characterizing the friction between a slid mass and the ground surface, for a dry broken rock mass which moves down in a straight path, a normal basal coefficient of friction of 32° is considered by Hsü (1975). Actually this angle varies a lot depending on the type of rock considered.

- Fahrböschung or apparent coefficient of friction, α or ϕ_{ap} (see Figure 2-3): the angle between the horizontal and the line connecting the crown of the head scarp with the most distal end at the toe of the deposit along the midstream path of the mass (Pudasaini and Hutter, 2007). The Fahrböschung has been considered by Heim (1932) as the angle of a straight energy line which expresses the rate of frictional dissipation of energy (Hsü, 1978).

- Energy line or Paushalgefälle (see Figure 2-3): the straight line connecting the centres of mass in the initial and end positions. It is called energy line since it counts

the drop of potential energy of the mass falling downslope due to the driving force of gravity (Pudasaini and Hutter, 2007).

- Travel angle of the centre of mass, ϕ_{CM} (see Figure 2-3): the angle of the energy line considered as the straight line connecting the centre of mass before and after failure.

- Excessive or exceeding travel distance, L_e: this concept is a peculiarity of this phenomenon and for this reason is also mentioned in the rock avalanche definition itself made by Hungr et al (2001) as reported in section 2.1.1. The term excessive derives from the fact that the mobility of rock avalanches has been compared to the one of a simple sled model (Heim, 1932), which assumes that all energy dissipation during motion is caused by friction. The travel angle of known rock avalanche events results to be much lower than the dry friction angle of soil or crushed rock. Even if it is the slope of the energy line which is taken into consideration the value still remains much lower than the friction angle (Hungr, 2002). Thus, more explicitly, the excessive travel distance, L_e, as called by Hsü (1975), is the difference between the travel distance of the considered event and the one of the same rock avalanche if it had hypothetically travelled dissipating energy only through normal dry broken rock friction at the base.

$$L_e = L - \frac{H}{\tan 32°} \qquad\qquad \text{[2-1]}$$

Some authors, e.g. Voight (1978) and Corominas (1996), argued about this definition since frictional parameters may be much less than 0.6 (tan32°). On the other hand they hardly assume values smaller than 0.45 and they never achieve the values registered for the Fahrböschung of some rock avalanche events (0.18). As a consequence the excessive travel distance actually exists but it should be necessary to take into account a different basal friction angle depending on the case studied.

- Size effect: this term is linked to the idea that the excessive travel distance is associated only with large volumes of more than $1 \times 10^6 \text{ m}^3$. Large masses seem to be displaced in a more economic manner than small ones (Erismann, 1979)

- Granular flow: "the collective motion of individual particles of granular material", where granular material refers to mixtures made up of discrete solid particles which are dispersed in a fluid or gas phase (Kern, 2000).

- Dilatancy: the change in volume that follows the shearing deformation in a granular body (Pudasaini and Hutter, 2007).

- Lubrication: the reduction of frictional resistance by introducing a further medium, called the lubricant, between the surfaces of two bodies displaced with respect to each other (Pudasaini and Hutter, 2007).

- Fluidisation: when the solid phase behaves like a fluid in a gas-solid or liquid-solid system (Pudasaini and Hutter, 2007).
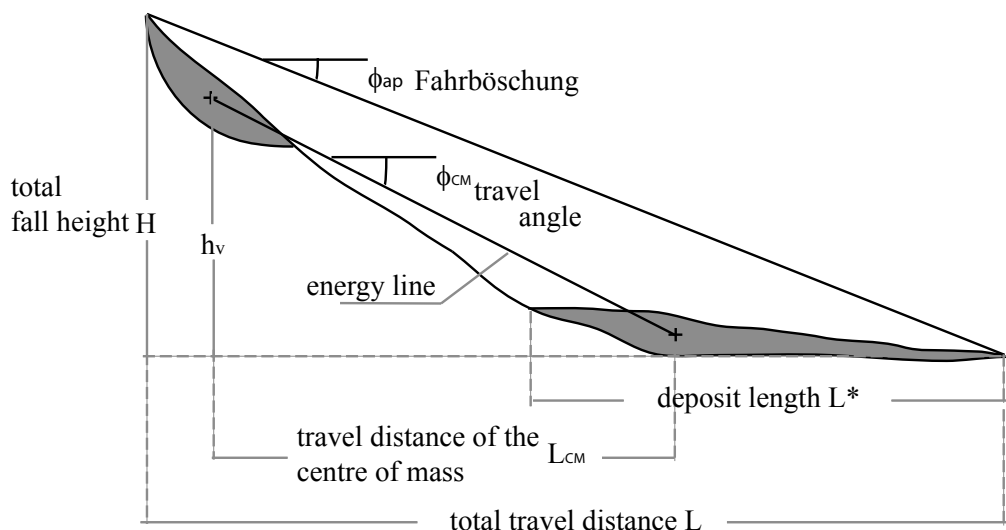
Figure 2-3 Terms and characteristics defining rock avalanche propagation

In order to better identify these characteristics and to give an idea of the dimensions and destructiveness of the phenomenon, some real events are illustrated in the next chapter giving more details to cases that will be the object of further considerations in the following.

Case histories

Rock avalanches are triggered by heavy earthquakes, abnormal precipitations, long term degradation of the rock material's strength, sudden temperature variation or sometimes by human actions e.g. the Vajont event in Italy originated as a consequence of the construction of a dam. They represent the most dangerous and lethal of all landslide phenomena.

According to Hungr (2002) it is possible to establish a certain frequency of these phenomena if occurrences are considered on an extensive mountainous area. Considering various inventories made in the past, the annual average frequency of a rock slope failure of more then $20*10^6$ m^3 is between 1/500 and 1/5000 per 10000 km^2, which reported to the area of European Alps means a return period of 70 to 700 years. Evans (2005) affirms that events of this kind occur in average every 2.7 years in the whole world and that in the Alps the frequency is one every century.

The largest rock avalanche of the last century is the one of Usoi where as a consequence of an earthquake of magnitude 9, 2.2 km^3 of rock has been triggered in the Pamir Mountains of Southeastern Tajikistan, blocking the valley and damming the lake Sarez. The most destructive rock avalanches actually took place in developing countries, where almost the 50% of the total deaths have been registered. One of the most lethal has been the Huascaran one in Peru in 1970, when two entire villages with 20000 inhabitants have been completely buried by the mass of debris (Evans et al, 2006).

In Table 2-2 are listed the principle characteristics of the cited events and of the Randa and the Six des Eaux Froides cases which will be useful in the following. Information are mainly taken from Voight and Pariseau (1978), Li (1983), Eisbacher and Clague (1984), Erismann and Abele (2001) and Evans (2005).

The Six des Eaux Froides rock avalanche (see Figure 2-4a) took place in 1946 in the Valais Canton in Switzerland. 5.8×10^6 m^3 of rock mass failed after four successive earthquake tremors of magnitude from 4.2 to 6.1, forming a deposit extended over 2 km length and 400 m width, quite similar to the one of a debris flow (Crealp, 1999). The presence of ridges and steep fronts of the final deposit put in evidence a rapid stop of the mass (Hsü, 1975 and Shreve, 1968). The site has been visited during the present research, in the framework of the INTERREG Rockslidetec project.

The Randa event took place in the Matter Valley in the southwestern Swiss Alps, involving the progressive failure of 30×10^6 m^3 of massive crystalline rock (Eberhardt et al. 2004). It is the result of two main events which took place the 18th of April and the 9th of May 1991. The interest of both events is that they occur over several hours, as a continuing rockfall (Schindler et al, 1993). It is the largest rock avalanche happened in Switzerland since the Goldau event in 1806. It has a characteristic steep conical deposit (see Figure 2-4b); the

cause of this peculiar morphology will be better analysed in section 3.4.3 where this event will be taken as a working example.

Event	Country	Year	Volume [$10^6 m^3$]	Fatalities	Fahrböschung
Flims	Switzerland	Prehistoric	10000		8
Köfels	Austria	Prehistoric	2300		10
Goldau	Switzerland	1806	35	457	12
Elm	Switzerland	1881	10	115	16
Frank	Canada	1903	36.5	70	14
Usoi	Tajikistan	1911	2000		
Six des Eaux Froides	Switzerland	1946	5.8		
Khait	Tajikistan	1949	75	12000	
Pandemonium Creek	Canada	1959	6.7		14
Vajont	Italy	1963	270	2000	19
Huascarán	Peru	1970	75	20000	14
Valpola	Italy	1987	34	27	
Randa	Switzerland	1991	20		

Table 2-2 Rock avalanches case histories
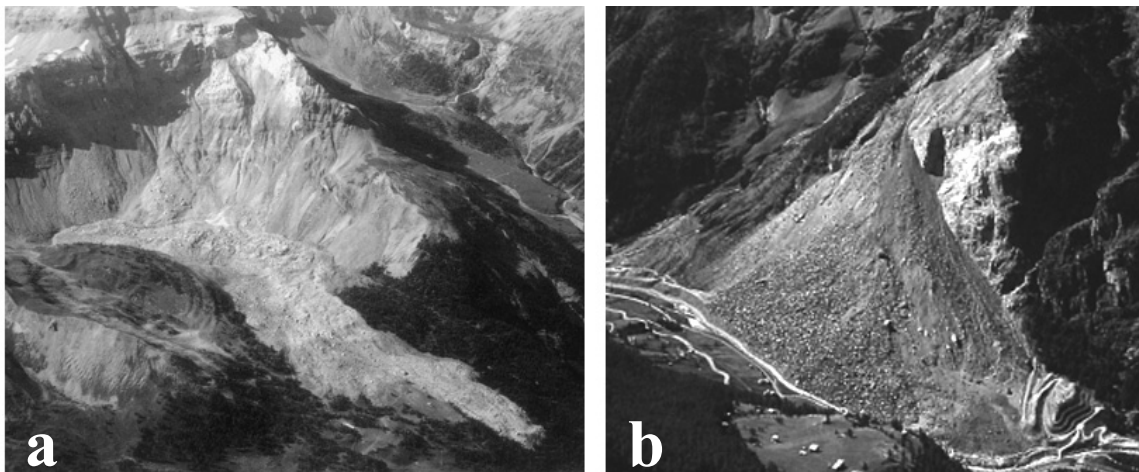
Figure 2-4 a) The Six des Eaux Froides deposit, Switzerland, courtesy of CREALP; b) The Randa deposit, Switzerland, source: Alpes du CAS, No. 6, 1998

Risk assessment

As aforementioned, the great energy developed by rock avalanches turns them into a difficult risk to assess. The only suitable way to prevent losses would be to design maps of the area affected by these phenomena as a tool for stakeholders of territorial management. According to the revision of nomenclature of Varnes (1978) made by Einstein (1988 and 1997), the definition of risk maps passes through several steps. First the *danger* must be identified geometrically and mechanically. This implies the recognition of instable volumes, their location and the type of failure mechanisms involved, but it doesn't include any forecasting. Afterwards the *hazard* (H_a) is defined as the probability of the danger to occur within a given period of time and the risk as the hazard multiplied by the potential worth of

loss, where loss can involve loss of life and injuries, capital loss, indirect risk and non-monetary environmental effects. Varnes (1984) defines *vulnerability* (V_u) as a number from 0 to 1 which expresses the degree of loss suffered by a given element, e.g. a house, in a set of *elements at risks* (E_r). Consequently the *total risk* (R_t) is given by the following formulation:

$$R_t = (H_a \times V_u) \times E_r$$ [2-2]

Derived from these definitions, danger maps, called also inventories, illustrate existing or potential slope instabilities, in hazard maps this is combined with the probability of occurrence and finally in risk maps the vulnerability of the area considered is added to the whole information. Hazard and risk maps constitute the base for decision making. In the case of rock avalanches, since technical countermeasures are sometimes so expensive to be generally unrealistic, the end product of mapping becomes zoning maps, which establish areas with limited construction permission. On the other hand the fact that the "return period" of a rock avalanche can be of more than 500 years makes the concept of risk itself to be hardly accepted by stakeholders and inhabitants of the exposed areas. For this reason it becomes of the greatest importance to increase the accuracy of identification of unstable volumes and to forecast the propagation of these destructive phenomena.

Once the unstable volumes and the possible scenarios of propagation are identified with accuracy, monitoring of the interested area and alert systems is one of the best tools to prevent fatalities as in the case of the Randa event, where monitoring systems have prevented life losses for one of the largest event registered in Switzerland in the last century (Bonnard et al, 1995).

One of the main concern is that most of the largest, most destructive and fatal rock avalanche events took and still take place in developing country. In these areas, the increase of squatter human settlements in regions potentially affected by several dangers and the lack of tools and funds to be used in forecasting of hazards, make the risk really high and difficult to be evaluated. The United Nation International Strategy for Disaster Reduction ISDR (see http://www.unisdr.org), aims at building disaster resilient communities by promoting increased awareness of the importance of disaster reduction as an integral component of sustainable development, with the goal of reducing human, social, economic and environmental losses due to natural hazards and related technological and

environmental disasters. The ISDR has as one of its four main objectives to improve scientific knowledge about disaster reduction: the more it is known about the causes and consequences of natural hazards and technological and environmental disasters on societies, the more it will be possible to be better prepared to reduce risks. Improvements in this sense for landslide hazards have been done by risk rating systems that propose a not expensive and useful tool to assess risk, e.g. the system developed by Saldivar-Sali and Einstein (2007) which is based on relatively simple characteristics, easily assessed in the field or generally easy to be recovered from historical records. In this framework, for the specific case of the complex and rare rock avalanche phenomena, simple empirical models for propagation forecasting are the most efficient from a cost-benefit point of view; if sufficiently reliable, they don't require complicated computations and expensive codes. As mentioned in the introduction the present study attempts to improve the understanding of the main mechanisms involved in rock avalanches and of the causes of their excessive mobility, to test the reliability of existing models and to propose new empirical formulations based on a well designed and extensive experimental campaign. Therefore this research could play an important role in the simplification and improvement of rock avalanche risk assessment.

2.2. Existing theories about rock avalanche excessive mobility

There are many theories which suggest different explanations for the rock avalanche excessive travel distance. Hungr (1990b and 2002), Shaller and Smith-Shaller (1996), Davies et al (1999) and Legros (2002) have attempted to summarize all these hypotheses and have mainly identified the following ones:

- Kent (1966) proposed that entrapped and compressed *air* could *fluidise* landslide. He based this hypothesis on the presence for some real cases of peculiar features such as the high degree of fluidity along with a remarkably high speed of movement and air blasts.

- Shreve (1968) suggested that a cushion of trapped *air* is formed at the base of the mass in motion and *lubricates* the rock avalanche, supporting it rather than fluidising it. This would lead the coarsest particles to fall to the base and the fine ones to be transported at the top (normal grading).

- Goguel (1978) supposed a *fluidisation* caused by the *steam* generated by vaporization of ground water that produces pore pressure in excess and thus reduces friction.

- Voight et al (1983) proposed for specific volcanic landslides a *fluidisation* by *volcanic gases.*

- Hsü (1975) supposed a *fluidisation* of the coarser *particles* operated by the layer of the *fine* ones coming from dispersion of rock dust.

- Heim (1882), supported afterwards by Abele (1974, 1994), Sassa (1988), Hungr (1990, 2002), Voight and Sousa (1994) and Legros (2002, 2006), suggested that the *water-saturated base*, once *liquefied* under the weight of debris, it is entrained along the path by the mass flowing and could function as a lubricant for the rock avalanche, behaving consequently as a debris flow.

- Melosh (1979) suggested a *loosening* caused by high-frequency *acoustic* vibrations due to the rapid shear of the granular material. "Sufficiently strong acoustic waves can momentarily relieve the static overburden pressure in limited regions of the rock mass, thus allowing sliding to occur in the unloaded region. If this happens frequently enough, flow of the entire rock mass results." This vibrational energy is generated externally by the boundary conditions of the movement.

- Several authors such as Heim (1932), Scheiddeger (1973), Davies (1982), Campbell (1989) and others, mentioned *mechanical fluidisation* as a possible explanation of rock avalanches high mobility. This should be due to the rapid shear of the granular material, assuming that "the bulk of material rides on a thin layer of highly agitated particles at low concentration" (Campbell, 1989). They suppose that the mechanical character of shearing changes at very high strain rates, that dilation occurs and consequently the contacts between the grains change from continuous sliding to intermittent collisions (Hungr, 1990). This would cause a decrease in the dynamic friction coefficient.

- Erismann (1979) proposed that the rock could *melt* by the *heat* generated from friction between stationary and moved material. When the event takes place in calcareous rocks, which do not melt when heated, he proposed a fluidization by

escaping of CO_2 gas produced by heat dissociation of limestone. Erismann pointed out also some interesting features of rock avalanches: i) the coherence problem, i.e. the displaced mass, although sometimes disintegrated into small fragments, shows a surprising congruence of its sequential order before and after the event; ii) the flow problem, i.e. in spite of this coherence the movement is characterized by a flowing behaviour; iii) the size effect problem as mentioned in section 2.1.1.

- Okura et al (2000) stated that the frequency of *collisions*, which increases with the number of blocks, could be a cause of longer total runout since it induces a higher acceleration in the front blocks. The fact that collisions could lead to longer runouts is also demonstrated by a simple model illustrated by Legros (2002). He considers two sliding blocks, in a first case held together and in a second case separated and allowed to fall one after the other. In both cases the centre of mass travels the same distance whereas the total runout is longer for the disconnected blocks where they collide with each other and one pushes the other one forward.

- Davies and McSaveney (1999) suggested that long runouts are due to the spreading of a coherent mass, which centre travels with a normal sliding friction law.

- Davies et al (1999) suggested afterwards that the excessive mobility is induced by *fragmentation* of the flowing mass. Failing as a coherent mass, the rock avalanche continuously collapses into smaller and smaller fragments. This process generates very high velocities in all directions and during runout this is translated to an isotropic dispersive stress throughout the moving mass, stopping the rear part of the mass and reducing the deceleration of the front part.

- Van Gassen and Cruden (1989) and also earlier Heim (1932) identified as a possible cause of the exceeding travel distance of large rock avalanches the *transfer of momentum* between the rear and the front part of the mass flowing. The rear particles enter the accumulation zone and collide with those slowing down ahead. Consequently the front and the rear parts interact through momentum transfer that induces propulsion of the front particles and deceleration of the rear ones as aforementioned for the model of the two blocks proposed by Legros (2002). These latter ones come to a stop reducing the mass of the moving material that is thus able to move further (see section 2.3).

Even if many of the mechanisms listed here could play an important role for some specific cases, it is difficult to decide which is the most significant one and how it controls the dynamics of the flow (Hungr, 1990). In addition, some of these hypotheses lack evidence in reality or in laboratory tests. As a consequence none of these mechanisms has been accepted as the main cause of rock avalanche excessive mobility (Legros, 2002) and several authors still argue about it, trying to find the most suitable explanation. Here the main arguments raised by Hungr (1990a, 1990b and 2002), Davies et al (1999) and Legros (2002 and 2006) are reported as representative.

These authors generally agree about the low possibility of some of the above mentioned theories:

- Air fluidization is found by all of them to be quite unrealistic, since the volume of air that the rock mass should incorporate to be fluidised has to be several times its own volume. In addition if a great quantity of air would be entrapped in the mass there should be the presence air bubbles or air jetting, which can be found only in volcanic rock avalanches.

- The theories based on gas pressure advanced by Shreve and Goguel are also considered quite unrealistic, as demonstrated by evidences of the inverse grading phenomenon in almost all the real events, and on the other hand the absence of great air jetting, craters, marginal fans etc. that should mark gas escape in rock avalanches (Cruden and Hungr, 1986).

- In the same way, the theory of mechanical fluidisation hasn't found evidence on several laboratory flume and ring shear tests where the internal friction coefficient has actually been found to have no systematic dependence on the shear strain rate even at high velocity of 5m/s (Hungr and Morgenstern, 1984a and b).

- The acoustic fluidisation theory is contradicted because, even if it has a sound theoretical and experimental basis at laboratory scale (Hungr, 1990b), there are no evidences in reality that the rock masses failed are able to produce high-frequency vibrations at sufficient intensity.

- Rock melting of Erismann was found as a peculiar phenomenon that could be present only in few rock avalanches such as the Köfels one where fused rocks (pumice) have been found in the deposit.

On the other hand the above-mentioned authors disagree for what concerns the transfer of momentum mechanism, suggested by Van Gassen and Cruden (1989), the fragmentation phenomenon, suggested by Davies et al (1999), and partly about the undrained lubrication theory.

- Hungr (2002) and Legros (2006) argument about the fact that rock fragmentation and the transfer of mechanical energy from the rear to the front of the rock avalanche, are energy consuming processes. Consequently they state that these mechanisms may partly explain the spreading of rock avalanches, but not the long runout of all of them, unless a source of additional energy is found, which doesn't seem the case in reality. In addition Erilchson (1991) has proved that the equations developed by Van gassen and Cruden (see section 2.3.2 and equations from 2-10 to 2-12) are wrong.

- In addition Legros (2002) observed that Davies and McSaveney (1999) theory on the spreading of a coherent mass is not supported by experimental evidence and is valid only for some real events. Studying a few well documented real cases he pointed out that the ratio of the height against the travelled distance measured from the centre of mass is also lower than the normal coefficient of friction of rocks.

- On the other hand Davies et al (1999) admit that the self-undrained loading has played a certain role in some cases, but they added that this concept is not sufficient to explain in general the long runout of rock avalanches, since it implies the permanent presence of extensive alluvial deposits in which undrained loading should occur, which is not actually always the case.

In support to their affirmations Davies et al (1999) make an interesting analysis of the runout process and according to it they classify the different mechanisms proposed in literature. They identify two processes in the propagation of a rock mass: translation mainly guided by basal friction and on the other hand deformation, affected by internal friction. The final deposit shape and distribution result from the total motion, which is a combination of

the two processes. As a consequence Davies et al (1999) divide the different mechanisms proposed in literature in three main categories: ones that imply a reduction of the basal friction; ones that imply a reduction of the internal friction and ones that don't belong to any of these first two. They have considered as belonging to the first category phenomena such lubrication by a basal air layer and mechanical fluidization; nonetheless mechanisms such air, water and acoustic fluidizations are classified in the second category as they induce a decrease of the internal friction angle. The transfer of momentum of Van Gassen and Cruden (1989) is considered by Davies et al as a rather different mechanism (third category) and even taken as a start to build up their theory of fragmentation, considering this process as the source of additional energy requested by other authors (see chapter 2.3). Nevertheless they questioned the fact that it is a general phenomenon that should take place at all scale and not only with large volumes. For this reason they considered as a counter proof of this theory the fact that tests carried out by Davies and McSaveney (1999) at small scale didn't provide any evidence of it. As a consequence they added a term derived from fragmentation, and they consider it as scale dependent.

Some of the mechanisms here introduced have been translated into mechanical models and they will be reported together with others in the following section.

2.3. Propagation studies approach

The main problems to be solved in rock avalanche modelling are the forecast of their travel path and distance, to estimate the velocity and the deposit profiles.

Models suggested in literature are obtained following different methods:

- Empirical: based on a statistical analysis of historical data

- Analytical and numerical: based on a mathematical description of the mechanisms involved in the phenomena

- Experimental: based on laboratory experiment results

Here follows an analysis of the different models belonging to theses classes, focusing on the empirical and experimental ones, which most concern the present study.

2.3.1. Empirical approach

In this category it is possible to distinguish further between geomorphologic and geometrical assessments (Hungr et al, 2005). The first one is a more qualitative method; it is based on the determination of the eventual rock avalanche path and deposit area, basing the analysis on past events in similar conditions and on the present topography. The first models attempting to quantitatively forecast rock avalanche propagation are based on the geometrical method. First Heim (1932), analysing several historical events, noticed the dependence of the travel distance upon the fall height, the topography and the volume of the rockslide. He defined the Fahrböschung, the travel distance and the fall height as mentioned in chapter 2.1.1 and illustrated in Figure 2-3 and, based on a simple sled model, he proposed that the travel distance (L) is simply obtained by:

$$L = \frac{H}{\tan(\alpha)}$$
[2-3]

where H and α are respectively the fall height and the Fahrböschung (see Figure 2.3).

The attribution of a travel angle remains a key problem of this model (Hungr et al, 2005). Inspired by this epoch-making work, several authors have attempted to find empirical expressions able to compute the Fahrböschung. Among others, Scheiddeger (1973), Li (1983) and Nicoletti and Sorriso-Valvo (1991) have proposed a relationship between the tangent of the Fahrböschung and the volume of the landslide by applying a linear regression on several historical data. Their equation has the following form:

$$\log_{10} f = a + b \cdot \log_{10} V$$
[2-4]

Where f is equal to H/L, a and b are constants and V is the volume expressed in m^3.

The accuracy of this equation depends significantly on the precision of the estimated geometrical characteristics, i.e. fall height and volume, which sometimes are really difficult to obtain. To ameliorate the model, Corominas (1996) has proposed a differentiation among different types of rock avalanches. In Table 2-3 the different coefficients proposed by the cited authors are summarized.

Authors	N	a	b	r	Comments
Scheiddeger (1973)	33	0.624	- 0.157	0.82	see Figure 2-5a
Li Tianchi (1983)	76	0.664	- 0.153	0.78	
Nicoletti and Sorriso-Valvo (1991)	40	- 0.527	- 0.085	0.37	volume expressed in 10^3 m^3
Corominas (1996)	204	- 0.047	- 0.085	0.79	all landslides
	47	0.210	- 0.109	0.87	rockfalls and rock avalanches
	16	0.231	- 0.091	0.91	obstructed
	6	1.078	- 0.233	0.92	deflected
	14	0.167	- 0.119	0.96	unobstructed

Table 2-3 Parameters of the regression equation of f versus rock avalanche volume (V) as described in equation [2-4], N is the number of events used for the analysis and r is the correlation coefficient. Inspired from Corominas (1996) and Hungr et al (2005)

Hungr (1990) considered the travel angle as not representative of the excessive mobility of large landslides. Corominas (1996) as well considered the Fahrböschung as an inefficient characteristic to denote excessive mobility of rock avalanche since there is a decreasing of the Fahrböschung also for small landslides. For this reason he suggested using the index L_r to express the degree of mobility of large landslides based on the Hsü (1975) concept of the excessive travel distance:

$$L_r = \frac{L_e}{H/\tan(32°)}$$

[2-5]

where L_e is defined by Hsü (1975) with the equation [2.1].

Also Nicoletti and Sorriso-Valvo (1991), proposed the use of the excessive travel distance, describing the ratio of L_e against the total travel distance (L), L_e/L, as a portion of H varying from 0.5H and 0.8H.

Li Tianchi (1983) proposed two relationships, see equations [2-6] similar to [2-4] based on linear regression between both the area (S) and the length of the deposit (L*, see Figure 2-3) and the interested volume (*V*) in order to predict, not only the traveled distance, but also the lateral and longitudinal spreading of the mass.

$$\log_{10} S = a + b \cdot \log_{10} V$$
$$\log_{10} L* = a + b \cdot \log_{10} V$$

[2-6]

Davies (1982) as well found a good fit between the length of the final deposit (L*) and the cubic root of the volume (see Figure 2-5b), underlining a certain homogeneity of the shape of the deposits.

Empirical methods are really useful in preliminary assessment and easy to apply. On the other hand, their statistical scatter is very large and they don't provide useful kinematics parameters. It is possible to establish only an envelope of values in between which the prediction could be situated. Therefore, if they are not sufficiently reliable, their use for risk management could be either dangerous or really expensive if too conservative. For this reason the necessity was born to improve those empirical models by considering also the physical rules involved in the phenomena, as illustrated in the following section.
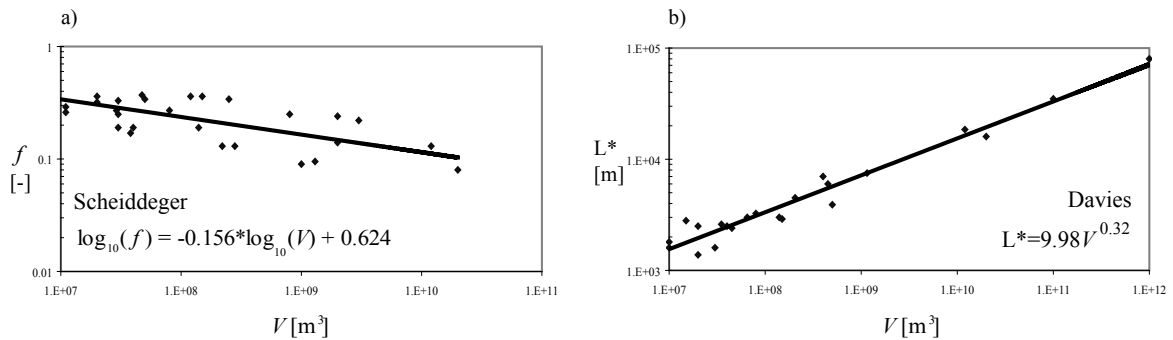
Figure 2-5 Empirical regressions of: a) Scheiddeger (1973), x axis: volume V [m^3], y-axis: f=H/L; b) Davies (1982,) x axis: volume V [m^3], y-axis: length of the deposit L[m]*

2.3.2. Analytical and numerical approaches

It is possible to distinguish three main groups of models in this category depending on how the mass is represented: the lumped mass model (Figure 2-6a), the discrete elements model (Figure 2-6b), and the fluid mechanics model (Figure 2-6c). The models of Heim (1932), Hsü (1975), Davies (1982) and Van Gassen and Cruden (1989), based on frictional law and energy dissipation, belong to the first category. Whereas the ones of Bagnold (1954) and Drake (1990, 1991) which take into account the interaction between particles, belong to the second one. The fluid mechanics models are more frequently used for debris flows, mudflows, lava and snow avalanches as in the case of the models of Hutter and Savage (1988), Hungr (1995), Pouliquen (1999), Denlinger and Iverson (2001), Pouliquen and Forterre (2002) and Ancey (2006). This approach is sometimes extended to dry granular flows, rockslides and rock avalanches (Mangeney-Castelnau et al, 2003 and 2005; Naaim et al, 1997; Pitman et al, 2003) when these are considered to be dense one-phase flows. In this section the most significant models are described according mainly to the review made by Hungr et al (2005) and Pirulli (2005).
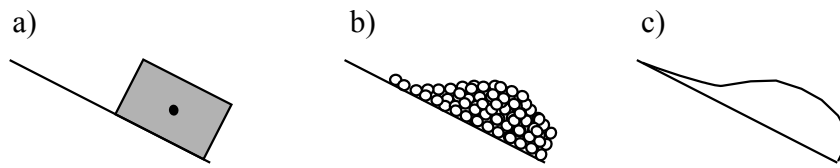
Figure 2-6 Schematic representation of rock avalanche analytical model approaches: a) lumped mass; b) discrete elements; c) fluid mechanics

Lumped mass

These models (called also sled or block models) represent the first attempt to describe the rock avalanche propagation (Heim, 1932). The flowing material is considered as a dimensionless point of mass M sliding along a path inclined of β, characterised by a constant friction angle φ (see Figure 2-7). "Internal deformation and its associated energy dissipation are neglected and the landslide is treated as a lumped mass" (Mcdougall, 2006). This is a rather simplistic representation of a rock avalanche. In addition in this way only the mobility of the centre of gravity is taken into account, neglecting lateral and longitudinal spreadings, which are of the greatest importance to design the area at risk. Nevertheless this model is useful to understand some mechanisms and the influence of various factors and rheological characteristics on the dynamic behaviour of rock avalanches. For this reason it is a representation often recalled in literature and it constitutes the base of most of the existing models. According to the work-energy theorem, the rate of change of kinetic energy and the gradient of the energy line change as follows:

$$d\left(\frac{Mv^2}{2}\right) = Mg\left[\sin\left(\beta\right) - \cos\left(\beta\right)\tan\left(\phi\right)\right]ds$$

$$\frac{dE}{Mg} = dz - d\left(\frac{v^2}{2g}\right) = -\tan\left(\phi\right)dx$$

[2-7]

Where M is the mass, *v* the velocity, E the total energy, β the slope angle and φ the friction angle as described in Figure 2-7.

If the position of the mass at start is given, it is possible to determine velocity and position of the block at any given time by means of the relationship of the energy loss. Starting from these notions, several authors have proposed different energy loss relationships, according to which parameters and mechanisms they believe important in the description of rock

avalanches propagation. They thus included basal resistance, momentum transfer, pore pressure, etc (McDougall, 2006).
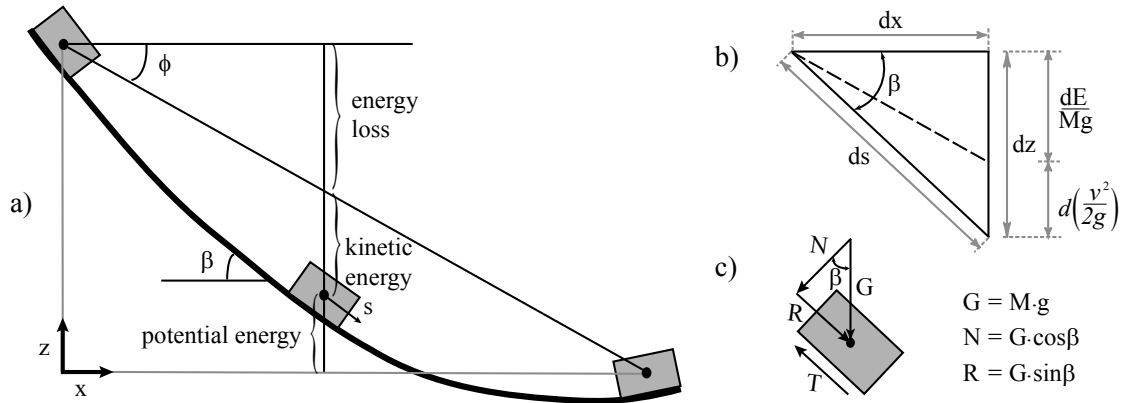
Figure 2-7 Derivation of the sliding block dynamic equation. a) Path profile; b) local slope geometry; c) force diagram. Adapted from Hungr et al (2005)

Körner (1976) noticed that the energy line described by equation [2.7] implies unrealistic high velocities of rock avalanche real events. For this reason he introduced a turbulent term, first suggested by Voellmy (1955) for snow avalanches, and, assuming the height of the block, h, constant, he obtained the following equation:

$$d\left(\frac{Mv^2}{2}\right) = Mg\left[\sin(\beta) - \cos(\beta)\tan(\phi) - g\frac{v^2}{gh\xi}\right]ds$$

$$\frac{dE}{Mg} = dz - d\left(\frac{v^2}{2g}\right) = \left[-\tan(\phi) - \frac{v^2}{h\xi}\right]dx$$

[2-8]

Where ξ [L/T^2] is the turbulent coefficient.

The energy line resulting form this solution is concave (see Figure 2-8), which means that velocities are lower and thus more realistic.

Another attempt to improve the sled model has been made by Hutchinson (1986), which proposed the presence of excess pore-fluid pressure, which is formed during failure and that, as the mass flows, dissipates through consolidation. In the case of the presence of a pore fluid pressure r_u, the friction angle assumes the following form, according to the principle of effective stress:

$$\tan\phi_b = (1 - r_u)\tan\phi$$

[2-9]

Therefore, in the case of the sliding consolidation model of Hutchinson, the energy line is convex (see Figure 2-8) and the velocities are even higher and consequently largely overestimated. Sassa (1988) with his "improved sled model" introduces as well the influence of pore-pressure. In his model, pore pressure changes during the flow due to the undrained loading of a saturated soil layer at the base of the rock avalanche. Consequently it is necessary to choose the appropriate set of r_u characterising the different parts of the path in order to have a good estimation of the velocities.
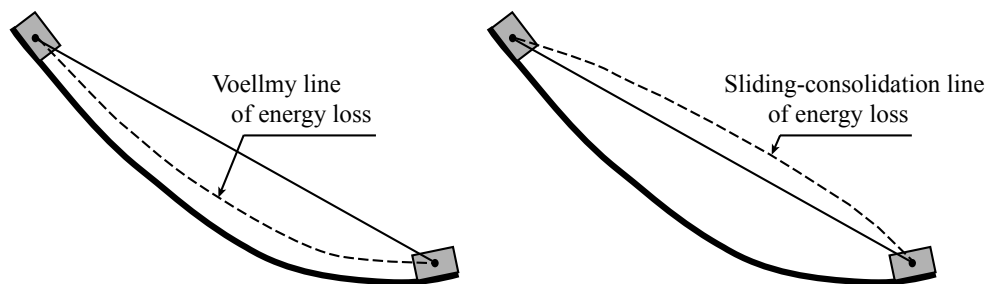
Figure 2-8 Energy lines of Voellmy and sliding-consolidation model (dashed lines) compared to the frictional one (straight bolded black line)

Another attempt to improve the simple sliding block model and to introduce other mechanisms in the rock avalanche behaviour has been made by Van Gassen and Cruden (1989). As already seen in section 2.2, they identified the reason of the significantly elongated shape of rock avalanches in a process of gradual deposition of the debris in the rear part of the mass while transferring its momentum to the forward part (Corominas, 1996). They based their formulation on the second Newton's law of motion for a mass (M) moving along an inclined path:

$$\frac{M}{2}\frac{d\left(v^2\right)}{ds}+v^2\frac{dM}{ds}=Mg\sin\beta-T \qquad\text{[2-10]}$$

Where v is the velocity, β the slope angle and T the resistance forces as illustrated on Figure 2-7. For a constant mass M, entering the accumulation zone with a velocity v_0 and a friction angle ϕ, the distance travelled by the centre of mass (L_{CM}, see Figure 2-3) is expressed by the following equation:

$$L_{CM}=-\frac{v_0^2}{2g\left(\sin\beta-\tan\phi\cos\beta\right)} \qquad\text{[2-11]}$$

If the mass instead of being constant is considered as exponentially decreasing along the path, equation [2-11] becomes:

$$L_{CM} = -1.93 \frac{v_0^2}{2g(\sin\beta - \tan\phi\cos\beta)}$$
[2-12]

This is more or less two times the distance travelled if the mass is supposed to be constant.

This theory has been strongly criticized by Hungr (1990a) who affirmed that to obtain equation [2-10] there should be an engine producing a thrust that propels the sliding mass along the runout surface as it happens for a rocket engine. In addition the equations used by Van Gassen and Cruden and developed by Cannon and Savage (1988) have been proved to be wrong by Erlichson (1991).

According to Hungr (2002) sled block models are not adequate to describe rock avalanche dynamics and they are a rather simplistic representation of the phenomenon. In addition in this way only the mobility of the centre of gravity is taken into account, neglecting lateral and longitudinal spreading which are of the greatest importance to design areas at risk.

Discrete elements

Discrete element method (DEM) assumes that the mass consists of separate, discrete particles and that the moving mass is the result of the interaction between the particles. This method is based on discontinuum mechanics, introduced first by Goodman et al (1968) in geomechanics (Pirulli,2005).

DEM models can be seen as a multiple sliding blocks model, where each block (particle) independently moves and interacts with the surface and with the other particles. By applying individual constitutive properties, contact laws, velocities, displacements and forces, the dynamic of each particle can be studied over a selected period of time (Pirulli, 2005). According to Cundall (1988), any particle may interact with any other particle and there are no limits on particle displacements and rotations. In the case of rock avalanche modelling, particles interact between them through friction and the equations of the conservation of mass, of energy and of momentum are used.

Particles are often represented by disc (2D) or sphere (3D). These shapes lead to simpler contact patterns and smaller computation times, but they don't represent the fragmented

blocky material constituting rock avalanche masses. Campbell and al. (1995) carried out a study on rock avalanche behaviour performing computer simulations of up to 1'000'000 two-dimensional discs. Simulations reproduced certain rock avalanche features, e.g. the preservation of the initial strata and the low apparent coefficient of friction related to larger volume; nevertheless the computations have lasted up to more than one year and as pointed out by Legros (2002) and Pirulli (2005) the disc shape of the particles produce low shear resistance and induce rolling, which, even if leading to long runouts, it is not a realistic representation of rock avalanche behaviour.

One of the most known code using this approach is the PFC developed by Itasca and used by several authors to simulate rock avalanches. EPAN3D, a DEM numerical code developed at the CETE Méditerranée (Aix en Provence, France), has been used to simulate a test carried out in the framework of the present work and will be better explained in section 5.2.

The long computing time, the limited number of particles that can be implemented and the large number of parameters that has to be determined, make this approach still to be developed to become a practical predicting tool.

Fluid mechanics

As an attempt to avoid these problems, fluid mechanics approach treats the moving mass as a homogeneous continuum (see Figure 2-6c), neglecting small scale interactions between the particles and concentrating on large scale field effects. The simplest form of dynamic analysis of rock avalanches is based on the St.Venant equations of unsteady flow. It is assumed that both depth and length of the flowing mass are large if compared with the characteristic dimension of the particles involved in the movement. Under this assumption, it becomes possible to replace the real moving mixture of solid and fluid phases by an "equivalent" fluid, whose rheological properties have to approximate the behaviour of the real mixture (Hungr, 1995). By this way, the dynamic behaviour of the flowing mass can be described by the mass and momentum conservation laws. Further, assuming that the vertical dimension of the flow is much smaller than its characteristic length, it is possible to use the so-called depth-averaged continuum flow models.

According to Pirulli (2005) the first to develop such models to be applied for granular flows were Savage and Hutter (1989). The key elements of their work are the derivation and

scaling of depth-average momentum and mass conservation equations, the formulation of shallow flow equations using Coulomb law for basal shear resistance and an earth pressure equation for the influence of Coulomb friction on longitudinal normal stresses, the development of numerical solution of the one-dimensional shallow flow equations using a Lagrangian finite scheme and the use of extensive experimental campaigns to validate the model.

Starting from this approach Hungr (1995) developed a model where different rheologies can be chosen and varied along the slide path or within the slide mass. In addition it is possible to take into account the rigidity and the coherence of the sliding mass and the effects of lateral confinement (Pirulli, 2005). Hungr and his co-workers translated this model into two numerical codes called DAN (Hungr, 1995) and DAN-3D (McDougall and Hungr, 2004) and performed an extensive back-analysis of a number of real cases to validate it.

Two other codes based on the continuum mechanics approach are interesting for the present work: RASH3D developed by Pirulli and Scavia (Pirulli, 2005) of Politecnico di Torino (Turin, Italy) and the model developed by Mohammed Naaim of Cemagref (Grenoble, France). As mentioned for EPAN3D in previous section, both models have been used to simulate a test carried out in the framework of the present work and will be better explained in section 5.2.

Flow-like models are able to describe the evolving geometry of a finite mass of a granular material and the associated velocity distribution; nonetheless results of the simulations depend on the value assigned to the constitutive parameters of the assumed rheology (Pirulli, 2005) to which sometimes the derived numerical codes are sensible. Therefore an important work of validation it is necessary in order to obtain a good accuracy in results.

2.3.3. Experimental approach

Due to the rareness of rock avalanches events, the number of well documented real cases is limited and data like unstable volume and coefficient of friction are difficult to recover with accuracy. Therefore, several authors have resorted to laboratory tests to validate and demonstrate the applicability of the afore-mentioned models. In addition other authors have carried out experimental campaigns to better understand the propagation mechanisms and to identify parameters influencing deposit characteristics, proposing sometimes new interpretations of the phenomena and new relationships between the parameters of interest

translated into empirical formulations. Despite the difficulty in matching the scaling laws, the use of a physical model enables studying the influence of each parameter of interest, by controlling and changing one at a time, with known and consistent experimental conditions. Therefore results can constitute a significant sample to fill up partly the limited amount of accurate field data.

Experiments usually reproduce idealized conditions and they can consist in ring shear tests, flume tests or three-dimensional granular flow tests, i.e. the flows are partially constrained or unconstrained. As mentioned in section 2.2 for the work of Hungr and Morgenstern (1984a) ring shear tests are typically used in this field to evaluate the behaviour of granular flow under high shear strain and at important velocity. Bagnold (1954) and Sassa (1988) also carried out such tests to measure the stresses developed in a sheared granular mass.

In the next sections follows a more detailed description of granular flow tests. These experiments represent the bases on which experiments and set-up of the present study have been designed and built up.

Flume tests

Flume tests consist in triggering nearly steady granular flows in inclined channels. Flume tests are mainly used to investigate the behaviour of two-dimensional granular flows. According to Drake (1991), although two-dimensional results are not directly applicable to three-dimensional granular flows, they are useful from a theoretical point of view since, when the effects of interstitial fluid are negligible, the experimental design preserves the essential physics of the interactions between particles in flows. Bagnold (1954), Hungr and Morgenstern (1984b), Drake (1990, 1991), Ancey et al (1997), Azanza et al (1997) and Pouliquen (1999) are among the authors who have resorted to this kind of experiments. In particular Drake (1990, 1991), studying the behaviour of plastic spheres of 6 mm diameter down a narrow channel, could identify two main regions in the flow (see Figure 2-9):

- – Frictional region: where momentum transfer is predominantly affected by persistent frictional interactions. This region consists of a quasi-static zone just over the bed and an overlying block-gliding zone, in which coherent blocks of grains move parallel to the bed

- Collisional region: where momentum transfer is predominantly affected by collisions. This region consists of three zones: a lower grain-layer-gliding zone, in which grains slide one over another; a middle chaotic zone, in which grain motions are highly random; an overlying zone, even more chaotic in which grains have gas-like behaviour and trace long curved paths.
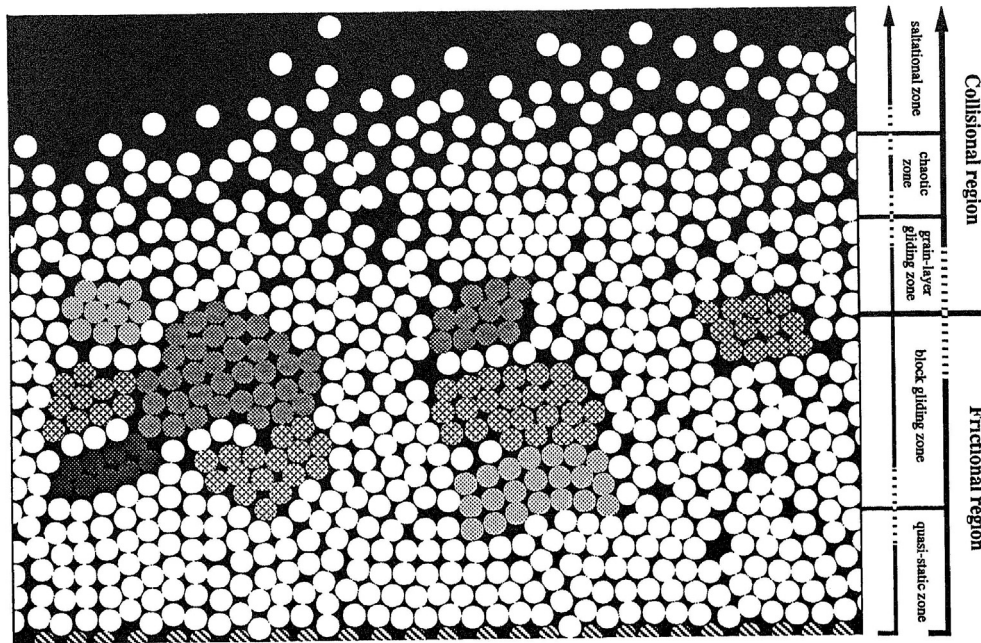
Figure 2-9 Different region in a granular flow, Drake (1990)

He also arrived to the important conclusion that density decreases linearly with the distance from the bed of the flow and that the continuum hypotheses (see section 2.3.2) are not verified only in a small zone near boundaries where large variations of velocities take place.

Three-dimensional granular flow

Even if flume tests are useful to understand granular flow behaviour, rock avalanches are unsteady three-dimensional phenomena. As a consequence, the best way to understand mechanisms involved is to carry out tests consisting in triggering tri-dimensional granular flows on designed topography.

In this framework, Hutter and his co-workers have carried out over several years an extensive experimental campaign with different and various experimental set-ups (it is possible to find a detailed overview of these tests in the book "Avalanche dynamics" of Pudasaini and Hutter, 2007) and that can be divided in three main classes:

1. Granular flows in narrow chute, e.g. Hutter and Koch (1991) and Greve and Hutter (1993).

2. Three-dimensional granular flows down an inclined plane without side confinement e.g. Koch et al. (1994) and Greve et al (1994).

3. Granular flow along irregular three-dimensional terrain: on curved and twisted channel (see Figure 2-10) or on inclined plane with obstacles on the pathway, e.g. Gray et al. (1999) and Pudasaini et al (2005).

The second class is the one that most interests the present study. Hutter and his co-workers have performed tests mainly consisting in unconfined or slightly confined granular flow on an inclined plane in the upper part, a cylindrically curved transition zone and a horizontal accumulation part (see Koch et al., 1994 and Greve et al, 1994). Some tests have been performed with a weakly parabolic channel in the upper part (see Gray et al, 1999 and Wieland et al, 1999). Nonetheless, even if of great interest for the design of the experimental set-up, these tests have been carried out mainly to demonstrate the efficiency and applicability of the model of Hutter and Savage (1988) and to verify its equations. As a consequence they are often taken as a reference in a more analytical and numerical framework rather than empirical and phenomenological as in the present case.
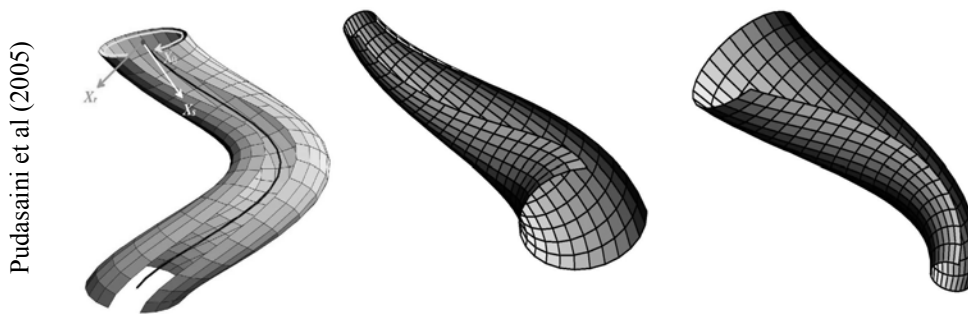
Figure 2-10 Example of the geometry of some tests carried out by Hutter and his co-workers (Pudasaini et al, 2005)

The work of Hutter and his co-workers has inspired several authors such as Bouzid (1999), Davies and Mcsaveney (1999), Denlinger and Iverson (2001) and Iverson et al (2004), McDougall and Hungr (2004), Patra et al (2005), etc. Most of these authors have also carried out experiments mainly to validate the model they developed. Among these, tests of Denlinger and Iverson are interesting for the device used to measure the thickness of the

flow (see Figure 2-11). They placed a series of bars above the channel and with a light they projected the shadow of the bars on the flow. The deformation of the shadows from straightness is related to the mass shape. A method based on a similar principle has been used in the present study.
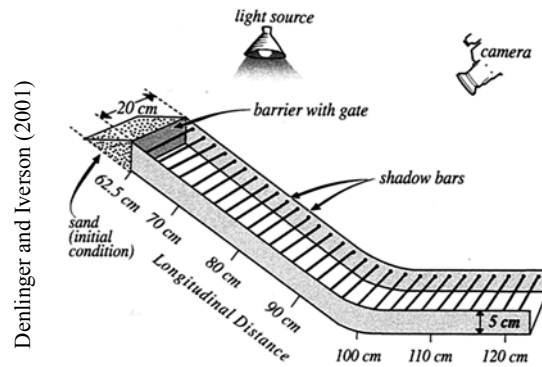
Figure 2-11 Experimental set-up of tests carried out by Denlinger and Iverson (2001)

Interesting for the present work are also the experiments performed by McDougall and Hungr (2004). These tests were performed to demonstrate the ability to simulate curved flow of the continuum model the geotechnical group of University of British Columbia has developed (McDougall, 2006): the material flowed from the chute onto a 20° approach slope and was then deflected by an inclined plane oriented obliquely to the approach direction (see Figure 2-12). In Chapter 5 experiments inspired from these deflection tests and carried out in the framework of the present work will be illustrated.

Figure 2-12 Experimental set-up of McDougall and Hungr (2004)

Among authors who performed granular flow experiments, Davies (1982) and Davies and McSaveney (1999, 2003) are among the few ones who have carried out tests to have a data set for developing empirical models and to understand the influence of parameters on the propagation at small scale. Of particular interest is the work of Davies and McSaveney (1999, 2003), who have studied the behaviour of small-scale dry granular avalanches which they compared to documented rock avalanche events. They performed tests that consisted in unconstrained dry granular flow (see Figure 2-13) of 0.1-1000 litres of sand on a plane inclined at 35° or 45° (see Table 2-4) and they analysed the length of the deposit, the travel distance and the Fahrböschung of the tests. Three real cases of unconstrained dry rock avalanches have been compared to laboratory tests: the South Ashbourton (New Zealand), with a slope at about 35° and which has a volume of less than one million cubic metres (300000 m^3); and the Elm (Switzerland) and the Frank slide (Canada) events with a slope of about 45° and which has larger volume (see Table 2-2). To carry out the analysis and to compare results to data coming form real events they defined some nondimensional variables: the normalised longitudinal extent of the deposit L*/h*, where L* (called normalised runout, R_h, by Davies and McSaveney) is the deposit length as defined in Figure 2-3 and h* is the cubic root of the volume; the normalized vertical fall height (h_v/h*), where h_v is the total height of the centre of mass before release as defined in Figure 2-3. The normalised length of the deposit has values "mainly within the range 1.5-3 for the laboratory data at both slopes, and is largely independent of fall height", see Figure 2-14. The South Ashburton value is not far form this range, on the other hand Elm and Frank events have much higher values of L*/h* between 5 and 7.

Figure 2-13 Image of a test carried out by Davies and McSaveney (1999)
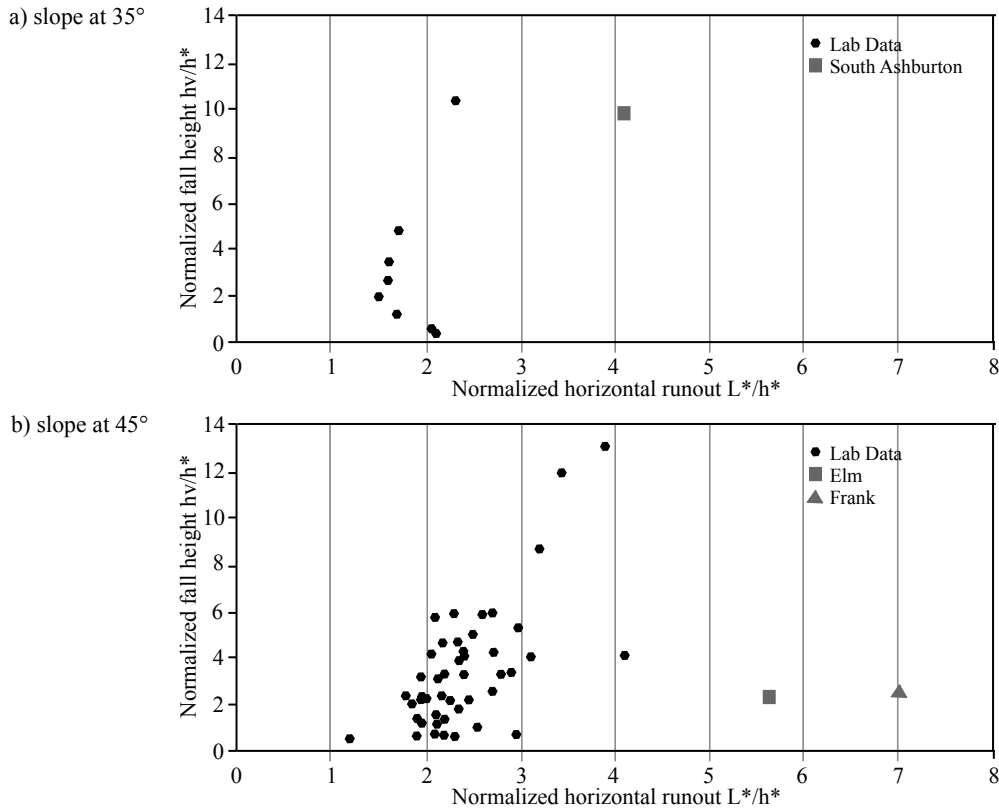
Figure 2-14 Davies and McSaveney (1999), plots of the normalised longitudinal length L*/h* against the normalised fall height h$_v$/h* for a) 35° and b) 45° slope

Therefore Davies and McSaveney conclude that "between volumes of about 10^5 m^3 and 10^7 m^3 the mechanism of deposit emplacement changes significantly from that seen in the laboratory". Afterwards, considering as well results of the empirical analysis performed by Davies (1982) and shown in Figure 2-5b, they defined two distinct empirical formulations for small scale and large scale events, reported in equation [2-13]. Davies and McSaveney (1999) suggest that this difference could be caused by some conditions that cannot be reproduced at laboratory scale such as rock fragmentation or the presence of saturated sub-strata and, as seen in section 2.2, to the spreading of a coherent mass.

$$L^* = 1.5 \div 3h^* \quad \text{at small scale}$$
$$L^* = 6 \div 10h^* \quad \text{at large scale}$$

[2-13]

Tests with blocks

Very few works have been found in literature that use blocks instead of gravel or sand. Moreover most of them, like the ones reported as representatives in Table 2-4 of Reik and Hesselmann (1976) and Rengers and Müller (1970), are not carried out with separated

elements but are small scale experiments of a jointed mass that is free to bend but not to disaggregate. The most interesting work that involves experiments with blocks is the one of Okura et al. (2000) who have performed tests with separated elements one on top of the other (see Figure 2-15). Perhaps due to the practical difficulty of performing these tests, no other record of this kind has been found in literature. They used a maximum of one thousand cubic blocks, each with 0.1 m side, that slide on a slope covered by granite slabs and inclined at 35°. These test conditions suggest that blocks would behave individually, rather like a rock fall than a rock avalanche. As already mentioned in section 2.2 with support of numerical simulations, they state that the frequency of collisions, which increases with the number of blocks, could be a cause of longer total runout since it induces a higher acceleration of the front blocks.

Figure 2-15 Experimental set-up of Okura et al (2000)

Scaling down

For the dimensional analysis of small-scale granular flows, two important works have been carried out. The one of Denlinger and Iverson (Denlinger and Iverson 2001; Iverson et al. 2004) and the one of Massey (1983) as reported by Davies and McSaveney (1999).

Among them Iverson and Denlinger (Iverson and Denlinger 2001, Denlinger and Iverson 2001, Iverson et al 2004), arrived at interesting conclusions concerning laboratory experiments by means of the assessment of dimensionless scaling parameters: Np the timescale ratio, NR the Reynolds number, c* the normalized intergranular cohesion and E* the normalised bulk stiffness. They state that large geophysical flows, where fluid effects are significant, can exhibit dynamics not evident at laboratory scale (especially miniature ones), where additionally there could be the presence of electrostatic phenomena which can bedevil results. On the other hand if fluid effects are negligible, which is one of the

hypotheses at the base of the present study, the model is simplified and the dynamics of the so defined "ideal granular avalanches" can be reproduced at small scale since it is controlled only by the geometry of the path and by the internal and the basal friction coefficients (Iverson and Denlinger, 2001). Nonetheless the scale must be large enough to satisfy the continuum assumption and to minimize the effects of microscopic forces.

Davies and McSaveney (1999) report more or less the same conclusions. They affirm that, with the exception of certain phenomena like rock fragmentation, or the presence of some environmental conditions as saturated substrate, or ground shaking due to the impact of the avalanche on the ground at the foot of the fall slope, granular avalanches at small scale can realistically reproduce the major features of large-scale rock avalanches. This happens only when laboratory tests respect three main conditions which regulate dynamic similitude: (1) there is consistent geometric similarity between small and large scale, including grain size and shape and surface roughness; (2) grain and air densities are the same at both scales; and (3) the drag coefficient of grains in the ambient gaseous medium is the same in laboratory tests and real events. Condition 1 is not satisfied when the grains of the material used are extremely small, as intergranular cohesive and electrostatic forces make grains interact differently than in field situation (Iverson et al, 2004). This is usually avoided by truncating the lower end of the grain-size distribution in the small-sizes. Condition 2 is usually respected, when tests are carried out in air at atmospheric pressure. Finally even if Condition 3 is difficult to be achieved at small scale, if sufficiently large particles are used air drag in the motion of granular material can be neglected if compared to other forces (Davies and McSaveney, 1999).

Drake (1991) makes also some similar conclusions regarding flow scale and limitations imposed by material properties. He affirms that the use of smaller particles satisfies the continuum hypotheses that suggest that particles diameter must be at least one tenth of the flow depth, but he states as well that it increases the effects due to air drag and electrostatic effects which strongly influence collisional properties, inducing a behaviour which differs from large scale events.

In the present study no particular scaling factor has been used, but the flow studied are dry and the fluid effects are negligible, in addition, as it is explained in next chapter, among tested material the one that better avoid electrostatic effects has been chosen.

Despite the fact that some phenomena are difficult to be reproduced at small scale, present laboratory tests support the hypotheses that the most important physics and mechanisms which govern propagation of large rock avalanches are likely to be understood through in deep observations of granular flows. The qualitative extrapolation of experimental results to a larger scale is a matter of great practical importance (Drake, 1991). Moreover physical modelling permits to control factors and initial conditions and therefore facilitates the comparison of theory with experiments. Finding a good agreement between the two is still superior to none and represents an improvement in the understanding of the full problem (Pirulli, 2005).

Resume table of already carried out laboratory tests

In order to offer an overview of the previous experimental studies carried out in this field and cited in the present work, a document (see Table 2-4) has been compiled with a classification of some of the significant references on granular and blocks flow physical modelling. The list is not exhaustive and only represents one categorisation approach. The aim is to provide the reader with an easy way to locate each experimental study in the framework of references. For example, if the reader is searching some references about sand unsteady flow, he can find them out looking in the granular material section, unsteady flow, and finally sorting out the tests where sand has been used. In this case the results would be Davies and McSaveney (1999, 2002, 2003), Davies et al. (1999), Denlinger and Iverson (2001), Iverson et al. (2004), Valentino et al. (2004) and Patra et al (2005). The search can be even more specific if the reader is interested only in some particular test, with a certain amount of material, a specific range of slope inclination or drop height.

Material	Flow type	Scale	Material, Diameter [mm]	Amount	Height [cm]	Slope [°]	Authors (year)
Granular	Steady	Small	Quartz sand, D = 0.035		50:90	33	Bagnold (1954)
			Plastic spheres, D = 6.0	2230-1280 particles/s	~250	42.75	Drake (1990, 1991)
			Glass beads, D = 0.3	<7.2 Kg/s/m	< 130	< 40	Ancey (1996)
			Steel beads, D = 3.0	1200-1700 particles/s	~60:~80	18:24	Azanza & al. (1997)
			Glass beads, D = 0.5, 1.3, 1.15		< 100	20:28	Pouliquen (1999)
Granular	Unsteady	Small	Silt, dry ice (oil, bentonite thixotropic flow)	< 160 cm3	60	41	Hsü (1975)
			Sand, rock flour, polystyrene beads	200 Kg/s	400:700	28.4:33.6	Hungr, Morgenstern (1984b)
			Plastic particles D=4 Glass beads D=3	500:5000 grains		40:60	Hutter, Savage (1988)
			Glass, vestolen, quartz, marmor beads, D= 2.5:5	1.5, 2.5, 3 litres	~200	Curved	Hutter, Koch (1991)
			Glass, vestolen, quartz, marmor beads, D= 2.5:5	< 3 dm3	~200	20:60	Greve & al. (1994)
			Silica sand, $D_{50} = 0.19$, Gravel, $D_{50} = 2.0$	0.1, 1, 10, 1000 litres	~100:150	35, 45	Davies, McSaveney (1999)
			Chick peas, D = 10.0	15000, 16000 peas	~90:~165	20:50	Bouzid (1999)
			Vestolen beads D=2:3.5; Marble chips D=2:4; Quartz chips D=4:5	< 3 dm3	~180	40	Wieland & al. (1999)
			Glass, aluminia, zirconia beads D = 14.0	100:600 particles	~50:100	15, 25	Okura & al. (2000)
			Dry quartz sand D = 0.5	290 cm3	~19.5	31.4	Denlinger, Iverson (2001)
			Fine silica, D = 0.19	1.8 litres	14, 21, 35	45	Davies, McSaveney (2002)
			Glass beads D = 0.5	62,231,524 grams	< 100	19-24	Pouliquen, Fortierre (2002)
			Ticino sand D = 0.6	22.5 dm3	~170	25	Valentino & al. (2004)
			Dry quartz sand D=0.5:1, angular; 0.25:0.5, round	380 cm3	~52	31.6	Iverson & al. (2004)
			Playground sand grains, D= 177–250 µm	43,425g		~24:~44	Patra & al (2005)
Granular	Unsteady	Small	Well graded polystyrene beads	~20 l		Deflection	McDougall, Hungr (2004)
Granular	Unsteady	Large	Water saturated sand and gravel	10 m3	~5000	31	Denlinger, Iverson (2001)
Blocks	Unsteady	Small	Jointed mass block 120x30x30; 120x120x30	~ 2 dm3		35, 40	Rengers, Müller (1970)
			Jointed mass, block 36x36x110	~ 2 dm3		20, 28, 36	Reik, Hesselmann (1976)
Blocks	Unsteady	Large	Square block $0.001{:}0.008$ m^3		290	35, 20	Okura & al. (2000)

Table 2-4 Flume, three-dimensional granular and blocks flow tests carried out in the past

The experiments carried out in the framework of the present study can be classified as unconstrained, unsteady, small scale granular and blocks flow tests on a simple geometry.

2.4.   Overview of the state of the art and contribution of the thesis

Long runout rock avalanches, or Sturzstroms, are defined as an extremely rapid, massive, flow-like motion of fragmented rock derived from a bed-rock failure and which exhibits much greater mobility than could be predicted using frictional models (Hungr et al, 2001). The volume of the mass in question is more than one million cubic metres. Rock avalanches represent the most dangerous and lethal one of all landslides phenomena, in particular in developing countries. Now, since their stabilization is almost impossible, the best way to prevent fatalities and damages is to define areas that could be affected by their occurrence. For this reason, it is necessary to understand and model the propagation mechanisms involved in these destructive phenomena which are still for most part unknown.

Several theories have been put forward to explain rock avalanche extended travel distance, but at the present time no general agreement has been achieved and there are still many questions to be answered and the debate is still open (Hungr, 2002). According to the classification made by Davies and McSaveney (1999) it is possible to distinguish between theories based on: 1) a reduction of the friction at the base; 3) a reduction of the friction within the mass; 3) other mechanisms.

Theories belonging to the first category are:

- Self undrained loading

- Lubrication by a basal air layer

- Mechanical fluidisation

Theories belonging to the second one are:

- Air fluidisation

- Water fluidisation

Finally the following theories belong to the third category:

- Acoustic fluidisation

- Momentum transfer

- Spreading of a coherent mass

- Fragmentation

Air fluidization and lubrication, steam fluidization and rock dissociation are theoretically plausible but there are no or few field observations supporting them. Some field evidence has been found for rock melting but only in a few specific cases. Mechanical fluidization has been contradicted by experiments. Acoustic fluidization theory has a sound theoretical and experimental basis at laboratory scale, but there is no evidence in reality that the failed rock masses are able to produce high-frequency vibrations at sufficient intensity. Rock fragmentation and the transfer of mechanical energy from the rear to the front of the rock avalanche may partly explain the spreading of rock avalanches, but not their long runout. The spreading of a coherent mass was for now not supported by evidence in the field. Lubrication by a liquefied saturated layer seems to have played a certain role in some cases, but this concept is not sufficient to explain in general the long runout of rock avalanches, since it implies the permanent presence of extensive alluvial colluvial or glacial deposits in which undrained loading should occur.

These theories have been translated into empirical, analytical and numerical models. Empirical formulations are based on regression analyses of data coming from field events. They are really useful in preliminary assessment and easy to apply, but their statistical scatter is very large. For this reason, the necessity was born to improve empirical models by considering also the physical laws involved in the phenomena. There are three main groups of analytical and numerical models: the sled block, the discrete elements, and the fluid mechanics ones. The models of Heim (1932), Hsü (1975) and Davies (1982), Van Gassen and Cruden (1989), based on frictional law and energy dissipation, belong to the first group. The ones of Bagnold (1954) and Drake (1990, 1991) which take into account the interaction between particles, belong to the second one. The models of Hutter et al. (1988, 1991),

Hungr (1995), Pouliquen et al. (1999, 2002), Derlinger and Iverson (2001) follow a continuum mechanics approach.

Since the number of well documented real cases is limited, due to the rareness of rock avalanches events, several authors have resorted to laboratory tests, some of them to validate their models, e.g. Hutter and his co-workers, Derlinger and Iverson (2001) and McDougall and Hungr (2004), and others to have a data set for validating and developing empirical formulations and to understand the influence of parameters on propagation at small scale, e.g. Davies and McSaveney (1999). Their work is of particular interest, since their approach is near to the one of the present study. They have studied the behaviour of small-scale dry granular avalanches which they compared to documented field events. For this reason they performed a dimensional analysis based on the work of Massey (1983) and they arrive at the conclusion that, with the exception of some particular phenomena (e.g. rock fragmentation), granular avalanches at small scale can realistically reproduce major features of large-scale rock avalanches. Denlinger and Iverson (2001) and Drake (1991) arrive also at similar conclusions. Often experiments have been used as a support or a counter proof to the theories mentioned for the rock avalanche long propagation, since even if many of the mechanisms listed in this chapter could have played an important role for some specific cases, none of them has been accepted as the main cause of rock avalanche excessive mobility (Legros, 2002).

In this framework, an extensive experimental study of dry unconstrained granular and little bricks tests has been carried out at the rock mechanics laboratory of the EPFL (Ecole Polytechnique Fédérale de Lausanne). It is possible to affirm that the main goal of the present research is to better understand mechanisms involved in rock avalanches and to improve the state of the art in assessing their propagation by means of analysis of the tests and comparison with existing theories and real cases. As a complementary part of the research, tests have also been used to compare and validate numerical codes. A multi-tool approach is used: intuitive and qualitative for the parametric study and quantitative for the empirical analysis.

2.4.1. Why physical modelling?

It is the belief of the Author that it is of the greatest importance to observe phenomena at small scale where things can be controlled and measured with accuracy, to understand in a more detailed way what happens in field events. Despite the difficulty in matching the scaling laws, the use of a physical model enables studying the influence of each parameter of interest, by controlling and changing one at a time, with known and consistent experimental conditions. Even the qualitative extrapolation of experimental results to a larger scale is a matter of great practical importance (Drake, 1991). The tests do not try to mimic reality, but they are an effort to understand the physics and mechanisms behind, through in deep observations that are unlikely to be done in field.

The choice to carry out a purely experimental research can be argued. Many authors believe that there are a lot of phenomena that it is impossible to reproduce in the laboratory, but still they resort to experiments to give evidence to their hypotheses. It is true that not all the mechanisms are reproducible at all scales, but comparing the two realities could help to identify which ones are peculiar to large events and which are not and then to understand the cause of the so-called size effect. In addition, many authors have proposed theories that should justify the excessive travel distance of rock avalanches, but if it is possible to reproduce the same phenomena at laboratory scale, these are not scale dependent anymore. In addition, most analytical and numerical models are scale independent and so it should be possible to test them at any scale, therefore results can also be useful to identify too simplistic models because if they cannot even describe the simple and ideal granular flows in the laboratory, there is little hope that they can be applied for large-scale events in a complex environment (Ancey, 2007). Experiments can then be useful to improve these models by identifying mechanisms and parameters that help to match better previsions and results and therefore make their extension to field events much more reliable.

3.   Preliminary experimental campaign

The first part of the present experimental study consisted of about hundred and fifty tests. The basic phenomenon studied is an unconstrained flow of a mass of granular material down an inclined board, followed at the toe by a horizontal plane on which the mass spreads and translates coming to rest when the momentum acquired from the fall is totally dissipated by collisions between the grains, intergranular and basal friction (Davies and McSaveney, 1999). The mass consists of dry rigid noncohesive grains and tests are carried out in an ambient gaseous medium at atmospheric pressure. They correspond to an idealized representation of dry unconstrained rock avalanches in the field.

Fall height, volume, releasing geometry and materials used for testing have been varied and their influence on deposit characteristics (such as length, width, height and morphology) and runout has been studied. The approach for this campaign has been mainly intuitive and qualitative. The analysis consists mainly in a parametric study, based on observations of the tests and comparison with known real events. Despite the intuitive approach, the results have been really useful for phenomenological studies and assessment of relevant physical parameters influencing rock avalanche propagation. In addition they represent the contribution of the EPFL rock mechanics laboratory (LMR) to the INTERREG "Rockslidetec" project between Italian, French and Swiss partners, the main goal of which has been to develop methodological devices to define areas that could be affected by large rock avalanches. The present work concerns mainly the action C.2 of the project (model development and laboratory experiments), where LMR main task has been to develop and carry out a research with a physical model at small scale. Part of these results has also been the object of a peer reviewed paper (Manzella and Labiouse, 2008a).

Furthermore, during this preliminary campaign, it has been possible to improve the experimental set-up and to develop and validate the measurement system and in particular the fringe projection method that will be illustrated in detail in chapter 4.

In this chapter the INTERREG project is described, the experimental set-up, the varied parameters and the measured characteristics are illustrated and the front velocity measurement device is explained in detail. Results of this first testing campaign are then presented.

3.1.   Interreg IIIA 'Rockslidetec'

The INTERREG IIIA "Rockslidetec" project between Italian, French and Swiss partners, had the main goal to develop methodological devices to define areas that could be affected by rock avalanche phenomena. The project has been organised in four actions:

- Action A: collection of an itemized list of historical rockslide events;

- Action B: rockslide geometrical characterization and determination of unstable volumes;

- Action C: study and modelling of rockslide run-out with comparison of different codes;

- Action D: promote the exchange between scientists and practitioners faced with managing these risks.

The partners were: Regione autonoma Valle d'Aosta, Politecnico di Torino, Università di Parma (Italy); Université Joseph Fourier-Grenoble, Pôle Grenoblois des Risques Naturels, CETE Lyon and Aix-en-Provence, Cemagref-Grenoble, Université de Savoie-Chambéry (France); Centre de Recherche pour l'Environnement Alpin (CREALP)-Sion, Ecole Polytechnique Fédérale de Lausanne (Switzerland). Each has specific skills in the field of investigation of the cliff, detection of potential landslides and modelling of rock avalanche propagation.

The EPFL Rock Mechanics Laboratory (LMR) has been involved mainly in action C for the bibliographical study and the physical modelling of propagation. As already mentioned,

since rock avalanches are luckily not so frequent, in the research field there is a lack of well known real cases on which it is possible to base proper back analysis studies or code validations. For this reason, physical modelling can constitute a significant sample to fill up partly the lack of accurate field data. In this context the first experimental campaign carried out by the LMR was very helpful for phenomenological studies and assessment of relevant physical parameters.

3.2.   Experimental set-up

The tests consist in triggering an unconstrained granular flow. The experimental set-up (see Figure 3-1) mainly consists of two rectangular boards joined by a hinge and connected by a sealing plastic band. The first panel (3 m length × 4 m width) is fixed horizontally on a concrete floor slab and the second one (4 m length × 3 m width) can be positioned at different angles. The panel dimensions are large enough to allow free-spreading along all the flow. Part of the tests has been carried out with a vertical board. Although this first configuration as well as the deposit observed were far away from reality, this preliminary work made it possible to detect some laboratory problems and consequently to improve the model as well as the methods of measurements and interpretation. For results shown in this chapter the inclination has been maintained at 45° degrees. Different amounts of material are poured into a wooden cuboidal reservoir measuring 20 cm height × 40 cm width × 65 cm length and placed on the tilting panel. The container is opened in an almost instantaneous way using a spring-loaded bottom gate and the material is released directly onto the slip surface.

A digital high speed camera is used to register a film of each test. The distance between the deposition area and the camera is 6 m and the camera is directed perpendicularly to the horizontal panel. This height has been chosen in order to register the whole test that can cover several metres. Characteristics of the camera used, process for recording and image analysis will be better explained in section 3.3.2. Descriptive pictures of the final deposit have been taken after each test.
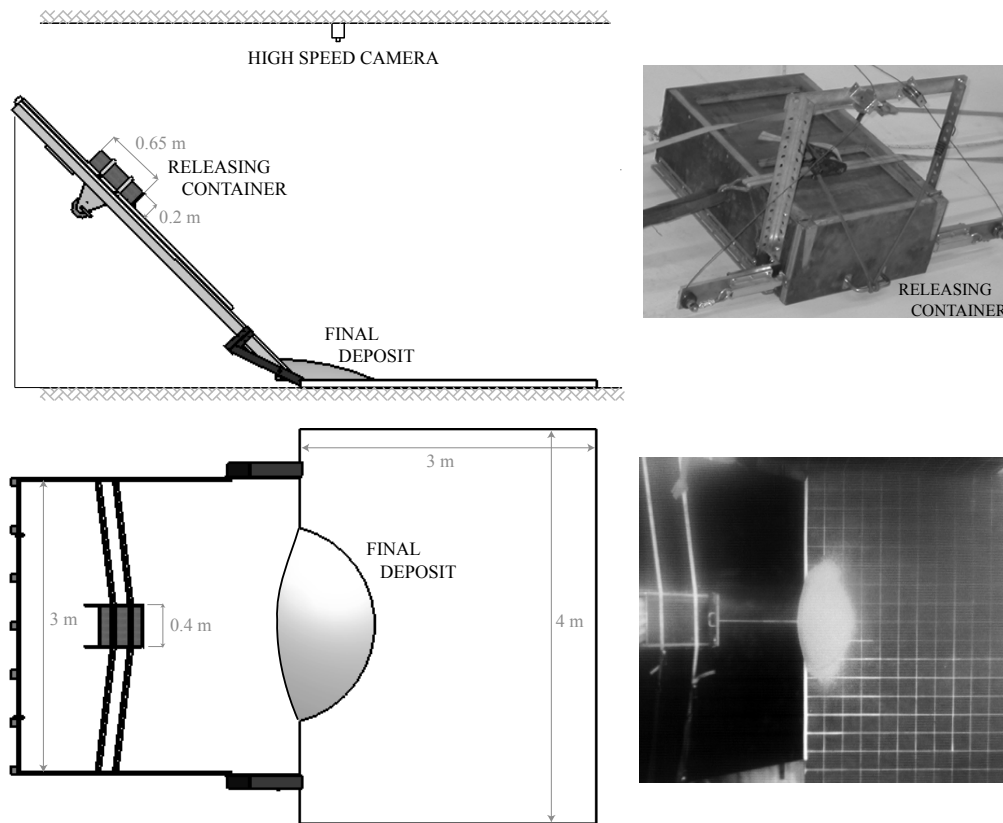
Figure 3-1 The experimental set-up and the releasing container

3.2.1. Factors

Two important terms have to be defined at this point that will be used in the following according to the definition of Fürbringer (2005): a response is any manifestation or consequence of a phenomenon. It can be a qualitative or quantitative property (response = dependent variable = consequence). A factor is any variable (or parameter) which has, in reality or probably, an influence on the studied phenomenon. The factors are considered as the possible causes of the response (factor = independent variable = cause).

The dynamics of rock avalanches is governed by topographic features of its path and on many other rheological and mechanical properties of the material such as the basal and internal angles of friction of the base and the material (Pudasaini and Hutter, 2007). In particular, granular flow experiments in the present study are influenced by the following factors (Davies and McSaveney, 1999):

- grain characteristic variables, i.e. diameter, angularity of the grains, and elasticity (coefficient of restitution);

- bulk characteristics, i.e. density, volume, grading;

- mass flow characteristic variables, i.e. flow depth and flow velocity;

- ambient characteristics, i.e. air density, air viscosity, humidity, gravitational acceleration;

- fall height;

- slope and runout surface characteristics, i.e. slope inclination to the horizontal, β [°], irregularity of the topography along the path, roughness and nature of the boards.

Among these factors likely to affect granular flows, some could not have been retained within the present research due to limitations imposed by the time available but also the existing conditions at the laboratory and by technologies on disposal, i.e. elasticity of the grains (coefficient of restitution), air density, air viscosity, humidity, flow depth and velocity. This preliminary experimental campaign has systematically evaluated the influence on the deposit morphology of the following parameters (see Figure 3-2):

- Volume, *V* [litres]

- Fall height, h [m]

- Geometry of the mass before failure

- The way the material is released

- Nature of released material, varying angularity and diameter of the grains, D [mm]
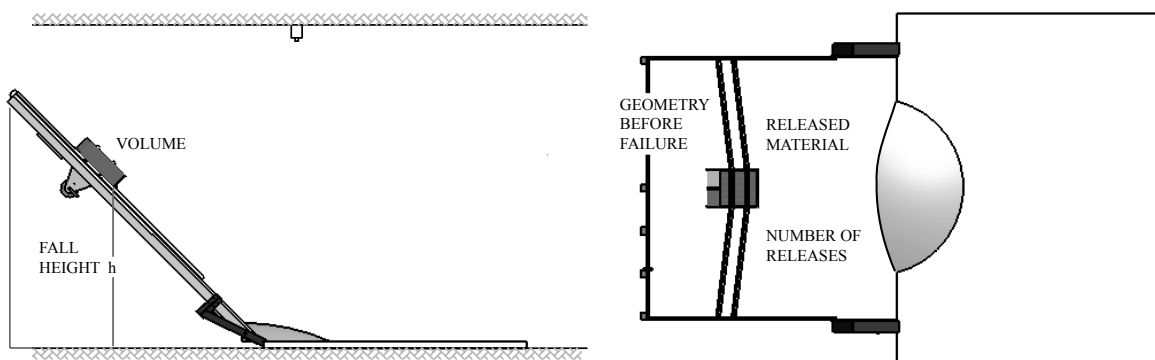
Figure 3-2 Factors varied during the preliminary campaign

The volumes used in the preliminary experimental campaign are of 10, 20, 30 and 40 litres. These volumes are released from 1 and 2 metres height. As it can be seen from Figure 3-2 the fall height is considered as the distance between the horizontal panel and the toe of the container which has been positioned and fixed along the tilting panel by a system of two belts. The range of variation of these factors has been chosen according to the limits of the experimental set-up.

In addition to the standard opening surface (20 cm × 40 cm), tests have been performed with an opening surface of 20 cm × 20 cm and 20 cm × 30 cm. The reduced opening surface was obtained by placing a separation panel inside the box. The three studied situations are schematically represented in Figure 3-3 by a simplified drawing where the mass shape of the granular material in the container is represented by a parallelopiped. Changing the opening surface of the reservoir, it has been possible to have the following conditions:

- Varying both volume (20, 30 and 40 litres) and filling depth (Figure 3-3a)

- Varying the filling depth, but maintaining constant the volume (20litres; Figure 3-3b)

- Varying the volume (20, 30 and 40litres), but keeping constant the filling depth (Figure 3-3c).

The material is arranged in the container trying to fill it entirely in height and width, varying the depth, keeping as much as possible a parallelepiped shape of the mass in order to reduce to the minimum the difference between the angles of repose at the back of the different materials. Indeed, it will be seen in section 3.5.4 that the way the material is arranged in the container before failure has a slight influence on propagation. Thus, in order to have a better consistency it is important to have a similar shape of the mass before failure.

Volumes have been released in one or more consecutive releases (for example 30 litres in one or in three subsequent releases of 10 litres each) to study the effects of a progressive failure on rock avalanches propagation. As shown in Figure 3-4 the second volume is released only when the first volume has completely come at rest and measurements have been completed on its deposit. So it is done for the successive ones.
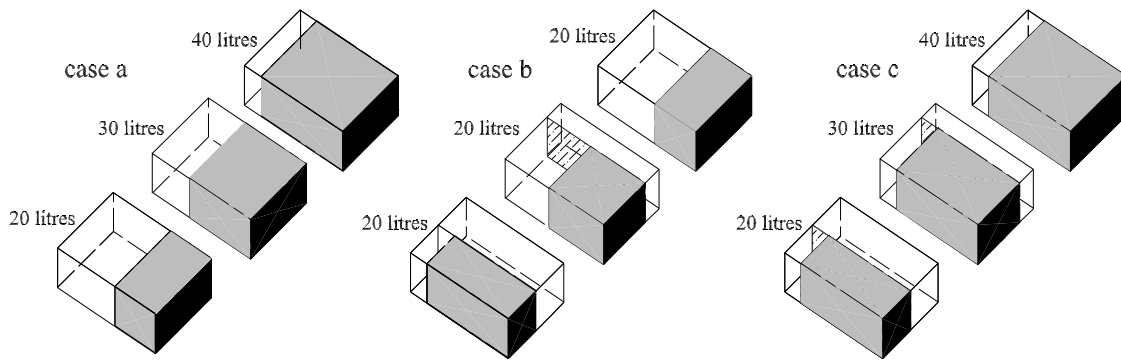
Figure 3-3 Changes in initial geometry (the opening gate is on the black filled side)
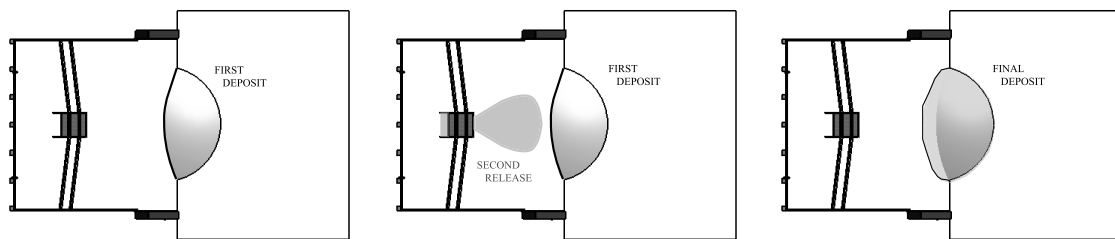
Figure 3-4 Consecutive releases

The three kinds of granular materials used for the tests are (see Figure 3-5 and Figure 3-6 for pictures and grain size distributions):

- Hs   : Hostun sand, a very fine sand

- Gr2 : Aquarium gravel 2, a gravel used for aquarium decoration, called Gr2 because its D90 value is 2 mm

- Gr4 : Aquarium gravel 4, also used for aquarium decoration, called Gr4 because its D90 value is 4 mm

The two types of gravels have mainly the same characteristics but grains of Gr4 have a greater diameter. The main characteristics of these materials are listed in Table 3-1. The unit weight of the material has been measured weighting a bucket of known volume, filled with non- compacted soils. The internal angle of friction (ϕ_i) is obtained measuring the slope to the horizontal assumed by the free surface of a heap at rest. The heap has been made pouring the material vertically in an almost steady way onto a horizontal surface (see Figure 3-8b). This measure has been compared for a better accuracy with the slope of the free

surface of a greater quantity of material poured into a box with transparent and smooth walls, put slowly at the horizontal position as shown in Figure 3-8a.

Material	Grains size [mm]	Unit weight [kN/m³]	Static friction angles internal [°]	on wood [°]	Dynamic friction angles on wood [°]
Hs	0.1-0.8	12.6	34 ± 1	34-40 ± 1	32 ± 1?
Gr2	0.5-4.0	14.9	34 ± 1	32 ± 1	30 ± 0.5
Gr4	1.0-4.0	15.0	37 ± 1	31 ± 1	27.5 ± 0.5

Table 3-1 Characteristics of the three granular materials used
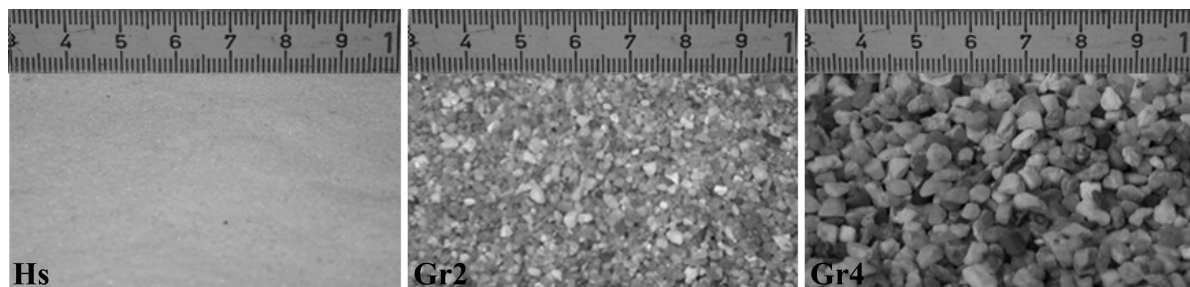
Figure 3-5 Granular materials used
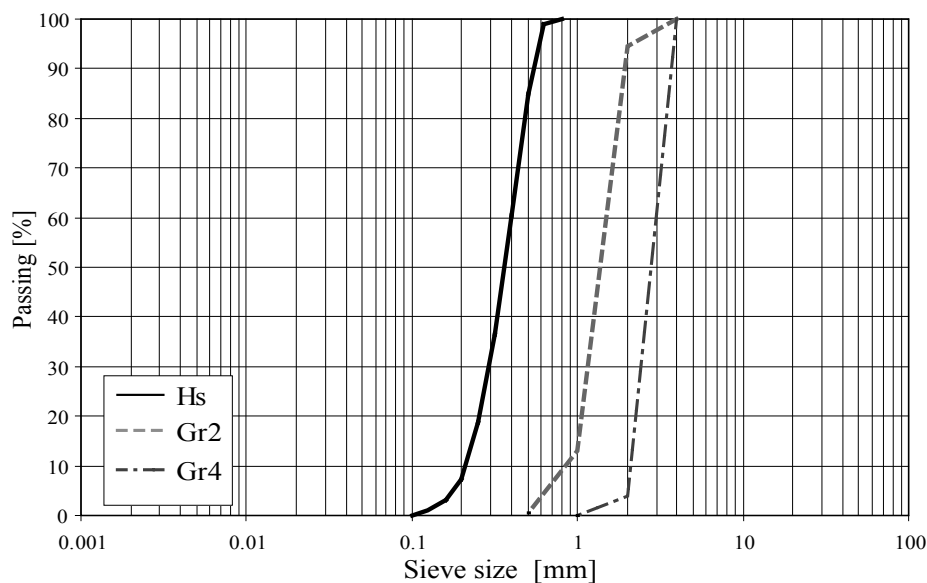
Figure 3-6 Grain size distribution of Hostun sand, Aquarium gravel2 (Gr2) and Aquarium gravel4 (Gr4)

The basal friction angle of the material (ϕ) has been estimated using tilting table tests. A tilting apparatus has been built at the laboratory (see Figure 3-7) and several tries have been made for each material. Hostun sand shows an abnormal behaviour as its basal friction angle was found to vary in a range between 34° and 40°, which is greater than its internal friction angle of 34°. In fact as soon as the grains are very fine a thin layer is stopped by the

asperities of the panel surface and probably also from electrostatic forces as stated by Drake (1991), Davies and McSaveney (1999) and Iverson et al, 2004 (see section 2.3.3). Consequently the first value (34°) of the range is referred to the moment when an upper layer of sand slides on another (see Figure 3-8c), the second value (40°) refers to the total departure of the material: this happens only when the thin layer of sand, firstly stopped, also slides. 34° is the value retained for the following since it is more realistic, taking into account that dry shattered rocks in nature have basal friction angles between 25° and 35°.

The basal dynamic friction angle of the material (ϕ_{dyn}) has been also estimated using the tilting apparatus. In this case two different kind of tests have been carried out to have a more accurate measure: first the material has been poured on the tilting panel as for the static case and then the slope has been increased, at the same time the panel has been constantly hit with a little hammer. Another way to carry out this test, which has conducted to the same results, is to pour continuously the material on the surface imposing a certain velocity, while increasing the slope angle. This is done at different angles. For both tests, the lowest angle for which the material does not stop on the inclined surface but continues to slide, is the dynamic friction coefficient. Also in this case it has been difficult to determine the value characterising the Hostun sand. The electrostatic effects are evident.
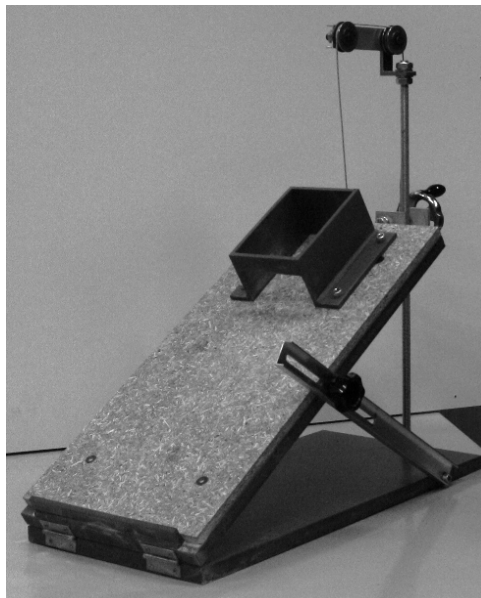
Figure 3-7 Tilting test set-up
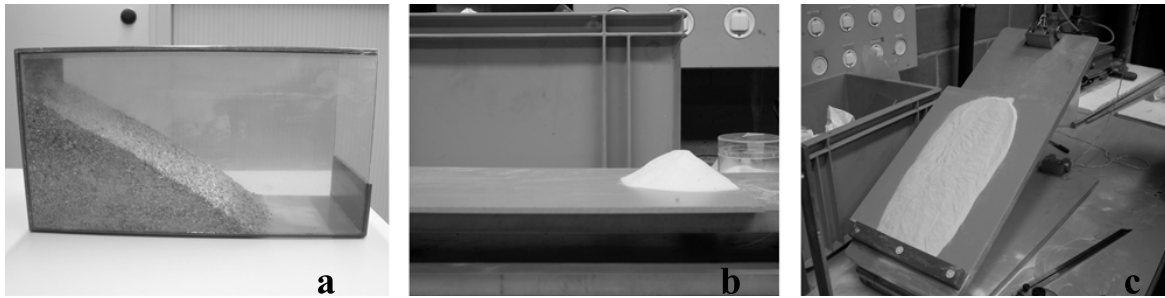
Figure 3-8 Measurement of: a) and b) internal and c) basal friction angles

3.3. Measurements

For each test, measurements of runout, width and length of the final deposit are taken manually while the front mass velocity is derived with a specific processing from films and images. At this state the deposit morphology is evaluated qualitatively from pictures of the mass at rest. Here follows a detailed description of the methods used.

The coordinates system (see Figure 3-9) used for measurements consists in:

- x coordinate: the direction of dip slope,

- y coordinate: the direction perpendicular to the x axis on the horizontal plane

- z coordinate: the direction perpendicular to the xy plane

3.3.1. Responses

The main characteristics measured are:

- Runout (R)

- Deposit width (W)

- Deposit length (L*)

- Deposit height (h_d)

- Velocity of the mass front (v_f)

When the mass has come to a halt, runout, width, height and length of the final deposit (see Figure 3-9) are manually measured with a tape. A standard procedure is used for all measurements whereby only the main part of the deposit is included. The zone where it is possible to start distinguishing single separated particles is not considered as part of the

deposit, i.e. the distance between two adjacent particles is more than one time the particle itself. Runout and length are measured along the x axis. Width is the projection on the y axis of the larger dimension in the direction perpendicular to the x axis.

In the literature, as seen in chapter 2, runout has usually been considered as the total horizontal travel distance between the head scarp and the toe of the deposit (L). In this study, as shown in Figure 3-9, runout (R) is considered as the distance travelled by the mass front on the horizontal panel as opposed to the total travel distance often used in literature. This measurement is not affected by intrinsic differences in length caused by the variation of some parameters such as fall height or slope inclination.

The displacement and the velocity of the mass front during sliding have been evaluated from analysis of the images. This is the result of a complex procedure which will be better explained in next section.
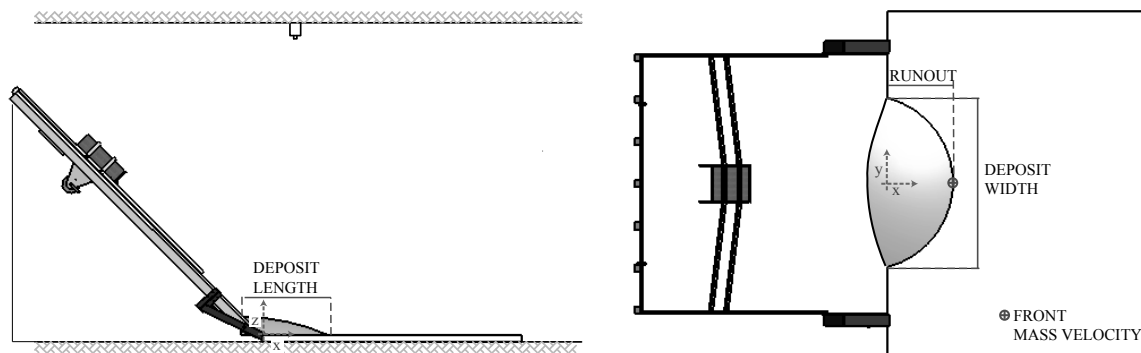
Figure 3-9 Measurements of the preliminary experimental campaign

3.3.2. Velocity by high speed camera

Each test is filmed by a high-speed digital camera. The displacement and the velocity of the mass front during the sliding are evaluated from the registered films. The operating speed of the camera ranges from 60 to 8000 frames per second. For higher recording rates, the resolution of the frames and the maximum recorded time decrease. Since a test usually lasts less than 2 seconds and the camera is placed at about 6 metres from the horizontal plane, it has been agreed that an operating speed of 60 frames per second with a frame resolution of 480x420 pixels constitutes a good compromise between accuracy of the measurement and data storage capacities. In order to cover the entire area of interest during motion, a wide-

angle lens is used, but this causes a radial distortion. As a consequence a calibration of the camera parameters had to be performed in order to systematically rectify the images.

Correction of distorted films

In the geometrical camera calibration, the objective is to determine a set of camera parameters that describe the mapping between 3-D reference coordinates and 2-D image coordinates (Heikkilä and Silvén, 1997). The correction of the films requires the determination of the following calibration parameters:

- The external or extrinsic parameters, which depend upon the 3-D position and orientation of the camera frame relative to an established world coordinate system. They are defined by the exterior orientation.

- The internal or intrinsic parameters, which are the camera geometrical and optical characteristics, e.g. focal length, radial and tangential distortion of the lenses. They are defined by the interior orientation.

Exterior orientation defines the position and angular orientation associated with an image at the time of exposure or image capture. Angular and rotational elements are defined which mathematically describe the relationship between a ground coordinate system and the image space coordinate system (that is derived with the interior orientation). Interior orientation defines the internal geometry of the bundle of rays as it existed at the time of image capture. The internal geometry of a camera is defined by the principal point (the point at which lines drawn between opposite corners of the images intersect and the distortions are equal to zero), the focal length (the distance between the film and the projection centre of the camera, when the lens is focused on a distant object) and the lens distortion (radial, tangential and asymmetric). These variables are computed by the interior orientation, which establishes a basic reference Cartesian system for each of the image, transforming the pixel coordinate system into the image space coordinate system.

To find these parameters it has been chosen the Camera Calibration Toolbox for Matlab (Strobl et al, 2007). This choice has been made according to the work of comparison between the different available methods performed by Heidenreich (2004), who has first applied this procedure at the LMR. The method proposed is based on the techniques of

Zhang (1999) and Heikkilä and Silvén (1996, 1997), which use images taken by the camera of a planar pattern at different positions. For this reason a sequence of images have been taken of a planar chessboard (9×9 alternate black and white squares each of 11.6 cm side) put in different position and at different orientations in the frame registered by the camera. The general concept in simple words is that the toolbox is able to identify distortions comparing the real dimensions of the chessboard with the one measured on the images.

The parameters resulting from the calibration are:

fc_1, fc_2 :   horizontal and vertical coordinates of the focal length [pixels]

cc_1, cc_2 :   horizontal and vertical coordinates of the principal point [pixels]

alpha_c   :   skew coefficient, defining the angle between the x and y sensor axis
(alpha_c is equal to zero for rectangular pixel)

k_c :   vector storing the radial (k_{c1}, k_{c2}, k_{c5}) and tangential distortions (k_{c3}, k_{c4})

As reported by Heidenreich (2004), the distortion model of Brown (1966) is used to compute the normalized pinhole projection x_d of a point P(x,y) on the image plane, combined with the radial and tangential distortion components:

$$x_d = \begin{bmatrix} x_{d1} \\ x_{d2} \end{bmatrix} = \left(1 + kc_1 \cdot r^2 + kc_2 \cdot r^4 + kc_5 \cdot r^6\right) \begin{bmatrix} x \\ y \end{bmatrix} + dx$$

$$dx = \begin{bmatrix} 2kc_3 \cdot x \cdot y + kc_4 \cdot \left(r^2 + 2x^2\right) \\ kc_3 \cdot \left(r^2 + 2y^2\right) + 2kc_4 \cdot x \cdot y \end{bmatrix}$$

[3-1]

Where $r^2 = x^2 + y^2$ (pinhole projection) and dx is the vector defining the tangential distortion which is due to imperfect centring of the lens components or other manufacturing defects. The camera model can thus be written as follows:

$$\begin{bmatrix} x_p \\ y_p \\ 1 \end{bmatrix} = KK \cdot \begin{bmatrix} x_{d1} \\ x_{d2} \\ 1 \end{bmatrix} = \begin{bmatrix} fc_1 & alpha\_c \cdot fc_1 & cc_1 \\ 0 & fc_2 & cc_2 \\ 0 & 0 & 1 \end{bmatrix} \cdot \begin{bmatrix} x_{d1} \\ x_{d2} \\ 1 \end{bmatrix}$$

[3-2]

where x_p and y_p are the horizontal and vertical coordinates of the point P in the distorted image and KK the camera matrix.

Matlab toolbox determines the values for these parameters based on image observations of the several points of intersection on the planar chessboard.

In the present case the intrinsic parameters are:

fc   =   [887.620 ; 886.396];

cc   =   [165.045; 233.512];

alpha_c   =   0.000;

kc   =   [-0.367; 0.663; -0.001; -0.002; 0.000]

In Figure 3-10 the total distortion effects, a distorted and a corrected image are visualised. The sequence of images can be now corrected and it is ready to be used to measure velocities and displacements of the front mass, as explained in the following section.
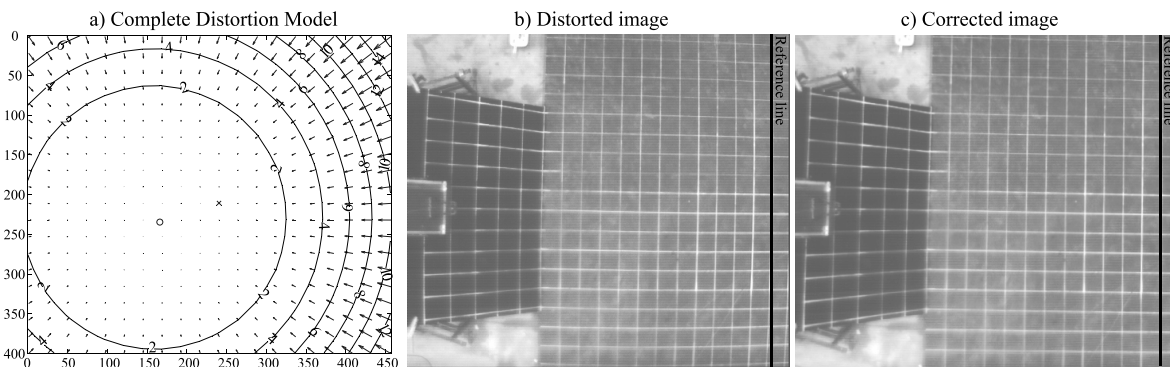
Figure 3-10 a) Total distortion model; b) distorted image; c) corrected image

Front mass velocity

The mass front is followed by means of a specialised software for image analysis (WINanalyze 1.4) which is able to automatically track objects in a film sequence (Heidenreich, 2004) and to register the *x*-displacement and compute the velocity *x'*. The accuracy of the measurement depends strongly on the visibility of the tracked object; in the present case it is impossible to place any visible track on the mass moving, since it will

change its characteristics and consequently bedevil the results. In addition grains are too small and, even if coloured, they could not be tracked from 6 metres distance. The only possibility has been to follow the front of the mass in movement along the x axis where there is a certain contrast between the granular material mass and the panel (see Figure 3-11). Accuracy depends then also on the material used (whether it is more contrasted with the panel or not), on light conditions and on the fact that it is not a specific point which is tracked but a front formed by several particles in movement. In average if the measure of the total displacement on the horizontal panel made by WINanalyze is compared with the runout measured by hand after each test, the uncertainty could reach approximately 1-2 cm.

Since the major problems to track the front have been encountered when the mass reaches the horizontal panel at the moment when it passes over the discontinuity between the tilting board and the horizontal one, it has been decided to analyse the velocity only on the horizontal panel. This is also justified by the fact that the propagation and spreading of the mass on the accumulation zone and the mechanisms developed in this phase are what mainly interest the present research. If the track is lost on the horizontal board due to sudden changes in contrast and light, it is possible to manually replace the position tracker; this operation leads to some discontinuity in the velocity plot; nonetheless, it is possible to deduce the general trend through curve fitting.

As it can be seen in the following, despite all these limitations, the measure of the front mass velocity revealed itself to be a very useful tool to compare tests and to identify particular mechanisms in the propagation and the accumulation of the mass.
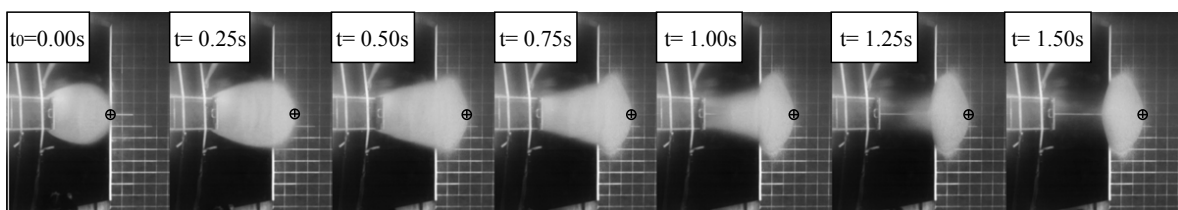
Figure 3-11 Track of the front mass

3.4. Testing programme and procedure

Among the series of tests carried out at the laboratory Table 3-2 shows the ones used for the analysis presented in this chapter. The testing programme has sometimes been changed in

progress with the tests based upon the results obtained and the difficulties encountered with the experimental set-up and the measuring devices adopted. The preliminary experimental campaign has consisted of about hundred and fifty experiments.

After the first tests, some improvements in the set-up have been made: boards have been replaced by new ones and the entire model has been located in a more suitable area of the laboratory, the handling system has been changed in order to ease the filling up of the box and the switching from one parameter value to another. To indicate the moment when these changes have been made, in Table 3-2 it is distinguished between first and second set-up.

Set-up	Series Number	Granular Material			h [m]		V [litres]				Number of releases				Releasing geometry height [cm]×width [cm]		
		Hs	Gr2	Gr4	1	2	10	20	30	40	1	2	3	4	20×20	20×30	20×40
First	1A		Gr2		1		10	20	30	40	1						20×40
	1B		Gr2		1			20	30	40	1	2	3	4			20×40
	2A	Hs			1		10	20	30		1						20×40
	2B	Hs			1				30		1	2	3				20×40
Second	4A		Gr2		1			20	30	40	1						20×40
	4B		Gr2		1			20	30	40	1	2	3	4			20×40
	5	Hs			1			20	30		1						20×40
	6A		Gr2			2		20	30	40	1						20×40
	6B		Gr2			2				40	1	2					20×40
	7	Hs				2			30		1						20×40
	8		Gr2			2		20			1				20×20		
	9		Gr2			2		20	30		1					20×30	
	10flat		Gr2			2		20			1						20×40
	11			Gr4		2			30		1						20×40

Table 3-2 Tests series of the preliminary campaign

Series of tests 1A - 4A and 2A - 5 have the same testing conditions but they have been performed with the two different experimental set-ups to verify if the changes made could affect tests consistency.

The 1A, 2A, 4A, and 6A test series have been used to study the volume influence on the run-out and deposit characteristics. The 1B, 2B, 4B and 6B test series have enabled the study of the influence of the type of release, i.e. all in once or in different consecutive releases. Furthermore, the 1A, 2A, 5, 6A, 7 and 11 test series have been used to evaluate the different behaviour of the three granular materials used. The 4A and 6A series have been

used to study the influence of the drop height and finally the 6A, 8, 9 and 10flat series have been dedicated to the assessment of the influence of the releasing geometry.

Limitations imposed by technologies, space and time at disposition and the physical properties of the material used constrain the factors and measurements that can reasonably be explored by physical experiments.

It is possible to resume the procedure of a test through the following consecutive steps:

1. The experimental set-up and measuring devices are checked.

2. In the case the height has to be changed, the reservoir is placed accordingly and is fixed to the panel with a system of belt.

3. The parameters of the camera which can be controlled are settled through the dedicated PC software, i.e. choice of the lens aperture, exposure time according to light conditions

4. The material is weighted with a precision balance, poured into the container and the free surface is smoothed by hand

5. The camera is started

6. The spring-loaded bottom gate of the reservoir is opened and the material is instantaneously released

7. The camera is stopped immediately after the material has come to rest and the part of the film that covers the test is registered.

8. The manual measurements (width, height, length and runout) are taken and reported on an Excel sheet

9. The material is swept away and the model is cleaned

This procedure is followed attentively for each test in order to assure consistency and repeatability. A test is performed three times for each set of parameters.

3.5.   Parametrical study and empirical interpretation

The preliminary experimental campaign has been first helpful for checking and improving the experimental set-up and the measuring devices, but it has already led to some interesting conclusions for a better understanding of the rockslide phenomenology and for the

definition of the most important parameters, as indicated in the purposes of the INTERREG project. The analysis has been qualitative, i.e. based on observations of the deposit morphology and comparisons with some known real events, and semi-quantitative, looking for the influence of the different factors varied on the mass propagation (front velocity) and on deposit characteristics (runout, length, width and height). A section will be dedicated to each parameter varied to systematically analyse its impact on responses.

3.5.1. Granular materials and influence on deposit morphology

The series used to investigate the different behaviour of the materials are 1A and 2A, 6A, 7 and 11. The greatest differences can be noticed comparing the tests made with Hostun sand and Aquarium gravel; the general trends are similar but the values vary significantly (see Figure 3-12): the deposit height of the Hostun sand tests can be up to 50% greater than with the Gr2 tests. On the other hand, length, width, run-out, and front mass velocity are smaller with sand than with gravel material. It can be that sand grains are so small that energy dissipated in shearing irregularities is higher, explaining in this way much shorter runout even if basal angles of friction are similar.
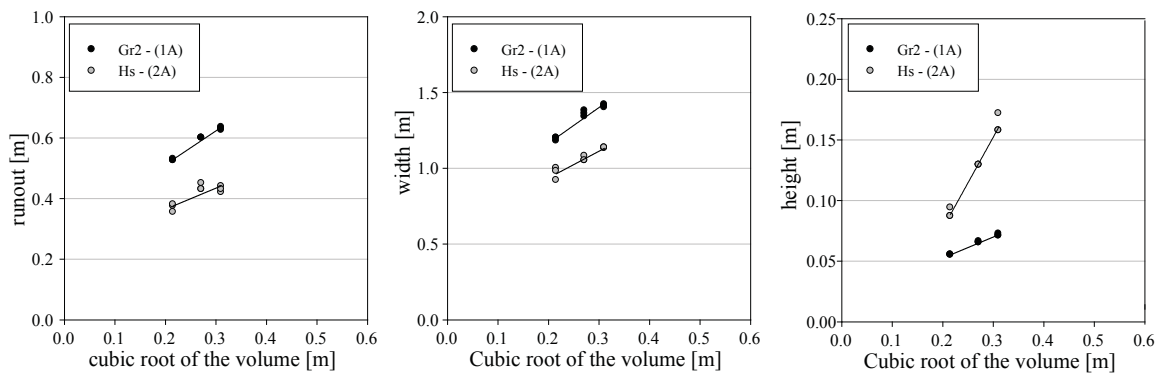
Figure 3-12 Comparison between Gr2 and Hs deposit run-out, width and height of the 1A and 2A series of experiments (1m drop height, 1 release, box opening 20 cm×40 cm)

A clear difference in the deposit morphology is detected (see Figure 3-13). The shape of the sand deposit, regular and compact, seem to agree well with many experiments described in the literature and carried out with sand (e.g. some experiments of Hutter and his co-workers, see Pudasaini and Hutter, 2007; Davies, 1997), while the Aquarium gravel deposit has well marked angular discontinuities: a central zone with a small slope and several ridges, but the front, rear and sides strongly inclined. The presence of ridges and steep front of the final

deposit put in evidence a rapid stop of the mass (Hsü, 1975 and Shreve, 1968). These morphological features are often detected in field events as well. As a matter of fact a similar morphology is noticed in situ at the Six des Eaux Froides (Valais, Switzerland) which has been visited during the present research, in the framework of the INTERREG Rockslidetec project, and in other rock avalanche deposits such as the one of Frank Slide (Hungr, 2004).
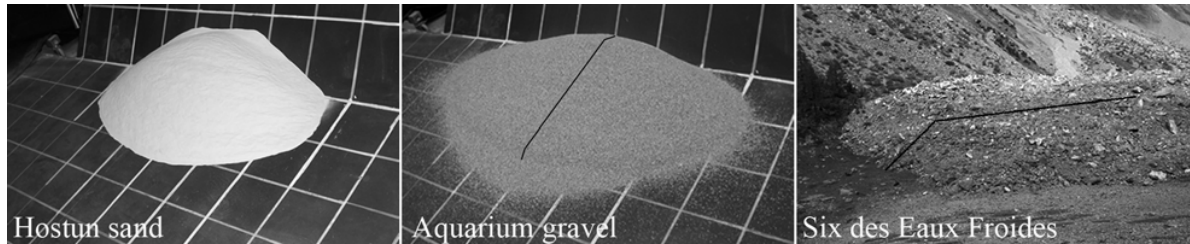
Figure 3-13 Influence of materials used on deposit morphology: comparison between Hostun sand, Aquarium gravel2 (30litres, 1m drop height, 1 release, box opening 20 cm×40cm) and Six des Eaux Froides (Valais, Switzerland)

Among all the tests reviewed in the literature, it has been noticed that gravel is seldom used and that most of the tests are performed with different kinds of sands or beads. One reason for this is that sand is a more suitable material for the validation of numerical models which are based on the fluid mechanics hypothesis (i.e. grain diameter should be less than 1/10 of the flow depth all along the slide to avoid a "bounce behaviour" and to assure a dense one-phase flow). On the other hand, as mentioned in section 2.3.3, this type of material is prone to effects due to air drag and electrostatic effects which influence strongly collisional properties inducing a behaviour which differs from large scale elements (Drake, 1991). This seems the case for Hostun sand, as it has been mentioned in section 3.2.1, because of the peculiar behaviour shown in tilting tests (see Figure 3-8).

Above a certain limit for which air drag and electrostatic effects are avoided or negligible, grain diameter and grading don't affect significantly propagation as indicated by tests performed by Davies (1997). This is confirmed by comparison with series 11 where the tests are carried out with the gravel Gr4 which has similar characteristics as the aquarium gravel 2 (Gr2) but with a larger diameter of the grains, as shown in Table 3-1 and Figure 3-5 and Figure 3-6. In fact, the morphology of the deposit is similar, except a more homogeneously rounded shape at the rear border in the case of Gr4. Slight differences have been also noticed within the deposit characteristics: using Gr4 with bigger grains diameter, runout

increases of 2% maximum, width remains almost constant; length and height increase of about 9%, showing a certain dilatancy (see Figure 3-14).

Even if the influence of the angularity of the grains hasn't been studied in the framework of the present research, intuitively it can be affirmed that this factor could have a great influence on the morphology and runout of the granular mass. To verify this statement, tests should be performed with spherical shaped particles with the same grain size distribution as Gr2. Beads and spheres of different materials are indeed often used in laboratory experiments (see Table 2.4) and have a more suitable shape for the modelling of particle contacts in discrete element codes. Nevertheless they produce a lower shear resistance and induce rolling with a behaviour which is far from the processes in rock debris. Fragmented rock particles are more angular and blocky, which increases voids within the mass, interlocking between the particles and inhibits rolling (Pirulli, 2005).

For the purposes of the present study, the choice has been made to use mainly Gr2. This material appears to be more representative of reality: no apparent electrostatic or air drag effects are registered, but grains are quite small allowing the mass to be still considered as a continuum. Moreover the angularity of the grains is more similar to the one of fragmented rock particles in the field. So it is for the final deposit morphology. In next chapter experiments with little bricks will be illustrated. These tests have been carried out also to verify the influence of the blocky shape on propagation.
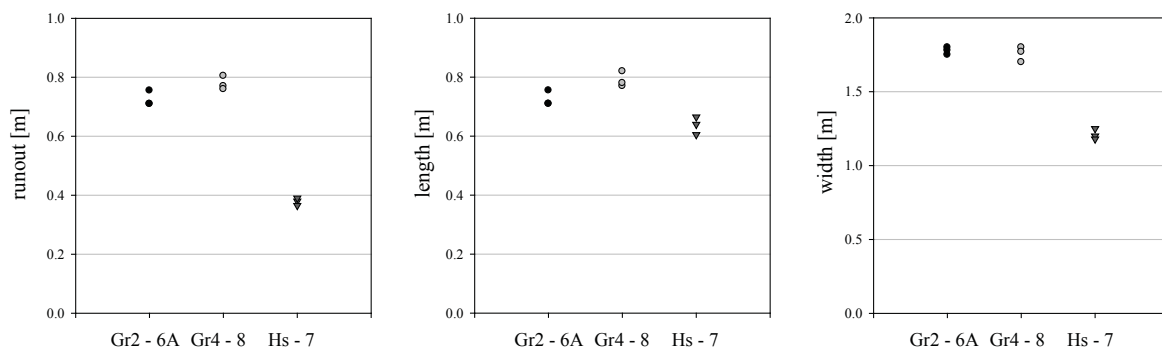
Figure 3-14 Comparison between Gr2, Gr4 and HS (30 litres, 2 m drop height, 1 release, box opening 20 cm×40 cm)

3.5.2. Volume and drop height

If test series 4A and 6A are considered, the volume of the released material has shown to influence the deposit characteristics (see Figure 3-15 for run-out, width and velocity plots). Even if the deposit morphology has shown not to be significantly affected, the geometry dimensions increase as the volume increases. On the other hand, the front velocities monitored from the high-speed camera remain similar for the different volumes until the mass is nearly at rest, and they only differentiate in the last part of the run-out. It can therefore be assumed that the volume has a significant influence only in the last part of the sliding event where the rear part of the mass seems to push or to run over the deposit which is already making up at the base. A transfer of linear momentum is likely to take place between the rear part of the deposit and the front one stopping.

The first plot in Figure 3-15 shows that there is an interaction between the volume and the fall height. It is apparent that the drop height has less and less influence on the runout as the volume increases. This agrees well with the theory of Legros (2002), which shows that the run-out distance of large rockslides depends primarily on the volume and less on the fall height.

On the other hand, an influence of the releasing height on the deposit morphology and on the propagation mechanism can be observed: when dropped from 2 m, the mass tends to flatten out. This is probably due mainly to the more significant mass potential energy. The propagation mechanism is shown in Figure 3-16 where it can be seen that when released from 1m the mass appears to follow a triangular propagation with an angle of about 15°, as detected on the images of the test, i.e. horizontal projection (see Figure 3-16c). In the second case (Figure 3-16d), with 2 m height, the mechanism is composed of two parts, one at the beginning that follows a triangular shape with the same opening angle (about 15°), and a second one which continues almost straight along the deepest slope after the mass front has reached a certain width. When released from a height of 1 m, the mass has not sufficient time and distance to develop the latter mechanism.
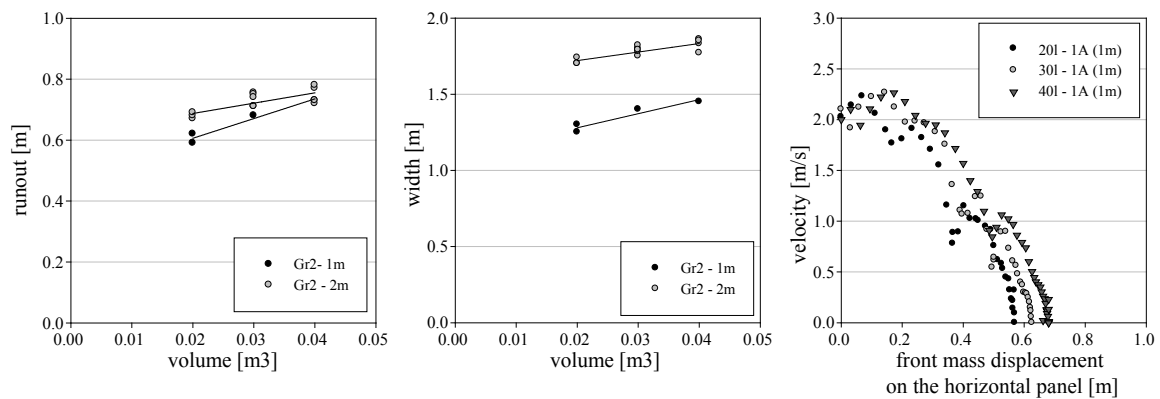
Figure 3-15 Volume and drop height influence on run-out, width and front mass velocity (1 release, box opening 20 cm×40 cm)
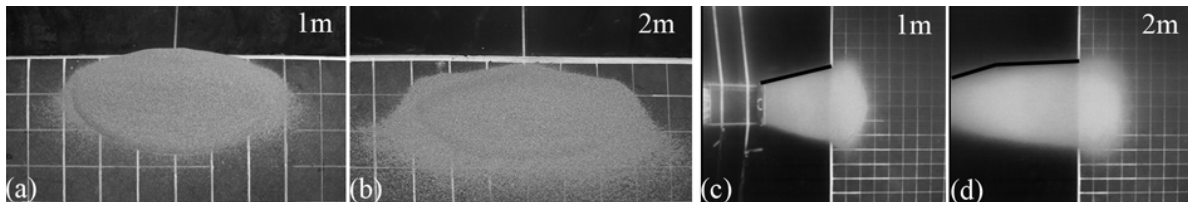
Figure 3-16 Final deposit pictures and difference in the propagation mechanism of a test made with 20 litres released from 1 and 2m height (1 release, box opening 20 cm×40 cm)

3.5.3. Consecutive releases

As already mentioned, to vary the number of consecutive releases means that the considered tests consist in releasing 40litres:

- once (40 litres)

- twice (20 over 20 litres) and

- four times (10 over 10 over 10 over 10 litres).

The series analysed here for this purpose are numbered 1B, 2B, 4B and 6B.

It can be observed that, by increasing the number of times by which a release of a certain volume is divided, the deposit length increases moderately, height increases significantly and run-out decreases (see Figure 3-17 and Figure 3-18). The width has a variable behaviour depending on the test configuration.

This behaviour can be explained after observing the effects of each release on the development of the deposit characteristics (see Figure 3-19 and Figure 3-20). It can be noticed that in actual fact, it is the first release which determines how far the entire volume will travel and the run-out does not evolve further during the test. The following releases are hindered by the deposit that has already taken shape at the base and they contribute mainly to building up the height of the deposit. In the case of consecutive releases, there is sufficient time for one mass of material to come to a standstill before the next one arrives as opposed to the previously discussed case (section 3.5.2) where there was a transfer of linear momentum between two moving masses.

In addition, the deposit morphology proved to be very dependent on the number of consecutive releases. When the mass is released at several times, a relatively conical deposit can be observed. As already mentioned above, each consecutive release arranges itself on the deposit formed by the previous release. This kind of behaviour is in agreement with in situ observations, like in the rather conical and narrow deposit of the Randa event in the Matter Valley (1991, Swiss Alps) which occurred over several hours. Even if the total volume of the failed mass was of 20 million m^3, the runout distance was significantly shorter than observed for other large rockslides of comparable volume. As explained by Eberhardt et al (2004), for cases where the slide mass does not fail as a singular event, the run-out and the characteristics of the final deposit do not depend on the entire failed volume but on the individual episodic events of smaller volumes.
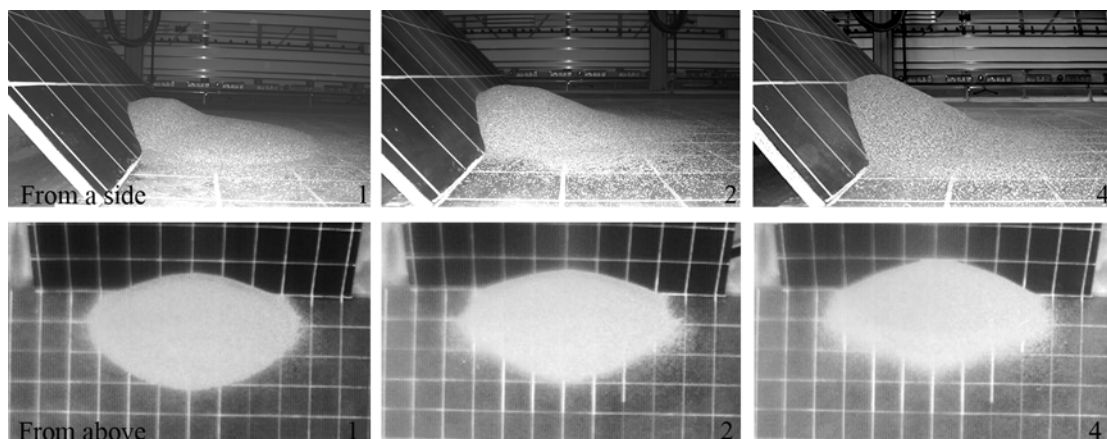
Figure 3-17 Influence of the number of consecutive releases on final deposit (40 litres, 1m drop height, box opening 20 cm×40 cm): pictures taken from a side (first row) and from above (second row) of 40 litres released in one (first column), two (second column) and four times (last column)
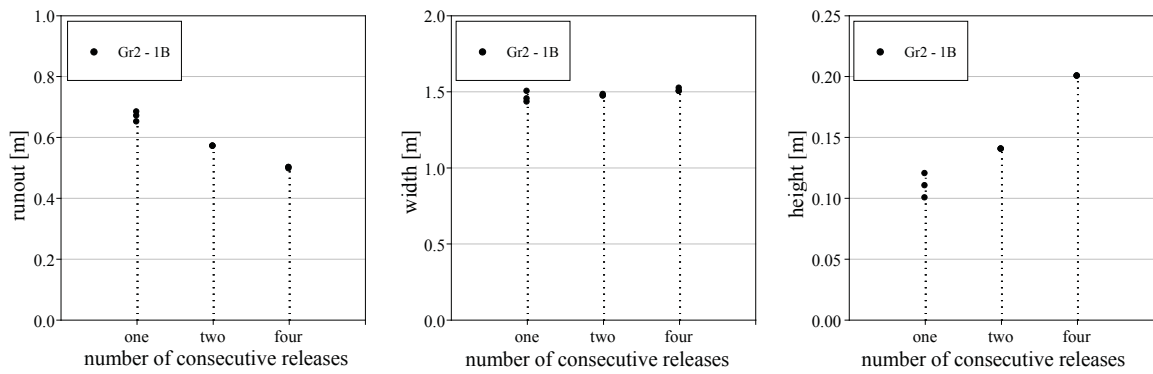
Figure 3-18 Influence of the number of consecutive releases on the final deposit characteristics (40 litres, 1m drop height, box opening 20 cm×40 cm)
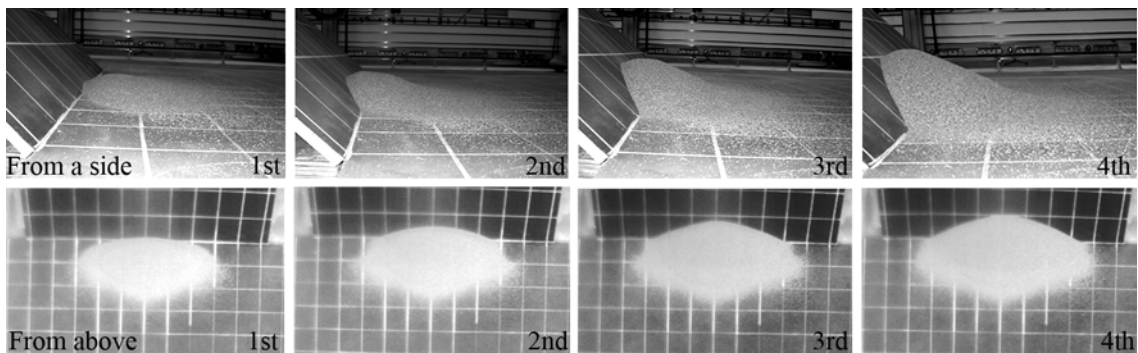
Figure 3-19 Evolution of the deposit with consecutive releases (1m drop height, box opening 20 cm×40 cm): pictures taken from the side (first row) and from above (second row) of the first release of 10 litres (first column). The second release of 10 litres (second column) made on the first release, the third (third column) made on the first two releases and the fourth release of 10 litres (last column) made on the first three releases.
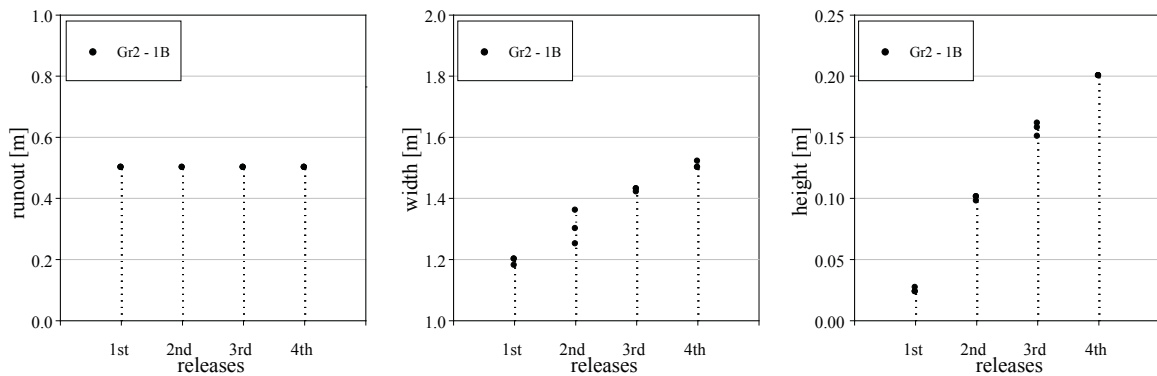
Figure 3-20 Evolution of the deposit characteristics with the consecutive releases (40 litres released in 4 times 10 litres, 1m drop height, box opening 20 cm×40 cm)

3.5.4. Geometry of the mass before failure

As mentioned in section 3.4, test series 1A and 4A have been useful in order to verify that the modifications of the experimental set-up haven't caused changes in the test results. A

difference of approximately 5% was observed between the deposit lengths of the two series. One explanation could be an unintended variation in the releasing geometry which means that the box has been filled up slightly differently in the two series. For test series 1A, the material has been rearranged after filling the box to create a flat surface more or less parallel to the opening of the box. However, for the 4A test series no rearrangement has been done after filling the box.

In order to verify the influence of this unintended variation in the releasing geometry, tests series 10flat has been carried out and compared with 6A (20 litres release). In series 10flat, the material has been left free to fall into the box without rearranging it afterwards (the word "flat" indicates this configuration), while in series 6A the material has been rearranged afterwards as in series 1A. The obtained results confirmed that the releasing geometry has a slight influence on the deposit morphology. To avoid this influence, the material in all other tests has been rearranged in the box prior to release to obtain the same conditions as in series 1A.

Moreover, analysing the influence of volume and releasing height, it can be noticed that, for the deposit characteristics, the regression lines do not pass through the origin of the coordinate axes but there is always a positive constant (see Figure 3-15). This could be due to the initial geometry. Normally the material has been poured into the box, covering the entire surface of the opening and resulting in varied depth of the filling (case a in Figure 3-3). Using series 6A, 8 and 9, the influence of the initial geometry on the deposit characteristics could be investigated. In section 3.2.1 and in Figure 3-3 the three studied situations are explained and schematically represented. Changing the opening capacity of the box (20cm height x 20cm width, 20cm height x 30cm width, 20cm height x 40cm width), first the filling depth has been varied maintaining the same volume (20 litres; case b in Figure 3-3) and then the volume (20, 30 and 40 litres) keeping almost the same filling depth (case c in Figure 3-3). The results have confirmed the hypothesis that the initial geometry has some influence on the deposit characteristics. Interesting remarks can be made observing the plots of the deposit widths (see Figure 3-21 case b and case c). By keeping the volume constant and increasing the width (case b) it is possible to observe an increase in the final deposit width. Otherwise, when varying the volume and the initial width (case c), the final deposit width varies accordingly to the initial width.

Differences in gate width also have little influence on runout. This can be due to the fact that the narrower shape of the container induces a kind of "arching" effect at the time of release. This leads to greater energy dissipation and consequently a shorter runout, when the opening gate decreases. This partly confirms results of Denlinger and Iverson (2001), who also performed tests varying the opening of the gate (even if not of the entire reservoir) and detected a decrease in the runout distance.

In some cases, the results are too scattered to establish a trend and the number of tests performed are not sufficient to draw any conclusion. However, they form a basis for future test design, which could be used to confirm the hypothesis that there are some slight interactions between the two parameters: volume and releasing geometry.
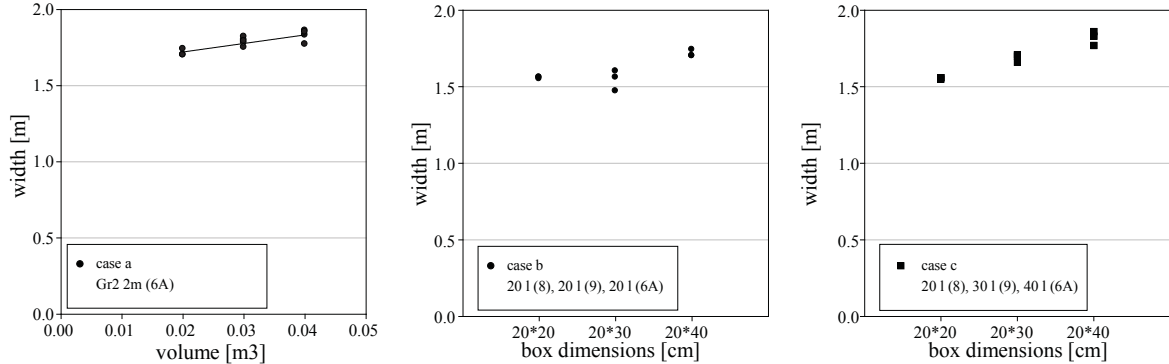
Figure 3-21 Influence of releasing geometry on deposit width (2m drop height, 1 release). The three cases studied are represented in Figure 3-3

3.5.5. Summary table

The following table is intended to give the reader a quick view of the qualitative relationships between the different factors and responses studied, as discussed above. The arrows indicate the following:

↗   : an increase of a parameter from a row chosen from the left column causes an increase of the characteristic at the head of the considered column;

↘   : an increase of a parameter from a row chosen from the left column causes a decrease of the characteristic at the head of the considered column;

↔   : an increase of a parameter from a row chosen from the left column has no significant effect on the characteristic at the head of the considered column.

-   : when no analysis has been done of the relationship

When a symbol is repeated twice it means that the influence is strongly marked.

Parameter	Runout	Deposit width	Deposit height	Deposit length	Deposit morphology	Mass front velocity
Materials From Hs to Gr2	↗	↗	↘↘	↗	Significantly different shape and features	↗
Materials From Gr2 to Gr4	↗ Slightly	↔	↗ Slightly	↗	Same features of the main deposit	↔
Volume	↗	↗	↗	↗	↔	↗ Only at the end
Fall height	↗	↗	↘	↗ Slightly	Different shape but same features	↗ Same behaviour
Number of releases	↘	Variable	↗↗	↗	Evolution to a "conic" shape	-
Each consecutive release	↔	↗	↗↗	↗	-	-
Releasing width; same volume	↗ Slightly	↗ Slightly	Variable	Variable	↔	↔
Constant releasing depth; different volume	↗	↗	↗	↗	↔	↔

Table 3-3 Summary table of the influences of factors on responses

3.6.   Conclusions on the preliminary campaign

From this preliminary experimental campaign, it is possible to draw several useful conclusions. The different parameters considered so far in the tests are:

- nature of released material: Hostun sand and two kinds of Aquarium gravels;

- material volume: 10-20-30-40 litres;

- releasing height: 1-2 m;

- releasing geometry: 20 cm x 40 cm, 20 cm x 20 cm and 20 cm x 30 cm;

- consecutive releases (for example 30 litres in one release or in three subsequent releases of 10 litres each).

The experiments have shown that deposit morphology is dependent on the type of material used: sand or gravel. The sand deposit shape, regular and compact, agrees well with many experiments described in the literature, while the Aquarium gravel deposit, which is quite irregular (a central zone with a small slope, but front, rear and sides strongly inclined), is in accordance with deposit characteristics of some real cases. The causes of the different gravel behaviour could probably be found in the shape and the angularity of the grains, although further tests need be carried out in the future to confirm this observation.

There is also a considerable difference in deposit morphology and dimensions when the event is the consequence of one large volume released at once or when the same volume is released in sequence. In the latter case, the characteristics of the final deposit do not depend on the entire volume but on the volume of the individual smaller volumes being released. This kind of behaviour is in agreement with in situ observations, such as the rather conical and narrow deposit of the Randa event in the Matter Valley (Swiss Alps) which occurred over several hours.

The analysis of the influence of the volume and drop height on the run-out shows that, even if an interaction exists between these two parameters, the run-out distance depends primarily on the volume and less on the drop height. Two different mechanisms of propagation can be observed when the sliding mass is released: triangular propagation with an opening angle of

about 15° detected on the horizontal projection, followed by a sliding along the deepest slope. The drop height influences this propagation as both the mechanisms are only observed when the mass is released from 2m. When the drop height is 1m, the mass reaches the horizontal panel before the second mechanism can develop. To end with, the final geometry depends to some extent on the initial geometry, especially with reference to the width.

For the range of parameters considered, the number of tests carried out is not yet sufficient to generalise the results obtained. In next chapter results obtained so far will be extended with tests performed with an improved experimental set-up. A new measuring device will allow to confirm and quantify the findings here presented and to study additional parameters and factors which could have an important influence on rock avalanche propagation. Among the new factors to be considered are the angle of the tilting panel, the roughness of the basal surface, and the use of bricks.

4.   Second experimental campaign

The second phase of the experimental study has consisted of about two hundreds tests. The basic phenomenon studied is the same as the one of the preliminary campaign: unconstrained flow of a mass of granular material down an inclined plane. In this case the mass consisted of dry rigid non-cohesive grains or small bricks, randomly poured into the reservoir before failure or piled orderly. The choice of the latter arrangement was motivated to model an idealised rock mass affected by discontinuity sets at the start.

Thanks to improvements in the experimental set-up it has been possible to easily vary some additional parameters such as the slope of the tilting panel, the material of the boards and consequently the roughness of the surface on which the mass flows and comes to rest. An innovative optical method based on fringes projection, developed and validated on preliminary experiments, permits to systematically retrieve the thickness of the final deposit and then to compute the position of its centre of mass. Additional responses have been as well evaluated, i.e the apparent coefficient of friction, the distance travelled by the centre of mass on the horizontal panel and the angle to the horizontal of the straight line connecting the centre of mass at the start and after deposition. Therefore the approach for this campaign has been more quantitative and it has been possible to formulate empirical models describing the relationships of the factors varied against the different responses considered. Part of these results are the object of a peer reviewed paper submitted recently (Manzella and Labiouse, 2008b).

In this chapter changes in the experimental set-up and improvements to the measuring device will be first illustrated, with particular attention to the fringe projection method which revealed to be a really useful measuring tool in granular avalanche experiments. The importance given to this description in the dissertation is due to the fact that the development and the adaptation of this method constitute one of the most significant parts of the present research, also in term of time dedicated to it, and one of the main objectives established beforehand. Then a parametrical study will be illustrated; a defined experiment is used as a benchmark and starting from this chosen test, the different parameters are varied and their effect on measured characteristics is described. Finally empirical analyses on the performed tests are presented and conclusions are drawn.

4.1. Improvements to the experimental set-up and measuring device

The geometry of the experimental set-up and the basic phenomenon studied haven't changed; the improvements have been done mainly to the tilting and releasing systems in order to be able to vary more easily the related factors. The parameters varied during the second experimental campaign are (see Figure 4-1):

- nature of released material: aquarium gravel2 and small bricks;

- arrangement of the bricks in the reservoir;

- slope angle (37.5°, 45°);

- fall height (1 m, 1.5 m);

- volume (20 l, 40 l);

- number of consecutive releases (40 litres in one or in two subsequent releases of 20 litres each);

- basal friction coefficient;

- discontinuity at the toe (sharp, curved).

In this section changes will be described in details together with a description of the fringe projection method (measuring tool).
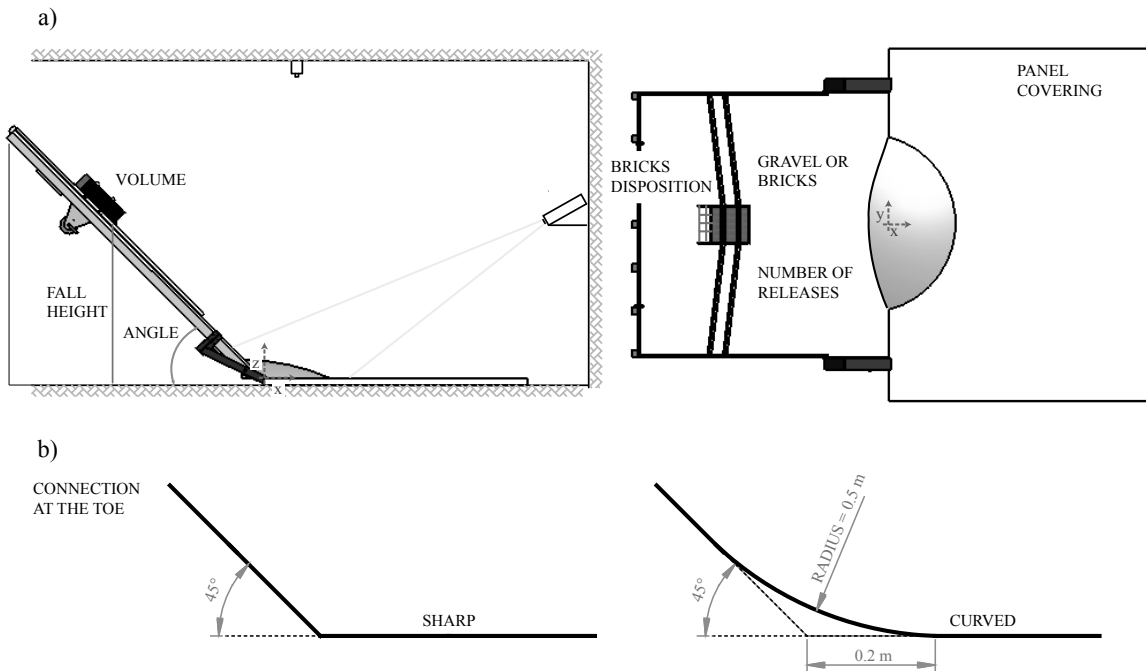
Figure 4-1 Factors varied: a) longitudinal and horizontal section of the model; b) Changes in the connection at the toe of the slope

4.1.1. New factors

Small terracotta bricks of 1.5 cm × 3.1 cm × 0.8 cm have been chosen as an additional material for this second campaign. This choice has been dictated by the fact that, as mentioned in chapter 2, very few works have been found in literature that use blocks instead of gravel or sand. Only one record has been found in literature of tests with several disaggregated blocks in the rock avalanche field (Okura et al, 2000), this is surely due to the practical difficulty of performing these experiments. Nonetheless, small bricks represent better the shape and the dimensions of the blocks relative to small topographic irregularities in real events. Therefore they could contribute to analyse phenomena which cannot be observed for gravel or sand flow at laboratory scale and consequently they could improve the understanding of the mechanisms involved in propagation.

Bricks have the characteristics listed in Table 4-1, where also the ones of the aquarium gravel2 are reported for comparison; more details about the latter material can be found in section 3.2.2. A tilting test has been used to measure the static and dynamic basal friction coefficients; a shear test has been carried out to measure the static friction at the interface between two bricks. Two different arrangements of the bricks before failure have been tested: poured in randomly in the container, called *Random bricks* (BrR) and shown in

Figure 4-2a, or piled orderly one on top of the other, called *Piled bricks* (BrP) and shown in Figure 4-2b. The choice of the latter arrangement was motivated to model a rock mass affected by discontinuity sets at the start and which during motion is free to disaggregate under the effect of gravity and collisions between the blocks. In order to arrange the bricks in the reservoir on the slope, they have been piled separately in a metallic box (see Figure 4-3a) that is gently inserted into the bigger one used for the test (see Figure 4-3b) and then totally removed. This preparation of piled bricks could take up to an entire day for tests with 40 litres. The longest dimension of the bricks (3.1 cm length) is perpendicular to the dip slope direction, whereas the larger surface (1.5 cm × 3.1 cm) is positioned parallel to the slope plane (see Figure 4-3b). For the 40 litres tests, bricks are thus disposed in 22 elements height × 11 elements width × 40 elements length (in the reservoir of 20 cm height × 40 cm width × 65 cm length). A space of one brick large has been left at each side to avoid a kind of vault effect. Despite the dimensions of a single element, the large quantity of blocks employed in a test (9680 bricks) makes the mass behave like a unique body. Single blocks can travel separately but the major part of the bricks is involved in the flow. This makes this work unique since it differs from the only tests of this kind performed before by Okura et al (2000) where experimental conditions and results suggest that blocks would behave individually, rather like a rock fall than a rock avalanche.

| Material | Size [mm] | Unit weight [kN/m³] | Static friction | | | Dynamic friction | |
			Internal [°]	On wood [°]	On forex [°]	On wood [°]	On forex [°]
Aquarium Gravel	D=0.5-4	14.3	34 ± 1	32 ± 1	28 ± 1	30± 0.5	23.5± 0.5
Random bricks	15x 31x 8	10.0	35 (interface)	-	30 ± 2		20± 0.5
Piled bricks	15x 31x 8	16.0	35 (interface)	-	30 ± 2		20± 0.5

Table 4-1 Gravel and bricks characteristics: size, unit weight, static friction angles

a)   b)
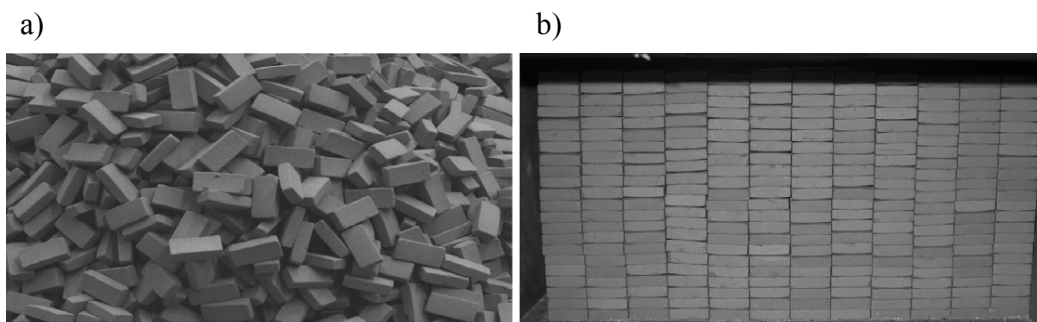
Figure 4-2 Bricks arrangements before release: a) random; b) piled
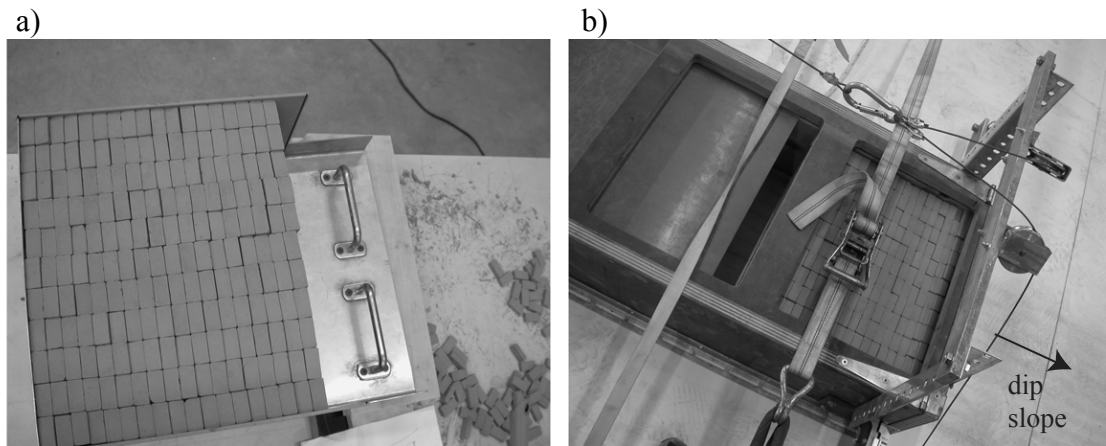
Figure 4-3 Set-up of piled bricks: a) preparation of the bricks in a metallic box; b) placement in the reservoir on the slope

Since the dynamics of rock avalanches is governed by topographic features of its paths and on the basal angle of friction (Pudasaini and Hutter, 2007), it has been chosen to vary other three factors within this campaign:

- The slope angle. Two inclinations have been chosen: 37.5° and 45° to the horizontal.

- The material of the panels' surface at the base, in order to change the basal friction. The surface of the model has been covered by two different materials: the one used so far, i.e. wood painted in black and a smoother one, i.e. a light PVC white sheet (forex). The respective angles of friction for Gr2 are reported in Table 4-1; bricks have been used only on forex.

- The "sharpness" of the discontinuity at the toe introducing a slightly curved connection. For the 45° slope the sharp angular connection between the two panels has been replaced by a smooth curve as shown in Figure 4-1b. The radius of the arc is of approximately 0.5 m.

4.1.2. Measurements and Fringe projection method

As for the preliminary experimental campaign, for each test, measurements of runout, width and length of the final deposit are taken manually while front mass velocity is derived from films with the specific process explained in section 3.3.2. In the case of bricks the front of the mass is sometimes difficult to be tracked and consequently it is necessary to replace the

pointer with the mouse; this operation leads to some discontinuities in the velocity plot, nonetheless, it is possible to deduce the general trend.

Principle of the fringe projection method

In order to recover the height information of the final deposit, several non-invasive techniques exist on the market, but some are really expensive, e.g. lasers and some are time consuming, e.g. theodolites. Inspired by the works of Denlinger and Iverson (2001), Pouliquen and Forterre (2002) and Desmangles (2003), it has been decided to employ a technique based on pattern projection. In phase-measuring profilometry, the depth information of the measured object is implicitly defined by certain trigonometric equations derived from image data (Zhang et al, 2007). The *fringe projection method* has been originally conceived for small objects and its adaptation and validation on present laboratory tests have been long lasting and sometimes difficult. Nonetheless once developed this technique constitutes a great tool for future research in this field since it provides a not expensive, rapid and easy to apply method. In addition all the necessary instruments were already in possession of the laboratory and further improvements, which have already been partly developed (see section 5.1.1), make it a promising technique to be easily employed in recovering the thickness of the mass in movement.

Alternating the superposition of two or more waves of light respectively in phase, i.e. constructive interference, and out of phase, i.e. destructive interference, causes alternating lines of dark and light. A fringe represents one wavelength of the source light and is measured from the centre of one bright line to the centre of the next. When fringes, i.e. parallel strips of dark and bright, are projected on an object, the strips will be straight and regularly spaced if the object is planar (see Figure 4-5a), whereas they will otherwise be distorted (see Figure 4-5b). Their divergence is related to the shape of the object that is coded in this fringe pattern. The geometrical relationship between the fringes pattern and the height of the object is schematically represented in Figure 4-4 and is expressed by the formula:

$$\Delta z = \frac{\Delta p}{\tan \psi} \qquad\qquad [4\text{-}1]$$

where Δp is the difference between the period of the fringes projected on the planar surface (p_p) and the apparent period (p_a) of the fringes projected on the object and Ψ is the angle between the incidence of light and the observation direction (Desmangles, 2003). Distortion of the pattern will be more evident and thus accuracy of Δz higher, if this angle is near to 90°. In any case Ψ must not be equal to 0°, i.e. the angle of incidence of the projection and the one of the observation direction must be different, otherwise the fringes will appear straight even on a non planar object.
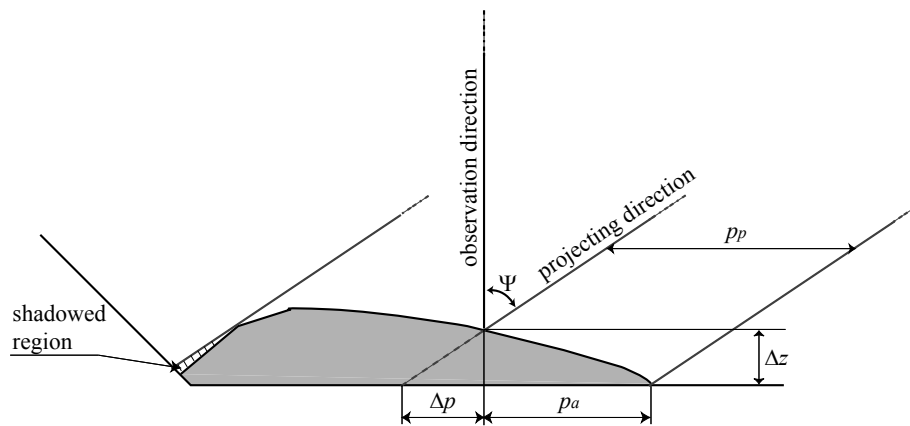
Figure 4-4 Schematic representation of the geometrical relationship between the period of the fringes and the height of the object, inspired from Desmangles (2003)

With equation [4-1] only the points which are located at the centre of the bright or dark light are taken into account. To have the height information of the entire frame it is possible to relate the height to the phase, using the so called phase map, instead of the period of the fringes. The phase in each pixel is obtained by means of different algorithms using the intensity, *I*. When a sinusoidal pattern is projected on a 3D object, the image can be modelled as:

$$I(i,j) = I_0 + I_M \cdot \cos \varphi(i,j) \qquad\qquad [4\text{-}2]$$

Where I_0 and I_M represent the background and the modulation intensities and $\varphi(i,j)$ denotes the phase in a given point *(i,j)* of the image. The phase map is a graphical representation of $\varphi(i,j)$ (Cochard and Ancey, 2007).

The method can be thus divided in three main steps:

1. creation of fringes and their projection on the object surface

2. registration of the object optical print (phase map)

3. retrieval of the height information from the phase map (phase unwrapping and calibration procedure)

1. To create fringes it is possible to resort to different techniques, e.g. an interferometer (Desmangles, 2003) or a micro-mirror projector (Cochard and Ancey, 2007). In the present case the pattern has been produced with Matlab by drawing parallel strips of different shades of grey at a fixed periodicity. A sequence of 256 greys starting from black (0) to white (255) has been used. These images have been projected with an EPSON EMP-7250 (a simple projector for PC) as a PowerPoint presentation. Images are captured with a NIKON COOLPIX 4500, a common and not expensive digital camera.

2. In order to obtain the phase map from equation [4-2] it is possible to use various algorithms (for further information see Creath, 1993 and Ghiglia and Pritt, 1998), which employ one or more images depending on the desired accuracy and on the velocity of the process. For a mass in relatively fast movement it is necessary to use an algorithm implying only one image, e.g. the method of Fourier used also in the framework of the present study for the benchmark exercise presented in Chapter 5.2. Nonetheless techniques using several images, called phase-shifting method, provide higher accuracy. Since most measurements undertaken for the present study are of the final deposit at rest it has been possible to use the phase-shifting method. More specifically formula [4-3] has been used that considers in each point the intensity $I(i,j)$ of three different captures of the projection of the same fringes pattern shifted each time of 1/3 of its period (see Figure 4-5).

$$
\begin{cases}
I_1(i,j) = I_0 + I_M \cdot \cos\big(\varphi(i,j)\big) \\
I_2(i,j) = I_0 + I_M \cdot \cos\big(\varphi(i,j) + \pi/3\big) \\
I_3(i,j) = I_0 + I_M \cdot \cos\big(\varphi(i,j) + 2\pi/3\big)
\end{cases}
\qquad [4\text{-}3]
$$

$$
\varphi = \arctan\left(\sqrt{3} \cdot \frac{I_2 - I_3}{2I_1 - I_2 - I_3} \right)
$$

With this equation it is possible to obtain the phase map of a certain frame on which fringes are projected. As shown in Figure 4-5 and Figure 4-7a in the present case the maps have been computed from pictures of the deposit and of what has been chosen to be the reference planar surface (where z is considered equal to zero). This is done by a Matlab routine (see

appendix I) developed by Michael Liebling (Biological Imaging Center, Beckman Institute California Institute of Technology) and adapted by Steve Cochard (Laboratoire d'Hydraulique Environnementale, LHE, EPFL), inspired from the work of Takajo and Takahashi (1988a and b).

a)

b)
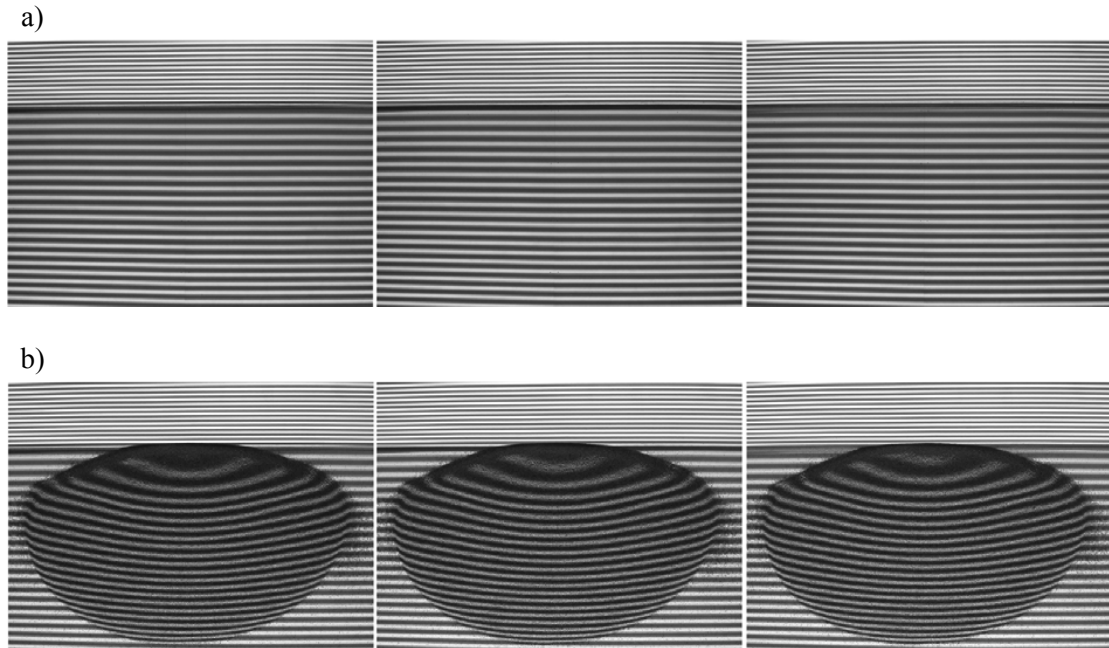
Figure 4-5 Images used for the phase calculation of a test of 40 litres of gravel released from 1 m height on a 45° inclined board covered with forex. On the planar surface and on the object, the same fringes are projected, shifted 1/3 of the period between each image. It is possible to observe the distortion of the fringes pattern caused by the shape of the deposit

This retrieval of the phase map is sometimes hindered by the presence of noises due to shadowed or hidden regions which blur the sharp frontiers of the phase (see Figure 4-4 and Figure 4-7a). Since all the information in these regions is lost, the direction of observation of the camera has been placed perpendicularly to the horizontal plane to avoid that there could exist any hidden parts of the deposit to the camera. Nonetheless shadowed regions could still appear, e.g. when the rear part of the deposit is not covered by the projected image. In this case it is possible to place the projector higher and more inclined, but a compromise has to be found between the effort made to avoid the shadow in some regions and the fact that the angle between the projecting and acquiring directions must be as close as possible to 90° (Cochard and Ancey, 2007). In the case of tests with bricks, the shape and the dimensions of each brick lead to several shadowed regions spread all over the surface of the deposit (see Figure 4-8a), this bedevil the retrieval of the phase map. It is possible to

solve the problem with the use of a larger wavelength, as it can be seen in Figure 4-8b. Even if this is done to a certain detriment of the accuracy, the results are still satisfactory and the deposit morphology can be computed.

3. The direct solutions to the equations [4-3], have a limited range from $-\pi$ to π and they are called the wrapped phases, see Figure 4-7a. An unwrapping process is needed to recover the original phases where the depth information is coded. Unwrapping a phase consists in developing the wrapped phase obtained with [4-3] by calculating the derivative of the phase and then correct all points with values greater than π or smaller than $-\pi$ by adding or subtracting a multiple of 2π. Then the phase derivative is integrated and the searched unwrapped phase is obtained (Zhang et al, 2007). The result of the phase unwrapping of a test carried out in the present research is shown in Figure 4-7b.

Calibration procedure and adaptations to laboratory tests

The calibration procedure involves the transformation of the position of the pixel *(i,j)* and the phase values into the x, y, z metric Cartesian coordinates system shown in Figure 4-1. The height of the object is proportional by a factor *P* to the difference between the unwrapped phase map of the object (φ_{obj}) and the unwrapped phase map of the reference planar surface (φ_{ref}) by means of the formula:

$$\Delta z = P \cdot \Delta \varphi = P \cdot \left(\varphi_{obj} - \varphi_{ref} \right) \tag{4-4}$$

According to equation [4-1] and Figure 4-4, *P* is a factor depending on the period of the fringes and on the geometry of the set-up:

$$P = p_p \big/ \left(2\pi \cdot \tan \psi \right) \tag{4-5}$$

Nonetheless, p_p and Ψ are difficult to be determined since this requires to accurately locate the position of the camera and the projector and the period of the fringes. An additional calibration should be done to report the image x, y coordinates to the set-up reference system (see Figure 4-7c). In the present research the instruments used for phase-shifting profilometry have been displaced for each test, changing the distance and the angle of incidence of the projection and the zoom of the camera. This allows covering only the area interested by the final deposit to increase accuracy (by decreasing the pixel dimensions) and

it is useful to minimise the shadowed regions and consequently noises on the phase map. Therefore a time-consuming calibration to determine p_p and Ψ each time the geometry of the set-up has been changed was unlikely to be done. For this reason, in order to simplify the process, instead of computing P, a factor F has been used that can be more easily obtained for each test. It is equal to the height of the deposit in a specific point with known image and Cartesian coordinates measured directly on the deposit over the $\Delta\varphi$ value at the corresponding point obtained with the calculations. Since $\Delta\varphi$ and Δz are directly proportional according to equation [4-4] a point that could be determined easily in both systems is the maximum of the two variables. So equation [4-4] for a general point (i,j) on the frame becomes:

$$\Delta z_{i,j} = F \cdot \Delta\varphi_{i,j} = \frac{z_{max}}{\Delta\varphi_{max}} \cdot \Delta\varphi_{i,j} \qquad\qquad [4\text{-}6]$$

To determine the x, y coordinates of the images, before each projection a frame with known dimensions has been delimited with a plastic band. Afterwards a script in Photoshop has permitted to crop the image according to the known area and to reduce to the minimum eventual distortions due to the camera lens (see Figure 4-6). A routine in MATLAB has been developed to automatically perform the whole calibration for all tests (see appendix I).

a)　　　　　　　　　　　b)
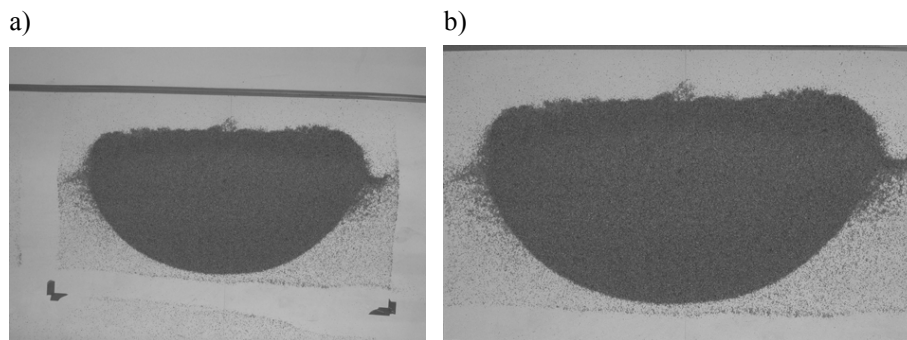
Figure 4-6 Work on the images done with Photoshop: a) original image; b) cropped image

A hypothesis to apply equation [4-6] is to have exactly the same conditions between the moment when photos of the deposit are taken to calculate φ_{obj} and the moment when photos of the reference surface are taken to calculate φ_{ref}. Even the slightest movement in the position of the instruments or a different adjustment in the photo camera parameters induces differences in the phase map and thus bedevils the results. In the present experiments a

significant time could pass between these two moments and the camera used does not allow some manual settings of the capture parameters, e.g. the focus. To force the automatic adjustment of the camera to be equal in all situations, darkness has been imposed in laboratory when fringes were projected. In addition the camera and the projector have been fixed to metallic frames separated from the testing boards to avoid that eventual vibrations due to the carrying out of a test could cause even the slightest difference in the position of the measuring devices. Despite all these precautions sometimes the two sets of three images relative to the reference plane (Figure 4-5a) and to the object (Figure 4-5b) have revealed a certain mismatch of the projection. To be able to exploit the measurements also in this case, even with a lower accuracy, a routine has been developed that reproduces the fringes pattern of a border section of the φ_{obj}, where no deposit is detected, to all the frame and use this as φ_{ref}.

The accuracy in the measurement of the height of the deposit varies from 3 mm for the best results to 5 mm. These values have been evaluated measuring the height of some points of the deposit with known x and y coordinates and comparing it with the height calculated with the fringe projection method. The accuracy has been considered satisfactory taking into account the fact that it is in the order of the maximum diameter of the gravel grains and of the smallest dimension of the bricks. Consequently for a large part of the tests even a layer of one element height could be detected. Spatial resolution in x and y directions is intrinsic to the recording media and the dimensions of the frame delimited by the plastic band. For this reason pictures have been taken with the highest possible resolution of 2272×1704 pixels and the zoom has been changed to cover only the area of interest. If an average frame is considered of 2 m $\times$ 1.5 m the dimension of a pixel is of about 0.8 mm. Figure 4-9 shows the final results obtained with the fringe projection method for a test of 40 l of gravel released from 1 m height on a 45° inclined smooth board.
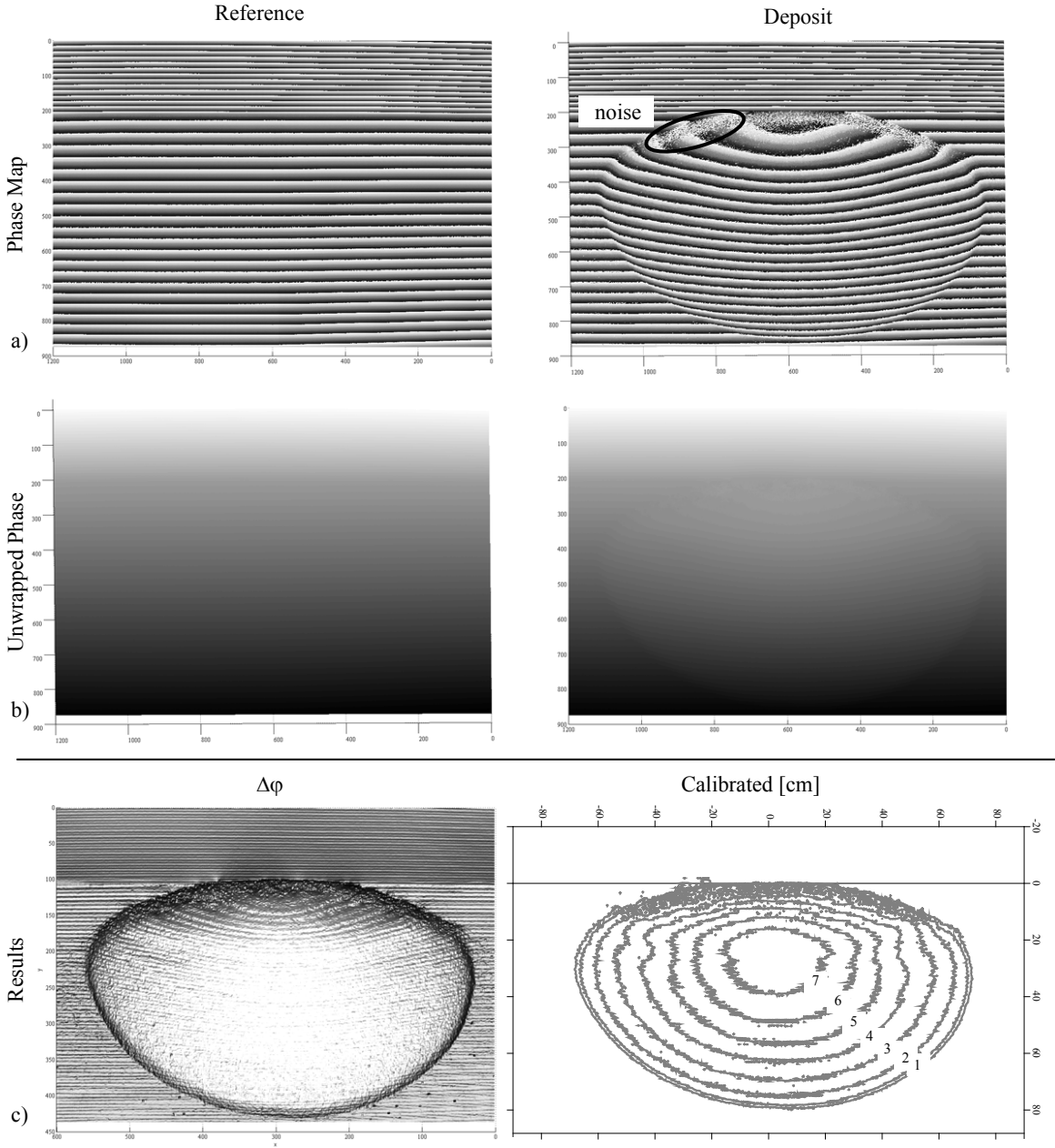
Figure 4-7 a) Phase map; b) phase unwrapping; c) results of the fringe projection method; release of 40 litres of gravel, from 1 m height, on a 45° inclined board covered with forex
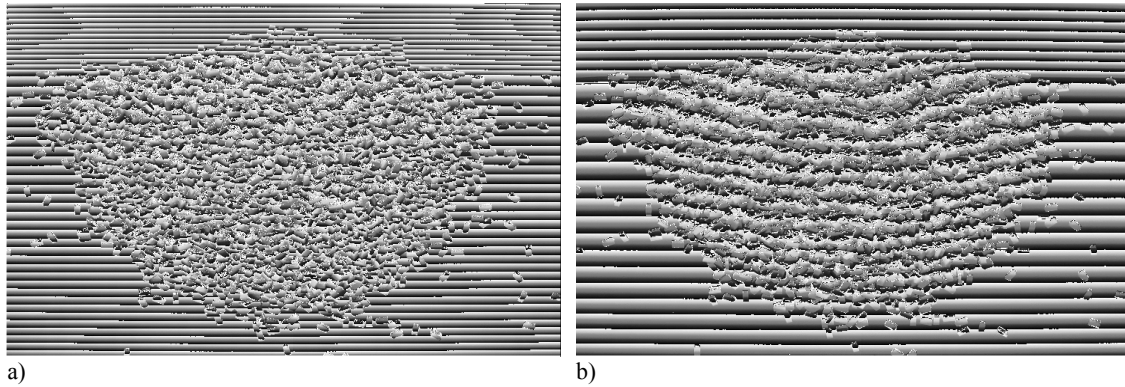
Figure 4-8 Comparison between the phase maps for tests with bricks: a) smaller wavelength normally used for gravel b) larger wavelength; it is possible to see how in a) it is difficult to distinguish the fringes projected on the deposit, whereas in b) the phase map can be retrieved; release of 20 litres of piled bricks, from 1 m height, on a 45° inclined board covered with forex
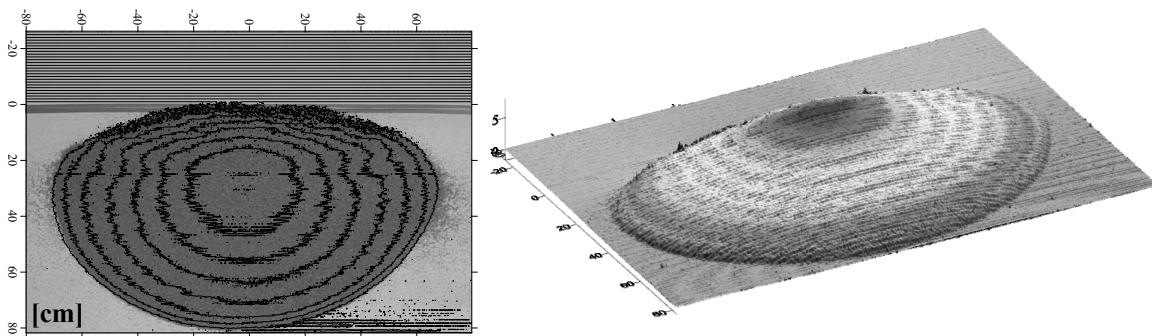
Figure 4-9 Fringe projection method results: level curves at each 1 cm overlapped on a deposit picture and 3D view; release of 40 litres of gravel, from 1 m height, on a 45° inclined board covered with forex

4.1.3. Testing programme and procedure

Among the series of tests carried out at the laboratory, Table 4-2 shows the ones used for the analysis illustrated in this chapter. The whole list with the measurements done follows in appendix II.

In the table, BrR refers to "Random bricks", i.e. bricks poured in randomly at start in the release container (see Figure 4-2a) and BrP to "Piled bricks", i.e. bricks piled orderly one on top of the other (see Figure 4-2b). Series 4A and 4B are a part of the same series reported in Table 3.2, where it has been possible to apply the fringe projection method.

- All the series and their related B ones have been used to verify whether the statements made in section 3.5.3 concerning the progressive failure of the mass.

- Series 4A together with 12, and so for the couples of series 13-14, 15-16, 17-18, 19-21, 20-22, 23-25, 24-26 have been used to test the influence of the fall height and volume on the responses considered.

- Series from 11 to 14 studied the behaviour of gravel flows on wood and can be compared to series from 15 to 18 which studied its propagation on forex.

- The couples of series 11-13, 12-14, 15-17, 16-18, 19-23, 20-24, 21-25 and 22-26 are useful to understand the influence of the slope angle.

- Comparing series from 15 to 18 and series from 19 to 26 and 28, 29 and 30 it is possible to understand the influence of the material used.

- The two consecutive series 19-20, 21-22, 23-24, 25-26 and 29-30 help to verify the effects of disposition of bricks before failure.

- Finally series from 27 to 28 have tested the effects of the sharpness at the toe of the slope.

Series Number	Granular Material			h [m]		V [l]		Release number		Slope [°]		Surface Material		Connection at the toe	
	Gr2	BrR	BrP	1	1.5	20	40	1	2	37.5	45	wood	forex	sharp	curved
4A	Gr2			1		20	40	1			45	wood		sharp	
4B	Gr2			1			40		2		45	wood		sharp	
12	Gr2				1.5	20	40	1			45	wood		sharp	
13	Gr2			1		20	40	1		37.5		wood		sharp	
14	Gr2				1.5	20	40	1		37.5		wood		sharp	
15	Gr2			1		20	40	1			45		forex	sharp	
15B	Gr2			1			40		2		45		forex	sharp	
16	Gr2				1.5	20	40	1			45		forex	sharp	
16B	Gr2				1.5		40		2		45		forex	sharp	
17	Gr2			1		20	40	1		37.5			forex	sharp	
17B	Gr2			1			40		2	37.5			forex	sharp	
18	Gr2				1.5	20	40	1		37.5			forex	sharp	
18B	Gr2				1.5		40		2	37.5			forex	sharp	
19		BrR		1		20	40	1			45		forex	sharp	
20			BrP	1		20	40	1			45		forex	sharp	
20B			BrP	1			40		2		45		forex	sharp	
21		BrR			1.5	20	40	1			45		forex	sharp	
22			BrP		1.5	20	40	1			45		forex	sharp	
22B			BrP		1.5		40		2		45		forex	sharp	
23		BrR		1		20	40	1		37.5			forex	sharp	
24			BrP	1		20	40	1		37.5			forex	sharp	
24B			BrP	1			40		2	37.5			forex	sharp	
25		BrR			1.5	20	40	1		37.5			forex	sharp	
26			BrP		1.5	20	40	1		37.5			forex	sharp	
26B			BrP		1.5		40		2	37.5			forex	sharp	
27	Gr2				1.5	20	40	1			45		forex		curved
27B	Gr2				1.5		40		2		45		forex		curved
28	Gr2			1		20	40	1			45		forex		curved
29		BrR		1		20	40	1			45		forex		curved
30			BrP	1		20	40	1			45		forex		curved

Table 4-2 Tests series considered for the second experimental campaign

Considering that the material covering the boards has been changed only once during the whole experimental campaign, it is here possible to resume the procedure of a test, as it has been done for the preliminary experimental campaign. The main steps are as following:

1. The experimental set-up and measuring devices are checked.

2. The container is placed according to the height and is fixed to the panel with a system of belts. The tilting panel is placed at 20°, the minimum possible angle, in order to be able to step on the board to pour the material into the reservoir and to place the piled bricks according to the procedure shown in section 4.1.1.

3. The tilting panel is placed at the desired angle according to the series of tests to be performed.

4. The parameters of the high speed camera are settled through the dedicated PC software, i.e. choice of the lens aperture, exposure time according to light conditions.

5. The camera is started

6. The spring-loaded bottom gate of the reservoir is opened and the material is instantaneously released.

7. The camera is stopped immediately after the material has come to rest and the part of the film that covers the test is registered.

8. A plastic band is placed around the area of the deposit (see Figure 4-6a) and the dimensions of the rectangular frame are manually measured and noted on the Excel sheet.

9. The projection of the fringes is started and the projector is placed according to the most suitable position to minimise shadowed regions and maximize accuracy as explained in previous section.

10. The photo camera is fixed to a metallic frame with acquiring direction perpendicular to the horizontal board. The zoom is changed to cover just the frame of interest, the aperture is fixed to the minimum (2.7), and the shutter speed is set between 1 s and ¼ s depending on the exterior light conditions.

11. The lights are switched off and fringes are projected, some shots are taken to verify the quality of the photos. The three images of the fringes shifted of one third of their period are projected on the deposit and pictures are taken in remote control in order to avoid any displacement of the camera. Lights are switched on while the camera is left on stand by.

12. The manual measurements of the deposit dimensions are taken and noted on an Excel sheet. The height of the highest point of the deposit on the horizontal panel is measured with a thin shank slowly inserted in the deposit, avoiding major disturbance of the mass. This will be useful to calculate the F factor of equation [4-6], as seen in previous section.

13. The material is swept away and the model is accurately cleaned.

14. The lights are switched off, the camera and the projector are remotely powered on and three shots of the fringes shifted of one third of their period on the reference plane are taken.

This procedure is followed attentively for each test in order to assure consistency and repeatability. A test is performed three times for each set of parameters, with the exception of tests with piled bricks that are carried out only two times due to limit in time.

4.2. Parametrical study

The whole experimental campaign carried out at the EPFL consists of about 300 tests that have already been partly illustrated in the previous chapter. This section only considers the tests (approximately 200) in which the height distribution of the deposit as well as its centre of mass position could be gathered by means of the fringe projection method. In this section considerations will be drawn on the influence of the factors considered. Also in this case the approach has been mainly intuitive and qualitative and analyses are based on observations and comparisons of the tests. The two experimental campaigns considered in the present study will be compared when this is possible.

The number of series considered is large (see Table 4-2). To better visualize and resume the results obtained for the factors considered, a test is chosen as representative and used as a

benchmark for comparison with the others. The benchmark concerns a mass of 40 litres of gravel released from 1 metre height on a 45° slope covered with forex. Results of this test are shown in Figure 4-10. As a support to the parametrical study, one experiment is then considered where one factor is varied relatively to the benchmark one. The tests considered for the comparison have the characteristics listed in Table 4-3. The first is the benchmark test (bold and italic) and for the following ones, only one parameter (bold and italic) at a time is varied. The main gathered data are also reported in the table, separated between manual and computed measurements.
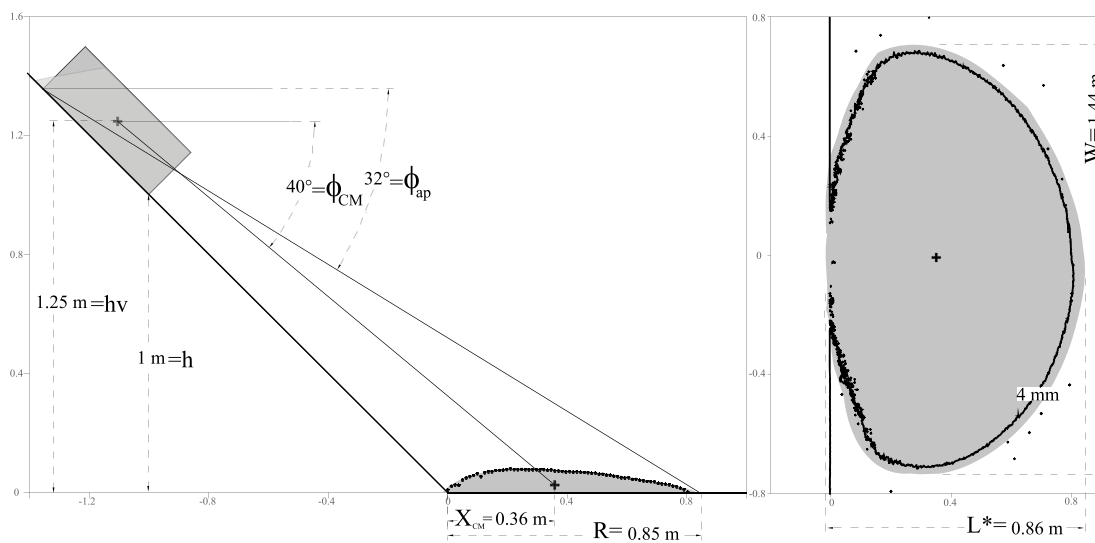
Figure 4-10 Gathered data release of 40 l of gravel, from 1 m height, on a 45° inclined board covered with forex

Material	Test conditions							Measures with tape			Computed data			Fig
	Slope	Fall	V	Base	Slope	Series		L*	R	W	X_{CM}	ϕ_{CM}	ϕ_{ap}	n°
	[°]	[m]	[l]	friction	Toe	number		[m]	[m]	[m]	[m]	[°]	[°]	[-]
Gr2	*45*	*1*	*40*	*smooth*	*sharp*	*15*		0.86	0.85	1.44	0.36	~40	~32	4-10
Gr2	45	1	*20+20*	smooth	sharp	15B		0.82	0.72	1.33	0.21	~43	~33	4-11
Gr2l	45	1	*20*	smooth	sharp	15		0.66	0.72	1.30	0.36	~40	~32	4-12
Gr2	45	*1.5*	40	smooth	sharp	16		0.87	1.06	1.57	0.53	~39	~32	4-13
Gr2	45	1	40	*rough*	sharp	4A		0.70	0.57	1.45	0.16	~43	~35	4-15
Gr2	*37.5*	1	40	smooth	sharp	17		0.86	0.75	1.40	0.24	~35	~28	4-16
BrR	45	1	40	smooth	sharp	19		0.93	0.84	1.40	0.37	~40	~32	4-18
BrP	45	1	40	smooth	sharp	20		1.23	1.15	1.39	0.39	~39	~28	4-19
Gr2	45	1	40	smooth	*curved*	28		1.03	1.27	1.70	0.73	~33	~27	4-21

Table 4-3 Test conditions and overview on the gathered data

In addition to the straightforward manual measurements, i.e. runout, width and length of the deposit, characteristics such as ϕ_{ap}, X_{CM} and ϕ_{CM} are computed.

In literature on rock avalanches it is possible to find several definitions of runout. Here it is considered as the distance travelled by the mass front on the horizontal panel as opposed to the total travel distance often used in literature. This measurement is not affected by intrinsic differences in length caused by the variation of some parameters such as fall height or slope inclination. The apparent coefficient of friction or Fahrboschüng, i.e. ϕ_{ap}, is considered as the angle to the horizontal of the straight line connecting the top on the inclined board of the mass before failure and the distal end of the deposit. X_{CM} represents the distance travelled by the centre of mass on the horizontal panel. Together with Z_{CM}, i.e. the height of the centre of the mass of the final deposit, X_{CM} is computed by a routine in MATLAB using the data gathered with the fringe projection method. ϕ_{CM} is the angle of the energy line, i.e. the angle between the horizontal and the straight line connecting the centre of mass at start and after deposition. To obtain ϕ_{ap} and ϕ_{CM}, the shape of the mass before release has been approximated as a cuboid (dark grey rectangle at the top of the slope in Figure 4-10) neglecting that, in reality, the rear part of the mass accumulates following the angle at rest of the material (light grey trapezoid overlapped to the rectangle at the top of the slope in Figure 4-10).

4.2.1. Consecutive releases

For all the sets of parameters studied in the second experimental campaign (see Table 4-2), the results obtained about the influence of consecutive releases confirm previous considerations stated in section 3.5.3; by means of the fringe projection method it is here possible to better visualise and quantify these statements as shown in Figure 4-11 for the same total volume of 40 litres released at once or at two different times (20 over 20 litres).
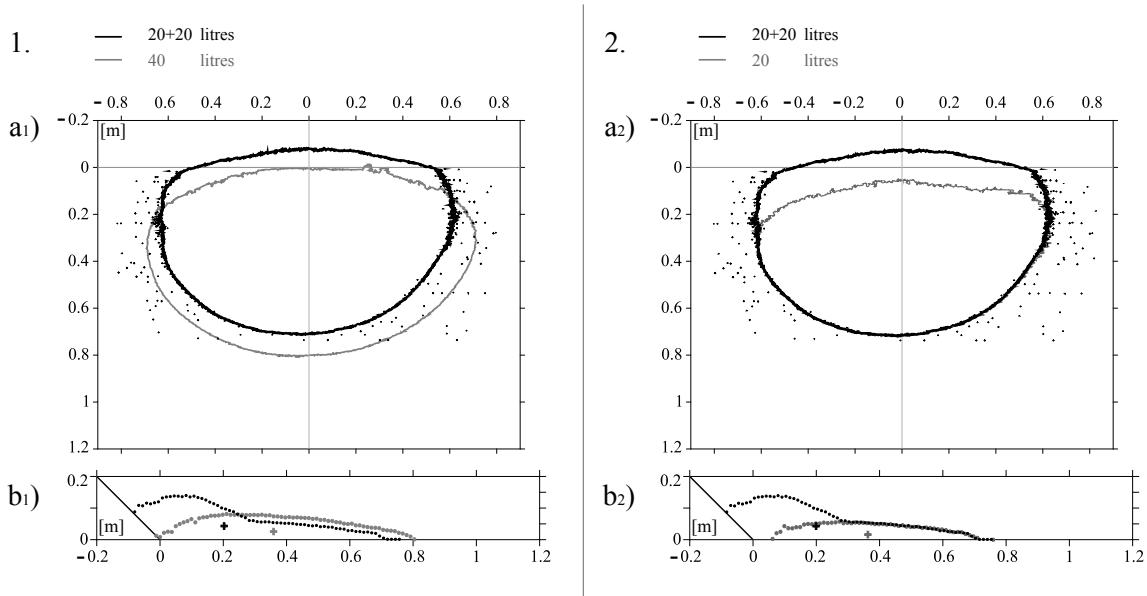
Figure 4-11 Influence of consecutive releases:1. a_1) horizontal and b_1) longitudinal deposit cross-sections of 40 l (grey) versus 20+20 l (black); 2. a_2) horizontal and b_2) longitudinal deposit cross-sections of 20 l (grey) versus 20+20 l (black)

As seen in section 3.5.3, by increasing the number of times by which the release of a certain volume is divided, the height of the deposit increases significantly and its runout decreases (see Figure 4-11a_1 and b_1). As a matter of fact, it is the first release which determines how far the entire volume will travel (see Figure 4-11a_2 and b_2). The following release is hindered by the deposit that has already taken shape at the base and it contributes mainly to building up the height of the deposit. As a consequence the centre of mass of the final deposit travels a shorter distance and the travel angle is higher. In addition, the deposit morphology proved to be very dependent on the number of consecutive releases. When the mass is released at several times, a relatively conical deposit can be observed. This kind of shape is very similar to the conical pile built up by sand particles flowing in a hourglass and is in agreement with in situ observations, as in the case of the Randa event in the Matter Valley (1991, Swiss Alps) which occurred over several hours.

4.2.2. Volume and fall height

Figure 4-12 illustrates for test with 20 litres (black markers and lines) compared with the reference one of 40 litres (grey markers and lines):

- the deposit horizontal section (plot a): the contour line is 4 mm above the horizontal panel to avoid noises caused by the fringe projection method error;

- the longitudinal cross-section of the deposit along the symmetry axis of the experiments (plot b);

- the position of the centre of mass (marked by a cross on b);

- the velocity of the mass front on the horizontal panel as a function of the travelled distance (plot c).

Similar figures will be used in the following for each tests listed in Table 4-3 (black markers and lines) compared with the reference one (grey markers and lines).

Figure 4-12 Influence of the released material volume: 20 l (black) versus 40 l (grey). Horizontal (a) and longitudinal (b) deposit cross-sections; front mass velocity on the horizontal panel (c)

As it can be supposed an increase of the volume leads to an increase of all the deposit characteristics. On the other hand, as already detected qualitatively in the preliminary campaign (see section 3.5.2), the deposit morphology does not suffer any significant change: the deposit is bigger but has mainly the same shape (see Figure 4-12a and b). This is valid for all the sets of parameters studied. Nonetheless the deposit morphology is slightly dependent on the releasing height. When dropped from a higher point, the mass tends to flatten out (see Figure 4-13a and b).
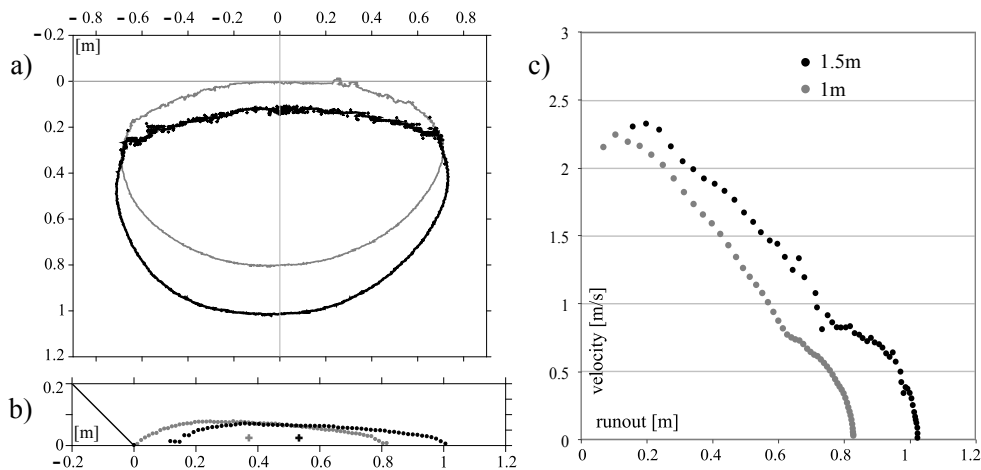
Figure 4-13 Influence of the fall height: 1.5 m (black) versus 1 m (grey). Horizontal (a) and longitudinal (b) deposit cross-sections; front mass velocity on the horizontal panel (c)

Observing Figure 4-12a and b, it is possible to notice that even if an increase of the volume induces a greater spread of the final deposit in all the directions and the runout is consequently longer, the centre of mass travels the same distance on the horizontal panel in both cases. This seems to confirm and give experimental evidence to the suggestion made by Davies (1982) and Davies and McSaveney (1999 and 2003) that the centre of mass of long-runout rock avalanches travels the same distance as if the coefficient of friction had been "normal" and that the exceeding travel distance is caused actually by the spreading of the mass. On the other hand, the exceeding travel distance is not always related only to an extra spreading of the mass. When the fall height increases (Figure 4-13a and b), the whole mass translates further and both the centre of mass and runout vary of the same length.

In addition it can be observed in Table 4-3 for series 15 and 16 that when the mass falls from a higher point, it reaches yes longer distance but the Fahrböschung is equal to approximately 32° for both fall heights. This is also confirmed by the back-analysis of real events performed by Corominas (1996) who affirmed that the fall height does not influence the value of ϕ_{ap} but does affect the horizontal travelled distance.

Front mass velocity

The front mass velocity pattern follows a rather similar behaviour for all the studied tests: an initial homogeneous decrease until there is a sudden attenuation of the deceleration, marked by a discontinuity in the plots, followed by a second part where the mass comes to rest. This is in agreement with the description of the behaviour of a loose material entering its

accumulation zone and with the theory of transfer of momentum given by Van Gassen and Cruden (1989) and even earlier by Heim (1932). These theories describe how a mass of debris flows like a stream along its course and how the front particles decelerate under the effect of friction after entering the accumulation zone (shown by a homogeneous deceleration in the velocity plot of e.g. Figure 4-12c and Figure 4-13c). Simultaneously the rear particles enter the accumulation zone at a higher velocity and collide with those slowing down ahead. Consequently the front and the rear parts interact through momentum transfer that induces a propulsion of the front particles (slower deceleration marked by a discontinuity on the front mass velocity plot in e.g. Figure 4-12c and Figure 4-13c) and a deceleration of the rear ones. Afterwards the material at the front deposits and comes to a complete stop (final part of the plot). According to Van Gassen and Cruden (1989), this process, detected here only for the front of the mass, develops throughout the accumulation zone causing the halt of the whole mass.
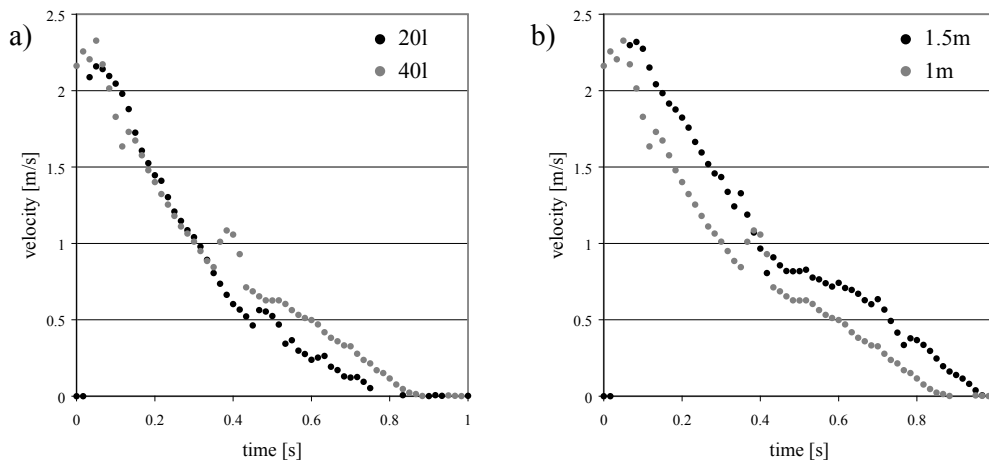
Figure 4-14 Plots of the front mass velocity against time: a) volumes of 20 l (black) versus 40 l (grey); b) fall heights of 1.5 m (black) versus 1 m (grey)

As can be observed in Figure 4-14, the plot of velocity against time follows a straight line in the first part describing a uniform decelerated motion of the front mass due to friction. The impulse given by the rear part of the mass affects this motion and provokes an attenuation of the initial deceleration, marked in the plot by another straight line but with a smaller gradient. This confirms the theory of Okura et al. (2000) which suggests that collisions between the individual blocks of the mass flow induce an acceleration of the mass front. In the case of a higher fall height, and thereby a higher initial potential energy, the mass enters

the accumulation zone with a greater velocity (Figure 4-14b). This leads to a simple translation of the velocity plot. For different volumes (Figure 4-14a), the slopes of the two straight lines, describing the uniform decelerated motion, also agree. Nonetheless the two plots overlap till the interaction between the rear and the front parts of the mass takes place. In the case of a greater volume this interaction lasts for a longer period of time leading to a translation of the straight line. Consequently it is possible to deduce that the volume has an influence primarily on the accumulation part of the process, where it affects the duration of the transfer of linear momentum between the rear and the front of the mass. This confirms what seen in section 3.5.2 and provides experimental evidence to what was stated by Heim (1932) and Van Gassen and Cruden (1989), who identified the cause of the long runout of large rock avalanches in this transfer of momentum. As seen in section 2.3.2 the equations developed in this framework by Van Gassen and Cruden to evaluate the distance travelled by the centre of mass have been demonstrated to be wrong by Hungr (1990a) and Erlichson (1991), nonetheless, as shown here, this transfer of momentum takes places in reality but it is likely to affects mainly the distance travelled by the front mass and consequently the runout.

4.2.3. Slope and basal friction

Data compiled in Figure 4-15 and Figure 4-16 show that a longer runout is induced by a lower base coefficient of friction and a higher slope angle. Nonetheless, these two parameters don't induce a similar increase of the travel distance of the centre of mass. When the slope angle decreases (Figure 4-16) or the base friction increases (Figure 4-15), the decrease in the forces acting in the direction of the flow in the first case and the increase in the resistant ones against the flow in the second case, do not allow the whole mass to pass over the break line leading to a different deposit morphology. In both cases, a part of the material still lies on the inclined board and consequently the centre of mass travels a shorter distance.
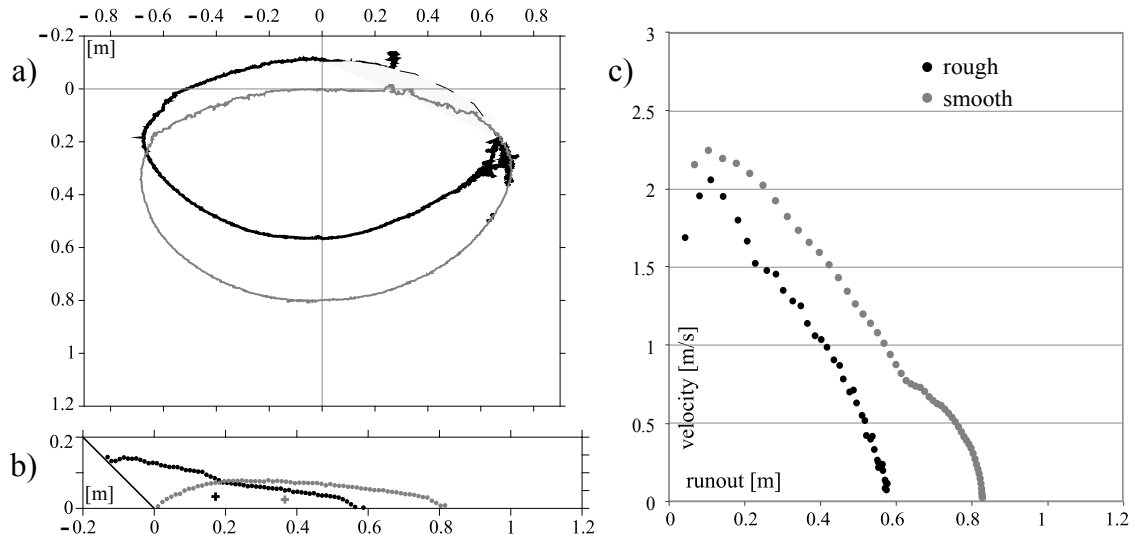
Figure 4-15 Influence of the board roughness: rough (black) versus smooth (grey). Horizontal (a) and longitudinal (b) deposit cross-sections; front mass velocity on the horizontal panel (c)
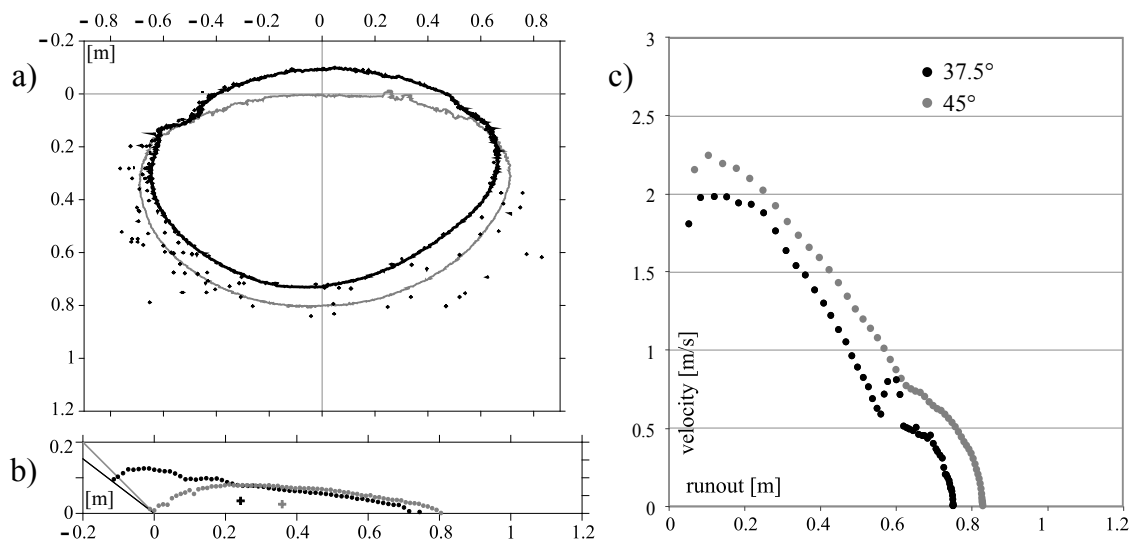
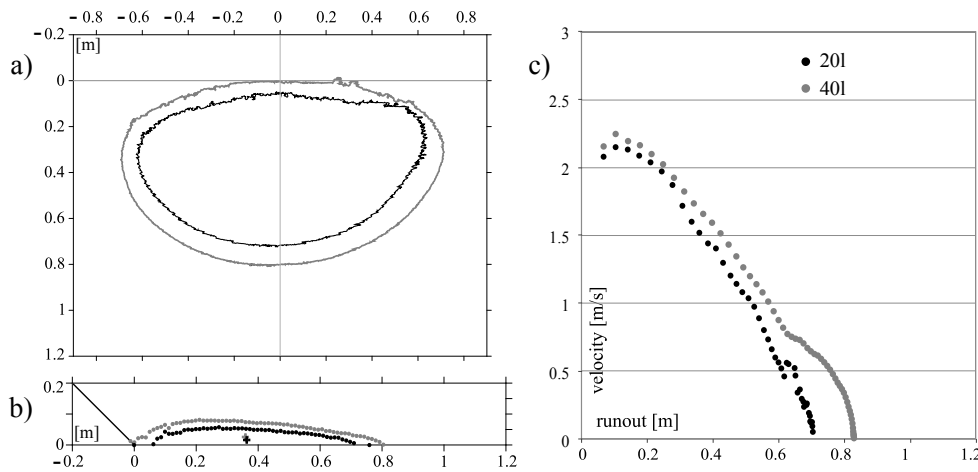*Figure 4-16 Influence of the slope angle: 37.5° (black) versus 45° (grey). Horizontal (a) and longitudinal (b) deposit cross-sections; front mass velocity on the horizontal panel (c)*

Logically, with a higher roughness of the base material, the travel angle of the centre of mass ϕ_{CM} increases (40° → 43°) since the effect of friction increases as well. On the other hand, for tests carried out on the same base material but with different panel inclinations, ϕ_{CM} would be predicted as constant if a simple frictional model is assumed for the energy dissipation (i.e. straight energy line model). Instead, ϕ_{CM} decreases (40° → 35°) when the slope angle decreases (45° → 37.5°). This could be explained by the fact that the velocity of

the mass is lower with a less inclined panel (see Figure 4-16c for the front mass velocity) and therefore also the energy dissipation through turbulence within the mass.

This is in agreement with Legros statement (2006) that energy dissipation is not constant but it is greater on steep slopes, where velocity is high, and it is reduced on gentle slopes, where velocity is low. Legros also suggests that the concept of a straight energy-line based on a simple frictional model is not adequate for modelling rock avalanches and that a velocity dependent term of energy dissipation should be taken into account to explain their mobility. For this reason it would be more adequate in numerical codes for rock avalanches to use a Voellmy-like model that combines frictional and turbulent behaviours. Nevertheless, even if the precision is higher, there is an additional rheological parameter to be calibrated (Pirulli and Mangeney, 2007).

Another possible explanation to the lower energy dissipation is the smoother transition between the two panels when the slope is gentler, suggesting that the energy line depends also on the set-up geometry. Evidence of this correlation can be found observing tests carried out in the extreme case of a 90° slope (preliminary tests carried out at the EPFL and shown in Figure 4-17, and tests by Davies, 1997), where ϕ_{CM} is very high, estimated above 60°. The shock of the particles falling almost vertically on the horizontal panel induces much greater energy dissipation. Therefore ϕ_{CM} seems to be dependent in a way to what is possible to call the "degree of sharpness" at the toe of the slope or the regularity of the path as called by Heim (1932). In order to confirm this effect of geometry on energy dissipation, some additional tests using a slightly curved transition zone between the two panels have been carried out and will be shown in section 4.2.5. This should allow verifying whether the loss of energy due to the current sharp discontinuity at the toe of the inclined board causes much shorter runouts and it will be useful to extend the findings to date.

Figure 4-17 Test at 90° slope; release of 40 l of gravel, from 1 m height, on a board covered with wood

4.2.4. Material used

Looking at the travel angle of the centre of mass (ϕ_{CM}) and the Fahrböschung (ϕ_{ap}) reported in Table 4-3, it can be noticed that for tests with the same slope angle (45°), one release, a sharp connection between the panels and the same base material (forex), ϕ_{CM} is similar for all the tests, approximately 40°, with a maximum variation of 1°. At the same time, ϕ_{ap} is approximately 32° degrees; tests with piled bricks (28°) make however an exception. Even if it has been demonstrated the apparent coefficient of friction to be physically meaningless (Legros, 2002), it can still be considered as a mobility index of landslides (Corominas, 1996). Therefore this lower value of 28° for ϕ_{ap} points out that tests with blocks arranged orderly at the start have a higher mobility. On the other hand, no major difference can be observed in either runout or mass centre position between tests with aquarium gravel and with bricks poured in randomly (Figure 4-18). Even if these two materials are very different for what concerns the dimensions and the shape of the grains, the morphology of the deposit does not seem to be affected by these changes in the case they are poured into the reservoir before failure. This seems in agreement with statements by Davies and McSaveney (1999) that grain size and grain-size distribution have negligible effects on runout. On the other hand, as already underlined by the value of the Fahrböschung, significant differences can be noticed when the bricks are piled orderly before failure (Figure 4-19). A greater spreading of the mass induces a more elongated shape of the final deposit putting in evidence the dependence of these deposit characteristics on the compactness and structure of the mass before failure.
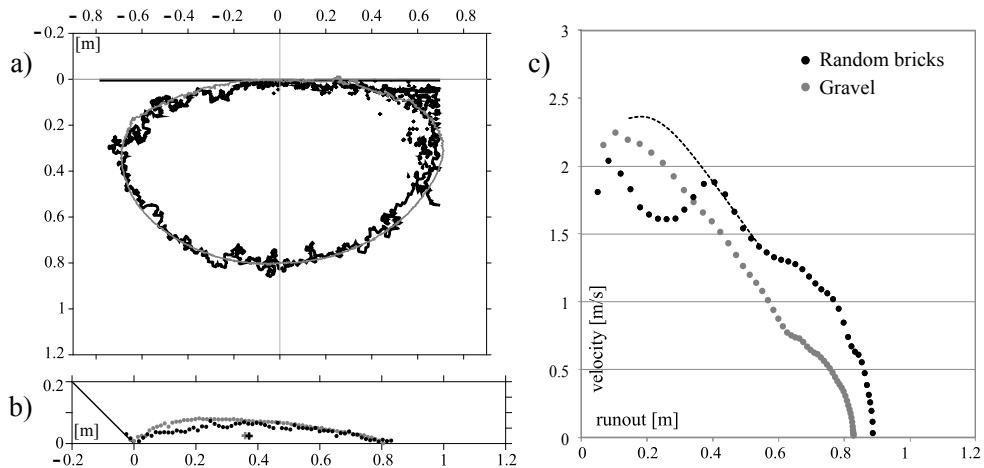
Figure 4-18 Influence of different material: Random bricks (black) versus Gravel (grey). Horizontal (a) and longitudinal (b) deposit cross-sections; front mass velocity on the horizontal panel (c)
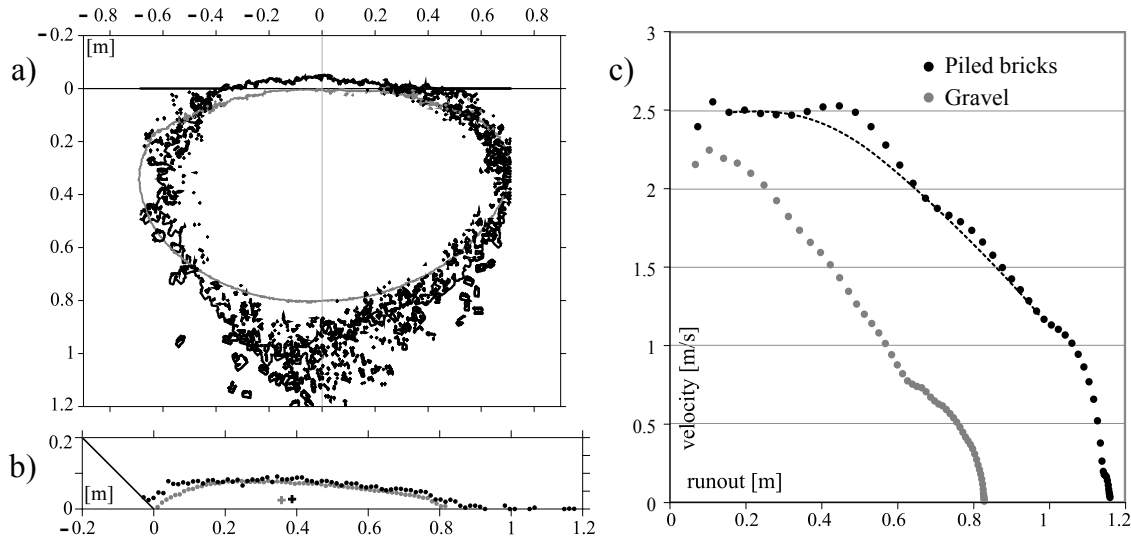
Figure 4-19 Influence of different material: Piled bricks (black) versus Gravel (grey). Horizontal (a) and longitudinal (b) deposit cross-sections; front mass velocity on the horizontal panel (c)

Mechanism of propagation

The difference between tests with piled bricks and tests with gravel and random bricks could rely intuitively to the fact that elements are structured at the beginning. In this case they interact less between them during the flow, hence less energy is dissipated in the first part of the process. This behaviour is confirmed by Figure 4-19c which shows that the front mass velocity is notably higher for piled bricks than for gravel or bricks arranged randomly. Consequently a longer propagation occurs.

One characteristic of rock avalanches is that they often start out with a relatively coherent mass, which shutters and crushes during the fall (Davies and McSaveney, 1999). In the case of piled bricks a similar process is reproduced, since the mass of bricks remains relatively compact at the beginning and disaggregates only afterwards. Evidence of this behaviour can be found observing the images of the tests. Both Aquarium gravel (Figure 4-20a) and bricks randomly poured into the box (Figure 4-20b) behave as a loose material and consequently there is a certain similarity between the mechanism of propagation in these two experiments. Nonetheless, when bricks are originally piled one on top of the other (Figure 4-20c), the mass behaves as a relatively compact body in the first part of the sliding where bricks remain packed together, until it reaches the horizontal panel and spreads out. On the inclined board, energy is consequently mainly dissipated through friction at the base, on the other hand, after the impact with the horizontal panel, the mass shatters and energy is dissipated mainly through friction/collisions between the bricks in the whole mass. The limited energy dissipation in the first part leads the mass to have a greater energy stored and a higher velocity when it enters the accumulation zone on the horizontal panel (see Figure 4-19c). This is a plausible explanation for the observed longer runout and X_{CM} (even if the variation of the centre of mass position is lower). On the contrary, in the case of gravel and of bricks simply poured into the box, a greater quantity of energy is dissipated from the beginning through both frictions at the base and within the mass. According to the distinction made by Drake (1990), it is possible to say that in the case of piled bricks the regime is mainly frictional on the inclined panel and then frictional-collisional in the accumulation zone. The abrupt change of flow direction seems to be the cause activating this passage to a different regime. On the other hand both regimes can be found in gravel and random bricks tests from the beginning of the slope because the mass is not structured at the start.
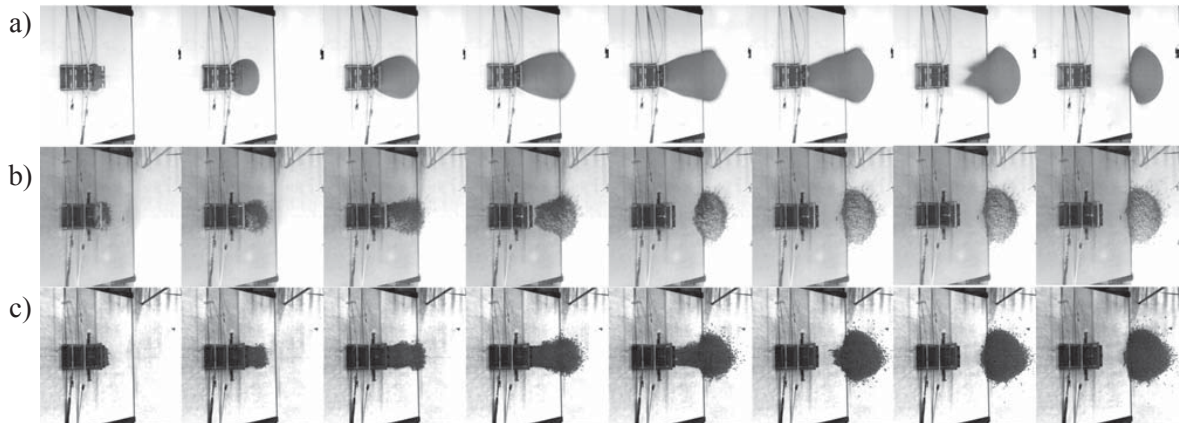
Figure 4-20 Images of the tests taken each 1/6 s : (a) test with aquarium gravel, (b) test with bricks originally randomly poured in, (c) test with bricks originally piled one on top of the other. Release of 40 l, from 1 m height, on a 45° inclined board covered with forex

The underlined differences in the propagation mechanism and in the runout distance of these tests give evidence to the fact that with bricks piled orderly at start it is possible to reproduce what Davies and McSaveney (1999) called the spreading of a coherent mass which, until now, was observed only in real events.

4.2.5. Connection at the toe of the slope

As aforementioned some series of tests have been carried out to verify whether the sharp discontinuity at the toe of the slope could have an influence on propagation, as suggested by the fact that ϕ_{CM} decreases (40° → 35°) when the slope angle decreases (45° → 37.5°). As a consequence the travel distance of the centre of mass seems to be dependent in a way to what is possible to call the "degree of sharpness" at the toe of the slope, confirming what already observed by Heim (1932) who affirms that the regularity of the pathway has an influence on rock avalanche propagation. Observing Figure 4-21 it is possible to notice how the change into a curved connection between the two panels leads to longer runout and X_{CM} and to a higher velocity. It is believed that this behaviour is due mainly to a lower loss of energy at the toe.

Noises of the contour line of the test with a smooth connection at the toe (Figure 4-21a) are due to the fact that to cover the whole area with the fringes, the projector has been displaced further at the expense of the quality of the projection.
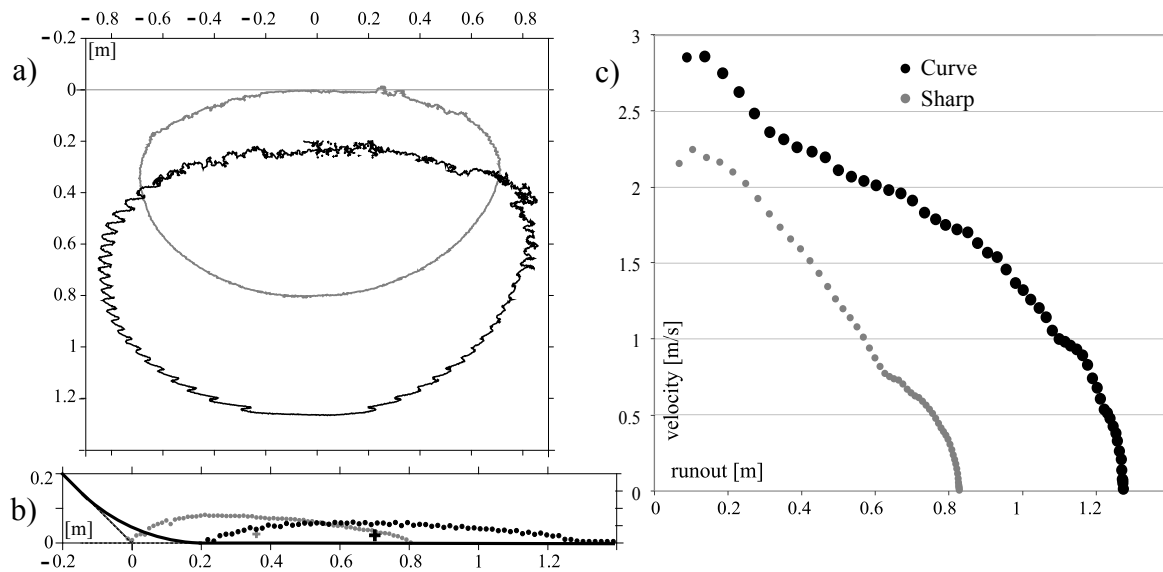
Figure 4-21 Influence of sharpness of the connection at the toe of the slope: smooth curved connection (black) versus sharp angular connection (grey). Horizontal (a) and longitudinal (b) deposit cross-sections; front mass velocity on the horizontal panel (c)

This is confirmed also comparing series 20 and 30, both performed with 40 litres of piled bricks (see Figure 4-22a and b). In the case of a smoother connection between the panels the morphology of the mass is evidently more elongated and the mass, its front and its centre, but not its rear, travel much further than in the case with a sharp discontinuity. As put in evidence in previous section, the longer runout of bricks piled orderly before failure could be due to the fact that in the first part of the slope the bricks remain structured and the regime is mainly frictional. Only when the mass reaches the toe and it looses its compactness due to the impact with the obstacle represented by the sharp discontinuity, the collisional regime increases its importance. In Figure 4-23 it is possible to observe how when the mass flows on a curved toe, it still travels a certain distance on the horizontal panel keeping its compactness. This reveals that the transition has been smoothed and energy has been even more "spared" than in others tests with piled bricks leading to an even longer propagation. As anticipated in the previous section, this confirms that the factor activating the shattering of the mass seems to be the impact with the horizontal panel. The fact that when the discontinuity is smoother there is a predominance of the frictional regime is also demonstrated by the fact that it has been possible to detect in the final deposit several pile of bricks which keep the initial structure (see Figure 4-24). As recalled by Erismann (1979) this "coherence problem" is detected in many large landslides: the mass, even if

disintegrated into small fragments, show a surprising congruence of the sequential order it had before failure. These considerations lead to the conclusion that experiments with bricks could help in studying and understanding mechanisms likely to happen in real rock avalanches. Therefore even if they don't fulfil the hypotheses of continuum mechanics, neither probably the similitude requirements and despite the difficulty in performing them, further experiments with bricks should be considered in the future, eventually testing different kinds of shapes, materials and dispositions.
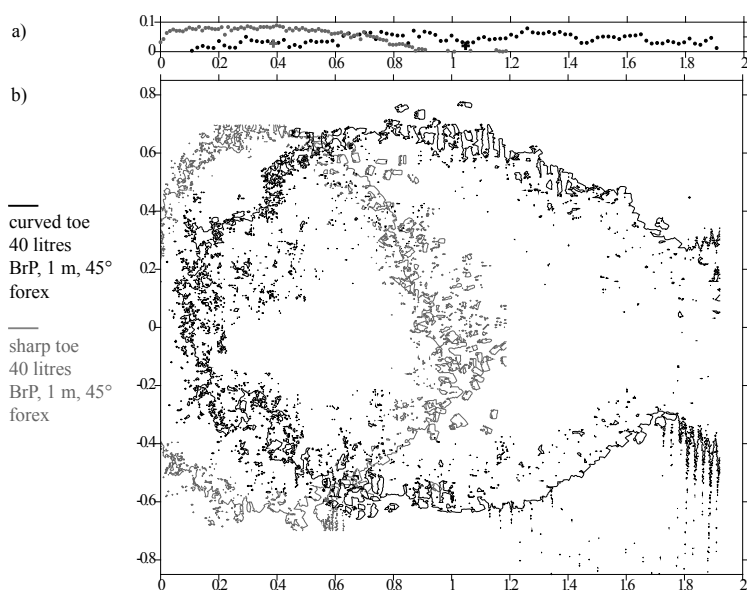
Figure 4-22 Influence of connection sharpness at the toe of the slope for a test with piled bricks: smooth curved connection (black) versus sharp angular connection (grey). Horizontal (a) and longitudinal (b) deposit cross-sections; the noise on the right boarder of the section is caused by the fact that the projector cannot cover more than 2 metres length
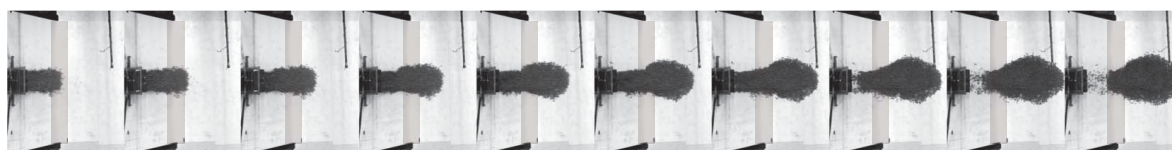
Figure 4-23 Flow of a 40 litres of piled bricks on a smooth curved toe and consequent propagation on the horizontal panel; the rectangle in light grey at the toe of the slope underlined the curved part
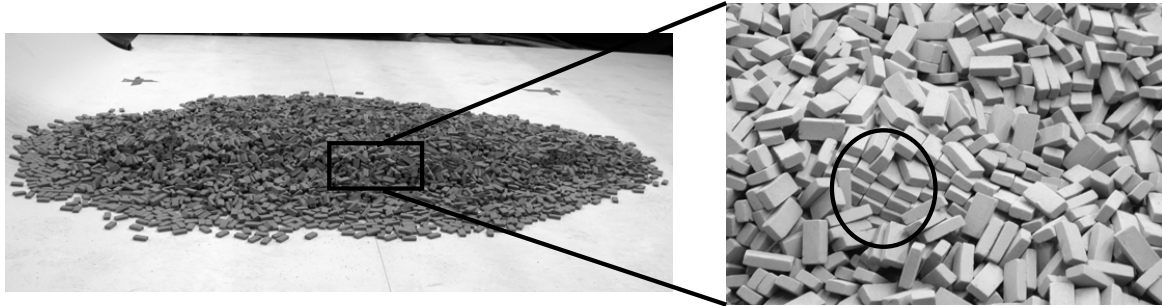
Figure 4-24 Evidence of the initial structure in a final deposit of a test of 40 litres of piled bricks with a curved discontinuity at the toe

4.2.6. Summary table

As in the previous chapter a synthesis of the qualitative relationships between the different factors and responses studied is given by means of a trend table where the arrows indicate the following:

↗ : an increase of a parameter from a row chosen from the left column causes an increase of the characteristic at the head of the considered column;

↘ : an increase of a parameter from a row chosen from the left column causes a decrease of the characteristic at the head of the considered column;

↔ : an increase of a parameter from a row chosen from the left column has no significant effect on the characteristic at the head of the considered column.

- : when no analysis has been done of the relationship

When a symbol is repeated twice it means that the influence is strongly marked.

Parameter	Runout	Deposit width	Deposit length	Deposit morphology	ϕ_{ap}	X_{CM}	ϕ_{CM}	Mass front velocity
Number of releases	↘	variable	↗	Evolution to a "conic" shape	↗	↘	↗	-
Volume	↗	↗	↗	↔	↔	↔	↔	↗ Mainly at the end
Fall height	↗	↗	↗ Slightly	Flatten out	↔	↗	↘ Slightly	↗ Same behaviour
Slope	↗	Variable	Variable	Flatten out	↗↗	↗	↗↗	↗
Basal friction	↘	Variable	Variable	Evolution to a "conic" shape	↗	↘	↗	↘
Materials From Gr2 to BrR	↗	Variable	Variable	Same features of the main deposit	↔	↗ Slightly	↔	↗
Materials From Gr2 to BrP	↗↗	↔	↗↗	Much more elongated	↘↘	↗ Slightly	↘ Slightly	↗↗
Sharp to Curved connection	↗↗	↗	↗	Much more spread	↘↘	↗↗	↘↘	↗↗

Table 4-4 Scheme of the influences of the factors on the responses

The factors studied in both experimental campaigns show similar trends with the exception of the influence of fall height on runout: in the second experimental campaign runout comes out to be dependent on this factor.

4.2.7. Conclusions on the parametrical study

From the parametrical study, it is possible to reach several useful conclusions. The different parameters considered are:

- number of consecutive releases (40 litres in one or in two subsequent releases of 20 litres each)

- volume (20 l, 40 l);

- fall height (1 m, 1.5 m);

- basal friction coefficient;

- slope angle (37.5°, 45°);

- nature of released material: aquarium gravel2 and small bricks;

- arrangement of the bricks before failure;

- discontinuity at the toe (sharp, curved).

The main results are:

1. The results obtained in the second testing campaign confirm the previous ones stated in section 3.5.3 that by increasing the number of times by which the release of a certain volume is divided, the height of the deposit increases significantly and its runout decreases. As a matter of fact, it is the first release which determines how far the entire volume will travel. Thanks to the fringe projection method it has been possible for this experimental campaign to better visualise these results and to confirm them with a more quantitative approach.

2. In the deposition process it is possible to distinguish an interaction between the rear and the front parts of the mass. The front mass enters the accumulation zone followed by a uniformly decelerated motion until the rear part approaches and forces the mass ahead to move further. This transfer of momentum between the rear and the front could partly explain the exceeding travel distance of rock avalanches. The greater the volume of the mass, the greater the duration of the interaction between

the rear and the front parts and the longer the runout. Nonetheless, this change in the position of the distal end of the deposit is not related to a variation of the travel distance of the centre of mass.

3. The exceeding travel distance is not always related to an extra-spreading of the mass. Tests with higher fall height show that the whole mass translates further and that the excess travel distance of the centre of mass and of the distal end are similar. The Fahrböschung is the same even if the runout is greater. Other factors causing longer runouts are: lower coefficient of friction, higher slope angle, the use of bricks ordered in piles and a smoother discontinuity at the toe of the slope. The latter induces the largest increase.

4. The concept of a straight energy-line based on a simple frictional model is not adequate to evaluate the distance travelled by the centre of mass. The experimental results are in agreement with Legros's statement (2006) that, for modelling of rock avalanches, only models that take into account a velocity dependent term of energy dissipation should be used, such as the Voellmy resistance model that combines frictional and turbulent behaviours. Moreover, the energy line seems to depend on the set-up geometry.

5. When bricks are piled orderly into the reservoir before failure, the mass behaves as a compact body on the inclined panel, i.e. the bricks remain packed together and energy dissipation takes place mainly through friction at the base. After the impact with the horizontal panel, the mass shatters and energy is then mainly dissipated through friction/collisions between the bricks. Having "spared" a part of the energy in the first part of the sliding, the mass enters the accumulation zone with a higher velocity and can consequently travel further on the horizontal panel. The final deposit has an elongated shape, with a lower apparent coefficient of friction (Fahrboschüng) but with a "normal" ϕ_{CM}. These tests with bricks piled orderly at the start could bring experimental evidence of the phenomena described as the spreading of a coherent mass by Davies and McSaveney (1999).

6. The loss of energy induced by the sharp discontinuity at the toe of the inclined board influences considerably the propagation of granular avalanche. Interesting

information about possible mechanisms of propagation and deposition comes out from the observation of the experiments with piled bricks: in the case of a smoother connection and a softer impact with the horizontal panel, the coherence of the mass all along the slope gives evidence of the "sparing" of energy and the regime seems to remain mainly frictional also on the horizontal panel. Instead, a sharp discontinuity along the pathway provokes the shattering of the mass and a frictional-collisional regime in the accumulation zone.

The last two points emphasize that blocks piled orderly at the start show a difference in flow behaviour and deposit characteristics compared to tests with aquarium gravel and blocks arranged randomly. This could mark an important step in the investigation of the processes involved in rock avalanches propagation and deposition and should be investigated further.

These semi quantitative results put in evidence the importance of certain factors in granular avalanches propagation and that should be considered in the setting up of empirical models: the volume, the fall height, the friction angle, the topography, i.e. the slope and the regularity of the pathway, the structure of the mass before failure. Another thing to be taken into account is whether the failure is progressive or not.

Factors which do not seem to influence runout are grain size and grain size distribution; this happens in laboratory tests only above a certain lower limit, since, when grain size is too small there could be some electrostatic effects which bedevil results. Nevertheless, the influence of these factors has not been studied in details in the present research and further tests are required to confirm these preliminary conclusions.

To describe the laboratory results with accuracy and verify whether it is possible to eventually extend the considerations made to real events with the necessary adaptations, in next section an attempt is made to translate the different effects detected into empirical formulations.

4.3. Empirical and statistical analysis of the results

In this section a more quantitative analysis of the laboratory results is carried out and empirical formulations will be studied. The aim is not yet to elaborate a model able to be applied directly to real cases. Indeed, it is well known that there are certain phenomena that it is not possible to reproduce with experiments carried out in laboratory. However according to the dimensional analysis presented in section 2.3.3, it is also demonstrated that the main mechanisms can be reproduced. Therefore even if the analyses performed here are valid only in the framework of the tests made, they contribute to understand which factors should be included in the modelling of real events, their importance and their variability.

A statistical analysis will be then carried out to evaluate the effects of several factors together on the chosen responses and to verify on the totality of the tests the considerations made with the parametrical and quantitative study.

4.3.1. Fahrböschung and exceeding travel distance

As described in section 2.3.1 the first empirical model attempting to describe rock avalanche runout is the one of Scheiddeger (see Table 2-3 and Figure 2-5). It has been verified whether this formulation is valid for the laboratory tests but the scatter is large and the accuracy is too low ($R^2 < 0.1$). This is probably due also to the fact that this formulation is not scale independent, since the volume has to be expressed in cubic metres.

The formulation of Davies and McSaveney (1999) has been thus preferred. They put in relation the apparent friction coefficient of tests with a nondimensional quantity h_v/h^*, i.e. the height of the centre of mass before release (see Figure 4-10) normalized by the cube root of the volume, h^*. As already mentioned in section 2.3.3, they performed as well tests consisting in unconstrained granular flows on a 45° slope with a sharp connection between the inclined and the horizontal planes. They compare the results obtained, i.e. a Fahrböschung between 32° and 42°, with data of the Elm and the Frank events which represent unconstrained real rock avalanches on a 45° slope. The values reported by Davies and McSaveney (1999) and represented in Figure 4-25 for these two real events differ to the ones founded in literature usually between 14° and 16° for both the Frank and the Elm rock avalanches. Nonetheless since it is here taken in consideration the work of Davies and McSaveney a value of the Fahrböschung of 20° for the Frank slide and of about 18° for the

Elm one are considered. In Figure 4-25 these values are reported together with the ones calculated for the present tests at 45° slope, covered by forex, with a sharp discontinuity at the toe. Results put into evidence low Fahrböschung for the experiments with bricks piled orderly before failure, confirming the influence of the structure of the mass on the mobility of rock avalanches seen in previous chapter. Still these values are far from the ones of real cases. It should be necessary to test lower releasing height or greater volumes to see whether going towards values of h_v/h^* similar to the ones of Elm and Frank events it would be possible to have also similar values of the Fahrböshung.
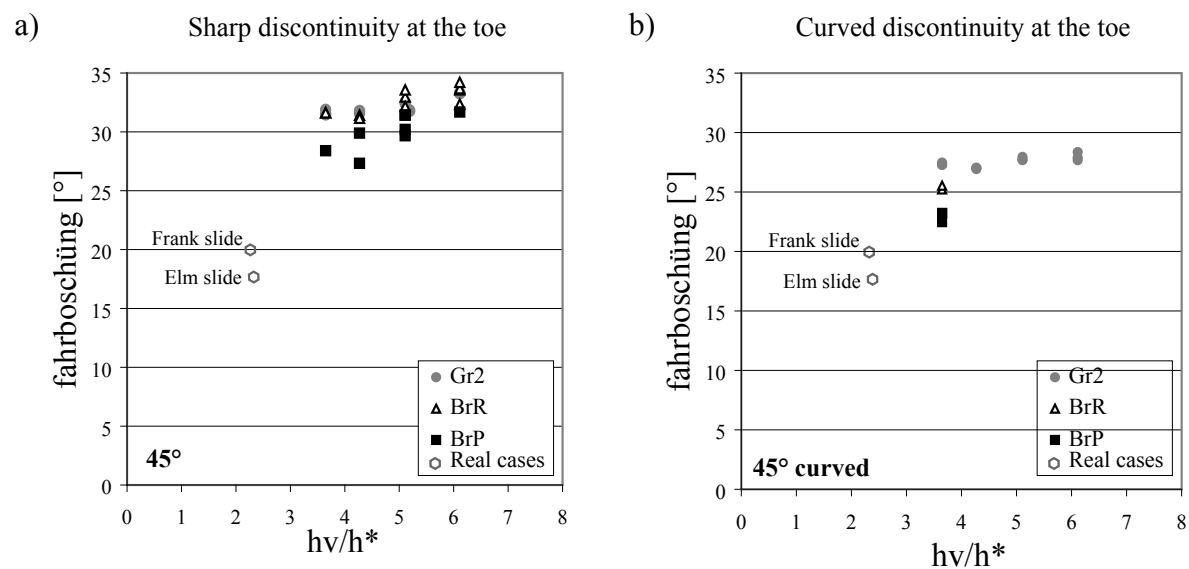
Figure 4-25 Fahrboschüng versus normalised height of the centre of mass before release: tests on 45° inclined panel covered with forex with either a sharp(a) or a curved (b) discontinuity at the toe

These results put in evidence the fact that a higher mobility is underlined by a lower apparent coefficient of friction, but they do not quantify how much this higher mobility differs from the one resulting from a normal sliding friction law. For this reason authors such as Hsü (1975), Hungr (1990a), Corominas (1996) and Davies and McSaveney proposed different kinds of variables to identify the rock avalanche exceeding travel distance. As seen in chapter 2.3 Hsü (1975) first proposed the exceeding travel distance to be the difference between the total travel distance, i.e. the horizontal projection of the line connecting the crown of the head scarp with the most distal end at the toe of the deposit along the midstream path of the mass, and the distance travelled following a purely frictional law (see equation [2-1]). Hungr (1990a) and Corominas (1996) proposed other formulations based on this first attempt according to equations [2-5] and [2-6]. In particular

it has been calculated for the present tests the index Lr of Corominas which expresses the degree of mobility of landslides putting in relation the exceeding travel distance as calculated by Hsü and the distance of the mass if it had travelled dissipating energy only through pure friction. Instead of using the 32° angle of basal friction proposed by these formulations, it has been used here the basal friction angle of each material measured by tilting tests, according to equation [4-7].

$$L_r = \frac{L_e}{H/\tan(\phi)} \qquad [4\text{-}7]$$

The plots of the L_r index reported in Figure 4-26 allow noting that:

- Piled bricks released on a plane with a sharp discontinuity at the toe and gravels released on a regular pathway with a curved slope don't exhibit an excessive mobility and remain in the range of a "normal" frictional behaviour

- Only the combination of bricks and curved slope does induce an excessive mobility of the distal end of the mass. It appears stronger when the bricks are piled at the start in the releasing container.

- Gravel and Bricks poured randomly before failure have a negative index when released on a slope with a sharp discontinuity at the toe. This underlines the great loss of energy occurring in the mass due to this discontinuity. It will be better quantified in the following section.

As only experiments with little bricks provide results with an excessive travel distance, this seems to confirm that this kind of laboratory tests could be more representative of the behaviour of jointed masses involved in rock avalanches.
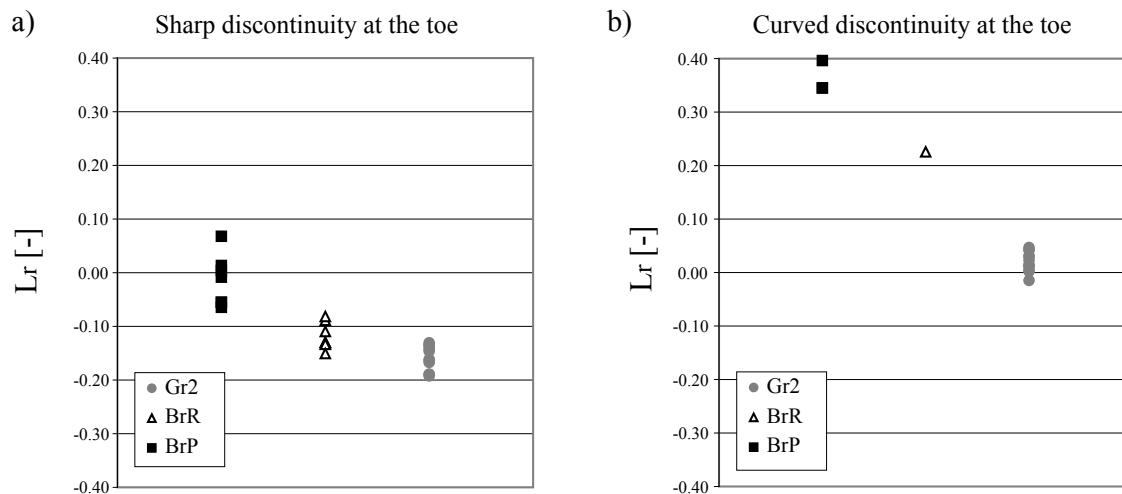
Figure 4-26 Degree of mobility L_r: for tests on a 45°inclined panel covered with forex with either a sharp (a) or a curved discontinuity at the toe (b)

4.3.2. Travel angle of the centre of mass and energy dissipation

The considerations made in the previous section are based on empirical formulas such as the Fahrböschung and the exceeding travel distance. Even if these evaluations give an idea of the mobility of granular avalanches, they nevertheless consider the mass as a whole and consequently its distal end travels as its centre of mass, hypotheses demonstrated to be physically meaningless by several authors, e.g. Hungr, Legros and Corominas. Therefore in this section the mobility of the centre of mass is analysed in details to be able to perform a proper comparison with a frictional model and to make considerations on energy dissipation. First the travel angle of the centre of the mass is assessed for all the experiments to determine which factors are the most influent. Then, having the position of the centre of mass before and after failure an attempt has been made to quantify the loss of energy due to friction at the base and within the mass.

In Figure 4-27a values of the travel angle of the centre of mass, ϕ_{CM}, are reported for all the experiments performed on forex considered in the second experimental campaign, with the exception of tests with consecutive releases. They are separated into gravel, bricks randomly poured into the reservoir and bricks piled orderly before failure. These categories are further distinguished into experiments at 45° and 37.5° with a sharp connection between the panels and tests at 45° but with a curved connection at the toe. It is possible to notice how, also in the case of the centre of mass, bricks piled orderly at the start and released on a plane with a

curved discontinuity at the toe show the lower values of ϕ_{CM}. There is a certain dependency of the travel angle also from the fall height as marked on the plot. Intuitively this can be due to the fact that a mass released from a higher point approaches the accumulation zone with a higher velocity. This allows the mass to pass over the discontinuity more easily, dissipating less energy.

As already mentioned in the parametrical study, gravel and bricks randomly poured into the container before failure have a rather similar behaviour. Nonetheless structured bricks behave differently and lead to lower values of the travel angle of the centre of mass, which diverge more from the two other materials as the transition between the panels is smoother.

It is possible to notice in Figure 4-27b how, within the test with the same material and the same arrangement before failure, the regularity of the pathway is a significant factor, as already pointed out by Heim in 1932. The more angular is the connection between the panels, the more shearing (friction) and collisions will develop within the sliding mass as it changes its flow direction, the larger will be the energy dissipation within the mass and the shorter the travel distance of the centre of mass.

On the other hand, when a structured mass at the start is moving down a regular slope (e.g. with a curved toe), the shattering process due to the change in flow direction is less marked, the structured mass moves further as a compact body and consequently travels as a whole a longer distance.

To better identify the interaction between the discontinuity at the toe of the slope and the arrangement of the mass at the start, a statistical analysis will be performed in section 4.3.5. On the other hand it is here important to quantify the energy loss to see whether these considerations are confirmed by a significant decrease in the loss of energy at the toe with an increase of the regularity in the pathway.
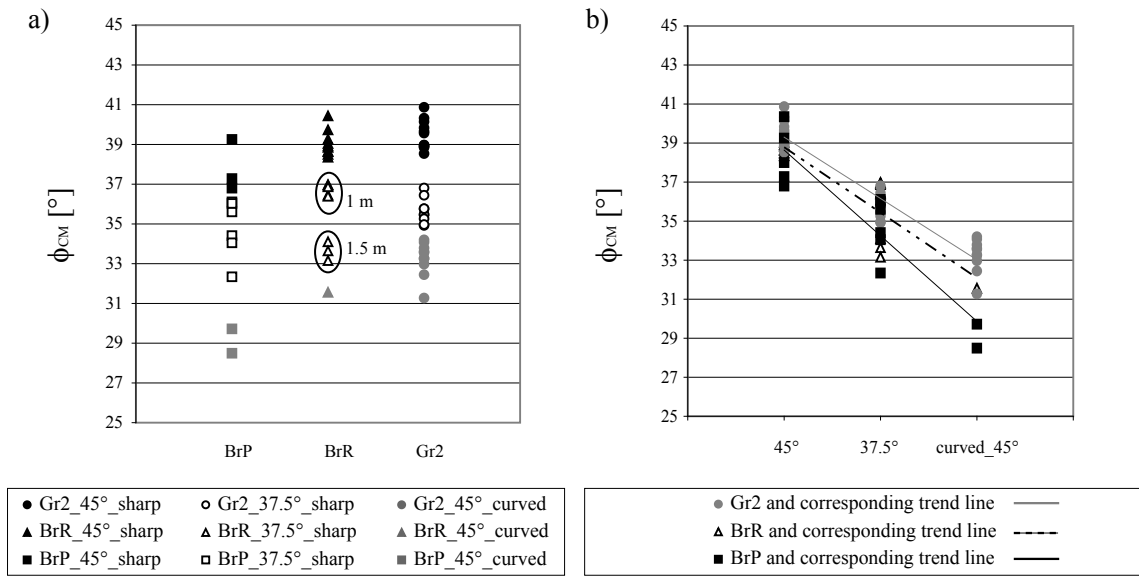
Figure 4-27 Travel angle of the centre of mass ϕ_{CM} for the one release experiments on forex: a) against the kind of material used (BrP, BrR, Gr2); b) against the characteristics of the connection at the toe (45°_sharp, 37.5°_sharp, 45°_curved)

Knowing the position of the centre of mass before and after propagation it is possible, according to equations [4-8], to calculate the total loss of energy E_{lt} and the loss of energy by friction at the base, E_{lf}, assuming a normal sliding friction law. The difference between these two energy values represents the energy loss by friction/collisions within the mass.

$$E_{lt} = Mgh_{CM} = MgL_{CM} \tan \phi_{CM}$$
$$E_{lf} = Mgh_f = MgL_{CM} \tan \phi$$

[4-8]

Where M is the mass expressed in Kg; g is the gravity acceleration [m/s^2]; h_{CM} and L_{CM} are difference in height [m] and the distance travelled by the centre of mass [m]; h_f is the height representing the energy loss of the mass by friction at the base. Figure 4-28 illustrates how these quantities are calculated for the experiment taken as a benchmark test for the parametrical study.

In order to have a variable that quantify the part of energy which is not dissipated by friction at the base, a relative energy loss ratio has been computed according to equation [4-9].

$$\frac{\Delta E}{E_{lt}} = \frac{E_{lt} - E_{lf}}{E_{lt}} = \frac{Mg\Delta h}{Mgh_{CM}} = \frac{\left(h_{CM} - h_f\right)}{h_{CM}}$$

[4-9]

As done for the travel angle of the centre of mass, in Figure 4-29a values of the energy loss ratio are reported for all the one release experiments performed on forex considered in the second experimental campaign. They are separated into gravel, bricks randomly poured into the reservoir and bricks piled orderly before failure and these categories are further distinguished into experiments at 45° and 37.5° with a sharp connection between the panels and tests at 45° but with a curved connection at the toe. In Figure 4-29b the ratio of energy loss is put in relationship with the degree of sharpness of the connection between the panels. Also in this case it is possible to notice the same trends as in the travel angle plots, which is expectable since the two variables are related. It is here confirmed that a model considering only energy dissipation at the base is not sufficient to explain the behaviour of a granular mass. A certain quantity of energy is lost at the toe and another part is dissipated along the slope. As suggested in the parametrical study, see section 4.2.4, energy seems to be dissipated mainly by friction at the base in the case of piled bricks; the more the material is structured the less the energy is dissipated within the mass on the slope till it reaches the horizontal panel and it shatters. In addition if the connection at the toe is progressive the shattering of the mass is partially avoided, inducing to an even more marked predominance of the frictional dissipation with values of $\Delta E/E_{lt}$ near zero.

Values below zero are of course physically meaningless. They could result either from imprecision in the determination of the centre of mass for blocky deposits (presence of voids due to shattering) or from a basal friction angle lower than the one determined in the tilting tests (the dynamic friction angle is known to be lower than the static one). The latter explanation is coherent with the statement by Legros that the centre of mass can travel longer distance than the one predicted by a normal sliding friction law. It is true that the data at disposition are not enough to affirm this with certainty but it is possible to deduce by general trends that the values obtained could be even lower considering an even more structured material or an even smoother topography. What can be said is that the structure of the mass before failure and its shattering during the flow has a significant influence on the travelling distance of the whole mass, both of its centre and of its distal end. The effects of these factors on runout and length of the final deposit will be more quantified in following section.
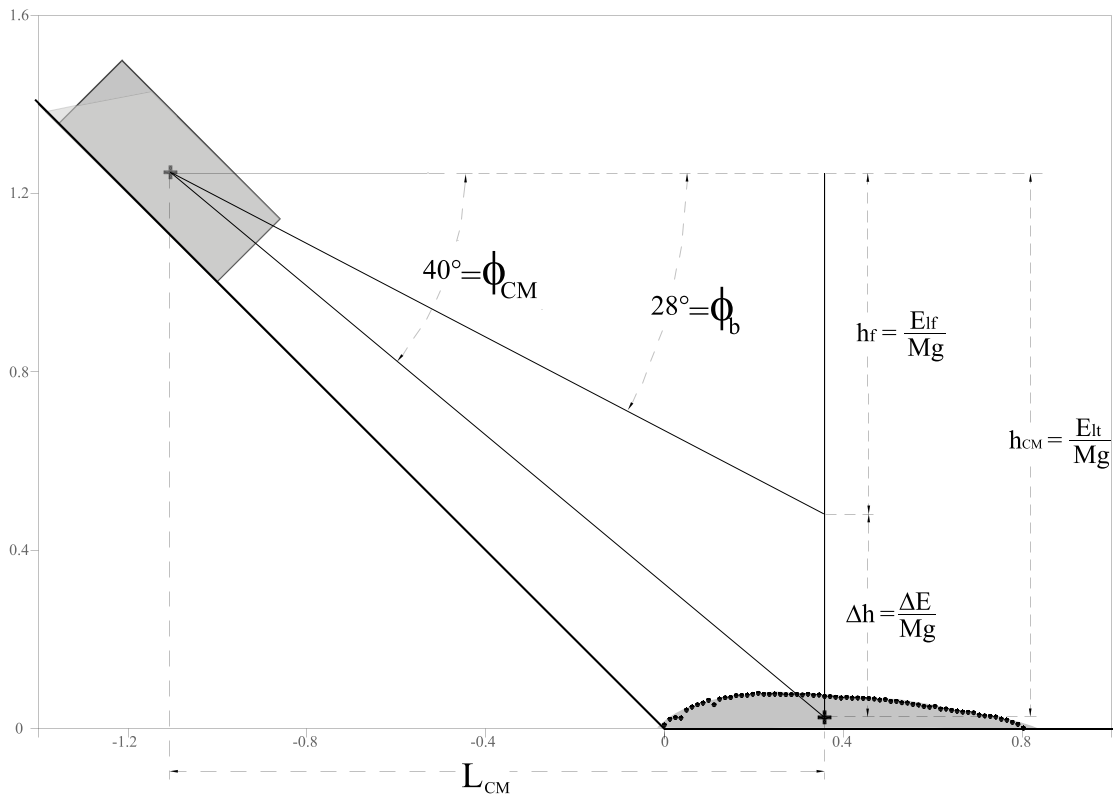
Figure 4-28 Gathered data for the evaluation of the dissipation of energy; benchmark experiment: release of 40 l of gravel, from 1 m height, on a 45° inclined board covered with forex
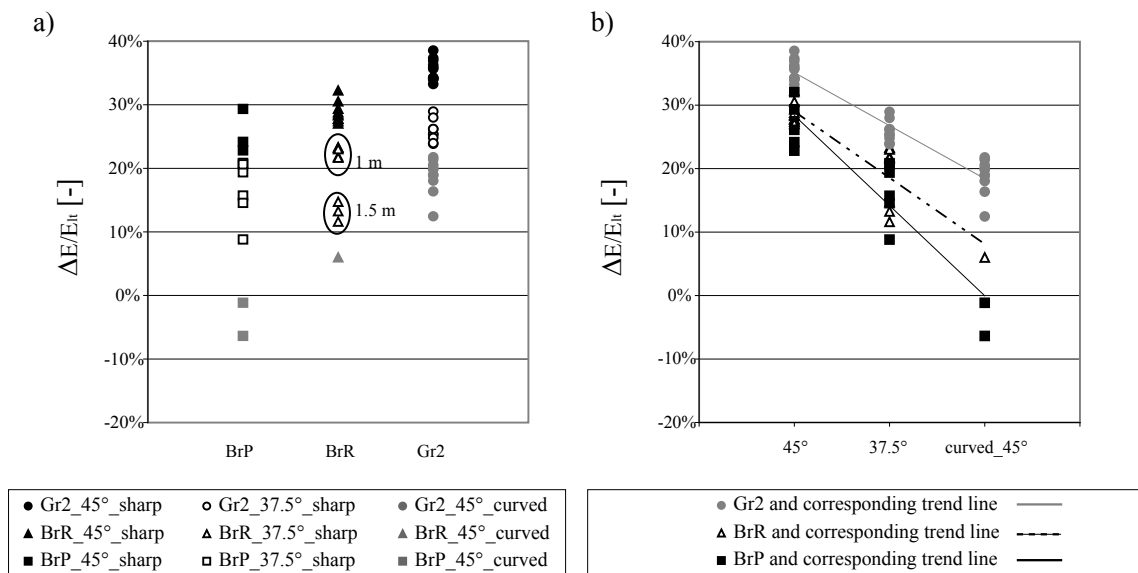
Figure 4-29 Relative energy loss ratio for the one release experiments on forex: a) against the kind of material used (BrP, BrR, Gr2); b) against the characteristics of the connection at the toe (45°_sharp, 37.5°_sharp, 45°_curved)

4.3.3. Lumped mass model and centripetal acceleration

In this section an attempt is made to verify whether it is possible to reproduce the tests carried out in the present study with a sled model which takes into account the centripetal acceleration.

As seen in section 2.3.2 for lumped mass models the flowing material is considered as a dimensionless point of mass M sliding along a path inclined of β, characterised by a constant friction angle ϕ. According to McDougall and Hungr (2004) a mass flowing on an irregular 3D terrain experiences centripetal acceleration, due to the curvature of the path. For a frictional model the acceleration consequently is:

$$a = g \cdot (\sin \beta - \tan \phi \cdot \cos \beta - \frac{v^2 \cdot \tan \phi}{r \cdot g})$$ [4-10]

Where a and v, are respectively the acceleration and the velocity of the centre of mass in the direction of the flow (Lagrangian system) and r is the radius of curvature.

For the geometry of the experimental set-up considered in the present study the path can be divided in three zones, the inclined slope at 45° before the curve, the curved part and the runout horizontal part as shown in Figure 4.30. In the first and last parts the centrifugal forces are equal to zero (r is infinite). For the curved part the calculations have been divided in steps of Δt and the slope has been updated of β-δ for each time step. To simplify the calculation, the velocity v in equation [4-10] of the term counting the centripetal acceleration, has been considered for each time step as the velocity $v(t)$ of the previous integration step, leading to the following equations of motion:

$$a\left(t + \Delta t\right) = g \cdot (\sin \beta - \tan \phi \cdot \cos \beta - \frac{v\left(t\right)^2 \cdot \tan \phi}{r \cdot g})$$

$$v\left(t + \Delta t\right) = \left[g \cdot (\sin \beta - \tan \phi \cdot \cos \beta - \frac{v\left(t\right)^2 \cdot \tan \phi}{r \cdot g}) \right] \cdot \Delta t + v\left(t\right)$$ [4-11]

$$x\left(t + \Delta t\right) = \left[\frac{g}{2} \cdot (\sin \beta - \tan \phi \cdot \cos \beta - \frac{v\left(t\right)^2 \cdot \tan \phi}{r \cdot g}) \right] \cdot \Delta t^2 + v\left(t\right) \cdot \Delta t + x\left(t\right)$$

Where x is the displacement of the centre of mass.

The calculations have been carried out also without taking into account the centripetal acceleration and results have been compared with laboratory data of some of the series of tests with gravel released at once. Results of the computations (both with and without centripetal acceleration) and of the laboratory tests are listed in Table 4-5 and shown in Figures 4-31 and 4-32. The average values on all the tests of the same series are reported.

Back-analysing the tests with a curved discontinuity at the toe, it has been possible to find an average dynamic friction coefficient at the base $\phi_{C\ 0}$ equal to ~24.5°. Using this value, two series with a sharp connection at the toe have then been back-analysed, decreasing the radius till the distance travelled by the centre of mass, measured with the fringe projection method and the computed one correspond.
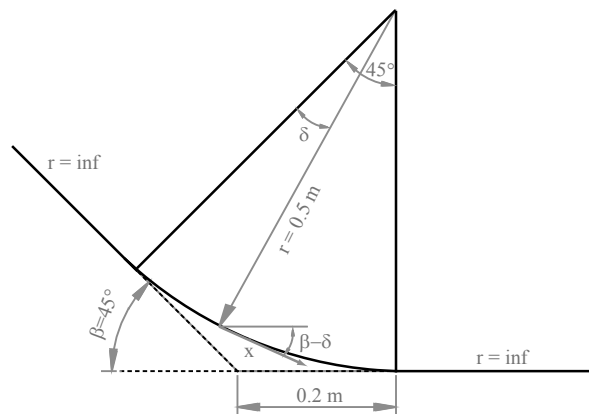
Figure 4-30 Curved connection at the toe

	Test conditions					Measured data		Computed data		
	One release of gravel on forex					Average values		with centripetal acceleration		without centripetal acceleration
Material	Slope	Fall	V	Slope	Series	X_{CM}	ϕ_{CM}	r	$\phi_{C\ 0}$	$\phi_{C=0}$
	[°]	[m]	[l]	Toe	number	[m]	[°]	[m]	[°]	[°]
Gr2	45	1	40	curved	28	~0.72	~34	0.5	~25	~32
Gr2	45	1.5	40	curved	27	~1.06	~33	0.5	~24.5	~32
Gr2	45	1	20	curved	28	~0.70	~34	0.5	~24.5	~32
Gr2	45	1.5	20	curved	27	~0.98	~33.5	0.5	~24.5	~32
Gr2	45	1	40	sharp	15	~0.36	~40.5	~0.005	24.5	~37.5
Gr2	37.5	1	40	sharp	17	~0.24	~35.5	~0.003	24.5	~33.5

Table 4-5 Test conditions, measured and computed data (with and without taking into account centripetal acceleration)

$\phi_{C\ 0}$ equal to ~24.5° is slightly higher than the measured ϕ_{dyn} (~23.5°) obtained with laboratory tilting tests (see section 4.1.1). In addition if the $\phi_{C=0}$ (travel angle computed with the sled model without the centripetal acceleration) is compared with the one measured for tests with the fringe projection method, ϕ_{CM}, a difference of about 2° is always detected. This is due to the fact that the lumped mass model does not allow considering the dissipation of energy within the mass and the spreading with the consequent flattening of the final deposit. As shown in Figure 4-31, for a release of 40 litres from 1 metre height there is a difference (Δh_{CM}=8 cm) between the height of centre of mass of the idealised sled model and the real one measured in laboratory.

It can be concluded from these observations that the lumped mass model can be useful to have a first approximation of the distance travelled by the centre of mass, but it does not take into account the loss of energy within the mass. In addition it cannot be used to predict the propagation of the distal end of the deposit because it considers the mass as a rigid block and it does not take into account the considerable spreading that takes place in the accumulation zone, which, as it has been observed previously, plays a significant role in the determination of the final runout.
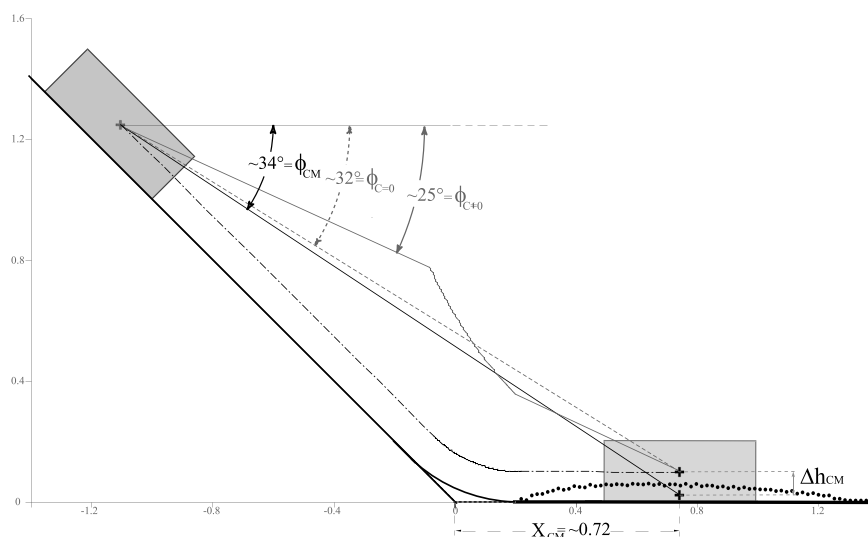
Figure 4-31 Straight energy line according to the measured ϕ_{CM} (filled black line) and the computed ones without taking into account the centripetal acceleration $\phi_{C=0}$ (dashed grey line); energy line accounting the centripetal acceleration $\phi_{C\ 0}$ (filled grey line); the path of the centre of mass in the case of the sled model is indicated with a black dashed-point line; test with 40 litres of gravel released at once from 1 metre height on a board at 45° covered with forex with a curved connection at the toe
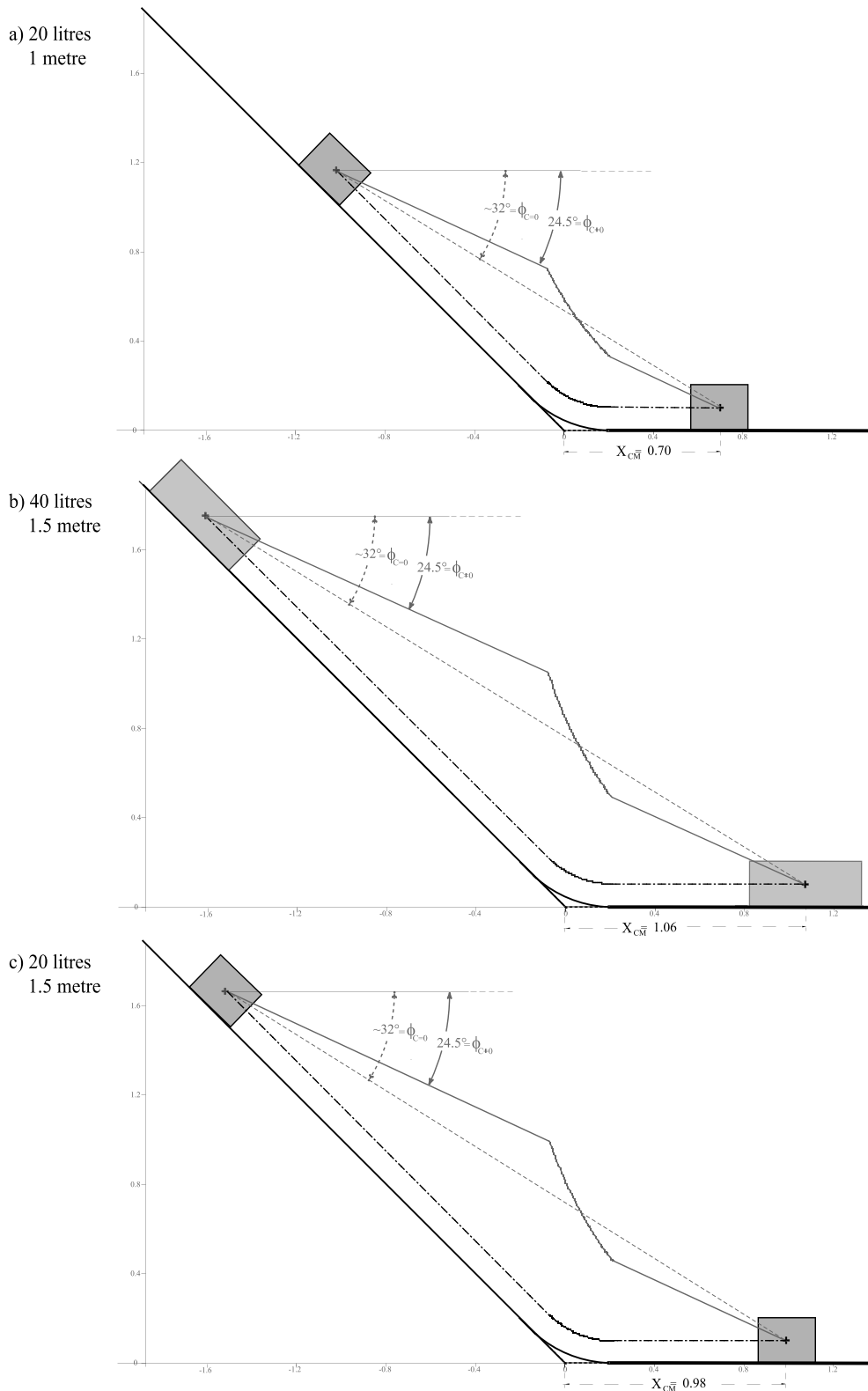
Figure 4-32 Straight energy line according to the computed travel angle without taking into account the centripetal acceleration $\phi_{C=0}$ (dashed grey line) and energy line accounting the centripetal acceleration $\phi_{C\ 0}$ (filled grey line); the path of the centre of mass is indicated with a black dashed-point line. a) test with 20 litres of gravel from 1 metre height; b) test with 40 litres of gravel from 1.5 metre height; c) test with 20 litres of gravel from 1.5 metre height

Maintaining constant the dynamic friction (ϕ_{dyn} or $\phi_{C\ 0}$) to 24.5° and varying the radius (r) of the curvature, different values of the distance travelled by the centre of mass (X_{CM}) are obtained and are plotted in Figure 4-33. It can be observed that the centripetal acceleration has a significant influence only for small values of r since the travel distance of the centre of mass starts decreasing significantly only for r less than 0.04 metre. In addition to obtain the measured X_{CM} of tests with a sharp discontinuity at the toe it is necessary to use values of the radius of less than 5 mm, in the order of the gravel grain size.

An accurate and systematic study of different curvature at the base should contribute to extend the considerations reported here.
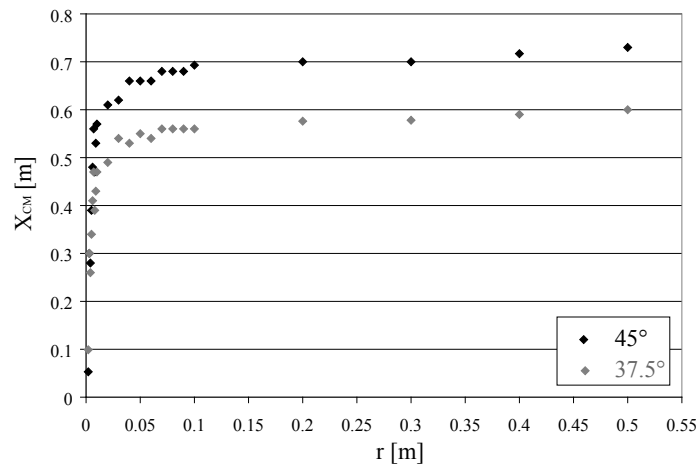
Figure 4-33 Travel distance of the centre of mass X_{CM} against the radius of the curvature predicted with a lumped mass model accounting for the centripetal acceleration (basal friction angle fixed to 24.5°); some noises are due to numerical imprecision; slope at 37.5° (grey) and 45° (black); release of 40 l, from 1 m height, on a inclined board covered with forex

4.3.4. Normalised length and runout of the deposit

According to Davies and McSaveney (1999), three non-dimensional factors have been computed, namely the normalized length (L*/h*), the normalized runout (R/h*) and the normalized vertical fall height (h_v/h*) which are respectively the deposit length, its runout on the horizontal panel and the total height of the centre of mass before release (see Figure 4-10), all normalized by the cube root of the volume, h*. Davies and McSaveney have used a factor, R_h/h*, defined as the normalized travel distance on the horizontal surface, but it is not clear whether this is equivalent to R/h* or L*/h* used here. Nonetheless their results seem to show little or no difference between these two values. In the tests analysed in the

present study these characteristics do not coincide (see section 3.3.1 and Figure 3-9), hence they are considered separately.

First only the tests with a sharp discontinuity at the toe have been considered to facilitate the comparison with results of Davies and McSaveney who have performed tests with the same configuration. Normalized length (see Figure 4-34a and b) does not depend on fall height and values of tests with gravel and blocks arranged randomly are in the range from 2 to 3.8. This is generally in agreement with the range of values obtained by Davies and McSaveney (1999), which lie between 1.5 and 3 (see Figure 2-14), as opposed to the real events considered, i.e. South Ashburton (New Zealand), Elm (Switzerland) and Frank slide (Canada) which have values between 4 and 7. They suggested that this difference between laboratory results and field observations could be caused by phenomena that occur only in field situations at large scale and that were not observed in laboratory (such as rock fragmentation during motion or the presence of saturated substrata).

Here as well it is confirmed that tests with blocks arranged in piles have particularly long spreading. Consequently they have higher values of L^*/h^*, between 3.2 and 4.3, which are closer to the values of the above-mentioned real events. It is possible to spot the same difference observing normalized runouts (see Figure 4-34c and d): tests with piled bricks have higher values than those with gravel or bricks poured randomly and are closer to real events. Despite the data scattering, it is also interesting to observe the linear dependency between the normalized runout and the normalized vertical fall height: R/h^* increases with the increase of h_v/h^*.
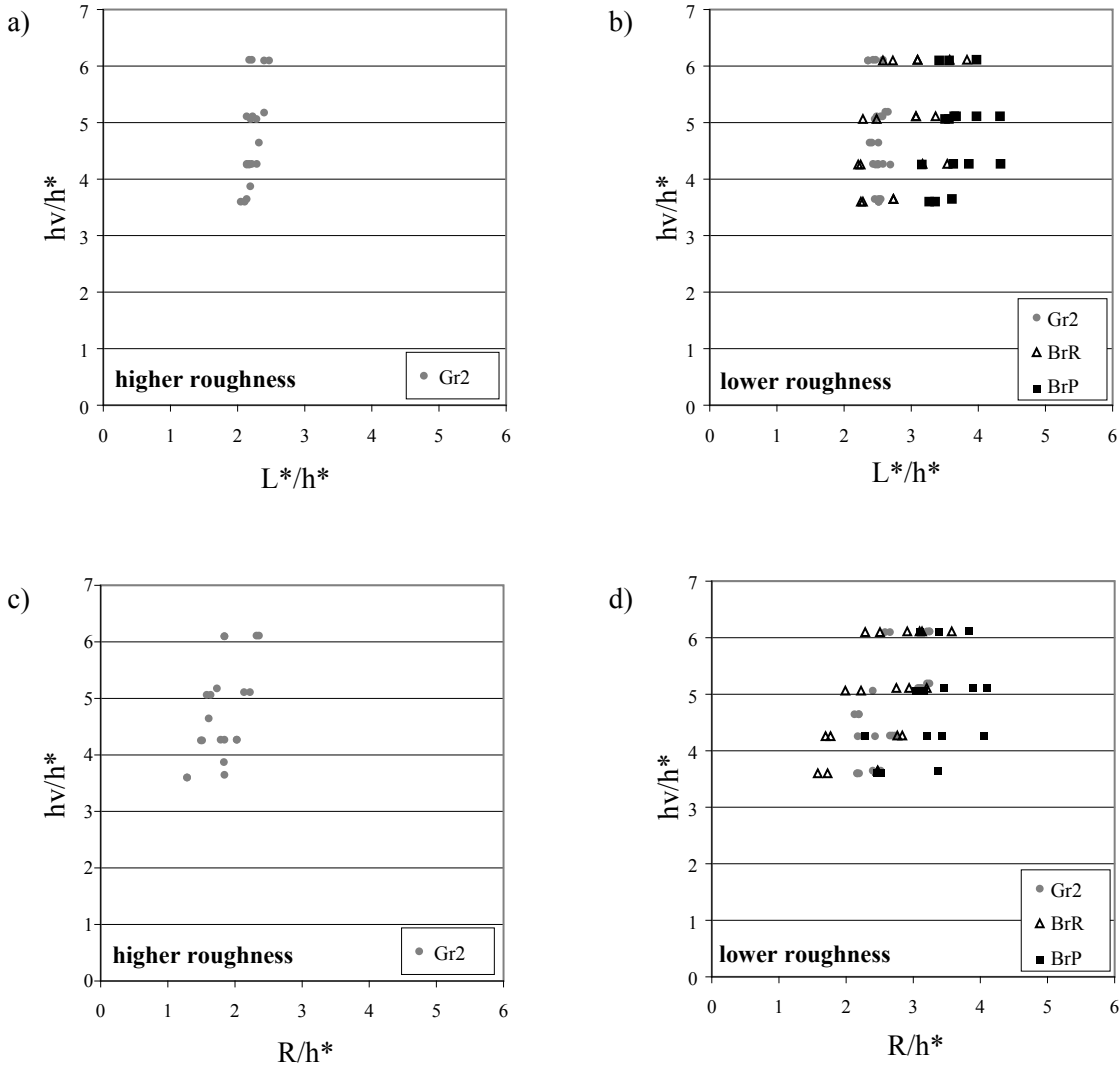
Figure 4-34 Normalised deposit length (L*/h*) plotted against normalized vertical fall height (h$_v$/h*), rough (a) and smooth (b) board surface with a sharp connection at the toe; normalised runout on the horizontal surface (R/h*) plotted against normalised vertical fall height (h$_v$/h*), rough (c) and smooth (d) board surface with a sharp connection at the toe. Gravel (grey circles), Random bricks (empty triangles) and Piled bricks (black squares)

From this analysis on all the tests (single release) it is possible to confirm what found with the parametrical study shown in section 4.2 and resumed in Table 4-4: runout is found to be dependent on fall height, on basal friction and on the structure of the bricks before failure; on the other hand length is slightly dependent on fall height and basal friction; nonetheless it is affected by the arrangement of the bricks.

These results can be translated in the following empirical formulations for what concerns the length of the deposit:

$$L^* = 2 \div 3.8 h^* \quad for\, Gr2 \ and \ for\, BrR$$
$$L^* = 3.2 \div 4.3 h^* \quad for\, BrP$$

[4-12]

And the following ones for what concerns runout:

$$R = a h_v + b h^*$$

[4-13]

Where *a* and *b* are two coefficients varying according to the basal friction and the material used. The data are too scattered to give a precise value of these two coefficients but it has to be considered that in the plots of Figure 4-34 are included data coming from tests carried out with different slope angles, which has been detected as a factor influencing runout (see Table 4-4). If the data are separated the scattering is less (see Figure 4-35) but the data set is not large enough to establish a general formulation. What can be said is that *a* varies accordingly for all the materials: when slope increases, *a* increases. On the other hand *b* is variable and it is impossible to establish a trend.
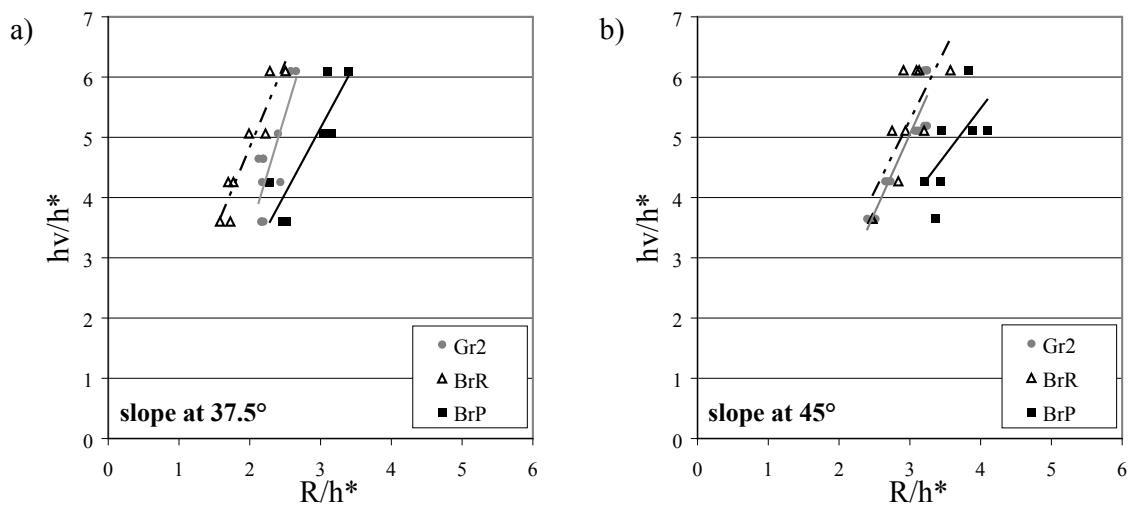
Figure 4-35 Normalised runout on the horizontal surface (R/h*) plotted against normalised vertical fall height (h_v/h*) of tests on forex with a sharp discontinuity at the toe, distinguished between a) slope at 37.5° and b) slope at 45°. Gravel2 (grey circles), Random bricks (empty triangles) and Piled bricks (black squares)

If tests with a curved discontinuity at the toe are considered these values change. As shown in the previous section the loss of energy due to the impact with the horizontal panel has a great influence on runout. It is interesting here to compare the different behaviour detected for tests with gravel and little bricks piled orderly before failure. In Figure 4-36a it can be seen how also in this case the length is not dependent on the fall height. In addition when gravel is used the difference in the connection at the toe does not influence a lot the length

of the deposit. So the range considered in equation [4-12] does not change significantly and results still agree with the ones of Davies and McSaveney. On the other hand a major difference is detected for tests with piled bricks where a change in the connection at the toe seems to influence significantly the length of the deposit. As already explained, the shattering process and the spreading of a mass structured at the start is induced by the change in flow direction at the toe of the slope. Now, when the connection between the panels is regular, the mass can keep further its structure, "sparing" energy and travelling further with a more elongated shape. In this case (i.e. piled bricks and curved connection), high values of both normalised length and runout are found, ranging between 5.1 to 5.6 times the cubic root of the volume h*, much closer to the ones evaluated on real events by Davies and McSaveney (between 4 and 7).

As shown in Figure 4-36b, also in the case of a curved connection between the panels the relationship between the normalized runout and the normalized height is clearly linear, but the coefficient *a* of equation [4-13] increases putting into evidence some interaction between this factor and fall height in the effect on runout.
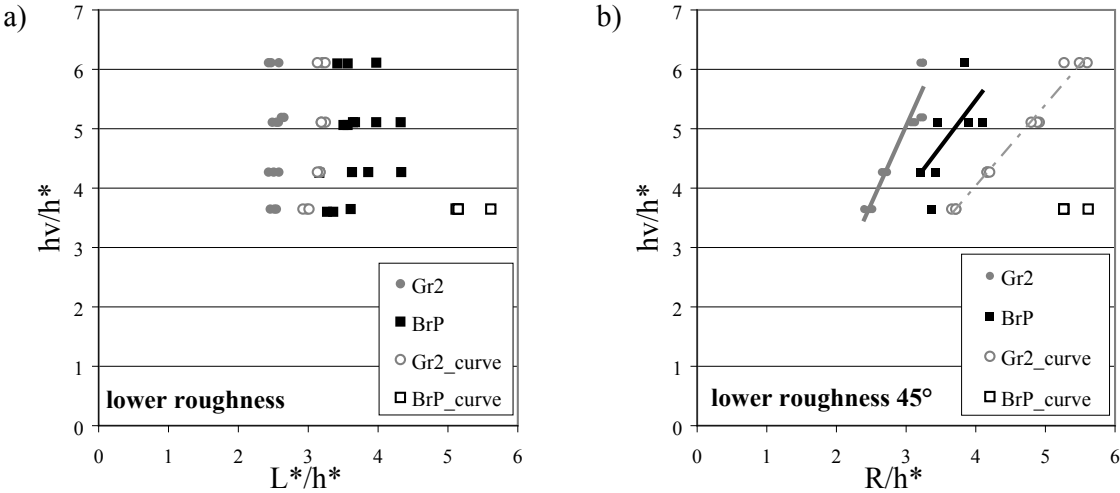
Figure 4-36 a) Normalised length (L/h*) and b) normalised runout (R/h*) on the horizontal surface plotted against normalised vertical fall height (h$_v$/h*). Slope at 45° covered by forex, Gravel2 (grey circles), Gravel2 with curved discontinuity (empty grey circles), Piled bricks (black squares) and Piled bricks with curved discontinuity (empty black squares)*

4.3.5. Statistical analysis of the results

In the previous sections the effects of different factors have been considered separately, qualitatively and quantitatively. Both analyses have been necessary to identify significant

factors within certain conditions; nevertheless none of them could capture the global picture. By means of the statistical method called analysis of variance (ANOVA), it is possible to consider at once the influence of several factors together verifying at the same time the presence of any interaction between them. When models exist describing a certain phenomena, this method is used to quantify the coefficients characterising the dependency between factors and a considered response. Since no empirical model has been yet developed able to describe in a comprehensive manner the propagation of rock avalanches, in the present study this method has been limited to verify the importance of the different factors and if any interaction could exist between them. For simplicity of use a linear model has been supposed between the factors and the responses considered, which will allow studying also first degree interactions. Despite these limitations this analysis has revealed to be really useful to verify what has been deduced from previous analyses and to identify additional interactions difficult to detect from a one factor at a time analysis.

In this section, the ANOVA method will be briefly presented according to the E-Handbook of Statistical Methods (NIST/SEMATECH, 2006) and the lecture notes of Fürbringer (2005) to which the reader is invited to refer for further information. More details will be also given in appendix III. Afterwards the analysis on the tests will be illustrated; considerations on the significant factors resulting from the ANOVA analysis will be made and then compared with the previous results achieved in the parametrical and empirical studies.

Analysis of variance: ANOVA

According to the E-Handbook of Statistical Methods (NIST/SEMATECH, 2006) and Fürbringer (2004), the initial techniques of the analysis of variance were developed by the statistician and geneticist R. A. Fisher in the 1920s and 1930s and it is used to detect significant factors in a multi-factor model. In the multi-factor model, there is a response (dependent) variable and one or more factor (independent) variables. This is a common model in designed experiments where the experimenter sets the values for each of the factor variables and then measures the response variable.

The matrix of the model is the matrix X which has one line per experiment, one column per factors of the model. In the present study linear models will be considered whose general formulation is as follows:

$$y_i = c_o + \sum_{i=1}^{N} c_i\, x_j + \sum_{1, j \neq i}^{N} c_{ij}\, x_i\, x_j + e_i$$

$$\vec{Y} = \begin{bmatrix} y_1 \\ \vdots \\ y_N \end{bmatrix} = X \begin{bmatrix} c_o \\ c_1 \\ \vdots \\ \vdots \\ c_{123\ldots K} \end{bmatrix} + \begin{bmatrix} e_1 \\ \vdots \\ e_N \end{bmatrix} = X\,\vec{c} + \vec{e}$$

[4-14]

Where $\vec{Y}$ is the column vector of the N experimental measurements of the response considered, $\vec{c}$ is the column vector of the model coefficients, $\vec{e}$ the column vector of the N experimental errors corresponding to each y_i experimental data and X is the matrix of the model.

The coefficients of the model can be estimated through the least square algorithm as in [4-15].

$$E(\vec{c}) = \left(X^T X\right)^{-1} X^T \vec{Y} - \left(X^T X\right)^{-1} X^T E(\vec{e})$$

$$E(\vec{c}) = \left(X^T X\right)^{-1} X^T \vec{Y}$$

[4-15]

With $E(\vec{c})$ is the estimated value of the coefficients of the model considering the estimated values of the error $E(\vec{e})$ equal to zero.

The coefficients of the model corresponding to the factors considered are called effects. The differences between the predicted values and the measured values are called residuals. The fundamental technique of the ANOVA is a partitioning of the total sum of squares (SS) into components related to the effects used in the model.

$$SS\_total = SS\_error + SS\_effects$$

[4-16]

Equation [4-16] summarizes how much of the variance in the data (total sum of squares) is accounted for by the factor effects (factor sum of squares) and how much is random error (residual sum of squares). In order to evaluate the significant factors it is necessary to compare the sum of squares of the effects with the sum of squares of the residuals. These have a chi-square distribution which results when independent variables with standard normal distributions are squared and summed. The effects mean squares of a significant effect are expected to be significantly greater than the mean square of the residual errors.

To compare them in a rigorous and objective way it is necessary to do an F test for the factor effects. An F-test (Snedecor and Cochran, 1983 as reported in NIST/SEMATECH, 2006) is used to test if the standard deviations of two populations are equal. The more this ratio deviates from 1, the stronger the evidence for unequal population variances. As a consequence higher is the probability (values near to 1), less the effect is significant since the factor and the residual have in this case similar variance. In next section the factors and responses considered are shown. In appendix III an example of the ANOVA analysis is reported.

Nondimensional factors and responses

In order to have scale independent formulations the two main following factors have been considered for the analysis of variance:

- $\dfrac{h_v}{h^*}$:   fall height of the centre of mass above the horizontal panel before failure (h_v, [m]) as defined in Figure 4-9 against the cube root of the volume (h^*, [m]);

- $\dfrac{\tan \phi}{\tan \alpha}$:   the tangent of the basal friction coefficient (ϕ) against the tangent of the slope angle (α). This last term represents the divergence from stability of the mass.

ANOVA has been performed separately for Gravel (Gr2), bricks randomly poured in the reservoir before failure (BrR) and piled orderly (BrP); then also for curved and sharp connections at the toe. An attempt has been made to include these two factors considering a degree of structure called **K** varying from 0 (loose material, i.e. BrR) to 1 (structured compact material, i.e. BrP) and a degree of smoothness of the connection at the toe called **S** varying from 0 (sharp angular discontinuity at 45°) to 1 (curved discontinuity after a 45° slope). This last factor has been introduced only for tests with gravel since not enough tests with bricks have been performed with **S**=1 to allow a proper analysis.

The ranges of variation of the factors are reported in Table 4-6, where h is the fall height considered in Figure 4-1.

Model for:	h [m]	h^* [m]	α [°]	ϕ [°]	Nondimensional factors [-]			
					h_v/h^*	$\tan\phi/\tan\alpha$	K	S
Gr2	1-1.5	0.27-0.34	37.5-45	28-32	3.6-6.11	0.53-0.81	0	0
BrR	1-1.5	0.27-0.34	37.5-45	30	3.6-6.11	0.58-0.75	0	0
BrP	1-1.5	0.27-0.34	37.5-45	30	3.6-6.11	0.58-0.75	1	0
BrR vs BrP	1-1.5	0.27-0.34	37.5-45	30	3.6-6.11	0.58-0.75	0-1	0
Curved vs Sharp (Gr2)	1-1.5	0.27-0.34	45	28	3.6-6.11	0.53	0	0-1

Table 4-6 Ranges of variation of the nondimensional factors considered in the ANOVA analysis

The nondimensional responses are:

- $\dfrac{R}{h^*}$:   the runout on the horizontal panel (**R**, [m]) as defined in Figure 4-9 against the cube root of the volume (**h***, [m]);

- $\dfrac{L^*}{h^*}$:   the deposit length (**L***, [m]) as defined in Figure 4-9 against the cube root of the volume (**h***, [m]);

- $\dfrac{W}{h^*}$:   the deposit width (**W**, [m]) as defined in Figure 4-9 against the cube root of the volume (**h***, [m]);

- $\dfrac{X_{CM}}{h^*}$:   the distance travelled by the centre of mass on the horizontal panel (**X**_{CM}, [m]) as defined in Figure 4-9 against the cube root of the volume (**h***, [m]);

- $\dfrac{\tan\phi_{ap}}{\tan\alpha}$:   the tangent of the apparent coefficient of friction or Fahrböschung (ϕ_{ap}) against the tangent of the slope angle (α);

- $\dfrac{\tan\phi_{CM}}{\tan\alpha}$:   the tangent of the travel angle of the centre of mass (ϕ_{CM}) against the tangent of the slope angle (α).

These factors and responses have been chosen since they have been found to be important in the previous analysis. Only two or three factors are considered at the same time. The first-

order model with second order interactions considered are as described in equation [4-17] respectively for 2 and 3 factors:

$$Y_i = a_0 + a_1 X_1 + a_2 X_2 + a_{12} X_1 X_2$$
$$Y_i = a_0 + a_1 X_1 + a_2 X_2 + a_3 X_3 + a_{12} X_1 X_2 + a_{13} X_1 X_3 + a_{23} X_2 X_3 + a_{123} X_1 X_2 X_3$$

[4-17]

Significant factors resulting from the ANOVA analysis

By means of the ANOVA the significant factors and interactions have been determined and are resumed in this section. An example of the whole ANOVA analysis is given in appendix III.

Analyses have been performed for gravel, bricks poured randomly into the reservoir and bricks piled orderly before failure. Results are similar so they are resumed in Table 4-7. If a factor has a different influence, depending on the material used or the arrangement of the blocks before failure, it is reported as variable. Additional analyses have been carried out for BrR and BrP to evaluate the effect of the degree of structure *K* (see Table 4-8).

factors			**interactions**
response	*hv/h**	*tanϕ/tanα*	*hv/h* & tanϕ/tanα*
R/h^*	**high**	**high**	low
L^*/h^*	variable	variable	low
W/h^*	**high**	low	**high**
X_{CM}/h^*	**high**	**high**	variable
$\tan\phi_{CM}/\tan\alpha$	low	**high**	low
$\tan\phi_{ap}/\tan\alpha$	low	**high**	low

Table 4-7 Resume of the three ANOVA analyses of the responses for tests with gravel (Gr2), bricks poured randomly into the reservoir before failure (BrR) and bricks piled orderly into the reservoir before failure (BrP), with a sharp discontinuity at the toe (S=0)

factors				**interactions**		
response	*hv/h**	*tanϕ/tanα*	*K*	*hv/h* & tanϕ/tanα*	*hv/h* & K*	*tanϕ/tanα & K*
R/h^*	**high**	**high**	**high**	low	low	low
L^*/h^*	low	**high**	**high**	low	low	low
W/h^*	**high**	low	**high**	low	low	low
X_{CM}/h^*	**high**	**high**	low	low	low	low
$\tan\phi_{CM}/\tan\alpha$	low	**high**	low	low	low	low
$\tan\phi_{ap}/\tan\alpha$	low	**high**	**high**	low	low	low

Table 4-8 ANOVA analysis of the responses for tests with bricks poured randomly into the reservoir before failure (K=0) and bricks piled orderly into the reservoir before failure (K=1) with a sharp discontinuity at the toe (S=0)

Another analysis has been performed only on the tests with gravel released on a 45° slope with forex with either a sharp or a curved transition at the toe, in order to evaluate the effect of the degree of smoothness of the connection at the toe called S (see Table 4-9).

factors			interactions
response	*hv/h**	*S*	*hv/h* & S*
R/h^*	**high**	**high**	low
L^*/h^*	low	**high**	low
W/h^*	**high**	**high**	low
X_{CM}/h^*	**high**	**high**	low
$\tan\phi_{CM}/\tan\alpha$	low	**high**	low
$\tan\phi_{ap}/\tan\alpha$	low	**high**	low

Table 4-9 ANOVA analysis of the responses for tests with gravel (Gr2) with a sharp discontinuity at the toe (S=0) together with a curved discontinuity at the toe (S=1)

It is possible to resume the results as follows:

1. Runout results to be dependent on the fall height, $\tan\phi/\tan\alpha$, i.e. the divergence from stability of the mass, the degree of structure (K) and the degree of smoothness (S).

2. Length of the deposit results to be dependent on the degree of structure (K) and the degree of smoothness (S) and it seems to be dependent only under certain conditions on $\tan\phi/\tan\alpha$. On the other hand it is independent from fall height.

3. Width of the deposit is dependent on fall height, on the degree of structure (K) and the degree of smoothness (S). On the other hand width results to be dependent on $\tan\phi/\tan\alpha$ only if the interaction with fall height is taken into account.

4. The travel distance of the centre of mass results to be dependent on fall height, $\tan\phi/\tan\alpha$ and the degree of smoothness (S). Nonetheless its dependency on the degree of structure (K) is low.

5. The travel angle of the centre of mass is as well dependent on $\tan\phi/\tan\alpha$ and on the degree of smoothness (S), but is independent from the degree of structure (K) and also from the fall height.

6. The Fahrböschung is dependent on $\tan\phi/\tan\alpha$, the degree of structure (K) and the degree of smoothness (S), but it is independent from the fall height.

The results of the ANOVA analysis confirm the considerations made in the previous section: all the factors studied have a strong influence on runout, while length is independent from fall height. Whether bricks are poured in randomly or piled orderly in the reservoir before failure, this doesn't influence significantly the travel distance and the travel angle of the centre of mass. Both the Fahrböschung and the travel angle of the centre of mass result to be independent from the fall height. All the responses vary significantly when the transition between the panels is smooth (rather than sharp), underling again the importance of considering the dissipation of energy within the mass in the study of rock avalanche propagation.

4.3.6.   Conclusions on the empirical and statistical analyses

According to Corominas (1996), an index Lr has been computed for the tests which represents the ratio between the exceeding travel distance as calculated by Hsü (1975) and the distance of the mass if it had travelled dissipating energy only through normal friction. Instead of using the 32° angle of basal friction proposed by these formulations, it has been used here the basal friction angle of each material measured by tilting tests. Results show that piled bricks released on a plane with a sharp discontinuity at the toe and gravels released on a regular pathway with a curved slope don't exhibit an excessive mobility and remain in the range of a "normal" frictional behaviour. Only the combination of bricks and curved slope does induce an excessive mobility of the distal end of the mass.

In order to have a variable that quantifies better energy losses, a relative energy loss ratio has been computed: values of ΔE confirmed that a model considering only energy dissipation at the base is not sufficient to explain the behaviour of a granular mass. Energy seems to be dissipated mainly by friction at the base in the case of piled bricks, the more the material is structured the less the energy is dissipated within the mass on the slope till it reaches the horizontal panel and shatters. In addition if the connection at the toe is progressive the shattering of the mass is partially avoided, inducing to an even more marked importance of the frictional dissipation with values of $\Delta E/E_{lt}$ near zero.

Back-anlysing tests results with a lumped mass model that takes into account centripetal acceleration can be concluded that it can be useful to have a first approximation of the

distance travelled by the centre of mass, but it is not adequate to evaluate the loss of energy within the mass and to predict the total runout.

According to Davies and McSaveney (1999) the length of the deposit scaled with the cube root of the volume has been calculated for all the tests. Values measured in the tests with aquarium gravel and blocks arranged randomly are in general agreement with the range of values Davies and McSaveney obtained. On the other hand, tests with blocks arranged in piles have longer spread and runout. A marked difference is detected for tests with a curved connection at the toe which are much closer to the ones evaluated on real events by Davies and McSaveney (between 4 and 7). The runout of the deposit is found to depend on volume and on the fall height following the equation

The results of the ANOVA analysis, confirm the considerations made: all the factors studied have a strong influence on runout, while length is independent from fall height. The structure of the mass before failure has a strong influence on runout and Fahrböschung. All the responses vary significantly when the transition between the panels is smooth (rather than sharp), underling again the importance of considering the dissipation of energy within the mass in the study of rock avalanche propagation.

5.   Complementary tests and benchmark exercises

In this chapter some additional experiments and a benchmark exercise are described. The necessity to put them separately is that not enough tests have been made to draw significant conclusions. Nonetheless the considerations made are interesting; moreover they introduce some possible developments of research in this field and consequently deserve to be mentioned.

Changes in the experimental set-up have been made to carry out a particular test which has made the object of an international benchmark exercise for "the 2007 International Forum on Landslide Disaster Management, Hong Kong - Landslide Runout Analysis Benchmarking Exercise". Numerical modellers from all over the world have been called to simulate real cases and a laboratory test. The Rock mechanics laboratory has been asked to carry out the above mentioned experiment. The particularity of this test is that a deflection is placed as an obstacle in the flow direction. This allows to validate codes on a particular topography and to check if they can simulate with sufficient accuracy even strongly curved flows.

The experimental set-up has been consequently modified and the measuring system has been improved in order to provide additional data. Thus, the fringe projection method has been adapted to measure the thickness of the flow during motion. These improvements are described in details. As for tests with a curved discontinuity, it is really important to illustrate here the experimental campaign made with the deflection in order to outline the main differences in mechanisms and propagation when the topography of the path changes.

In the last part of this chapter, the results of a benchmark exercise made in the framework of the INTERREG "Rockslidetec" project are shown. One of the experiments made with the standard geometry of the set-up, has been simulated with the codes developed by three partners: the Cemagref code and RASH3D (Politecnico di Torino), based on a continuum mechanics approach and EPAN3D (CETE), based on a discrete approach.

These benchmark exercises evidence a possible application of the tests carried out at the LMR and they underline the importance of the validation of numerical codes and models on well-defined laboratory tests since this contributes to understand advantages and limits of the codes, improving their development and their use and consequently enhancing forecast of rock avalanche propagation.

5.1.   Deflection experiments

As described on the web site (http://hkieged.org/LDM2007), the 2007 International Forum on Landslide Disaster Management has been held in Hong Kong from 10 to 12 December 2007, organized under the auspices of the Joint Technical Committee on Landslides and Engineered Slopes (JTC-1) of the ISSMGE, ISRM and IAEG. The Forum has been also one of the key activities marking the 30th Anniversary of landslide disaster management in Hong Kong. It comprises a compact and intense session for about 60 invited experts from different countries to share experiences and thoughts on the state-of-the-art and best practices. It addresses focused subjects of direct relevance to landslide disaster management. Highlights of the Forum include a benchmarking exercise on landslide debris mobility modelling. The benchmarking exercise is a novelty, covering an important and evolving area in landslide risk assessment and management. In this framework the EPFL Rock Mechanics Laboratory has been asked to carry out a laboratory test that is the object of this exercise.

As mentioned in section 2.1.1 deflections are described as "topographic obstacles on the path forcing a change in former direction of progression of more than 60°" (Corominas, 1996). According to Heim (1932) and as reported by Nicoletti and Sorriso-Valvo (1991) when a mass is deflected, it is decelerated and the effect on final deposit morphology depends on the angle of impact. If the deflection plane is orthogonal to the direction of progression, case of the opposite wall obstruction in Figure 2.1c, the avalanche is split in two parts of similar volumes, on the other hand if the angle is oblique the partition is not equal and the mass can be entirely deflected (Figure 2.1d). In addition deflections often cause partial runup and overthickening of the mass in movement (Corominas, 1996). When the deflection is strong and significantly increases dissipation of energy, it is reasonable to say that this kind of rock avalanche belongs to the third category established by Nicoletti and Sorriso-Valvo (1991): low mobility rock avalanche, determined by high energy dissipation. In fact, these kinds of landslides are also often characterized by runup, partition of the debris and fall-back ridges which indicate forced stopping and significant energy dissipation.

Testing the ability of mathematical models to predict the behaviour of ideal granular avalanches that move cross an irregular topographic surface is indeed a critical step towards

understanding and predicting the propagation of rock avalanches real events (Iverson et al, 2004b). Even if some authors agree with the fact that topography of the path strongly influences rock avalanche mobility, there are few attempts to systematically study its effect (Nicoletti and Sorriso-Valvo, 1991). In this framework both experimental campaigns with a curved discontinuity (see previous chapter) and with the deflection, could provide significant reliable data to verify phenomena that depend on the topography of the path and that were only observed empirically.

5.1.1. Set-up and testing configurations

The configuration of the set-up is inspired from tests carried out at the University of British Columbia (Vancouver, Canada) by McDougall and Hungr (2004). These tests were performed to demonstrate the ability of their numerical code (DAN3D) to simulate curved flow (McDougall, 2006): the material flowed from the chute onto a 20° approach slope and was then deflected by an inclined plane oriented obliquely to the approach direction. Following these first tests, the LMR has also introduced in the flow direction a deflector on the inclined plane.

The approach slope is in this case of 37.5°. According to McDougall (2006), two further angles are necessary to define the deflection plane:

- δ: the deflection angle, which is the plan angle between the approach direction and the intersection of the deflection and approach planes

- α_d: the deflection plane true dip angle

As shown in Figure 5-1, δ is equal to 62° and α_d to 22.6°. The panels are covered by forex and the materials used are Aquarium gravel2 and Hostun sand, whose characteristics are summarized in Table 5-1 and illustrated in details in section 3.2.2. As described in section 3.2.2, the material is arranged in the box to try to fill it entirely in height and width, varying the depth. At the back the angle of repose of the sand is approximately 70° to the inclined panel, as shown also in Figure 5-1. The material is released by the sudden removal of the downslope wall of the reservoir.

Material	Grain size distr. [mm]	Unit weight [kN/m³]	Static friction angles	
			Internal [°]	On forex [°]
Aquarium Gravel	D=0.5-3	14.3	34 ± 1	28 ± 1
Hostun sand	D=0.32-0.8	12.6	34 ± 1	32 ± 1

Table 5-1 Characteristics of the granular materials used for the deflection experiments

Eight experiments, two for each series listed in Table 5-2, have been carried out with this set-up, varying the material, the releasing height and the volume. The first series called Def_1 is considered as the reference configuration (bold, italic) and for the following ones, only one parameter (bold, italic) at a time is varied. In Figure 5-2 deflection tests are compared in pair, overlapping the contour of the final deposit and the position of the centre of mass respectively of Def_2 (a), Def_3 (b) and Def_4 (c) over the results from the series Def_1 (Gravel, 1 m, 30 l). In Figure 5-3 images taken by the high speed digital camera are illustrated for the same four test configuration. Each capture is at an interval of 1/6 of a second. This allows observing how the flow is deviated when it reaches the deflector and how the variation of a parameter affects the propagation. Since experiments have good reproducibility, only one of the two tests belonging to the same series has been represented in these images to facilitate the interpretation.
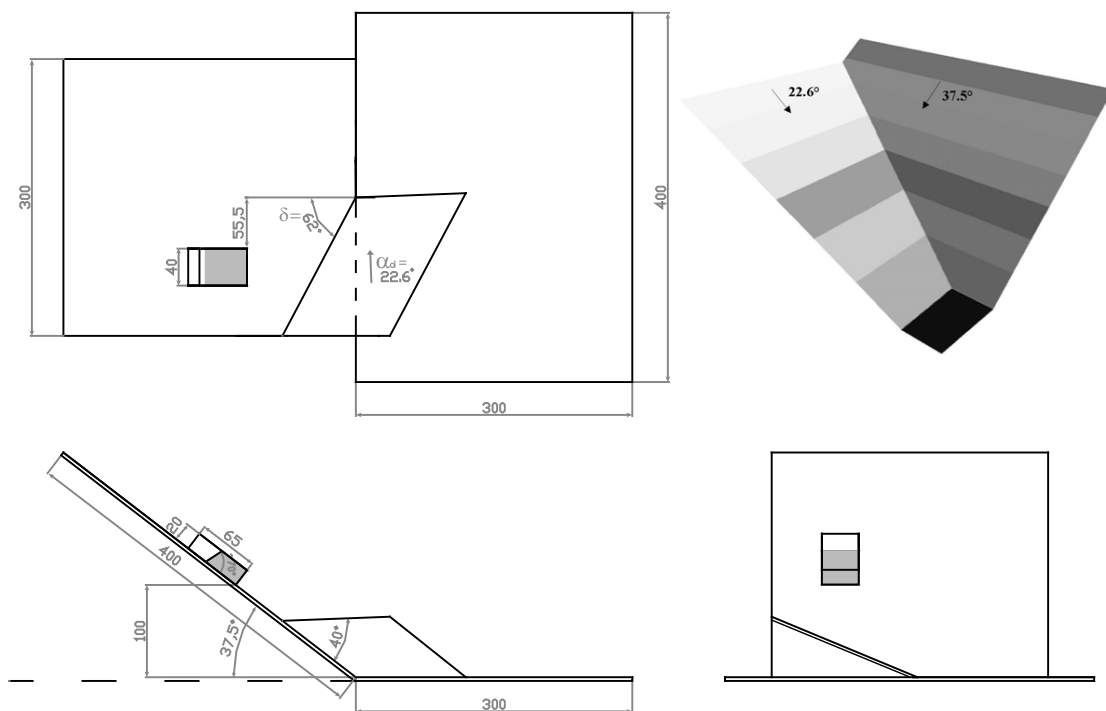
Figure 5-1 Deflection experimental set-up

Series	Material	Fall height [m]	Volume [l]
Def_1	*Gravel*	*1*	*30*
Def_2	Gravel	1	*40*
Def_3	Gravel	*1.5*	30
Def_4	*Hostun sand*	1	30

Table 5-2 Deflection experiments test conditions

5.1.2. Experimental results

It is possible to observe that an increase of the volume doesn't affect the propagation mechanism. As it is shown in Figure 5-3 the tests Def_1 and Def_2 are really similar from the release to 1.5 seconds. From this moment on, things start changing since the quantity of material is different. Even if the shape of the deposit remains almost the same, in the case of 40 l the deposit develops a little bit more in the upslope part of the deflector and as a consequence the centre of mass recedes. This is mainly due to the fact that when the front part of the mass reaches the deflection, it dissipates most of its energy. This induces a decrease of the velocity that leads to a complete stop of the first part of the mass on the deflector and at the toe before the rear part has completely reached it. As in the case of the consecutive releases seen in sections 3.5.3 and 4.2.1, the mass that has already come to a stop works as a kind of dam for the approaching material. The rear part of the mass has enough energy to overcome the deflection but it is then hindered by the deposit that has already taken shape on it and at the base and it consequently builds up upslope of the deflector. This is opposed to the standard case of an inclined plane without deflection (chapter 3 and 4) where there was a transfer of linear momentum between the two moving parts of the mass, the first one still coming to a stop and the rear one approaching. The fact that the in the case of 30 litres the mass travels slightly further than in the case of 40 litres on the horizontal panel it seems explained by the fact that since in the first case the mass approaching doesn't cover the entire width of the deflector, some material partly contours on the side the obstacle formed by the heap taking shape at the base.

In all three cases where gravel is used (Def_1, Def_2 and Def_3), the mass stretches out mainly on the deflector. A minor part reaches the toe on the horizontal panel and a small quantity remains on the approaching panel at 37.5°. Even when the mass is released from a higher point and has consequently a higher potential energy (Def_3), the runout on the horizontal part doesn't change significantly. This confirms the fact that a great quantity of

energy is dissipated when the flow is deflected. Therefore topographic obstacles hinder the flow of granular avalanches and lead to shorter runouts as stated by Hsü (1975) and reported by Nicoletti and Sorriso-Valvo (1991).

On the other hand Nicoletti and Sorriso-Valvo (1991) reported as well the consideration of Moore and Mathews (1978) who believe that landslides can make large changes in direction with little loss of velocity. This statement is not completely in opposition to the one of Hsü (1975), since the quantity of energy loss strongly depends from the sharpness of the obstacles the landslide encounters on its path. As demonstrated by tests with a sharp and curved connection at the toe, even if the change in direction is the same, the first configuration leads to much shorter runouts. Also in the case of a strong deflection in the flow it is presumable that if the discontinuity would be progressive and smoother also the energy loss would be limited, as it happens when a child slides in a sinuous tube-shaped slide. In addition in a strongly sinuous path the mass is in a way canalised and therefore it can be imagined that its initial structure is held together by the borders. In this case as in the case of bricks piled orderly before failure it could happen that less energy is dissipated within the mass and as a consequence compensates part of the energy spent at the base to overcome obstacles.
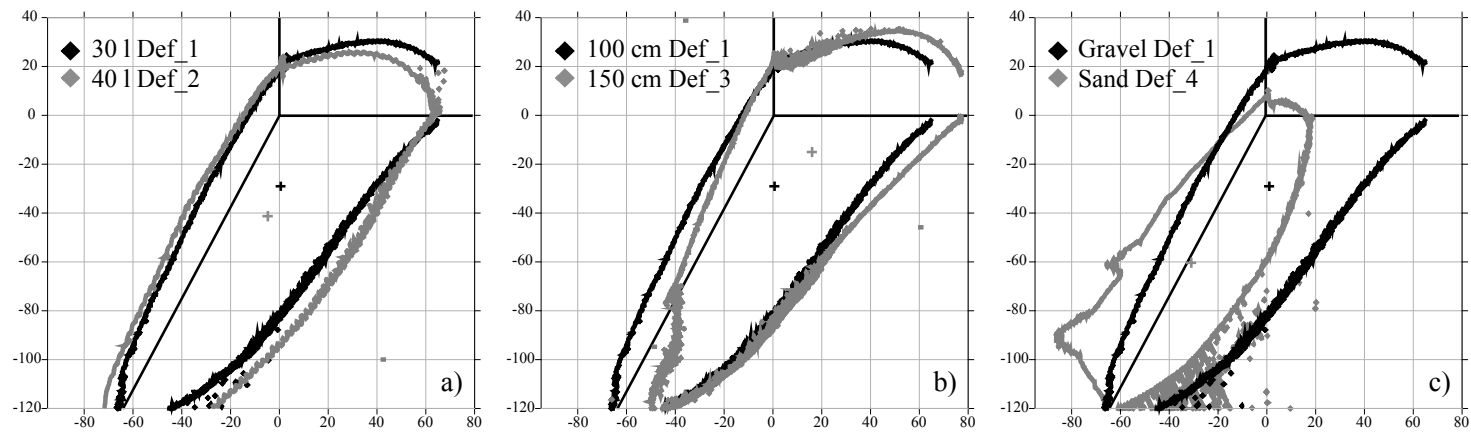
Figure 5-2 Final deposit and position of its centre of mass on the xy plane for the deflection tests. Contour line at 1 mm. Black markers: gravel, 30 l, 100 cm (Def_1) and grey markers: a) gravel, 40 l, 100 cm (Def_2); b) gravel, 30 l, 150 cm (Def_3); c) Hostun sand, 30 l, 100 cm (Def_4)
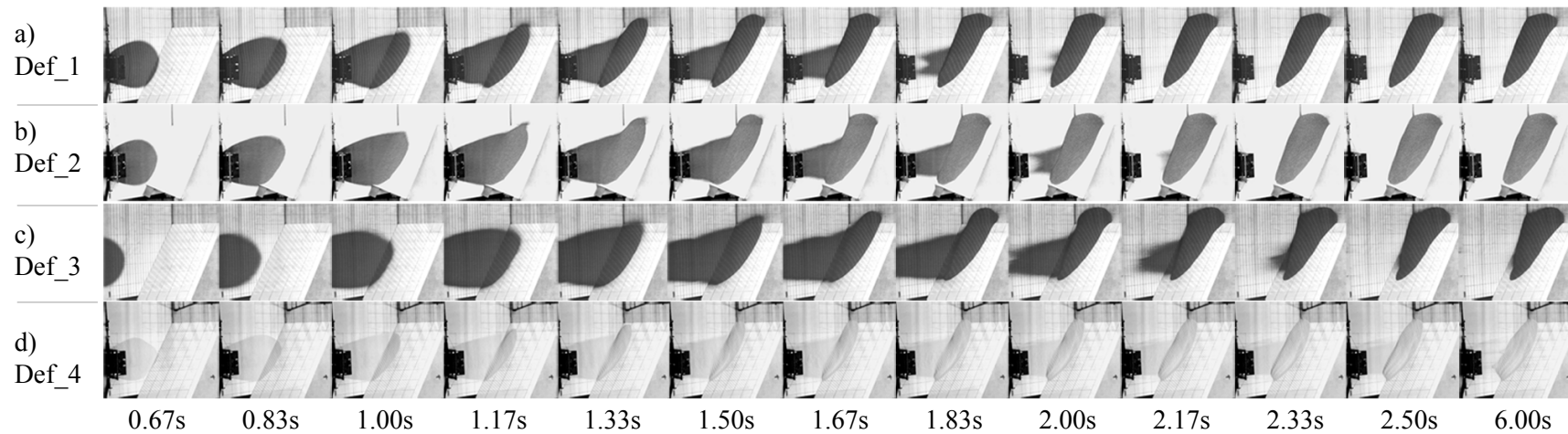
Figure 5-3 Comparison of the propagation in the deflection tests. Def_1: gravel, 30 l, 100 cm; Def_2: gravel, 40 l, 100 cm; Def_3: gravel, 30 l, 150 cm; Def_4: Hostun sand, 30 l, 100 cm. Images each 1/6 of a second. Time= 0s is the moment the gate opens

As already detected in previous experiments with gravel and Hostun sand (see section 3.5.1), the morphology and the dimensions of the deposit markedly change when the Hostun sand is used (Figure 5-2c and Figure 5-3d). This is due partly to the higher coefficient of friction between the sand and the forex, which induces greater energy dissipation on the approaching plane and reduced velocities all along the flow. As for the other tests a great part of the remaining energy is dissipated when the mass is deflected and consequently the front already comes to a stop on the deflector. The rest of the mass slowly reaches the deposit already made up downslope forming a rather ellipsoidal and thicker accumulation in the upper part, where the centre of mass is also located. The reduced velocities could also be due to the fact recalled in section 3.5.1 that the Hostun sand shows some peculiar behaviour: since it is an extremely fine material, a thin layer is probably stopped on the panel surface by some electrostatic effect. In the last part of the process consecutive layers of fine sand still approaching come to a stop, leading to a deposit developed more in height and less in lateral and longitudinal extension than the one observed for the test with gravel. This phenomenon is marked also from transverse ridges in relation to the direction of the flow detected on the final deposit; the sudden halt of the front caused by the loss of energy due to the deflection cause the oncoming mass "to pile up as transverse ridges" (Shreve, 1968 as reported by Hsü, 1975).

5.1.3. Data provided as a benchmark

The test used for the benchmark exercise of the 2007 International Forum on Landslide Disaster Management belongs to the series Def_4 in Table 5-2 (30 litres of Hostun sand released from 1 metre height). Hostun sand has been chosen because it is a more suitable material for the validation of numerical models which are based on the fluid mechanics hypothesis, i.e. grain diameters should be less than 1/10 of the flow depth all along the slide to avoid "bounce behaviour" and to assure a dense one-phase flow (Hungr, 2007).

A contour plan of the final deposit is shown in Figure 5-4 (dimensions in cm). Intersections are visible on the deposit due to a slight mismatched between the rendering of the topography and the fringe projection results.
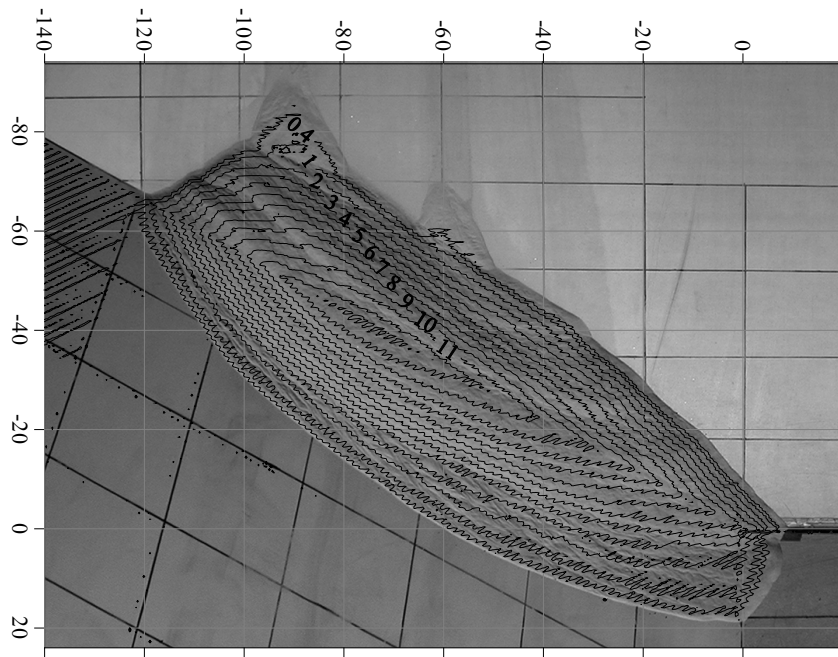
Figure 5-4 Final deposit contour lines overlapped to a photo of the final deposit of the benchmark test (Def_4)

The sequence of flow is illustrated in Figure 5-5, showing a sequence of images taken at 0.14 second intervals. The thickness of the mass in movement has been obtained thanks to recent developments of the fringe projection method explained in the following section.

Measurement of the thickness of the flow: fringe projection with Fourier

As already mentioned in section 4.1.2, during the first part of the present PhD the fringe projection method has been adapted and developed using the tools at disposition at the laboratory to measure the thickness and the morphology of the final deposit. The possibility to apply this method during motion has been only recently developed thanks to Professor Pierre Jacquot and Sebastien Equis of the Nanophotonics & Metrology Laboratory (EPFL) and it still requires some additional adaptations to be systematically used. For these reasons, it has been used only for the test submitted as a benchmark. Nonetheless, these developments could be very useful for future experiments and consequently are here illustrated.

As explained in section 4.1.2, the fringe projection method consists in projecting alternate lines of dark and light (fringes) on the deposit surface. When fringes are projected on a planar surface, they are straight and equally spaced, whereas on a rough surface they are distorted and this distortion is related to the shape of the object (Desmangles, 2003).

Consequently, it is possible to retrieve the information on the deposit thickness deriving it from the departure from straightness of the fringes. This information is contained in the object optical print (phase map); for the volume and the morphology of the final deposit the phase map is calculated using a formula which implies the use of three different images. Since the flow is relatively fast, it is not possible during motion to register the three different images useful for the calculations of the phase; thus, it is necessary to appeal to the Fourier method to analysis the fringes. As reported by Cochard and Ancey (2007) the Fourier transformation profilometry (FTP) was introduced by Takeda et al (1982), to which the reader can refer for further information. A fundamental principle when processing a signal using Fourier analysis is to manipulate the spectrum of a signal rather than manipulating the signal itself. In this way it is possible to use only one image at the different instant of the flow, projecting continuously the same image of the fringes and taking several pictures of the mass in movement. The MATLAB procedure used, kindly put at disposition of the laboratory by Equis Sebastien, is shown in Appendix I.

Since the quality of the images of the film was not sufficiently high, the accuracy is of about 1 cm in the thickness of the flow (evaluated only for the final deposit comparing calculated and measured heights) and there are some noises in the lateral part of the area taken into consideration (see Figure 5-5). The use of a high speed camera and a projector with higher resolutions and a fixed set-up geometry would lead to a much higher precision.

5.1.4. Conclusions about deflected experiments

Results of this small experimental campaign with deflector and the conclusions drawn from the comparison of tests with sharp and curved connection at the toe of the slope seen in the previous chapter confirm the fact that the topography of the path can induce important loss of energy within the mass. These considerations are in agreement with the statement of Nicoletti and Sorriso-Valvo (1991): "three-dimensional boundary surfaces strongly influence flow dynamics because transverse shearing and cross-stream momentum transport occur where topography obstructs or redirects motion". For these reasons it becomes of the utmost importance to include this factor in the modelling of rock avalanches propagation and it has been the reason for which an experiment of this kind has been chosen for the benchmark exercise of the Hong Kong Landslide Runout Analysis Benchmarking Exercise.
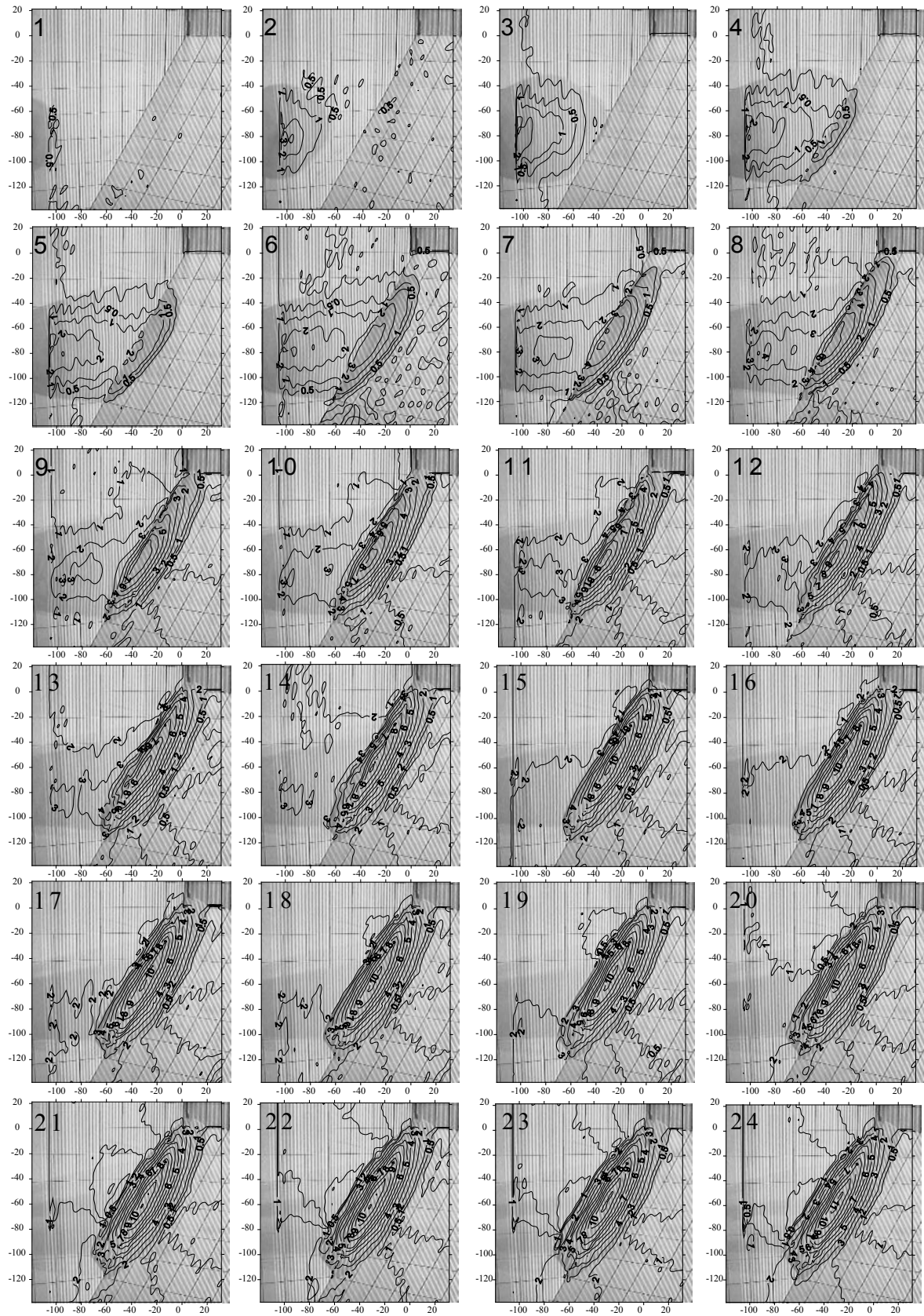
Figure 5-5 Sequence of images and thickness of the flow at 0.14 second intervals. Contour lines in cm

5.2.   Numerical modelling in the "Rockslidetec" framework

This section illustrates the results of a collaboration born among the partners of the action C of the INTERREG IIIA "Rockslidetec" project, with the aim of studying rock avalanche propagation by means of physical and numerical modelling. This part is also the object of a paper (Manzella et al, 2008) which has been accepted for the 11th International Symposium on Landslides (ISL) to be held in Xi'an in July 2008.

Since rock avalanches are luckily not so frequent, there is a lack of well known real cases on which to base proper back analysis studies or code validations. For this reason experimental results can constitute a base of comparison for the validation of numerical models. In particular in the INTERREG IIIA action C framework one specific experiment has been used as a benchmark by Cemagref (Grenoble, France), Politecnico di Torino (Turin, Italy) and CETE Méditerranée (Aix en Provence, France), respectively in collaboration with Mohamed Naaim, Marina Pirulli and Jean-François Serratrice. The results of the simulations have been useful to compare the three codes and underline their specific characteristics.

In this chapter the three codes are described, then the results of the exercise of the numerical modeling are presented and compared.

The test on which the partners worked has the following characteristics: a release of 20 litres of aquarium gravel from 1 m height on a 45° inclined panel of wood with a sharp discontinuity at the toe. As aforementioned aquarium gravel has a quite homogeneous grain size distribution with a diameter D= 0.5-3 mm. Its unit weight is of 14.3 kN/m^3. Its internal static friction angle is ϕ_i=34° and the one at the base between the gravel and the panel surface is ϕ= 32°.

Thanks to the fringe projection method and the film registered with the high speed camera it has been possible to furnish to the partners the digital elevation model of the final deposit and images of the flow each 1/60 second.

5.2.1. Numerical models

Three numerical models are considered for this benchmark exercise. Two of them are based on a continuum mechanics approach while the third, EPAN3D, on a discrete element method.

As reported by Pirulli in Manzella et al (2008), models based on continuum mechanics treat the moving mass as a homogeneous continuum, assuming that both depth and length of the flowing mass are usually large if compared with the characteristic dimension of the particles involved in the movement. Under this assumption, it becomes possible to replace the real moving mixture of solid and fluid phases by an "equivalent" fluid, whose rheological properties have to approximate the behaviour of the real mixture (Hungr, 1995). By this way, the dynamic behaviour of the flowing mass can be described by the mass and momentum conservation laws. Further, assuming that the vertical structure of the flow is much smaller than its characteristic length, the codes integrate the balance equations in depth, obtaining the so-called depth-averaged continuum flow models (Savage and Hutter, 1989).

On the other hand a code such as EPAN3D (CETE Méditerranée) based on a discrete element method (DEM) assumes that the mass consists of separate, discrete particles and that the moving mass is the result of the interaction of the particles. The forces acting on each particle are computed taking into account the initial configuration and the relevant physical laws. According to Cundall (1988) any particle may interact with any other particle and there are no limits on particle displacements and rotations. In the case of rock avalanche modelling, particles interact between them through friction and the equations of the conservation of mass, of energy and of momentum are used. The velocity distribution field and the thickness of the mass in movement are obtained by the computation of the dynamics of a discretized deformable mass on a grid.

As reported by Naaim in Manzella et al (2008), in Cemagref model the domain is restricted to rock avalanches made of dry and cohesion-less grains. The Bagnold's profile is adopted to represent the variation of velocity within the depth of the flow. A friction model issued from the recent progress on granular material flows (Pouliquen, 1999) is chosen to represent the momentum loss at the substratum level. The pressure distribution inside the flowing

material is considered as isotropic, which means that the earth pressure coefficient is taken equal to 1. Afterwards, the shallow water equations were extended to large rock avalanche flows over a complex topography. The variables of the equations are the depth and the velocities. The system of equations is written in curvilinear coordinates. Each component of this model was largely tested using both analytical solutions and laboratory experiments.

The RASH3D code (Pirulli, 2005) originates from a pre-existing model (SHWCIN). An extension of SHWCIN for simulating dry granular flows was initially introduced by Mangeney-Castelnau et al. (2003). Pirulli (2005) proposed further modifications to SHWCIN to reduce observed mesh-dependency problems, permit simulation of motion across irregular 3D terrain, incorporate the influence of internal strength and allow the selection of more than one possible basal resistance relationship. As input data the code requires the digital elevation model of the studied area, the identification of the boundary of the source area and the geometry of the initial volume. As for the rheological characteristics of the flowing mass, three different rheologies are implemented in RASH3D at the present time: 1) the simple frictional rheology, based on a constant friction angle and shear forces are independent of velocity; 2) the Voellmy flow relation, which consists of a turbulent term, accounting for velocity-dependent friction losses, and a Coulomb or basal friction term for describing the stopping mechanism; 3) the quadratic rheology, where the total friction is provided by a yield term and a viscous term as defined in the Bingham equation and a term representing the turbulence contribution. The RASH3D code has been widely validated simulating laboratory tests (e.g. Mangeney et al., 2003; Pirulli, 2005) and back analysing real cases (e.g. Pirulli et al., 2007; Pirulli and Mangeney, 2007).

As reported by Serratrice in Manzella et al (2008), the objective of EPAN3D (CETE Méditerranée) is to simulate a destructive rock mass of large volume, its propagation along a mountain slope then the accumulation and the spreading out in the valley. Calculation starts from the topography of the site defined in three dimensions by a precise digital terrain model (DTM). The unstable volume of rock is discretized in small elements of volume. After failure, these elements slide on the DTM, until they find equilibrium at the bottom of the valley where they accumulate and spread out. The moving rock cluster is permanently associated with the morphology of the slope by updating the DTM at each calculation step. The energy is dissipated primarily through friction between the sliding elements and at the

base. Each elementary volume is supposed to take the shape of a paraboloid with elliptic section. The volume of the sliding elements also evolves according to a bulking law that depends on the distance covered from failure. Finally, the initial unit weight of the rock is given. On the whole, calculations are based on ten mechanical parameters. Calculations allow following the position of all the sliding elements at every time, the extent and shape of the cluster, from the time of release until its complete stabilization.

5.2.2. Simulation results

To simulate the benchmark test the partners have used the following data depending on their codes:

- For his code, based on a "frictional" model, Cemagref used a friction coefficient equal to 0.62 corresponding to the tangent of the friction angle at the base (ϕ= 32°). No calibration has been made.

- The RASH3D simulation was also based on a model of the type "frictional". The basal friction angle was fixed at 42°, after calibration on the results of the laboratory test.

- For the EPAN3D code the released mass was divided in 1911 elementary volumes arranged in seven layers according to a cubic network. A back-analysis of the laboratory test allowed a calibration of the parameters of the constitutive model.

Digitalization of the geometry of the model (an inclined panel at 45° degrees and a horizontal panel) as well as the definition of the zone of departure (0.25 m x 0.20 m x 0.4 m box filled with 20 litres of granular material) were in charge of the teams, but there should not be any significant difference.

In Figure 5-6, Figure 5-7 and Figure 5-8 the simulation results are shown. Although relatively far from observations made on the extension and the morphology of the gravel deposit, the results obtained by Cemagref are relevant compared to the others, if it is taken into account that no parameter calibration has been made (class A prediction). As can be seen from Figure 5-8, the calculation made by RASH3D reproduces well the velocity of propagation of the rear and front of the mass, but less the final deposit shape, especially in the transversal direction. Besides, the chosen angle of friction is far from the experimental value. Observing Figure 5-6 and Figure 5-7 it is found that the deposit morphology and

dimensions are better simulated by the model EPAN3D, but it has to be taken into account that they result from a back-analysis and from the calibration of 11 parameters, not all with physical meaning.

In Table 5-3 the predictions of the three codes are qualitatively compared with the observations made during the laboratory test. The symbols +, +/- and - mean respectively good, average, imperfect adequacy, for the characteristic indicated on the corresponding line.
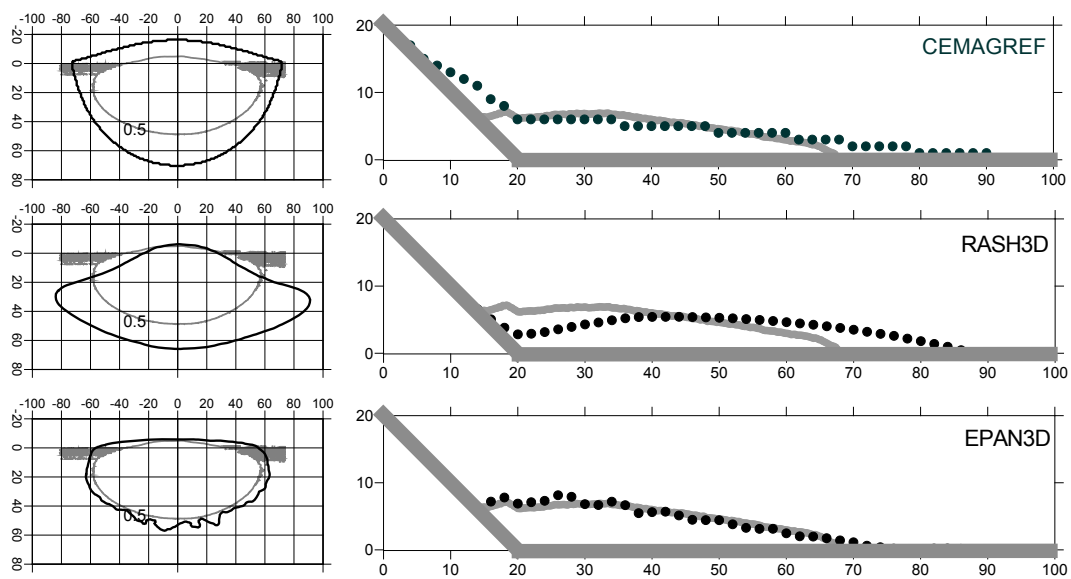
Figure 5-6 Horizontal section and longitudinal section along the symmetry axis of the observed deposit (light grey) and the codes simulations (black markers)
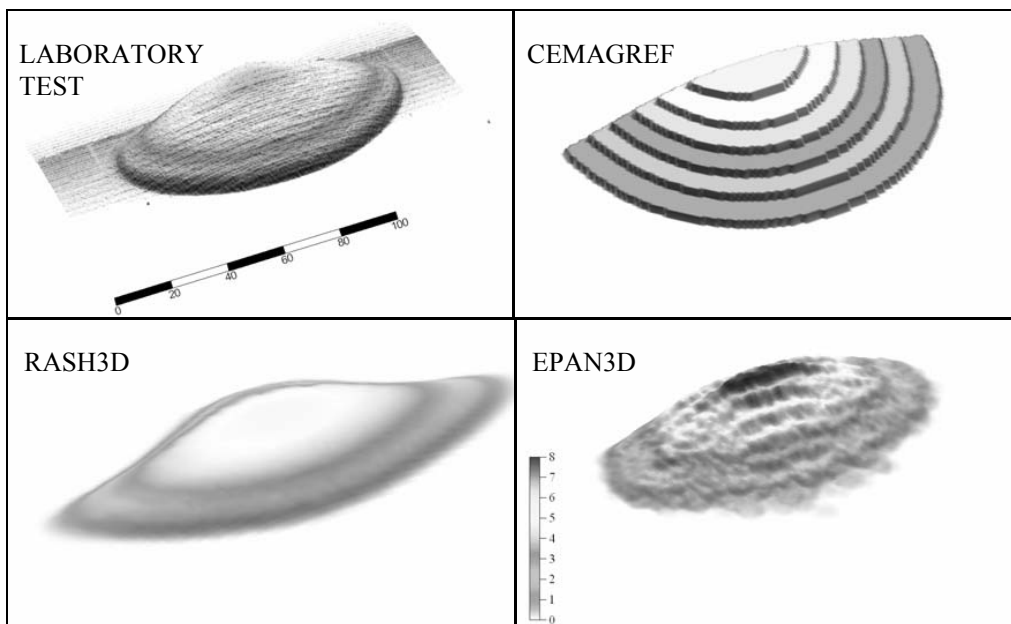
Figure 5-7 3D view of the observed deposit and the codes simulations; data are presented at the same scale
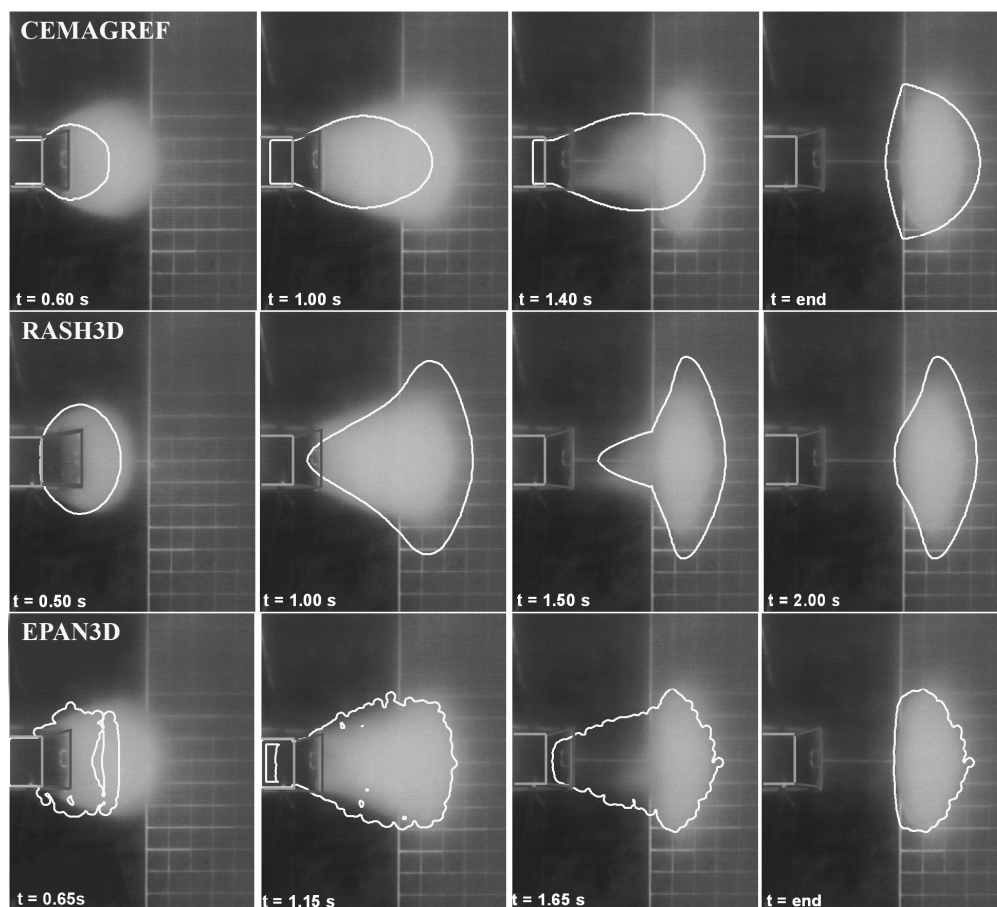
Figure 5-8 Comparison between the mass propagation and spreading observed in laboratory (images in background) and those modelled by the three codes; the outline represented in white concerns the 1 mm thickness contour line

		Cemagref	RASH3D	EPAN3D
Model		Frictional	Frictional	Pouliquen
Analysis		Without calibration	Back-analysis	Back-analysis
Number of parameters		1	1	11
Propagation	Runout	-	-	+
	Velocity	-	+	-
Deposit Dimensions	Longitudinal ext.	-	+/-	+
	Lateral extension	+/-	-	+
	Height	+/-	+/-	+
Deposit Morphology	General shape	-	-	+
	Front	-	+/-	+/-
	Rear	-	-	+

Table 5-3 Qualitative comparison among the codes; +, +/- and - stand respectively for good, average, imperfect adequacy with the laboratory observations and measurements

Since only one test has been used for this work of comparison, it is important to put the above-mentioned statements into perspective. Only a comparison of the codes among several test configurations would allow a proper analysis. On the other hand this study underlines the importance of the validation of numerical codes on well-defined laboratory tests since this contributes to understand advantages and limits of the codes, improving their development and their use and consequently enhancing forecast of rock avalanche propagation.

6. Conclusions and prospects

Laboratory experiments hold an important role in improving the modelling of rock avalanches since they contribute to better understand mechanisms involved and to assess the parameters influencing propagation by means of analysis of the tests, comparison with existing theories and real events. Tests analysed in the present study consist in unconstrained flows of granular materials and small bricks down an inclined board which ends with a horizontal accumulation zone.

Two main experimental campaigns have been carried out at the EPFL Rock Mechanics Laboratory. The first represents a preliminary study which has been useful to test the experimental set-up, to improve the measuring devices and to assess the most important factors governing the propagation of granular avalanches. In the second experimental campaign these first results are extended with tests performed with an improved experimental set-up. A new measuring device allows to confirm and quantify the findings and to study additional factors which could have an important influence on rock avalanche propagation.

The different parameters considered in the preliminary tests are:

- nature of released material: Hostun sand and two kinds of Aquarium gravels;

- material volume: 10-20-30-40 litres;

- fall height: 1-2 m;

- releasing geometry: 20 cm x 40 cm, 20 cm x 20 cm and 20 cm x 30 cm;

- consecutive releases (for example 30 litres in one release or in three subsequent releases of 10 litres each).

Runout, width and length of the final deposit are measured manually while front mass velocity is derived with specific processing from films taken by a high speed camera.

The experiments have shown that:

1. Deposit characteristics and morphology are dependent on the type of material used: sand or gravel. The sand deposit shape, regular and compact, agrees well with many experiments described in the literature, while the aquarium gravel deposit, which is quite irregular (a central zone with a small slope, but front, rear and sides strongly inclined), is in accordance with deposit characteristics of some real events. On the other hand no major differences have been encountered between tests with the two gravels leading to the conclusion that grain diameter doesn't seem to affect significantly propagation as indicated by tests performed by Davies (1997).

2. There is also a considerable difference in deposit characteristics and morphology when the event is the consequence of one large volume released at once or when the same volume is released in sequence. In the latter case, the characteristics of the final deposit do not depend on the entire volume but on the volume of the individual released masses. This kind of behaviour is in agreement with the rather conical and narrow deposit of the Randa event (Switzerland) which has been the consequence of a progressive failure.

3. Two different mechanisms of propagation can be observed on the inclined board when the mass is released: triangular propagation with an opening angle of about 15° (measured on the horizontal projection), followed by a sliding along the deepest slope. The drop height influences this propagation as both the mechanisms are only observed when the mass is released from 2 m.

4. In the deposition process it is possible to distinguish an interaction between the rear and the front parts of the mass. The mass front enters the accumulation zone followed by a uniformly decelerated motion until the rear part approaches and forces the mass ahead to move further. This transfer of momentum between the rear and the

front could partly explain the exceeding travel distance of rock avalanches. The greater the volume of the mass, the greater the duration of the interaction between the rear and the front parts and the longer the runout.

5. The geometry of the deposit depends to some extent on the geometry of the mass before failure, especially with reference to the width.

The parameters considered in the second experimental campaign are:

- number of consecutive releases (40 litres in one or in two subsequent releases of 20 litres each)

- material volume (20 l, 40 l);

- fall height (1 m, 1.5 m);

- basal friction coefficient;

- slope angle (37.5°, 45°);

- nature of released material: aquarium gravel2 and small bricks;

- arrangement of the bricks before failure;

- discontinuity at the toe (sharp, curved).

The fringes projection method, a new optical technique developed recently, has been adapted to the present tests. This allows retrieving the height of the final deposit and then to compute the position of its centre of mass. Therefore, the analysis of the experimental results is no longer limited to data such as runout and apparent coefficient of friction (Fahrböschung), but it also allows considering the distance travelled by the mass centre and its travel angle. In this way it has been possible to better visualise the results and to confirm them with a more quantitative approach.

Results of the second experimental campaign put in evidence the importance of certain factors in granular avalanches propagation and that should be considered in the setting up of empirical models: the volume, the fall height, the friction angle, the topography, i.e. the

slope and the regularity of the pathway, the structure of the mass before failure. Another thing to be taken into account is whether the failure is progressive or not. In particular:

6. The results obtained in the second testing campaign confirm that by increasing the number of times by which the release of a certain volume is divided, the height of the deposit increases significantly and its runout decreases.

7. Factors causing longer runouts are: larger volume, greater fall height, lower coefficient of friction, higher slope angle, the use of bricks ordered in piles and a smoother discontinuity at the toe of the slope. The latter induces the largest increase.

8. Deposit morphology doesn't seem to depend on volume. An increase of the mass released induces a homogeneous increase of all the deposit characteristics maintaining the same deposit shape; nonetheless the centre of mass travel the same distance, while runout, width and length increases.

9. Tests with higher fall height show that the whole mass translates further and that the exceeding travel distance of the centre of mass and of the distal end are similar. The Fahrböschung is nearly the same even if the runout is greater.

10. The concept of a straight energy-line based on a simple frictional model is not adequate to evaluate the distance travelled by the centre of mass. For modelling of rock avalanches, only models that take into account a velocity dependent term of energy dissipation should be used, such as the Voellmy resistance model that combines frictional and turbulent behaviours. Moreover, the energy line seems to depend on the set-up geometry.

11. When bricks are piled orderly into the reservoir before failure, the mass behaves as a compact body on the inclined panel, i.e. the bricks remain packed together and energy dissipation takes place mainly through friction at the base. After the impact with the horizontal panel, the mass shatters and energy is then mainly dissipated through friction/collisions between the bricks. Having "spared" a part of the energy in the first part of the sliding, the mass enters the accumulation zone with a higher velocity and can consequently travel further on the horizontal panel.

12. The regularity of the pathway is a significant factor, as already pointed out by Heim in 1932. The more angular is the connection between the panels, the more shearing (friction) and collisions will develop within the sliding mass as it changes its flow direction, the larger will be the energy dissipation within the mass and the shorter the travel distance of the centre of mass and of the distal end.

13. According to Corominas (1996), L_r represents the ratio between the exceeding travel distance as defined by Hsü (1975) and the distance of the mass if it had travelled dissipating energy only through normal friction at the base. Results of L_r show that piled bricks released on a plane with a sharp discontinuity at the toe and gravels released on a regular pathway with a curved slope don't exhibit an excessive mobility and remain in the range of a "normal" frictional behaviour. Only the combination of bricks and curved slope does induce an excessive mobility of the distal end of the mass.

14. From tentative considerations about the energy losses along the path, it appears that a model considering only energy dissipation at the base is not sufficient to explain the behaviour of a granular mass. On the other hand, in the case of piled bricks, energy seems to be dissipated essentially by friction at the base on the inclined board till the mass reaches the horizontal panel and shatters. In addition if the connection at the toe is progressive the shattering of the mass is partially avoided, inducing an even more marked predominance of the frictional dissipation at the base.

15. A lumped mass model which takes into account the centripetal acceleration can be a good tool to reproduce the distance travelled by the centre of mass of the tests but not to evaluate the energy losses within the mass and the total runout.

16. According to Davies and McSaveney (1999) the nondimensional values of the length, L*, and of the runout, R, against the cubic root of the volume, h*, has been calculated for all the tests. The length is found to be independent from the fall height. The results can be translated in the following empirical formulations for what concerns one release tests with a sharp discontinuity at the toe:

$$R = ah_v + bh^*$$

Where *a* and *b* are two coefficients varying according to the basal friction, slope angle and the material used. When slope increases, *a* increases. And for the length:

$$L^* = 2 \div 3.8 h^* \qquad \text{for Gravel and Random bricks}$$
$$L^* = 3.2 \div 4.3 h^* \qquad \text{for Piled bricks}$$

Values measured in the tests with aquarium gravel and blocks arranged randomly are in general agreement with the range of values Davies and McSaveney obtained (1.5-3). On the other hand, tests with blocks arranged in piles have longer spread than those reported by Davies and McSaveney (1999).

17. A marked difference is detected for tests with a curved connection at the toe which are much closer to the ones evaluated on real events by Davies and McSaveney (between 4 and 7):

$$L^* = 5.1 \div 5.6 h^*$$

18. The results of the ANOVA analysis, i.e. a statistical method used to consider at once the influence of several factors together, confirm the considerations made: all the factors studied have a strong influence on runout, while the length of the deposit is independent from fall height. The structure of the mass before failure has a strong influence on runout and Fahrböschung. All the responses vary significantly when the transition between the panels is smooth (rather than sharp), underlining again the importance of considering the dissipation of energy within the mass in the study of rock avalanche propagation.

Some additional experiments have been carried out with a deflection placed as an obstacle in the flow direction. Results of this complementary experimental campaign with deflector confirm the fact that the topography of the path can induce important losses of energy within the mass and has a strong influence on propagation. For these reasons it is of the greatest importance to include this factor in the modelling of rock avalanche.

One of the experiments made with a standard geometry of the set-up, has been simulated with the codes developed by the partners of the INTERREG IIIA "Rockslidetec" project: even if each code has reproduced some aspects of the test none could simulate accurately all

its characteristics. This benchmark exercise puts into evidence the importance of the validation of numerical models on well-defined laboratory tests, since this contributes to understand advantages and limits of the codes, improving their development and their use.

6.1. Outlooks

In the present research an extensive set of parameters has been taken into considerations. Nonetheless the range of variation of each factor studied is contained due to limit of space and time. Therefore to generalise conclusions drawn and to formulate a comprehensive empirical model to quantify the effects of all the parameters studied it would be necessary in future research to extent these ranges, e.g. larger volumes up to 100 litres and smaller fall height. The experimental set-up should be consequently adapted.

From the analysis of the results it has been possible to detect the importance of some factors, i.e. topography, nature of the released material and structure of the mass before failure and along the pathways, but few detailed studies of their effects have been found in literature and should be thus further investigated. Different curvature between the inclined and horizontal panels and other angle of deflection could be studied for this purpose. These last tests could be also important to evaluate the influence of the centripetal acceleration.

To better analyse energy dissipation and transfer of momentum along the path it would be necessary to know the morphology of the mass during motion and to compute the position and the velocity of its centre of mass along the path. For this reason measuring devices should be improved to be able to apply the Fourier method in fringes projection: the use of a high speed camera with high definition of the captures would make it possible to increase the accuracy obtained in the present study.

Some factors such as the angularity and grading of granular material or the arrangement of blocks have been found in the present research to have some influences on rock avalanche propagation but they couldn't be further investigated and should be considered in future tests.

Finally as suggested by the work done with the codes of the INTERREG III partners, simulations on a larger sample of tests should be performed as a help to the interpretation of the experimental results and of the improvement of numerical models.

In this framework a PhD thesis at the LMR will follow the present research to study these aspects and to extend the findings to date.

References

Abele, G. 1974. Bergstürze in den Alpen, ihre Verbreitung, Morphologie und Folgeerscheinungen. Wissenschaftliche Alpenvereinshefte, 25: 1-230.

Abele, G. 1994. Large rockslides: their causes and movement on internal sliding planes. Mountain Research & Development, 14(4): 315-320.

Abele, G., Erismann, T.H., and Heuberger, H. 1997. Rockslide movement supported by the mobilization of groundwater-saturated valley floor sediments. Zeitschrift fur Geomorphologie, 41(1): 1-20.

Ancey, C. 2006. Dynamique des avalanches. Presses Polytechniques Universitaires Romandes en co-édition avec Cemagref éditions

Ancey, C. 2007. http://lhe.epfl.ch/

Ancey, C., and Cochard, S. 2006. Understanding avalanches. Physics World, 19(7): 29-31.

Ancey, C., Evesque, P., and Coussot, P. 1997. Analogy between granular flows down an inclined channel and the motion of a bead down a bumpy line. In Powder & Grains, pp. 475-478.

Azanza, E., Chevoir, F., and Moucheront, P. 1997. Experimental study of rapid granular flows in a two-dimensional channel. In Powder &Grains, pp. 455-458.

Azanza, E., Chevoir, F., and Moucheront, P. 1999. Experimental study of collisional granular flows down an inclined plane. Journal of Fluid Mechanics, 400: 199-227.

Azzoni, A., Chiesa, S., Frassoni, A., and Govi, M. 1992. The Valpola Landslide. Engineering Geology, 33(1): 59-70.

Bagnold, R.A. 1954. Experiments on a gravity free dispersion of large solid spheres in Newtonian fluid under shear. PRSL, 225: 49-63.

Bonnard, C., Noverraz, F., Lateltin, O., and Raetzo, H. 1995. Large landslides and possibilities of sudden reactivation. Felsbau, 13(6): 401-407.

Bouzid, I. 1999. Contribution à l'étude des écoulements granulaires appliqués aux éboulements rocheux en grande masse, Université Claude Bernard, Lyon.

Campbell, C.S. 1989. Self-lubrication for long runout landslides. Journal of Geology, 97(6): 653-665.

Campbell, C.S., Cleary, P.W., and Hopkins, M. 1995. Large-scale landslide simulations: global deformation, velocities and basal friction. Journal of Geophysical Research, 100(B5): 8267-8283.

Cannon, S. H., Savage, W. Z. 1988. A mass-change model for the estimation of debris-flow runout. Journal of Geology, 96 (2): 221-227

Cochard S., and Ancey, C. 2008. Tracking the free surface of time-dependent flows: Image processing for the dam-break problem. Experiments in Fluids, 44 (1): 59-71.

Corominas, J. 1996. The angle of reach as a mobility index for small and large landslides. Canadian Geotechnical Journal, 33(2): 260-271.

Crealp, 1999. Eboulement du Six des Eaux Froides – mai 1946. Causes et mécanisme de l'éboulement. Centre de Recherche sur l'environnement Alpin - CREALP

Creath, K. 1993. Temporal phase measurement methods. In Interferogram Analysis. Ed. Robinson, DW., and Reid, GT. Institute of Physics Publishing. Bristol and Philadelphia

Cruden, D.M., and Hungr, O. 1986. The Debris of the Frank Slide and Theories of Rockslide Avalanche Mobility. Canadian Journal of Earth Sciences, 23(3): 425-432.

Cruden, D.M., and Varnes, D.J. 1996. Landslide types and processes. Special Report - National Research Council, Transportation Research Board, 247: 36-75.

Cruden, D.M., and Martin, C.D. 2007. Before the frank slide. Canadian Geotechnical Journal, 44(7): 765-780.

Cundall, P.A. 1988. Formulation of a Three-Dimensional Distinct Element Model - Part I. A Scheme To Detect And Represent Contacts In A System Composed Of Many Polyhedral Blocks. International journal of rock mechanics and mining sciences & geomechanics abstracts, 25(3): 107-116.

Davies, T.R., McSaveney, M.J., and Hodgson, K.A. 1999. A fragmentation-spreading model for long-runout rock avalanches. Canadian Geotechnical Journal, 36(6): 1096-1110.

Davies, T.R.H. 1982. Spreading of rock avalanche debris by mechanical fluidization. Rock Mechanics Felsmechanik Mécanique des Roches, 15(1): 9-24.

Davies, T.R.H. 1995. Rock avalanche runout - Preliminary model studies. In International Symposium on Prediction of Rapid Landslide Motion.

Davies, T.R.H. 1997. Runout of Dry Granular Avalanches. Research report of the Department of Natural Resources Engineering, Lincoln University, New Zealand.

Davies, T.R.H., and McSaveney, M.J. 1999. Runout of dry granular avalanches. Canadian Geotechnical Journal, 36: 313-320.

Davies, T.R.H., and McSaveney, M.J. 2002. Dynamic simulation of the motion of fragmenting rock avalanches. . Canadian Geotechnical Journal, 39: 789-798.

Davies, T.R.H., and McSaveney, M.J. 2003. Runout of Rock Avalanches and volcanic debris avalanches. In International conference on fast slope movements. Naples. 11-13 May, Vol.2.

Denlinger, R.P., and Iverson, R.M. 2001. Flow of variably fluidized granular masses across three-dimensional terrain 2. Numerical predictions and experimental tests. Journal of Geophysical Research B: Solid Earth, 106(B1): 553-566.

Denlinger, R.P., and Iverson, R.M. 2004a. Granular avalanches across irregular three-dimensional terrain: 1. Theory and computation. Journal of Geophysical Research B: Solid Earth, 109.

Denlinger, R.P., and Iverson, R.M. 2004b. Flow of variably fluidized granular masses across three-dimensional terrain, 2, Numerical predictions and experimental tests. Journal of Geophysical Research B: Solid Earth.

Desmangles, A.I. 2003. Extension of the fringe projection method to large object for shape and deformation measurement, Ph.D. thesis n°2734, Ecole Polytechnique Fédérale de Lausanne, CH

Drake, T.G. 1990. Structural features in granular flows. Journal of Geophysical Research, 95(B6): 8681-8696.

Drake, T.G. 1991. Granular flow. Physical experiments and their implications for microstructural theories. Journal of Fluid Mechanics, 225: 121-152.

Eberhardt, E., Stead, D., and Coggan, J.S. 2004. Numerical analysis of initiation and progressive failure in natural rock slopes - the 1991 Randa rockslide. International Journal of Rock Mechanics and Mining Sciences, 41(1): 69-87.

Einstein, H.H. 1988. Landslide Risk Assessment Procedure. In Fifth International Symposium on Landslides, Vol.2, pp. 1075 -1090.

Einstein, H.H. 1997. Landslide risk - systematic approaches to assessment and management. In Landslide Risk Assessment. Honolulu, pp. 25-50.

Eisbacher, G.H., and Clague, J.J. 1984. Destructive mass movements in high mountains: hazard and management - Geol Soc. of Canada, Paper 84-16, 230 p.

Eisbacher, G.H., and Claque, J.J. 2007. Destructive mass movements in high mountains: Hazard and management. Geol. Survey of Canada, Paper 84-16, Otawa: Canadian Government Publishing Centre, pp 1-230, 1984.

Erlichson, H. 1991. A mass-change model for the estimation of debris-flow runout, a second discussion: Conditions for the application of the rocket equation. Journal of Geology, 99: 633-634

Erismann, T.H. 1979. Mechanisms of large landslides. Rock Mechanics Felsmechanik Mécanique des Roches, 12(1): 15-46.

Erismann, T.H., and Abele, G. 2001. Dynamics of Rockslides and Rockfalls. Springer-Verlag, Berlin Heidelberg. 316 pages. ISBN 3-540-67198-6.

Evans, S.G. 2005. Single event landslides resulting from massive rock slope failure: characterising their frequency and impact on society. NATO Science Series IV, Earth and Environmental Sciences, 49: 53-73.

Evans, S.G., Clague, J.J., Woodsworth, G.J., and Hungr, O. 1989. The Pandemonium Creek rock avalanche, British Columbia. Canadian Geotechnical Journal, 26(3): 427-446.

Evans, S.G., Scarascia Mugnozza, G., Strom, A.L., Hermanns, R.L., Ischuk, A., and Vinnichenko, S. 2006. Landslides from massive rock slope failure and associated phenomena. In Landsildes from Massive Rock Slope Failure, pp. 3-52.

Fahnestock, R.K. 1978. Little Tahoma Peak rockfalls and avalanches, Mount Rainier, Washington, USA. In Rockslides and Avalanches. 1. Natural Phenomena, pp. 181-196.

Fürbringer, J.M. 2005. Material and notes of the lectures of Design of Experiments. Doctoral school- EPFL.

Ghiglia, D.C., and Pritt, M.D. 1998. Two-dimensional phase unwrapping. Ed. John Wiley & sons.

Goguel, J. 1978. Scale-dependent rockslide mechanisms, with emphasis on the role of pore fluid vaporization. Rockslides and Avalanches, 1: 693-705.

Goguel, J., and Pachoud, A. 1972. Géologie et dynamique de l'écroulement du Mont Granier dans le massif de la Chartreuse, en novembre 1248. Bull. BRGM, 3(1): 29-38.

Goodman, R.E., Taylor, R.L., and Brekke, T.L. 1968. A model for the mechanics of jointed rock. J. Soil Mech. Found. Div., Proc. ASCE, 94(SM3): 637-659.

Gray, J.M.N.T., and Hutter, K. 1997. Pattern formation in granular avalanches. Continuum Mech. Thermodyn., 9: 341-345.

Gray, J.M.N.T., Wieland, M., and Hutter, K. 1999. Gravity-driven free surface flow of granular avalanches over complex basal topography. Proc. Roy. Soc. Lond. A 455: 1841-1874

Greve, R., and Hutter, K. 1993. Motion of a granular avalanche in a convex and concave curved chute: experiments and theoretical predictions. Phil. Trans. R. Soc. A 342: 573-600.

Greve, R., Koch, T., and Hutter, K. 1994. Unconfined flow of granular avalanches along a partly curved surface. I. Theory. Proc. R. Soc. Lond., 445: 399-413.

Guzzetti, F. 2000. Landslide fatalities and the evaluation of landslide risk in Italy. Engineering Geology, 58(2): 89-107.

Heidenreich, B. 2004. Small and half-scale experimental studies of rockfall impacts on sandy slopes. Ph.D. thesis n°3058, Ecole Polytechnique Fédérale de Lausanne

Heikkilä, J., and Silvén, O. 1996. Calibration procedure for short focal length off-the-shelf CCD cameras. Proc. 13th International Conference on Pattern Recognition, Vienna, Austria, p. 166-170.

Heikkilä, J., and Silvén, O. 1997. *A Four-step Camera Calibration Procedure with Implicit Image Correction. IEEE Computer Society Conference on Computer Vision and Pattern Recognition (CVPR'97), San Juan, Puerto Rico, p. 1106-1112.*

Heim, A. 1882. *Der Bergsturz von Elm. Z. Dtsch. Geol. Ges., 34:74-115.*

Heim, A. 1932. *Bergsturz und menschenleben. Frets und Wasmuth, Zurich.*

Hewitt, K. 1988. *Catastrophic Landslide Deposits in the Karakoram Himalaya. Science, 242(4875): 64-67.*

Hsü, K.J. 1975. *Catastrophic Debris Streams generated by Rockfalls. Geol. Soc. Am. Bull., 86,I: 129-140.*

Hungr, O. 1981. *Dynamics of Rock Avalanches and Other Types of Mass Movements.*

Hungr, O. 1990a. *Momentum-Transfer and Friction in the Debris of Rock Avalanches - Discussion. Canadian Geotechnical Journal, 27(5): 697-697.*

Hungr, O., 1990b. *Mobility of rock avalanches. Reports of the National Research Institute for Earth Science and Disaster Prevention, Tsukuba, Japan, 46: 11-20.*

Hungr, O. 1995. *A model for the runout analysis of rapid flow slides, debris flows, and avalanches. Canadian geotechnical journal: 610-623.*

Hungr, O. 2002. *Rock avalanche motion: Process and modeling. In Proceedings of NATO Advanced Research Workshop, Massive Rock Slope Failure: New Models for Hazard Assessment, pp. 66-69.*

Hungr, O. 2006. *Rock avalanche occurrence, process and modelling. In Landslides from Massive Rock Slope Failure. pp. 243-266.*

Hungr, 2007 *Personal communication.*

Hungr, O., and Morgenstern, N.R. 1984a. *High velocity ring shear tests on sand. Geotechnique, 34(3): 415-421.*

Hungr, O., and Morgenstern, N.R. 1984b. *Experiments on the flow behaviour of granular materials at high velocity in an open channel. Geotechnique, 34(3): 405-413.*

Hungr, O., and Evans, S.G. 2004. *Entrainment of debris in rock avalanches: An analysis of a long run-out mechanism. Bulletin of the Geological Society of America, 116(9-10): 1240-1252.*

Hungr, O., Corominas, J., and Eberhardt, E. 2005. *Estimating landslide motion mechanism, travel distance and velocity. In Proceedings of the International Conference on Landslide Risk Management, pp. 99-128.*

Hungr, O., Evans, S.G., Bovis, M.J., and Hutchinson, J.N. 2001. *A review of the classification of landslides of the flow type. Environmental and Engineering Geoscience, 7(3): 221-238.*

Hutchinson, J.N. 1986. *A sliding consolidation model for flow slides. Canadian geotechnical journal, 23(2): 115-126.*

Hutter, K., and Savage, S.B. 1988. Avalanche dynamics: the motion of a finite mass of gravel down a mountain side. In ISL, Vol.1, pp. 691-697.

Hutter, K., and Koch, T. 1991. Motion of a granular avalanche in an exponentially curved chute: experiments and theoretical predictions. Phil. Trans. R. Soc. Lond., 334: 93-138.

Iverson, R.M., and Denlinger, R.P. 2001. Flow of variably fluidized granular masses across three-dimensional terrain I. Coulomb mixture theory. Journal of Geophysical Research B: Solid Earth, 106(B1): 537-552.

Iverson, R.M., Logan, M., and Denlinger, R.P. 2004. Granular avalanches across irregular three-dimensional terrain: 2. Experimental tests. J. Geophys. Res., 109(F1).

Kent, P.E. 1966. The transport mechanism in catastrophic rock falls. The Journal of Geology 74, pp. 79–83

Kern, M. 2000. Inverse grading in granular flow. Ph.D. thesis n°2287, Ecole Polytechnique Fédérale de Lausanne

Koch, T., Greve, R., and Hutter, K. 1994. Unconfined flow of granular avalanches along a partly curved surface. II. Experiments and numerical computations. Proc. R. Soc. Lond., 445: 415-435.

Körner, H.J. 1976. Reichweite und Geschwindigkeit von Bergstürzen und Fließschneelawinen. Rock Mechanics Felsmechanik Mécanique des Roches, 8(4): 225-256.

Legros, F. 2002. The mobility of long-runout landslides. Eng. Geol., 63: 301-331.

Legros, F. 2006. Landslide mobility and the role of water. In Landslides from massive rock slope failure. Edited by Evans, G.S., Scarascia Mugnozza, G., Strom A. and Hermanns L.R. NATO Sciences Series, IV. Earth and Environmental Sciences, V.49, 233-242

Lehman, M., Jacquot, P., and Facchini, M. 1999. Shape measurements on large surfaces by fringe projection. In Exp. Tech., Ecole Polytechnique Fédérale de Lausanne, CH, pp. 31-35.

Leoniv, N.N. 1960. The Khait, 1949 earthquake and geological conditions of its occurrence. Izvestia of the Academy of Sciences of the USSR, Geophysical Series, 3: 409-424

Li, T. 1983. A mathematical model for predicting the extent of a major rockfall. Zeitschrift für Geomorphologie, 27(4): 473-482.

Liebling, M., Blu, T., and Unser, M. 2004. Complex-wave retrieval from a single off-axis hologram. Journal of the Optical Society of America A: Optics and Image Science, and Vision, 21(3): 367-377.

Mangeney-Castelnau, A., Bouchut, F., Vilotte, J.P., Lajeunesse, E., Aubertin, A., and Pirulli, M. 2005. On the use of Saint Venant equations to simulate the spreading of a granular mass. Journal of Geophysical Research B: Solid Earth, 110(9): 1-17.

Mangeney-Castelnau, A., Vilotte, J.P., Bristeau, M.O., Perthame, B., Bouchut, F., Simeoni, C., and Yerneni, S. 2003. Numerical modeling of avalanches based on Saint Venant equations using a kinetic scheme. Journal of Geophysical Research B: Solid Earth, 108(11).

Manzella, I., Labiouse, V. 2007. Rock avalanches: experimental study of the main parameters influencing propagation. Proc. 11th ISRM, 9-13 July, 2007, Lisbon, 1: 657-660.

Manzella, I. & Labiouse, V. 2008a. Qualitative analysis of rock avalanches propagation by means of physical modelling of non-constrained gravel flows. Rock Mech. and Rock Engineering Journal, 41 (1): 133-151

Manzella, I., Labiouse, V. 2008b. Gravel and small bricks flow experiments to investigate parameters and mechanisms involved in rock avalanches. Submitted to the Engineering Geology Journal.

Manzella, I., Pirulli, M., Naaim, M., Serratrice, JF., and Labiouse, V. 2008. Numerical modelling of a rock avalanche laboratory experiment in the framework of the "Rockslidetec" alpine project. Accepted for the 10th International Symposium on landslide and Engineered Slopes to be held from the 30th of June to the 4th of July 2008 in Xi'an, China

Massey, B.S. 1983. Mechanics of fluids. Van Nostrand Reinhold (UK) Co. Ltd.

McDougall, S. 2006. A new continuum dynamic model for the analysis of extremely rapid landslide motion across complex 3D terrain, PhD thesis, University of British Columbia, Vancouver, Canada.

McDougall, S.D., and Hungr, O. 2003. Objectives for the development of an integrated three-dimensional continuum model for the analysis of landslide runout. In Debris-Flow Hazards Mitigation: Mechanics, Prediction, and Assessment, 1: 481-490.

McDougall, S., and Hungr, O. 2004. A model for the analysis of rapid landslide motion across three-dimensional terrain. Canadian Geotechnical Journal, 41(6): 1084-1097.

Melosh, H.J. 1979. Acoustic Fluidization - New Geologic Process. Journal of Geophysical Research, 84(NB13): 7513-7520.

Meunier, M., and Ancey, C. 2004. Towards a conceptual approach to predetermining long-return-period avalanche run-out distances. Journal of Glaciology, 50(169): 268-278.

Moore, D.P., and Mathews, W.H. 1978. Rubble Creek landslide, Southwestern British Columbia. Can J Earth Sci, 15(7): 1039-1052.

Naaim, M., and Ancey, C. 1995. Modelisation of dense avalanches. In Snow and avalanches. 1992. Edited by G. Brugnot. Chamonix. Cemagref: 173-181.

Naaim, M., Vial, S., and Couture, R. 1997. Saint Venant approach for rock avalanches modelling. In Multiple Scale Analyses and Coupled Physical Systems: Saint Venant Symposium.

Nicoletti, P.G., and Sorriso-Valvo, M. 1991. Geomorphic controls of the shape and mobility of rock avalanches. Geological Society of America Bulletin, 103(10): 1365-1373.

O'Brien, JS., Julien, PY., Fullerton, WT. 1993. Two-dimensional water flood and mudflow simulation. Journal of Hydrological Engineering, 119(2): 244-261.

Okura, Y., Kitahara, H., and Sammori, T. 2000a. Fluidization in dry landslides. Eng. Geol., 56: 347-360.

Okura, Y., Kitahara, H., Sammori, T., and Kawanami, A. 2000b. The effects of rockfall volume on runout distance. Eng. Geol., 58(2): 109-124.

Pariseau, W.G., and Voight, B. 1979. Rockslides and Avalanches: Basic Principles.

Patra, A.K., Bauer, A.C., Nichita, C.C., Pitman, E.B., Sheridan, M.F., Bursik, M., Rupp, B., Webber, A., Stinton, A.J., Namikawa, L.M., and Renschler, C.S. 2005. Parallel adaptive numerical simulation of dry avalanches over natural terrain. Journal of Volcanology and Geothermal Research, 139(1-2): 1-21.

Pirulli, M. 2004. Numerical analysis of three potential rock avalanches in the Alps. Numerische untersuchungen dreier potenzieller bergstürze in den Alpen, 22(2): 32-39.

Pirulli, M. 2005. Numerical modelling of landslide runout, a continuum mechanics approach. PhD Thesis, Department of Structural and Geotechnical Engineering, Politecnico di Torino, Italy.

Pirulli, M., Bristeau, M.O., Mangeney, A., and Scavia, C. 2007. The effect of the earth pressure coefficients on the runout of granular material. Environmental Modelling and Software, 22(10): 1437-1454.

Pirulli, M., Mangeney, A. 2007. Results of back-analysis of the propagation of rock avalanches as a function of the assumed rheology. Rock Mech. and Roch Engineering Journal, 41 (1): 59-84

Pitman, E.B., Nichita, C.C., Patra, A., Bauer, A., Sheridan, M., and Bursik, M. 2003a. Computing granular avalanches and landslides. Physics of Fluids, 15(12): 3638-3646.

Pouliquen, O. 1999. Scaling laws in granular flows down rough inclined planes. Physics of Fluids, 11: 542-547.

Pouliquen, O., and Forterre, Y. 2002. Friction law for dense granular flows: application to the motion of a mass down a rough inclined plane. J.Fluid.Mech., 453: 133-151.

Pudasaini, S.P., Hsiau, S.S., Wang, Y., and Hutter, K. 2005. Velocity measurements in dry granular avalanches using particle image velocimetry technique and comparison with theoretical predictions. Physics of Fluids, 17(9): 1-10.

Pudasaini, S.P., and Hutter, K. 2007. Avalanche Dynamics: Dynamics of Rapid Flows of Dense Granular Avalanches. Springer.

Reik, G., and Hesselmann, F.J. 1976. A study of kinematic and dynamic aspects of rock slides by means of model tests. In ISMES meeting: Rockfall dynamics and protective works effectiveness. Bergamo, Italy. 20-21 May, 90: 97-122.

Rengers, N., and Müller, L. 1970. Kinematische Versuche an geomechanischen Modellen. Rock Mech., Suppl.1: 20-31.

Saldivar-Sali, A., and Einstein, H.H. 2007. A landslide risk rating system for Baguio, Philippines. Engineering Geology, 91(2-4): 85-99.

Sander, B. 1948. Einführung in die gefügekunde der geologischan körper.

Sassa, K. 1988. Special lecture: geotechnical model for the motion of landslides. In Landslides. Proc. 5th symposium, Lausanne, 1988. . Lausanne, 1: 37-55.

Savage, S.B. 1984. Mechanics of rapid granular flows. Advances in Applied Mechanics, 24: 289-366.

Savage, S.B., and Hutter, K. 1989. Motion of a finite mass of granular material down a rough incline. Journal of Fluid Mechanics, 199: 177-215.

Scheidegger, A.E. 1973. On the prediction of the reach and velocity of catastrophic landslides. Rock Mechanics Felsmechanik Mécanique des Roches, 5(4): 231-236.

Schindler, C., Cuenod, Y., Eisenlohr, T., and Joris, C.L. 1993. The events of Randa, April 18th and May 19th 1991 - an uncommon type of rockfall. Die Ereignisse vom 18. April und 9. Mai 1991 bei Randa (VS) - ein atypischer Bergsturz in Raten, 86(3): 643-665.

Serratrice, J.F. 2006. Modélisation des grands éboulements rocheux par épandage. Application aux sites de La Clapière (Alpes-Maritimes) et de Séchilienne (Isère). Bulletin des Laboratoires des Ponts et Chaussees (263-264): 53-69.

Shreve, R.L. 1966. Sherman Landslide Alaska. Science, 154(3757): 1639.

Shreve, R.L. 1968. The Blackhawk landslide. Geological Society of America, Special Paper, 108: 1-47.

Snedecor, G.W., and Cochran, W.G. 1989. Statistical Methods, Eighth Edition, Iowa State University Press.

Strobl, K., Sepp, W., Fuchs, S., Paredes, C. and Arbter K. 2007. Camera Calibration Toolbox for Matlab. www.vision.caltech.edu/bouguetj/calib_doc/

Takajo, H., and Takahashi, T. 1988a. Least-squares phase estimation from the phase difference. J. Opt. Soc. Am. A, 5(3): 416-425.

Takajo, H., and Takahashi, T. 1988b. Noniterative method for obtaining the exact solution for the normal equation in least-squares phase estimation from the phase difference. J. Opt. Soc. Am. A, 5(11): 1818-1827.

Takeda, M., Ina, H., and Kobayashi, S. 1982. Fourier-transform method of fringe-pattern analysis for computer-based topography and inteferometry. Journal of the Optical Society of America, 72(1): 156-160.

References

Valentino, R., Barla, G., and Montrasio, L. 2004. *DEM simulation of dry granular flow in laboratory flume tests. In Ninth International Symposium on Landslides: Evaluation and Stabilization. Rio de Janeiro. 28 June-02 July, 2: 1489-1496.*

Van Gassen, W., and Cruden, D.M., 1989. *Momentum transfer and friction in the debris of rock avalanches. Can. Geotech. J., 26: 623-628.*

Varnes, D.J. 1978. *Slope movement and types of processes. Landslides: Analysis and Control: 11-33.*

Varnes, D.J.D.J. 1984. *International Association of Engineering Geology Commission on Landslides and other mass movements on Slopes, Landslide Hazard Zonation: A Review of Principles and Practice.*

Voellmy, A. 1955. *Über die Zerstörungskraft von Lawinen. Schweizerische Bauzeitung, 73(12-15): 159-162.*

Voight, B. 1978. *Lower Gros Ventre Slide, Wyoming.*

Voight, B., and Pariseau, W. G. 1978. *Rockslides and Avalanches: An Introduction. In: Rockslides and Avalanches, 1 (Voight, B., ed.). Amsterdam, Oxford, New York: Elsevier. Dev. Geotech. Eng.,14A: 1–67.*

Voight, B., and Sousa, J. 1994. *Lessons from Ontake-san: a comparative analysis of debris avalanche dynamics. Engineering Geology, 38(3-4): 261-297.*

Wieland, M., Gray, J.M.N.T., and Hutter, K. 1999. *Channelized free-surface flow of cohesionless granular avalanches in a chute with shallow lateral curvature. J.Fluid Mech.: 73-100.*

Zhang, Z. 1999. *Flexible camera calibration by viewing a plane from unknown orientations. In Proceedings of the IEEE International Conference on Computer Vision. Kerkyra, Greece. IEEE, 1: 666-673.*

Zhang, H., Su, H., and Su, X.Y. 2007. *A Phase Unwrapping Algorithm for 3D Reconstruction. In Proceedings of the ACIS International Conference on Software Engineering, Artificial Intelligence, Networking, and Parallel/Distributed Computing. ACIS : 666-673.*

Sources

Les Alpes, 1998 of the Club Alpin Suisse - CAS, No. 6

NIST/SEMATECH 2006. http://www.itl.nist.gov/div898/handbook/ E-Handbook of Statistical Methods.

http://hkieged.org/LDM2007 The 2007 International Forum on Landslide Disaster Management

www.geonet.org.nz GeoNet web page

http://www.unisdr.org United Nations International Strategy for Disaster Reduction

www.vajont.net

Appendix I: fringe projection method

Code of Steve Cochard (Environmental Hydraulics Laboratory, LHE-EPFL) for the retrieving of the unwrapped phase:

```
a =[1 2 3];
disp('read w64')
w1(:,:,a(1)) = rgb2gray(imread('flat_64_1.tif'));
w1(:,:,a(2)) = rgb2gray(imread('flat_64_2.tif'));
w1(:,:,a(3)) = rgb2gray(imread('flat_64_3.tif'));

w64=double(w1);
disp('phase')
phi_64 = phasestep(w64);
figure, s1 = surf(phi_64), set(s1,'linestyle','none'), drawnow
clear w64
disp('unwrap')
s_64 = unwrap2(phi_64,'mirror');
figure, s2 = surf(s_64), set(s2,'linestyle','none'), drawnow
clear phi_64

disp('read x64')
w2(:,:,a(1)) = rgb2gray(imread('fig_64_1.tif'));
w2(:,:,a(2)) = rgb2gray(imread('fig_64_2.tif'));
w2(:,:,a(3)) = rgb2gray(imread('fig_64_3.tif'));

x64=double(w2);
disp('phase')
alpha_64 = phasestep(double(x64));
clear x64
tic
disp('unwrap')
t_64 = unwrap2(alpha_64,'mirror');
toc


s64 = s_64(1:2:end,1:2:end);
t64 = t_64(1:2:end,1:2:end);

figure, s1 = surf(t64), set(s1,'linestyle','none'), drawnow
couleur = t64-s64;
l = light('position',[0 0.6 0.3]);
set(s1,'CData',couleur);
set(s1,'FaceColor','interp');
set(s1,'FaceLighting','phong');

xlabel('x')
ylabel('y')
zlabel('z')
view(-60,10);

[f1,f2]= freqspace(25,'meshgrid');
Hd = zeros(25,25); d = sqrt(f1.^2+f2.^2) < 0.2;
Hd(d) = 1;
couleur = filter2(Hd,couleur);
set(s1,'CData',couleur);
[dx,dy] = gradient(couleur);

dx([1:100,end-100:end],[1:100,end-100:end]) = 0;
dy([1:100,end-100:end],[1:100,end-100:end]) = 0;
save('t64','t64')
save('s64','s64')
```

Code of Irene Manzella (Rock Mechanics Laboratory, LMR- EPFL) for calibration and the retrieving of the deposit profile:

```
dif_phase=t64-s64;
fheight = dif_phase';
hdep = input('hdep=');
r=length(fheight(:,1));
c=length(fheight(1,:));
inc=input('panel inclination=');
widI=length(fheight(:,1))
lenI=length(fheight(1,:))
figure(1)
s1 = surf(fheight), set(s1,'linestyle','none')
l = light('position',[0 0.6 0.3]);
set(s1,'FaceColor','interp');
set(s1,'FaceLighting','phong');
minasseZ=floor(min(min(fheight)));
maxasseZ=ceil(max(max(fheight)));
set(gca,'ZLim',[minasseZ maxasseZ])
set(gca,'ZTick',[minasseZ:0.5: maxasseZ]);
xlabel('x')
ylabel('y')
zlabel('dif_phase')
view(0,0);
hold;
Zmin = input('Zmin=');
varXP=1;
cyclevol=1;
varloop=1;
varcycle=1;
wid=input('image width=');
len=input('image length=');
XP=input('image XP=');
while varXP>0;
    while cyclevol>0;
        while varloop>0;
            Z=fheight;
            Z= Z-Zmin;
            figure(2)
            s2 = surf(Z), set(s2,'linestyle','none')
            l = light('position',[0 0.6 0.3]);
            set(s2,'FaceColor','interp');
            set(s2,'FaceLighting','phong');
            minasseZ=floor(min(min(Z)));
            maxasseZ=ceil(max(max(Z)));
            set(gca,'ZLim',[minasseZ maxasseZ])
            set(gca,'ZTick',[minasseZ:0.5: maxasseZ]);
            xlabel('x')
            ylabel('y')
            zlabel('dif_phase')
            view(0,0);
            hold;
            figure(3)
            s3 = surf(Z), set(s3,'linestyle','none')
            l = light('position',[0 0.6 0.3]);
            set(s3,'FaceColor','interp');
            set(s3,'FaceLighting','phong');
            minasseZ=floor(min(min(Z)));
            maxasseZ=ceil(max(max(Z)));
            set(gca,'ZLim',[minasseZ maxasseZ])
            set(gca,'ZTick',[minasseZ:0.5: maxasseZ]);
            xlabel('x')
            ylabel('y')
            zlabel('dif_phase')
            view(90,0);
            hold;
            DX=(len/lenI);
            DY=(wid/widI);
            NX=len-DX
            NY=wid-DY
            Zcol=reshape(Z,[],1);
```

```
'write 1 if you want to introduce phase pick manually (the max is not centered)'
'0 if you want phase pick to be an average around the maximum (the max is
centered)'
varh=input('varh=');
if varh>0;
    pick=input('pick=');
else
    [maximo,posmax]=max(Zcol);
    aroundpick=[Zcol(posmax-3) Zcol(posmax-2) Zcol(posmax-1) Zcol(posmax)
    Zcol(posmax+1) Zcol(posmax+2) Zcol(posmax+3)]
    pick=mean(aroundpick)
end
fact=hdep/pick
Zmm=Zcol*fact;
size(Zmm)
max(Zmm)
n=length(Zcol(:,1));
Zzero= zeros(n,1);
for i=1:n
if Zmm(i)<0
    Zzero(i)=0;
else
    Zzero(i)=Zmm(i);
end
end
m=length(Zmm(:,1));
XYZpan=zeros(m,3);
i=0;
for h=0:DX:NX
    for j=0:DY:NY
        i=i+1;
        XYZpan(i,1)=h;
        XYZpan(i,2)=j;
        if (h<XP)
            XYZpan(i,3)=(XP-h)*tand(inc);
        end
    end
end
XYZpan(:,1)=(XYZpan(:,1)-XP);
XYZpan(:,2)=(XYZpan(:,2)-wid/2);
XYZpan_mat=reshape(XYZpan(:,3),r,c);
XYZdep0=zeros(m,3);
XYZdep0(:,1)=XYZpan(:,1);
XYZdep0(:,2)=XYZpan(:,2);
XYZdep0(:,3)=Zzero;
XYZdep0_mat=reshape(XYZdep0(:,3),r,c);
XYZdep0_pan=zeros(m,3);
XYZdep0_pan(:,1)=XYZpan(:,1);
XYZdep0_pan(:,2)=XYZpan(:,2);
XYZdep0_pan(:,3)=Zzero+XYZpan(:,3);
XYZdep0_pan_mat=reshape(XYZdep0_pan(:,3),r,c);
figure(4)
subplot(2,2,1)
s4 = surf(XYZdep0_mat), set(s4,'linestyle','none')
l = light('position',[0 0.6 0.3]);
set(s4,'FaceColor','interp');
set(s4,'FaceLighting','phong');
xlabel('x')
ylabel('y')
zlabel('XYZdep0_mat')
view(150,50);
subplot(2,2,2)
s4 = surf(XYZdep0_mat), set(s4,'linestyle','none')
l = light('position',[0 0.6 0.3]);
set(s4,'FaceColor','interp');
set(s4,'FaceLighting','phong');
xlabel('x')
ylabel('y')
zlabel('XYZdep0_mat')
view(90,0);
subplot(2,2,3)
s4 = surf(XYZdep0_mat), set(s4,'linestyle','none')
l = light('position',[0 0.6 0.3]);
set(s4,'FaceColor','interp');
```

```
            set(s4,'FaceLighting','phong');
            xlabel('x')
            ylabel('y')
            zlabel('XYZdep0_mat')
            view(0,90);
            subplot(2,2,4)
            s4 = surf(XYZdep0_mat), set(s4,'linestyle','none')
            l = light('position',[0 0.6 0.3]);
            set(s4,'FaceColor','interp');
            set(s4,'FaceLighting','phong');
            xlabel('x')
            ylabel('y')
            zlabel('XYZdep0_mat')
            view(0,0);
            hgsave('XYZdep0_mat')
            hold;
            'write 1 if you want to introduce a different Zmin, 0 if you want to quit the
loop'
            varloop=input('varloop=');
            if varloop<1
                Zmin = Zmin;
            else
                Zmin = input('Zmin=');
                Z=fheight;
                Z= Z-Zmin;
            end
        end

    m=length(XYZdep0(:,1));
    Nx=zeros(m,1);
    Ny=zeros(m,1);
    Nz=zeros(m,1);
    D=zeros(m,1);
    i=0;
    for h=0:DX:(NX-DX)
        for j=0:DY:(NY-DY)
            i=i+1;
            Nx(i)=(XYZdep0(i,1)+DX/2)*(XYZdep0(i,3)+XYZdep0(i+1,3));
            Ny(i)=(XYZdep0(i,2)+DY/2)*(XYZdep0(i,3)+XYZdep0(i+1,3));
            Nz(i)=(XYZdep0(i,3)/2)*(XYZdep0(i,3)+XYZdep0(i+1,3));
            D(i)=XYZdep0(i,3)+XYZdep0(i+1,3);
        end
    end
    Ntotx=sum(Nx)
    Ntoty=sum(Ny)
    Ntotz=sum(Nz)
    Dtot=sum(D)
    xc=Ntotx/Dtot
    yc=Ntoty/Dtot
    zc=Ntotz/Dtot
    Vtot=sum(D/2*DX*DY)
    'write 1 if you want to introduce a different Zmin, 0 if you want to quit the loop'
    cyclevol=input('cyclevol=');
    if cyclevol<1
            Zmin = Zmin;
        else
            Zmin = input('Zmin=');
            Z=fheight;
            Z= Z-Zmin;
            varloop=1;
        end
    end
    figure(5)
    subplot(2,1,1)
    s5 = surf(XYZdep0_pan_mat), set(s5,'linestyle','none')
    l = light('position',[0 0.6 0.3]);
    set(s5,'FaceColor','interp');
    set(s5,'FaceLighting','phong');
    xlabel('x')
    ylabel('y')
    zlabel('XYZdep0_pan_mat')
    view(150,50);
    subplot(2,1,2)
    s5 = surf(XYZdep0_pan_mat), set(s5,'linestyle','none')
```

```
    l = light('position',[0 0.6 0.3]);
    set(s5,'FaceColor','interp');
    set(s5,'FaceLighting','phong');
    xlabel('x')
    ylabel('y')
    zlabel('XYZdep0_pan_mat')
    view(0,0);
    hold;
    'write 1 if you want to introduce a different XP, 0 if you want to quit the loop'
    varXP=input('varXP=');
    if varXP<1
                cyclevol = 0;
    else
    wid=input('image width=');
    len=input('image length=');
    XP=input('image XP=');
    varloop=1;
    cyclevol =1;
    end
end
hgsave('XYZdep0_pan_mat')
XYZdep=zeros(m,3);
XYZdep(:,1)=XYZpan(:,1);
XYZdep(:,2)=XYZpan(:,2);
XYZdep(:,3)=Zmm;
XYZdep_mat=reshape(XYZdep(:,3),r,c);
XYZdep_pan=zeros(m,3);
XYZdep_pan(:,1)=XYZpan(:,1);
XYZdep_pan(:,2)=XYZpan(:,2);
XYZdep_pan(:,3)=Zmm+XYZpan(:,3);
XYZdep_pan_mat=reshape(XYZdep_pan(:,3),r,c);
figure(6)
s6 = surf(XYZdep_mat), set(s6,'linestyle','none')
l = light('position',[0 0.6 0.3]);
set(s6,'FaceColor','interp');
set(s6,'FaceLighting','phong');
xlabel('x')
ylabel('y')
zlabel('XYZdep_mat')
view(150,50);
hgsave('XYZdep_mat')
figure(7)
s7 = surf(XYZdep_pan_mat), set(s7,'linestyle','none')
l = light('position',[0 0.6 0.3]);
set(s7,'FaceColor','interp');
set(s7,'FaceLighting','phong');
xlabel('x')
ylabel('y')
zlabel('XYZdep_pan_mat')
view(0,0);
hgsave('XYZdep_pan_mat')
results=zeros(1,11);
results(1,1)=len;
results(1,2)=wid;
results(1,3)=XP;
results(1,4)=widI;
results(1,5)=lenI;
results(1,6)=Zmin;
results(1,7)=fact;
results(1,8)=xc;
results(1,9)=yc;
results(1,10)=zc;
results(1,11)=Vtot;
results
save('xyzpan','XYZpan','-ASCII')
save('xyzdep','XYZdep','-ASCII')
save('xyzdep0','XYZdep0','-ASCII')
save('xyzdep_pan','XYZdep_pan','-ASCII')
save('xyzdep0_pan','XYZdep0_pan','-ASCII')
save('XCM','xc','-ASCII')
save('YCM','yc','-ASCII')
save('ZCM','zc','-ASCII')
save('VOL','Vtot','-ASCII')
```

Code of Equis Sebastien (Nanophotonics & Metrology Laboratory, EPFL) for the retrieving of the unwrapped phase with the Fourier method:

```
%Fringe analysis with Fourier method
clear all
close all
clc
%--------------------
ti = cputime;
%---------------------------------------------------------------------------
%---------------------------------------------------------------------------
% identify on the image significant points
base=imread('base.bmp');
image(base)
% a=input('xmax=');
% b=input('ymax=');
%---------------------------------------------------------------------------
%open the image files
Ii = double(imread('base.bmp'));
% Iie = Ii(1:b,1:a,1);
Iie = Ii(1:end,1:end,1);
If = double(imread('flow.bmp'));
% Ife = If(1:b,1:a,1);
Ife = If(1:end,1:end,1);
%---------------------------------------------------------------------------
[n1,n2] = size(Iie);
%---------------------------------------------------------------------------
%---------------------------------------------------------------------------
%filtering in Fourier space
rnoyau = 24;
[x,y] = meshgrid(-rnoyau:rnoyau,-rnoyau:rnoyau);
%elliptical filter
r = 2*x.^2+y.^2+2*x.*y;
noyau = (sqrt(r) < 0.7*rnoyau);
%positioning the filter in the Fourier domain
posfil = zeros(n1,n2);
posfil(54,96) = 1;
mask = conv2(posfil,double(noyau));
maskf = mask(rnoyau:rnoyau+n1-1,rnoyau:rnoyau+n2-1);
%--------------------
%recenter the FT (a shift in real domain changes the phase of FT)
%Shift theorem of FT
M = zeros(n1,n2);
vect =ones(max(n1,n2),1);
for k =1:max(n1,n2)
    Mtemp = diag(vect,2*k-max(n1,n2)-1);
    M = M+Mtemp(1:n1,1:n2);
end
M = exp(i*pi*M);
%---------------------------------------------------------------------------
%inverse FT and phase extraction
FT_Iie_fil = fftshift(fft2(Iie));
FIie_fil = ifft2(FT_Iie_fil.*maskf).*M;
Pi = atan2(imag(FIie_fil),real(FIie_fil));

FT_Ife_fil = fftshift(fft2(Ife));
FIfe_fil = ifft2(FT_Ife_fil.*maskf).*M;
Pf = atan2(imag(FIfe_fil),real(FIfe_fil));
%---------------------------------------------------------------------------
figure(3)
%plotting of the extracted phases still wrapped (carrier not removed)
subplot(1,2,1);imagesc(Pi);colormap gray;axis image
subplot(1,2,2);imagesc(Pf);colormap gray;axis image
%---------------------------------------------------------------------------
%---------------------------------------------------------------------------
% modulo 2pi substraction: RECOMMENDED in this case
Pm = Pf-Pi;
Pm = Pm-2*pi*round(Pm/2/pi);

Pm_unw2 = unwrap2(Pm,'mirror');
Pm_unw2 = Pm_unw2-min(min(Pm_unw2));
%--------------------
figure(7)
```

```
%plotting the wrapped phase due to the fluid only
imagesc(Pm);colormap gray;axis image;title('Wrapped Phase')
%---------------------
figure(8)
%plotting the unwrapped phase due to the fluid only
imagesc(Pm_unw2);axis image;colorbar;title('Unwrapped Phase')
%------------------------------------------------------------------------
%------------------------------------------------------------------------
%computation time
tf = cputime-ti
save('Pm_unw2','Pm_unw2')
```

Appendix II: tests and measurements of the second campaign

		Test conditions					Manual measurements			Computed data		
Series	Material	slope [°]	h [m]	V [litres]	Base friction	Slope toe	L* [m]	R [m]	W [m]	X_{CM} [m]	ϕ_{CM} [°]	ϕap [°]
4A	Gr2	45	1.0	20	rough	sharp	0.62	0.49	1.25	0.17	43.9	35.3
4A	Gr2	45	1.0	20	rough	sharp	0.60	0.55	1.40	0.24	42.1	34.3
4A	Gr2	45	1.0	40	rough	sharp	0.70	0.57	1.45	0.16	43.8	35.1
4B	Gr2	45	1.0	20+20	rough	sharp	0.68	0.50	1.44	0.09	45.0	36.1
12	Gr2	45	1.5	20	rough	sharp	0.59	0.63	1.40	0.33	41.6	36.0
12	Gr2	45	1.5	20	rough	sharp	0.60	0.64	1.40	0.33	41.5	35.9
12	Gr2	45	1.5	40	rough	sharp	0.76	0.76	1.60	0.34	41.5	35.3
12	Gr2	45	1.5	40	rough	sharp	0.73	0.73	1.60	0.36	41.2	35.7
13	Gr2	37.5	1.0	20	rough	sharp	0.59	0.41	1.25	0.09	38.3	31.1
13	Gr2	37.5	1.0	40	rough	sharp	0.72	0.44	1.40	0.04	38.9	31.4
13	Gr2	37.5	1.5	40	rough	sharp	0.78	0.54	1.60	0.09	37.8	32.0
14	Gr2	37.5	1.5	20	rough	sharp	0.67	0.50	1.50	0.11	37.7	31.9
14	Gr2	37.5	1.5	20	rough	sharp	0.65	0.50	1.50	0.12	37.6	31.9
15	Gr2	45	1.0	20	smooth	sharp	0.68	0.74	1.30	0.37	39.6	31.5
15	Gr2	45	1.0	20	smooth	sharp	0.66	0.72	1.30	0.36	39.7	31.8
15	Gr2	45	1.0	20	smooth	sharp	0.70	0.73	1.29	0.34	40.1	31.7
15	Gr2	45	1.0	40	smooth	sharp	0.84	0.82	1.45	0.34	40.3	31.9
15	Gr2	45	1.0	40	smooth	sharp	0.87	0.86	1.48	0.36	40.9	31.4
15	Gr2	45	1.0	40	smooth	sharp	0.86	0.85	1.44	0.36	39.8	31.6
15B	Gr2	45	1.0	20+20	smooth	sharp	0.86	0.74	1.32	0.21	42.6	32.9
15B	Gr2	45	1.0	20+20	smooth	sharp	0.82	0.72	1.33	0.21	42.6	33.1
15B	Gr2	45	1.0	20+20	smooth	sharp	0.84	0.74	1.32	0.19	43.0	32.9
16	Gr2	45	1.5	20	smooth	sharp	0.70	0.88	1.36	0.52	38.9	33.3
16	Gr2	45	1.5	20	smooth	sharp	0.66	0.87	1.37	0.52	39.0	33.4
16	Gr2	45	1.5	20	smooth	sharp	0.67	0.88	1.37	0.51	39.0	33.3
16	Gr2	45	1.5	40	smooth	sharp	0.85	1.05	1.56	0.56	38.5	32.6
16	Gr2	45	1.5	40	smooth	sharp	0.88	1.07	1.57	0.53	38.9	32.4
16B	Gr2	45	1.5	20+20	smooth	sharp	0.91	0.89	1.47	0.41	40.6	34.0
16B	Gr2	45	1.5	20+20	smooth	sharp	0.89	0.88	1.52	0.39	40.8	34.1
16B	Gr2	45	1.5	20+20	smooth	sharp	0.91	0.90	1.48	0.38	40.9	33.9
17	Gr2	37.5	1.0	20	smooth	sharp	0.68	0.59	1.28	0.17	36.8	28.8
17	Gr2	37.5	1.0	20	smooth	sharp	0.67	0.61	1.30	0.20	36.4	28.6
17	Gr2	37.5	1.0	20	smooth	sharp	0.73	0.66	1.29	0.25	35.5	28.1
17	Gr2	37.5	1.0	40	smooth	sharp	0.86	0.75	1.40	0.24	35.5	28.0
17	Gr2	37.5	1.0	40	smooth	sharp	0.86	0.74	1.41	0.23	35.8	28.1
17	Gr2	37.5	1.0	40	smooth	sharp	0.86	0.74	1.41	0.23	35.8	28.1
17B	Gr2	37.5	1.0	20+20	smooth	sharp	0.78	0.61	1.38	0.06	38.5	29.5
17B	Gr2	37.5	1.0	20+20	smooth	sharp	0.80	0.63	1.32	0.09	37.8	29.2
17B	Gr2	37.5	1.0	20+20	smooth	sharp	0.81	0.66	1.40	0.12	37.4	28.9
18	Gr2	37.5	1.5	20	smooth	sharp	0.64	0.72	1.44	0.35	34.9	29.9
18	Gr2	37.5	1.5	20	smooth	sharp	0.64	0.70	1.42	0.32	35.3	30.1
18	Gr2	37.5	1.5	40	smooth	sharp	0.84	0.82	1.60	0.35	35.0	29.6
18B	Gr2	37.5	1.5	20+20	smooth	sharp	0.87	0.72	1.44	0.21	36.5	30.4
18B	Gr2	37.5	1.5	20+20	smooth	sharp	0.86	0.71	1.44	0.19	36.8	30.5

		Test conditions					**Manual measurements**			**Computed data**		
Series	**Material**	slope [°]	h [m]	V [litres]	Base friction	Slope toe	L* [m]	R [m]	W [m]	X_{CM} [m]	ϕ_{CM} [°]	ϕap [°]
19	BrR	45	1.0	20	smooth	sharp	0.86	0.75	1.35	0.37	31.4	39.3
19	BrR	45	1.0	20	smooth	sharp	0.96	0.77	1.33	0.32	31.2	40.4
19	BrR	45	1.0	40	smooth	sharp	0.93	0.85	1.40	0.39	31.6	39.2
20	BrP	45	1.0	40	smooth	sharp	1.23	1.15	1.39	0.39	28.4	39.3
20	BrP	45	1.0	20	smooth	sharp	1.09	0.87	0.98	0.32	29.9	40.4
20B	BrP	45	1.0	20+20	smooth	sharp	1.16	0.87	1.32	0.27	31.3	41.1
21	BrR	45	1.5	20	smooth	sharp	0.97	0.85	1.35	0.54	33.6	38.7
21	BrR	45	1.5	20	smooth	sharp	1.04	0.97	1.45	0.54	32.4	38.6
21	BrR	45	1.5	40	smooth	sharp	1.05	1.01	1.62	0.54	33.0	38.9
21	BrR	45	1.5	40	smooth	sharp	1.05	0.94	1.55	0.54	33.6	38.9
21	BrR	45	1.5	20+20	smooth	sharp	0.84	0.84	1.35	0.52	33.7	39.0
22	BrP	45	1.5	40	smooth	sharp	1.50	1.40	1.42	0.67	29.7	37.3
22	BrP	45	1.5	40	smooth	sharp	1.38	1.33	1.47	0.70	30.2	36.8
22B	BrP	45	1.5	40	smooth	sharp	1.27	1.05	1.29	0.30	32.6	41.8
23	BrR	37.5	1.0	20	smooth	sharp	0.61	0.48	1.14	0.16	36.9	30.2
23	BrR	37.5	1.0	20	smooth	sharp	0.60	0.46	1.18	0.16	37.0	30.4
23	BrR	37.5	1.0	40	smooth	sharp	0.77	0.59	1.33	0.19	36.4	29.7
23	BrR	37.5	1.0	40	smooth	sharp	0.78	0.54	1.31	0.15	36.9	30.2
24	BrP	37.5	1.0	20	smooth	sharp	0.90	0.62	1.11	0.20	36.1	28.5
24	BrP	37.5	1.0	40	smooth	sharp	1.15	0.86	1.28	0.22	35.6	27.0
24	BrP	37.5	1.0	40	smooth	sharp	1.18	0.84	1.18	0.19	36.0	27.2
25	BrR	37.5	1.5	20	smooth	sharp	0.74	0.68	1.31	0.48	33.6	30.2
25	BrR	37.5	1.5	20	smooth	sharp	0.70	0.62	1.25	0.53	33.2	30.8
25	BrR	37.5	1.5	40	smooth	sharp	0.78	0.68	1.39	0.22	36.5	30.8
25	BrR	37.5	1.5	40	smooth	sharp	0.85	0.76	1.49	0.44	34.1	30.1
26	BrP	37.5	1.5	20	smooth	sharp	1.01	0.92	1.13	0.60	32.3	28.3
26	BrP	37.5	1.5	20	smooth	sharp	0.97	0.84	1.24	0.63	32.1	28.9
26	BrP	37.5	1.5	40	smooth	sharp	1.22	1.08	1.50	0.40	34.4	27.7
26	BrP	37.5	1.5	40	smooth	sharp	1.24	1.04	1.38	0.43	34.0	28.0
26B	BrP	37.5	1.5	20+20	smooth	sharp	1.17	0.92	1.41	0.27	35.6	28.9
27	Gr2	45	1.5	20	smooth	curved	0.88	1.49	1.54	1.00	33.3	27.9
27	Gr2	45	1.5	20	smooth	curved	0.85	1.43	1.68	0.97	33.6	28.4
27	Gr2	45	1.5	40	smooth	curved	1.11	1.68	1.74	1.12	32.4	27.7
27	Gr2	45	1.5	40	smooth	curved	1.09	1.67	1.77	1.06	33.0	27.7
27	Gr2	45	1.5	40	smooth	curved	1.09	1.64	1.79	1.04	33.3	27.9
27B	Gr2	45	1.5	20+20	smooth	curved	0.96	1.52	1.58	1.00	33.5	28.8
27B	Gr2	45	1.5	20+20	smooth	curved	1.07	1.49	1.74	0.82	35.4	29.0
28	Gr2	45	1.0	20	smooth	curved	0.86	1.13	1.48	0.68	34.1	27.0
28	Gr2	45	1.0	20	smooth	curved	0.85	1.14	1.55	0.71	33.6	26.9
28	Gr2	45	1.0	40	smooth	curved	1.00	1.25	1.66	0.70	34.2	27.5
28	Gr2	45	1.0	40	smooth	curved	1.03	1.27	1.70	0.73	33.8	27.3
29	BrR	45	1.0	40	smooth	curved	1.20	1.52	1.44	0.89	31.6	25.2
30	BrP	45	1.0	40	smooth	curved	1.92	1.92	1.25	1.04	29.7	22.5
30	BrP	45	1.0	40	smooth	curved	1.76	1.80	1.40	1.15	28.5	23.2

Appendix III: ANOVA analysis

According to the E-Handbook of Statistical Methods (NIST/SEMATECH, 2006) and Fürbringer (2005), the initial techniques of the analysis of variance were developed by the statistician and geneticist R. A. Fisher in the 1920s and 1930s and it is used to detect significant factors in a multi-factor model. In the multi-factor model, there is a response (dependent) variable and one or more factor (independent) variables. This is a common model in designed experiments where the experimenter sets the values for each of the factor variables and then measures the response variable. The level is considered as the state, i.e. the value of a factor.

Once established the factors to be considered, natural variables are standardised for the sake of numerical accuracy and generality of the designs. In this way all variables will be centred on zero and will vary in the interval -1 and 1. The standardised variable x_j is derived by the transformation of the natural variable u_j:

$$x_j = \frac{u_j - u_j(0)}{\Delta u}$$
$$u_j = u_j(0) + x_j \Delta u$$

[1]

Where $u_j(0)$ is the center of the interval of the natural variable and Δu is the half of the natural interval. The matrix of experiments is built considering the level x_{ij} of the factor j (column) in the experiment i (rows). The matrix of the model is the matrix X which has one line per experiment, one column per factors of the model. In the present study linear models will be considered whose general formulation is as follows:

$$y_i = c_o + \sum_{i=1}^{N} c_i \, x_j + \sum_{1, j \neq i}^{N} c_{ij} \, x_i \, x_j + e_i$$

$$\vec{Y} = \begin{bmatrix} y_1 \\ \vdots \\ y_N \end{bmatrix} = X \begin{bmatrix} c_o \\ c_1 \\ \vdots \\ \vdots \\ c_{123\ldots K} \end{bmatrix} + \begin{bmatrix} e_1 \\ \vdots \\ e_N \end{bmatrix} = X \, \vec{c} + \vec{e}$$

[2]

Where $\vec{Y}$ is the column vector of the N experimental measurements of the response considered, $\vec{c}$ is the column vector of the model coefficients, $\vec{e}$ the column vector of the N experimental errors corresponding to each y_i experimental data and X is the matrix of the model expressed by [3].

$$X = \begin{pmatrix} 1 & x_{11} & x_{12} & \cdots & x_{11}x_{12} & x_{11}x_{13} & \cdots \\ 1 & x_{21} & x_{22} & \cdots & x_{21}x_{22} & x_{21}x_{23} & \cdots \\ 1 & x_{31} & x_{32} & \cdots & x_{31}x_{32} & x_{31}x_{33} & \cdots \\ \vdots & \vdots & \vdots & & \vdots & \vdots & \\ 1 & x_{N1} & x_{N2} & \cdots & x_{N1}x_{N2} & x_{N1}x_{N3} & \cdots \end{pmatrix}$$

[3]

The coefficients of the model can be estimated through the least square algorithm as in [4].

$$\vec{Y} = X \, \vec{c} + \vec{e}$$

$$X^T \vec{Y} = X^T X \, \vec{c} + X^T \vec{e}$$

$$(X^T X)^{-1} X^T \vec{Y} = \vec{c} + (X^T X)^{-1} X^T \vec{e}$$

$$\vec{c} = (X^T X)^{-1} X^T \vec{Y} - (X^T X)^{-1} X^T \vec{e}$$

$$E(\vec{c}) = (X^T X)^{-1} X^T \vec{Y} - (X^T X)^{-1} X^T E(\vec{e})$$

$$E(\vec{c}) = (X^T X)^{-1} X^T \vec{Y}$$

[4]

With $E(\vec{c})$ is the estimated value of the coefficients of the model considering the estimated values of the error $E(\vec{e})$ equal to zero.

$(v_{ij}) = (X^T X)^{-1}$ is called the matrix of dispersion and the derived matrix of correlation is the matrix (r_{ij}) whose elements correspond to the correlation coefficients of the model coefficients c_i and c_j which are calculated according to [5].

$$r_{ij} = \frac{v_{ij}}{\sqrt{v_{ii}}\sqrt{v_{jj}}} = \frac{\mathrm{cov}(c_{ij})}{\sqrt{\mathrm{var}(c_i)}\sqrt{\mathrm{var}(c_j)}} \qquad [5]$$

This matrix is important because it allows calculating the Variance Inflation Factors (VIF) which are the diagonal elements of the inverse of the correlation matrix and predicts the quality of the estimation of the coefficient c_i of the model. More a VIF is close to 1 better is the estimator of the corresponding coefficients. Inflation factors greater than 8 or 10 indicate bad design which must be avoided (Feneuille, 1985 as reported by Fürbringer, 2005).

Once calculated the coefficients of the model and verified that they are well predicted by means of the VIF it is possible to perform an ANOVA analysis. The coefficients of the model corresponding to the factors considered are called effects. The differences between the predicted values and the measured values are called residuals. The fundamental technique of the ANOVA is a partitioning of the total sum of squares (SS) into components related to the effects used in the model.

$$SS\_total = SS\_error + SS\_effects \qquad [6]$$

Equation [6] summarizes how much of the variance in the data (total sum of squares) is accounted for by the factor effects (factor sum of squares) and how much is random error (residual sum of squares).In order to evaluate the significant factors it is necessary to compare the sum of squares of the effects with the sum of squares of the residuals. These have a chi-square distribution which results when independent variables with standard normal distributions are squared and summed. The effects mean squares of a significant effect are expected to be significantly greater than the mean square of the residual errors.

To compare them in a rigorous and objective way it is necessary to do an F test for the factor effects. In order to do this test the sum of squares (SS) must be standardized by its degree of freedom (DF) to obtain the mean squares. The total degree of freedom is equal to the number of data, for each factor the degree of freedom is the number of levels minus one whereas the degree of freedom of the mean is 1 and the ones of the residual are the total degrees of freedom minus the sum of the factor degrees of freedom. Using the F-distribution is a natural candidate because the test statistic is the quotient of two mean squares which have a chi-square distribution, i.e. the ratio between the mean square of the factor versus the mean square of the error. This statistic follows an F distribution with k and n degrees of

freedom, respectively the ones of the considered effect and of the residual error. An F-test (Snedecor and Cochran, 1983 as reported in NIST/SEMATECH, 2006) is used to test if the standard deviations of two populations are equal. The more this ratio deviates from 1, the stronger the evidence for unequal population variances. As a consequence higher is the probability (values near to 1), less the effect is significant since the factor and the residual have in this case similar variance.

In order to have scale independent formulations the two main following factors have been considered for the analysis of variance:

- $\dfrac{h_v}{h^*}$:   fall height of the centre of mass above the horizontal panel before failure (h_v, [m]) as defined in Figure 4-9 against the cube root of the volume (h^*, [m]);

- $\dfrac{\tan\phi}{\tan\alpha}$:   the tangent of the basal friction coefficient (ϕ) against the tangent of the slope angle (α). This last term represents the divergence from stability of the mass.

ANOVA has been performed separately for Gravel (Gr2), bricks randomly poured in the reservoir before failure (BrR) and piled orderly (BrP) and for curved and sharp connections at the toe. An attempt has been made to include these two factors considering a degree of structure called K varying from 0 (loose material, i.e. BrR) to 1 (structured compact material, i.e. BrP) and a degree of smoothness of the connection at the toe called S varying from 0 (sharp angular discontinuity at 45°) to 1 (curved discontinuity after a 45° slope). This last factor has been introduced only for tests with gravel since not enough tests with bricks have been performed with S=1 to allow a proper analysis.

The ranges of variation of the factors are reported in Table 4-61.

Model for:	h [m]	$h*$ [m]	α [°]	ϕ [°]	Nondimensional factors [-]			
					$hv/h*$	$\tan\phi/\tan\alpha$	K	S
Gr2	1-1.5	0.27-0.34	37.5-45	28-32	3.6-6.11	0.53-0.81	0	0
BrR	1-1.5	0.27-0.34	37.5-45	30	3.6-6.11	0.58-0.75	0	0
BrP	1-1.5	0.27-0.34	37.5-45	30	3.6-6.11	0.58-0.75	1	0
BrR vs BrP	1-1.5	0.27-0.34	37.5-45	30	3.6-6.11	0.58-0.75	0-1	0
Curved vs Sharp (Gr2)	1-1.5	0.27-0.34	45	28	3.6-6.11	0.53	0	0-1

Table 1 Ranges of variation of the nondimensional factors considered in the ANOVA analysis

The nondimensional responses are:

- $\dfrac{R}{h^*}$:   the runout on the horizontal panel (R, [m]) as defined in Figure 4-9 against the cube root of the volume ($h*$, [m]);

- $\dfrac{L^*}{h^*}$:   the deposit length ($L*$, [m]) as defined in Figure 4-9 against the cube root of the volume ($h*$, [m]);

- $\dfrac{W}{h^*}$:   the deposit width (W, [m]) as defined in Figure 4-9 against the cube root of the volume ($h*$, [m]);

- $\dfrac{X_{CM}}{h^*}$:   the distance travelled by the centre of mass on the horizontal panel (X_{CM}, [m]) as defined in Figure 4-9 against the cube root of the volume ($h*$, [m]);

- $\dfrac{\tan\phi_{ap}}{\tan\alpha}$:   the tangent of the apparent coefficient of friction or Fahrböschung (ϕ_{ap}) against the tangent of the slope angle (α);

- $\dfrac{\tan\phi_{CM}}{\tan\alpha}$:   the tangent of the travel angle of the centre of mass (ϕ_{CM}) against the tangent of the slope angle (α).

These factors and responses have been chosen since they have been found to be important in the previous analysis. Only two or three factors are considered at the same time. The first-

order model with second order interactions considered are as described in equation [7] respectively for 2 and 3 factors:

$$Y_i = a_0 + a_1 X_1 + a_2 X_2 + a_{12} X_1 X_2$$
$$Y_i = a_0 + a_1 X_1 + a_2 X_2 + a_3 X_3 + a_{12} X_1 X_2 + a_{13} X_1 X_3 + a_{23} X_2 X_3 + a_{123} X_1 X_2 X_3$$

[7]

According to the number of experiments and the level of the factors the model matrix is built. The VIF of the model have been found to be really near to 1 in the order of 1.001, therefore the least square derivation of the coefficients should give a good estimation of the effects.

By means of the ANOVA the significant factors and interactions have been determined.

Here follows an example of an ANOVA analysis. First in Table 2 the model matrix with the normalised value of the factors considered and in the last column the corresponding values of the response R/h* are shown. Afterwards the ANOVA table of the factors of influence on R/h* for tests with gravel and a sharp discontinuity is illustrated in Table 3. When the F test gives values <<1 then the factor is detected as having a high influence on the response, otherwise its influence is considered as low if near to 1.

Constant	$X_1=h_v/h^*$	$X_2=\tan\phi/\tan\alpha$	$X_1\&X_2=h_v/h^*\ \&\ \tan\phi/\tan\alpha$	$Y=$ Response $=R/h^*$
1	-1.00	0.14	-0.14	2.19
1	-1.00	0.14	-0.14	2.16
1	-1.00	1.00	-1	1.29
1	-1.00	1.00	-1	1.29
1	-0.96	-1.00	0.96	2.51
1	-0.96	-1.00	0.96	2.49
1	-0.96	-0.34	0.32	1.78
1	-0.96	-0.34	0.32	1.67
1	-0.48	0.14	-0.06	2.25
1	-0.48	0.14	-0.06	2.43
1	-0.48	1.00	-0.47	1.51
1	-0.48	1.00	-0.47	1.49
1	-0.47	-1.00	0.46	2.65
1	-0.47	-1.00	0.46	2.69
1	-0.47	-0.34	0.15	1.79
1	-0.47	-0.34	0.15	2.03
1	0.16	0.14	0.02	2.37
1	0.16	0.14	0.02	2.40
1	0.16	1.00	0.16	1.58
1	0.16	1.00	0.16	1.64
1	0.20	-1.00	-0.20	3.07
1	0.20	-1.00	-0.20	3.13
1	0.20	-0.34	-0.06	2.22
1	0.20	-0.34	-0.06	2.13
1	0.99	0.14	0.13	2.65
1	0.99	0.14	0.13	2.58
1	0.99	1.00	0.98	1.84
1	0.99	1.00	0.98	1.84
1	1.00	-1.00	-1	3.21
1	1.00	-1.00	-1	3.24
1	1.00	-0.34	-0.34	2.32
1	1.00	-0.34	-0.34	2.36

Table 2 Model Matrix and R/h* for tests with gravel with a sharp discontinuity at the toe

$Y=$ Response $=R/h^*$		Value	SS	DF	mean square	F statistic	F test	importance
	constant	$a_0=$ 2.20	155.32	1	155.32			
$X_1=$	h_v/h^*	$a_1=$ 0.29	2.68	7	0.38	3.27	0.014	high
$X_2=$	$\tan\phi/\tan\alpha$	$a_2=$ -0.58	10.75	3	3.58	30.62	$2.26*10^{-8}$	high
$X_1\&X_2=$	$h_v/h^*\ \&\ \tan\phi/\tan\alpha$	$a_{12}=$ -0.07	0.15	1	0.15	1.27	0.18	low
	residuals		1.87	24	0.08			

Table 3 ANOVA table of R/h* for tests with gravel with a sharp discontinuity at the toe

Curriculum Vitae

Irene Manzella
Italian, 31 years old, woman, single
Avenue du Château 62
1008 Prilly, Switzerland
+41 76 4798791, irenemanzella@gmail.com
Web: http://personnes.epfl.ch/irene.manzella

EDUCATION

Currently: PhD student since 2004 at the Rock Mechanics Laboratory of EPFL (Lausanne). Subject of the thesis: Dry rock avalanche propagation: unconstrained flow experiments with gravel materials and little bricks.

Courses successfully attended in the framework of the Doctoral school: Design of experiments; Geodynamical processes of slope instability, incl. recognition and mitigation; Photogrammetry; Prevention, control and management of environmental risks and crisis situations; Scientific communication; Speckle metrology.

2005: Attendance to the IGAR workshop "Data analysis and modelling in environmental sciences towards risk assessment and impact on society", Lausanne, Switzerland.

2004: Attendance to the FORM-OSE Post-graduate Training School "Living with hydro-geomorphological risks: from theory to practice", Strasbourg, France.

2002: Master of advanced study in "Settlements upgrading for cooperation and development", Politecnico di Milano, Faculty of Architecture, Mantua, Italy. Report: "Progetti di cooperazione in zone ad alto rischio. Il caso nicaraguense".

2002: Workshop in Nicaragua to follow a project regarding planning and upgrading of rural and half urban communities in El Viejo (dep. Chinandega).

2002: Program of training for the municipal committee of El Viejo, Nicaragua, for the natural disasters prevention, mitigation and attention.

16th Oct 2001: Degree in Environmental and Territorial Engineer, specialization: Land Protection, Politecnico di Milano.

Master thesis: "Experimental study about the spatial parameters of influence on woody debris entrapment facilities in torrents".

2001: Working out of the thesis (7 months) at the Hydraulic laboratory of the Technische Universität München, Munich and Obernach, Germany.

PROFESSIONAL EXPERIENCE

Currently: Assistant since December 2003 at LMR, EPFL Lausanne. Working for the INTERREG IIIA Rockslidetec project on propagation of rock avalanches; physical modelling.

2003: Consulting (3 months) for the hydro-geological survey for the upgrading of a petrol station of ERG Petroli S.p.A.

2003: Holding (4 months) a temporary teaching post in the scientific high school 'Antonelli' and the technical high school 'Fauser', Novara, Italy. Mathematics classes.

2002: Consulting (3 months) to the NGO INDES, Managua, Nicaragua. Evaluation of dangers, vulnerabilities and hazards of Managua.

2002: Consulting (2 months) to Engineer Riccardo Massara, Novara, Italy. Hydro-geological hazards.

2002: Trainee (3 months) at the Benedini office, Mantua, Italy. Dimensioning of sewerage systems.

MAIN PUBLICATIONS

Manzella, I., Labiouse, V. (2008): Qualitative analysis of rock avalanches propagation by means of physical modelling of not constrained gravel flows. Rock Mech. & Rock Eng. Journal, 41 (1), 133-151

Manzella, I., Labiouse, V. (2007): Rock avalanches: experimental study of the main parameters influencing propagation. Proc. 11th ISRM, 9-13 July, 2007, Lisbon, V.1, 657-660

Not yet published and further informal publications:

Manzella, I., Labiouse, V. Gravel and small bricks flow experiments to investigate parameters and mechanisms involved in rock avalanches. Submitted to Engineering Geology Journal.

Manzella, I., Pirulli, M., Naaim, M., Serratrice, JF., and Labiouse, V. 2008 Numerical modelling of a rock avalanche laboratory experiment in the framework of the "Rockslidetec" alpine project. Accepted for the 10th International Symposium on landslide and Engineered Slopes to be held from the 30th of June to the 4th of July 2008 in Xi'an, China

Manzella, I., Labiouse V. (2006): INTERREG IIIA 'Rockslidetec' project. Final report. Internally published, English version and French abstract

Manzella, I., Labiouse V. (2005): Modélisations physiques pour l'étude de la propagation des avalanches rocheuses. Sols et Roches : bulletin des laboratoires de mécanique des sols et des roches, No 35

MEMBERSHP: IACMAG committee for enhancing membership, Ingénieurs du monde, AIAT (Associazione Ingegneri per l'Ambiente e il Territorio)

LANGUAGES: Italian mother tongue, fluent English and French, good Spanish and German